Modeling and Experimental Evaluation of a Load-Sensing and Pressure Compensated Hydraulic System

A thesis submitted to the

College of Graduate Studies and Research

In Partial Fulfillment of the Requirements for the Ph.D. Degree in the

Department of Mechanical Engineering

University of Saskatchewan

By

Duqiang Wu

Permission to Use

The author agrees that the libraries of University of Saskatchewan may make it freely available for inspection. I further agree that the permission for copying this thesis in any manner, in whole or in part, for scholarly purposes, may be granted by the professors who supervised this work or, in their absence, by the Head of the Department or Dean of the College in which this thesis work was conducted. It is understand that any copying, publication or use of this thesis or parts thereof for financial gain shall not be allowed without my written permission. It is also understood that due recognition shall be given to me and to the University of Saskatchewan in any scholarly use which may be made of any material in this thesis. Requests for permission to copy or to make other use of material in this thesis, in whole or in part, should be addressed to:

Head of the Department of Mechanical Engineering

University of Saskatchewan

Engineering Building

57 Campus Drive

Saskatoon, Saskatchewan, S7N 5A9

Canada

Abstract

Heavy load equipment, such as tractors, shovels, cranes, airplanes, etc, often employ fluid power (i.e. hydraulic) systems to control their loads by way of valve adjustment in a pump-valve control configuration. Most of these systems have low energy efficiency as a consequence of pressure losses across throttle valves. Much of the energy is converted into heat energy which can have determinantal effects on component life and the surrounding environment.

From an energy efficiency point of view, an ideal hydraulic system is one that does not include any throttling valve. One such circuit is made of a variable pump and motor load (pump/motor configuration). The velocity of the load is controlled by manipulating the pump displacement or by changing the rotary speed of the pump shaft. In such a system, the transient response of the load is often unsatisfactory because it is difficult to quickly and accurately manipulate the pump displacement or change shaft speed. Thus circuit design must be a compromise between the energy efficiency of the pump/motor system and the controllability of a pump/valve/motor combination.

One possible compromise is to use a pump-valve configuration which reduces energy losses across the valve. One way to achieve this is by controlling the pressure drop across the valve and limiting it to a small value, independent of load pressure. Based on this idea, a type of hydraulic control system, usually called load-sensing (LS), has recently been used in the flow power area. This type of system, however, is complex and under certain operating conditions exhibits instability problems. Methods for compensating these instabilities are usually based on a trial-and-error approach.

Although some research has resulted in the definition of some instability criterion, a comprehensive and verifiable approach is still lacking.

This research concentrates on identifying the relationship between system parameters and instability in one particular type of LS system. Due to the high degree of non-linearity in LS systems, the instabilities are dependent on the steady state operating point. The study therefore concentrates first on identifying all of the steady state operating points and then classifying them into three steady state operating regions. A dynamic model for each operating region is developed to predict the presence of instabilities. Each model is then validated experimentally. This procedure, used in the study of the LS system, is also applied to a pressure compensated (PC) valve. A PC valve is one in which the flow rate is independent in variations to load pressure.

A system which combines a LS pump and a PC valve (for the controlling orifice) is called a load sensing pressure compensated (LSPC) system. This research, then, examines the dynamic performance of the LSPC system using the operating points and steady state operating regions identified in the first part of the research.

The original contributions of this research include: (a) establishment of three steady state operating conditions defined as “Condition I, II & III”, which are based on the solution of steady state non-linear equations; (b) the provision of an empirical model of the orifice discharge coefficient suitable for laminar and turbulent flow, and the transition region between them; (c) and the development of an analytical expression for orifice flow which makes it possible to accurately model and simulate a hydraulic system with pilot stage valve or pump/motor compensator. These contributions result in a practical and reliable method to determine the stability of a LS or LSPC system at any operating point and to optimize the design of the LS or LSPC system.

Acknowledgements

The author would like to express his gratitude to Drs. Richard Burton and Greg Schoenau for their invaluable guidance, advice and encouragement throughout the research of the project. Additionally, a particular gratitude is also owed to Engineer, Doug Bitner, for his substantial assistance in the experiments.

The author acknowledges the financial assistance in the firm of a scholarship from the University of Saskatchewan and support from NSERC research grants.

Finally, a great debt of gratitude is owed to my family, for their support and love, particularly my wife, Wenjun Guo, for taking care of my daughter, Jasmine, and my son, Daniel.

Table of Contents

Content of Figures

Content of Tables

Abbreviation

LS	The Load sensing hydraulic system
PC	The Pressure Compensated flow control valve
LSPC	The Load Sensing Pressure Compensated hydraulic system
SSOP	The Steady State Operating Points of the LS or LSPC system
TF	The Transfer Function of a dynamic system

Nomenclature

Δ	Differential of variables	
"$_0$"	Subscript which represents the operating point of a variable	
$\boldsymbol{A}$	State matrix	
A_p	Cross-sectional area of pump pistons	[m^2]
A_{pc}	Flow cross-sectional area of the hydrostat orifice	[m^2]
A_{pcs}	Cross-sectional area of the hydrostat spool	[m^2]
A_y	Cross-sectional area of the control piston of the pump	[m^2]
A_r	Cross-sectional area of the LS spool in the LS regulator	[m^2]
A_s	Flow cross-sectional area for the charge orifice	[m^2]
A_T	Flow cross-sectional area for the discharge orifice	[m^2]
a_1, a_0	Coefficients of s polynomial associated with the TF denominator	
$\boldsymbol{B}$	Input-state matrix	
B_m	Damping coefficient of the motor	[Nms]
B_{pc}	Damping coefficient of the hydrostat spool in the PC valve	[$Nm^{-1}s$]
B_{pc}^*	Overall damping coefficient of the hydrostat spool which has considered the effect of the hydraulic damping on the damping hole	[$Nm^{-1}s$]
B_r	Damping coefficient of the LS spool	[$Nm^{-1}s$]
B_y	Effective damping coefficient of control piston of LS pump	[$Nm^{-1}s$]
B_{sp}	Simplified constant (damp coefficient) of the control piston and swash plate assembly	[Nms]
$b_{xv1,}$ b_{xv0}	Coefficients of s polynomial in the numerator of flow gain TF of the PC system	[s^{-1}],[s^{-2}]
$B_{psL1,}$ b_{psL0}	Coefficients of s polynomial in the numerator of flow pressure coefficient TF of the PC system	[s^{-1}],[s^{-2}]
b_1, b_0	Coefficients of s polynomial associated with the TF numerator	
$\boldsymbol{C}$	State output matrix	
C_c	Flow contraction coefficient on orifices	
C_d	Discharge coefficient for orifices	

C_{dc}	Discharge coefficient of the adjustable orifice in the PC valve	
C_{dv}	Discharge coefficient of the hydrostat orifice in the PC valve	
$C_{d\infty}$	The discharge coefficient of orifices when the flow becomes fully turbulent	
C_p	Dynamic gain of the LS pump	$[m^3s^{-1}rad^{-1}]$
C_{pss}	Steady state gain of the LS pump	$[m^3s^{-1}rad^{-1}]$
C_v	Flow velocity coefficient (approximately 0.98)	
c_{ml}	Leakage coefficient of the motor	$[m^3s^{-1}Pa^{-1}]$
c_{pl}	Leakage coefficient of the pump	$[m^3s^{-1}Pa^{-1}]$
$\boldsymbol{D}$	Input output matrix	
D_{damp}	Diameter of the damping hole	[m]
D_h	Hydraulic diameter of orifices	[m]
D_m	Volumetric displacement of the motor	$[m^3]$
D_p	Volumetric displacement of the pump	$[m^3]$
D_{pc}	Diameter of circular type hydrostat orifice	[m]
D_{pcs}	Spool diameter	[m]
D_{pmax}	The maximum volumetric displacement of the pump	$[m^3]$
e	Overall random error of the measurement system	
e_c	A/D converting error	
e_s	Sensors' random error	
F_{ff}	Steady state flow force exerted on a spool	
F_L	Load resistant force	[N]
F_{pc}	Pre-compression of the spool spring at the initial displacement for the PC system	[N]
F_{pr}	Initial pre-compression in the balance spring of LS spool	[N]
F_{sp}	Spring force	[N]
F_{ext}	External force	[N]
G	Transfer function	
G_p	Pump transfer function	
$G_{pinloop}$	TF of the inner closed loop of the LS pump	$[rad \cdot m^2N^{-1}]$
G_{psL}	Flow-pressure coefficient transfer function	$[m^5s^{-1}N^{-1}]$

G_{xv}	Flow gain transfer function	$[m^2s^{-1}]$
H_L	Transfer function of the load: $P_L(s)/Q_L(s)$	
H_p	Overall pressure feedback gain of the load sensing pump	
J_{sp}	Average total moment of inertia of swash plate, yoke and piston assembly	$[Nms^2]$
K	Linearization coefficient, gain of the A/D converter	
K_1, K_2	Linearization coefficient with respect to the 1st and 2nd independent variables	
K_c	Flow-pressure coefficient	$[m^5s^{-1}N^{-1}]$
K_{cpc}	Flow-pressure coefficient of hydrostat orifice of PC valves	$[m^5s^{-1}N^{-1}]$
K_{cr1}	Flow-pressure coefficient for the "charge" orifice of the LS regulator	$[m^5s^{-1}N^{-1}]$
K_{cr2}	Flow-pressure coefficient for the "discharge" orifice of the LS regulator	$[m^5s^{-1}N^{-1}]$
K_{cv}	Flow-pressure coefficient of the fixed orifice of PC valves	$[m^5s^{-1}N^{-1}]$
K_{dxy}	Linearization coefficient with respect to the yoke speed	$[Nm^{-3}]$
K_p	Linearization coefficient with respect to the pressure	$[s^{-1}]$
K_{pr2}	Pressure torque constant	$[m^3]$
K'_{pr2}	Pressure torque constant	
K_{pr3}	Pressure torque constant	$[m^3rad^{-1}]$
K'_{pr3}	Pressure torque constant	$[rad^{-1}]$
K_{ps}	Linearization coefficient with respect to the pump pressure	$[s^{-1}]$
K_{psL}, K_c^*	Flow-pressure coefficient of the PC system at high frequency region or with fully opened hydrostat orifice	$[m^5s^{-1}N^{-1}]$
K_{psL}^*	Flow-pressure coefficient of the PC system at steady state	$[m^5s^{-1}N^{-1}]$
K_{py}	Linearization coefficient with respect to the control pressure	$[s^{-1}]$
K_q	Flow gain of orifices	$[m^2s^{-1}]$
K_{qpc}	Flow gain of hydrostat orifice of PC valves	$[m^2s^{-1}]$
K_{qr1}	Flow gain for the "charge" orifice	$[m^2s^{-1}]$
K_{qr2}	Flow gain for the "discharge" orifice	$[m^2s^{-1}]$

K_{qv}	Flow gain of fixed orifice of PC valves	[m^2s^{-1}]
K_{sp}	Angular effective spring coefficient	[$Nm \cdot rad^{-1}$]
K'_{sp}	Angular effective spring coefficient	[$Nm^{-2}rad^{-1}$]
K_x	Linearization coefficient with respect to a displacement	[$Nm^{-3}s^{-1}$]
K_{xr}	Linearization coefficient with respect to the displacement of the LS spool	[$Nm^{-3}s^{-1}$]
K_{xv}	Flow gain of the PC system at high frequency region or with fully opened hydrostat orifice.	[m^2s^{-1}]
K_q^*		
K_{pc}^*	Flow gain of the PC system at steady state	[m^2s^{-1}]
K_{xy}	Linearization coefficient with respect to the yoke displacement	[$Nm^{-3}s^{-1}$]
k_{ff}	Coefficient related to steady state flow force ($k_{ff} = 2C_dC_v\cos 69°$)	
k_{pc}	Spring coefficient of the hydrostat spool spring	[Nm^{-1}]
k_{pc}^*	Overall Spring coefficient of the hydrostat spool spring which has considered the effect of the steady state flow force	[Nm^{-1}]
k_r	Spring coefficient of balance spring of the LS spool	[Nm^{-1}]
k_y	Spring coefficient of pre-compression spring against swash plate	[Nm^{-1}]
L	The axial length between hydrostat orifice and the center of conduit	[m]
L_{damp}	Length of the damping hole	[m]
M_{pc}	Mass of the hydrostat spool in the PC valve	[kg]
m, n	Power of factors in the empirical modification coefficient of the Reynolds number	
m_r	Mass of the LS spool	[kg]
N	The number of the pump pistons	
N_{pc}	The number of the hydrostat orifices in the perimeter of the spool	
N_{xv}	The index number of turns on the needle valve	
P_1	The minimum pump pressure at operating condition II	[Pa]
P_2	The maximum pump pressure at operating condition II	[Pa]

P_d	Pressure differential setting across a simple orifice in the LS system or across a PC valve in the LSPC system	[Pa]
P_L	Load pressure	[Pa]
P_{L1}	Load pressure with the highest load	[Pa]
P_{L2}	Load pressure of the second load	[Pa]
ΔP_{L1}	Pressure drop across the orifice controlling the highest load	[Pa]
ΔP_{L2}	Pressure drop across the orifice controlling the second load	[Pa]
P_{Ls}	Load pressure at the end of LS line	[Pa]
P_m	Intermediate pressure between the fixed orifice and hydrostat orifice in the PC system.	[Pa]
P_{mb}	Downstream pressure of the motor	[Pa]
P_{pc}	Pressure setting associated with the pressure drop across fixed orifice in the PC system	[Pa]
P_T	Fluid pressure in the tank	[Pa]
P_s	Pump pressure	[Pa]
P_{sh}	Pressure of the end of the hydrostat spool at which the pressure is larger than the pressure in the other side	[Pa]
P_{sL}	Pressure drop across the PC system	[Pa]
P_y	Control piston pressure of the pressure control pump	[Pa]
Q	Flow rate	[m^3s^{-1}]
Q_L	Load flow rate	[m^3s^{-1}]
Q_{L1}	Load flow rate with the highest load	[m^3s^{-1}]
Q_{L2}	Load flow rate of the second load	[m^3s^{-1}]
Q_{Lpc}	Flow rate through the hydrostat orifice of the PC system	[m^3s^{-1}]
Q_{Lv}	Flow rate through the fixed orifice of the PC system	[m^3s^{-1}]
Q_{ml}	Leakage flow rate of the motor	[m^3s^{-1}]
Q_{pl}	Leakage flow rate of the pump	[m^3s^{-1}]
Q_{pmax}	The maximum flow suction from tank	[m^3s^{-1}]
Q_{r1}	Flow rate through the “charge” orifice	[m^3s^{-1}]
Q_{r2}	Flow rate through the “discharge” orifice	[m^3s^{-1}]
Q_s	Pump flow delivering	[m^3s^{-1}]

Q_y	Flow rate into control piston	[m^3s^{-1}]
Re	Reynolds number on an orifice	
Re_c	Reynolds number on hydrostat orifice in a PC system	
Re_v	Reynolds number on adjustable orifice in a PC system	
R_p	Moment arm of the pump piston	[m]
R_r	The radius of round orifices for the control piston	[m]
R_{pc}	The radius of the crescent orifice of the hydrostat in the PC valve	[m]
R_{py}	Moment arm of the control piston about pump shaft	[m]
R_{sh}	Hydraulic damping of the damping hole at the center of the end surface of the hydrostat spool	[sNm^{-5}]
T	Temperature	[°C]
T_{mf}	Resistant torque of the motor load	[Nm]
T_{sp}	Angular effective spring pretension	[Nm]
T'_{sp}	Angular effective spring pretension	[Nm^{-2}]
t	time	[s]
U	Input variable vector	
u	input	
V	Volume of a chamber	[m^3]
V_m	Volume in the chamber between the flow valve (a simple orifice or a PC valve) and the motor	[m^3]
V_p	Volume of the pump chamber	[m^3]
V_{pcm}	Volume in the chamber between the fixed orifice and the hydrostat orifice of the PC system	[m^3]
V_{sh}	Volume of the chamber at the end of the hydrostat spool with high chamber pressure	[m^3]
V_{sh0}	Volume of the chamber at the end of the hydrostat spool with high chamber pressure at condition which the hydrostat orifice is just closed	[m^3]
V_y	Volume of the control piston chamber of pump	[m^3]
V_{ymin}	Minimum volume of the control piston chamber of pump	[m^3]

w	Width of the rectangular orifice	[m]
w_r	Width of the rectangular orifice for the control piston	[m]
w_{pc}	Width of the Equivalent rectangular type of the hydrostat orifice of the PC system	[m]
w_v	Width of the fixed orifice of the PC system	[m]
X	State variable vector	
x	Independent variable, opening of the orifice	[m]
x_{pc}	Displacement of the hydrostat spool and also opening of hydrostat orifice	[m]
x_{pci}	The initial displacement of the hydrostat spool	[m]
x_{pcmax}	The maximum displacement of the hydrostat spool	[m]
x_r	The initial displacement of the LS spool of LS regulator	[m]
x_{ri}	The initial displacement of LS spool	
x_{rmax}	The largest width of the regulator orifice	[m]
x_{spring_def}	The deformation of the hydrostat spring at $x_{pc} = 0$	[m]
x_v	Opening of adjustable or fixed orifice	[m]
x_{vmax}	The maximum opening of adjustable orifice	[m]
x_y	Displacement of the control piston	[m]
x_{ymax}	The maximum displacement of the control piston	[m]
Y	Output variable vector	
y	Dependent variable	
z	The 2nd independent variable of a multi-variable function	
β	Bulk module of the fluid	[Nm^{-2}]
δ	Laminar flow coefficient of orifices	
δP_{pcc}	The minimum value of the pressure drop across a PC system	[Nm^{-2}]
ε	Modification coefficient of discharge coefficient, or Reynolds number	
ϕ	Rotary speed of the motor	[s^{-1}]
η	Ratio of discharge coefficients of adjustable orifice and hydrostat orifice, C_{dv}/C_{dc} in the PC valve	

λ_{pc}	Factor associated with the areas of the adjustable orifice and hydrostat orifice	
λ_2	Factor associated with the areas of the adjustable orifice and hydrostat orifice	
μ	Absolute viscosity of fluid	[Nsm^{-2}]
ρ	Flow density	[kgm^{-3}]
θ	Motor's angle, flow jet angle of spool orifice (approximately 0.69)	[rad]
θ_{sp}	Swash plate angle of the pump	[rad]
θ_{spmax}	Maximum of swash plate angle of the pump	[rad]
υ	Kinematical viscosity of fluid	[m^2s^{-1}]
ω	Rotary speed on pump shaft	[$rad \cdot s^{-1}$]
ω_L	Undamped natural frequency of the motor load	[s^{-1}]
ω_{Ls}	Damping break frequency of the LS line	[s^{-1}]
ω_{Lsp}	Non-dominant undamped natural frequency of the LS pump	[s^{-1}]
ω_r	Undamped natural frequency of the LS spool	[s^{-1}]
ω_{sp}	Undamped natural frequency of the swash plate	[s^{-1}]
ω_y	Break frequency of the control chamber	[s^{-1}]
ω_{ysp}	Equivalent break frequency	[s^{-1}]
ζ	Damping ratio	

Chapter 1 Introduction

1.1 Project Background

The motion of many manipulators in engineering (steering control of vehicles, the arm control of crane equipment and robots, control of moving parts of off-road equipment and airplanes, etc) is often fulfilled using flow control in hydraulic systems. Essentially, there are two ways in which flow control can be accomplished: using a variable displacement pump and using an orifice opening via a proportional valve (pump-valve system). In the first instance, a variable displacement pump can be used to change the flow rate without the use of a controlling orifice (valve). This is accomplished by varying the swash-plate angle of the pump or the input speed from the electric motor. This type of flow control is very efficient because energy losses across a controlling orifice are avoided. However, controlling the swash-plate can be quite complex and in some instances, can introduce additional sources of inefficiencies.

An alternate configuration is one of a pump and controlling orifice (via a valve downstream from the pump). This configuration results in a pressure drop across the controlling orifice which translates to an inherent energy loss. This pressure drop, however, can be used as a controlling signal within the valve or can be fed back to a control valve at the pump to improve transient responses and reduce energy losses.

Flow control systems with a pump-valve configuration are often found in applications involving multi-loads. Systems of this type must meet two conditions: (1) the pump must provide enough flow to the control valves to sustain a constant pump supply pressure, and (2) the control valves should be of proportional type. If energy consumption is to be minimized then the pump should be of the demand flow type in

which the valve flow requirements match the flow delivered by the pump. To accomplish this, some sort of "load sensing" function is required.

In the past decade, load-sensing systems (here-after denoted as LS systems) have found increasing usage in fluid power applications, especially in automobiles and off-road equipment [Book and Goering, 1997]. One of the many advantages associated with these systems is the high energy-saving potential; that is, the pump attempts to match the power requirements to the changing load power requirements with minimal control losses. However, stability problems and undesirable interactions amongst loads have been reported [Lantto, et al, 1990 and Lantto, et al, 1991].

A load sensing pump is one in which a pressure (or pressure differential) is fed back to a controller within a pump to adjust the swash-plate angle and subsequently, the pump's flow (see Figure 1.1). The LS pump system consists of a variable displacement pump (A in Figure 1.1), the actuating yoke and control piston (B) of the swash-plate, and the critically lapped adjusting valve (C). When the physical load (D) experiences an incremental increase, then a corresponding incremental increase in pressure P_L is sensed in the feedback sensing line (E); the pressure change acts on the spool of the compensator piston (G). A force unbalance on the spool translates the spool to the right porting fluid in the swash-plate piston (B) to the tank. A decrease in the fluid pressure at this point increases the swash-plate angle, which in turn increases the flow rate from the pump. This increase in flow encounters the controlling orifice (higher resistance) (F) and as a result, the pressure increases. This pressure is sensed in the pump feedback line (H), which acts on the right hand side of the compensator piston (G). The pressure rises until a force balance across the compensator is re-established. At this point, the pressure drop across the controlling orifice (F) is re-established and the flow restored to its

original value. Flow control is thus established. This type of pump is called a "load sensing" pump. A system that consists of a load sensing pump, a simple proportional valve and its load(s) is commonly called as load sensing (LS) system.

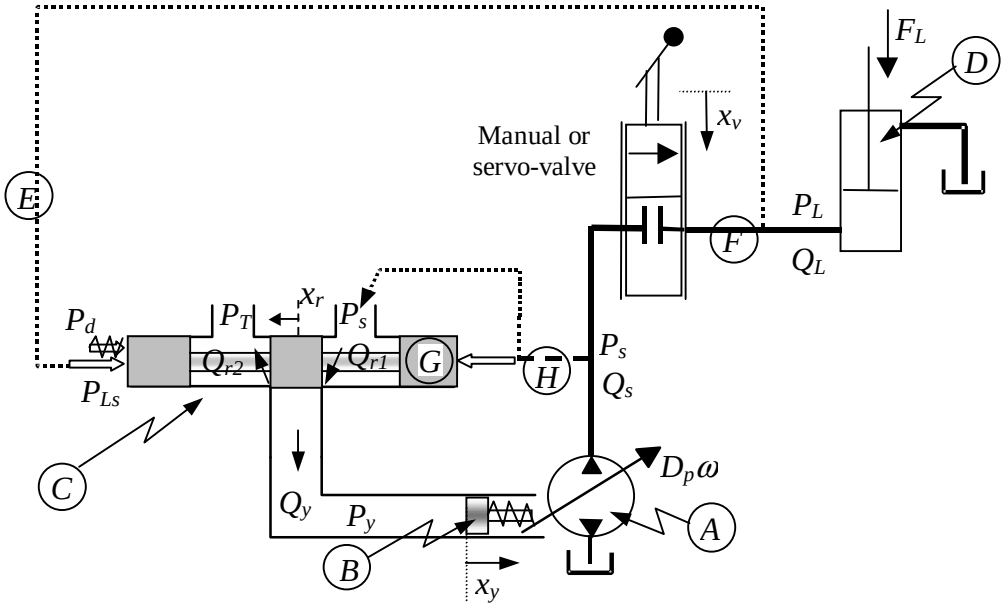

Figure 1.1 Schematic of Load Sensing (LS) System

The prime advantage of the LS system is that the supply pressure P_s is controlled to be marginally higher than the down stream pressure P_L (typically, 1MPa). Thus, the energy loss across the valve is minimized compared to valve-based systems. Only a variable displacement pump-motor combination is more energy efficient.

In LS systems, the system response is affected by dynamic changes in the load conditions. This can be illustrated in Figure 1.2. With reference to this figure, consider the following scenario. In (a), the steady state loading conditions are shown. In (b), a sudden increase in P_L occurs. As a result the flow through the valve decreases momentarily as seen in (c). P_s also increases but at a smaller rate than P_L (d) because of the capacitance in the lines between the pump and valve. But the pressure difference across the load sensing compensator forces the spool to respond such that the pump

starts to increase its stroke; therefore, the pump flow Q_s increases as illustrated in (d). Q_L also starts to increase because of the small increase in P_s from step (d). As a result of the increase in pump flow, P_s will now increase rapidly as illustrated in (e). Q_L increases because the pressure drop across the valve increases, but also the pump flow starts to decrease due to the reestablishment of the pressure balance across the pump compensator. This continues until the pressure drop across the control valve is reestablished (f).

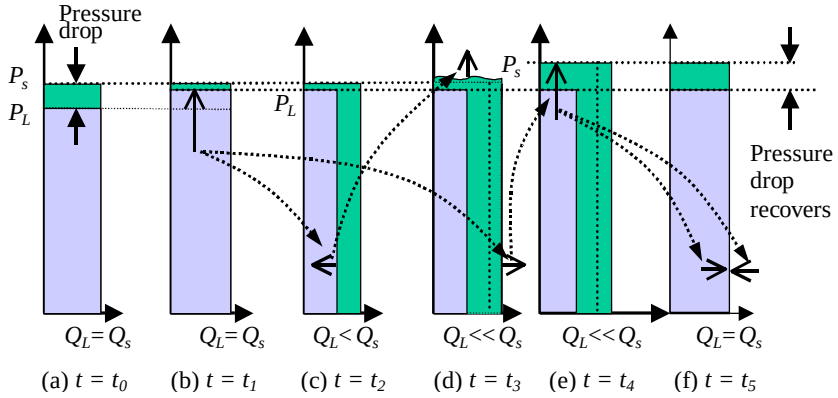

Figure 1.2 Time Sequenced Pressure and Flow of a LS System during Transition

The response of Q_L and Q_s are shown in Figure 1.3, which reflects the above sequences. It is clear that both Q_L and Q_s are load dependent during the dynamic change in P_L. Since the object is to make Q_L independent of the load, statically and dynamically, the LS system is in error. This translates into a perturbation in the speed of a rotary or linear load. In some cases, if the operating point is close to critical values in term of stability, this perturbation can drive the system to an unstable situation.

A second problem arises when this kind of system is connected to two loads as shown in Figure 1.4 [Ramachandran and Ukrainetz, 1985; Ukrainetz, et al, 1986, and Lantto, et al, 1991]. Consider the following sequences as illustrated in Figure 1.5 and

with reference to Figure 1.4. In (a), the steady state load pressure for load #1 is P_{L1} and for load #2, P_{L2}. Because of the design of the circuit, the pump compensator responds to the highest load pressure (P_{L1}) via the shuttle valve (see Figure 1.4). It is assumed that flows to the loads are Q_{L1} and Q_{L2} as shown in (a). The pump delivers the sum of these two flows Q_s. Consider an increase in the load pressure P_{L1} as shown in (b). Q_{L1} starts to decrease (c). But, because of the pump compensator, the pump is directed to increase flow Q_s as shown in (d). As a result, *Ps* increases (e) and Q_{L1} starts to increase (e). But because P_s increases, the pressure drop across the other flow control valve increases also shown in (e). This results in an increase in the flow, Q_{L2}, through the other valve (f); thus, the load speed will increase accordingly. Thus changes in the loading conditions in the higher load will affect the flow to the second system. The response of both loads in terms of flow to the pressure increase is shown in Figure 1.6. It is clear that the first system flow Q_{L1} can recover but the second system cannot. Thus, the aforementioned problems do require some consideration when it comes to implementation.

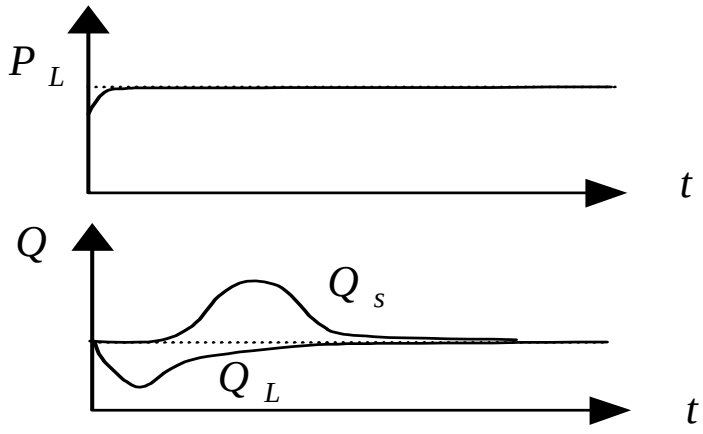

Figure 1.3 Transient of a LS System Perturbed by its Load

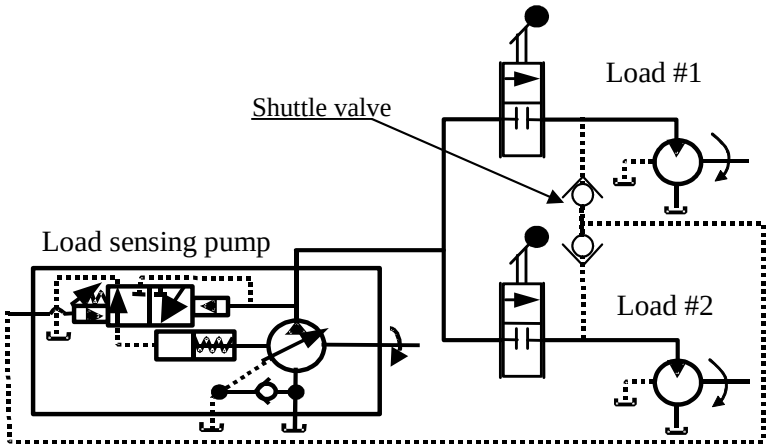

Figure 1.4 Schematic of a LS System with Multiple Loads

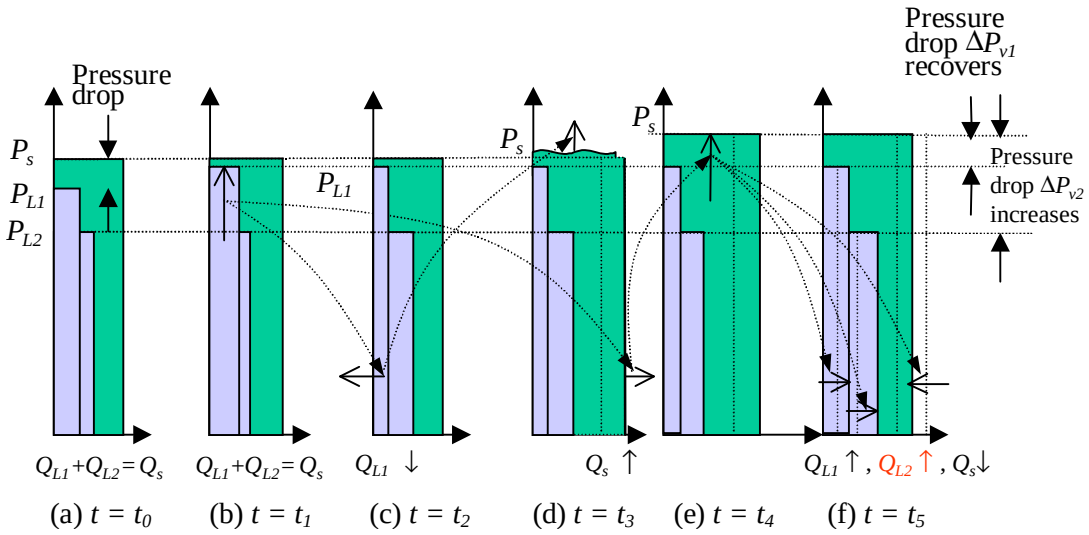

Figure 1.5 Time Sequenced Pressures and Flows of a Multi-Load LS System during Transition

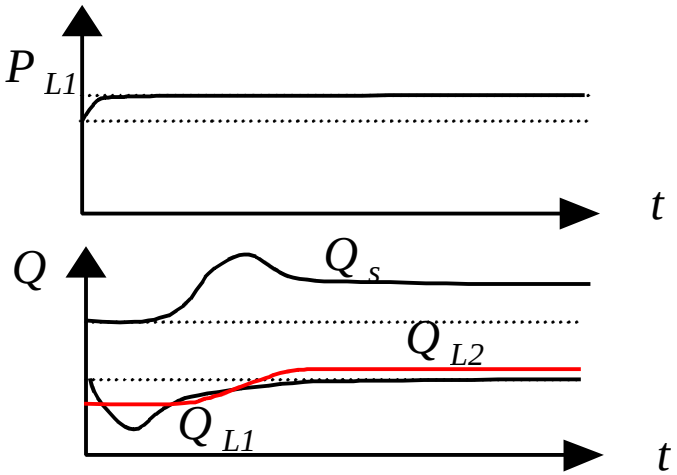

Figure 1.6 Transition of a Multi-Load LS System Perturbed by its Highest Load

A second type of flow control structure consists of a pump, compensator valve (more commonly known as a hydrostat), and a fixed orifice (Figure 1.7). The system consists of valves (or valve combination) in which the pressure(s) is piloted to a pressure compensator valve (A) in Figure 1.7, (located downstream from a fixed or adjustable orifice (E)). This compensator valve modulates its opening in order to maintain a fixed pressure drop (P_s - P_m) across the fixed or variable orifice (E).

Consider the situation in which the load (D) experiences a change during operation; subsequently, the pressure, P_L, would also change. This causes an instantaneous decrease in the pressure drop, $P_m - P_L$, which results in a decrease in the flow rate, Q_L, to the load. The "unperturbed" flow through the fixed orifice (E) encounters a resistance at (B). Because of the very small chamber volume between the fixed and compensator orifice, the intermediate pressure, P_m, would suddenly increase. The pressure increase is sensed in the feedback sensing line (C) and is exerted on the spool of the compensator valve (A). The orifice created by the compensator spool is modulated by the force unbalance across the spool (created by P_s, P_m and a bias spring, P_{pc}). An increase in P_m increases the compensator spool orifice opening, x_{pc}, which results in an increase in the flow, Q_L, through the compensator. The increase in the flow rate via the compensator (A), in turn, results in a decrease in P_m. The aforementioned processes continue until a new force balance is re-established across the compensator spool (A). The original pressure drop across the fixed orifice is restored and flow control is accomplished. Thus for a specific orifice setting, the flow is independent of the variation in P_L (and similarly, P_m).

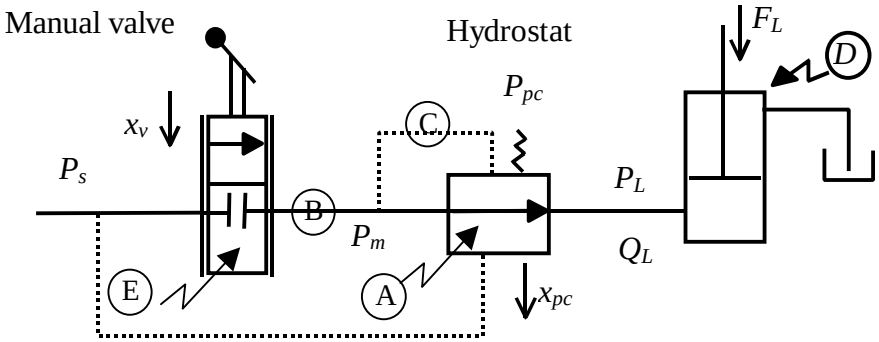

Figure 1.7 Schematic of Pressure Compensated (PC) System

For the LS system previously discussed, a problem associated with changes in the load was identified. This same situation exists for this kind of PC system. However, because the mass of the spools of the compensator is small compared to the mass of the pump swash plate, the response of the valve is very fast compared to the pump and rapid flow recovery is possible. When used in circuits with multiple loads, the second problem discussed previously does not exist because each load is isolated by a separate PC valve and hence P_s is approximately constant. For all PC systems, the supply from the pump is established by the pressure compensator on the pump or from the relief valve setting. This means that a substantial pressure drop exists across all (PC) flow control valves. This can result in substantial energy losses in the system. This loss is highly dependent upon the load pressure and the supply pressure set at the pump.

Although both LS and PC systems are based on pressure (or pressure differential) feedback control, there are some differences in their operation. The key components of PC systems are hydrostats, which are automatically adjusted in order to maintain a constant flow independent of the load. The main components of LS systems usually are variable displacement pumps, which are demand flow systems; that is, they only deliver what is required independent of the loading condition.

The above discussion has shown that the dynamic behavior of the LS system is affected by variations in the load pressure. The PC systems also show this dependency but because of their response, it is minimal (good controllability). But PC systems, being valve based, are not energy efficient compared to the LS systems. Thus it is desirable to be able to combine the advantages of the PC system with those of the LS system. This gives rise to a new configuration called a LSPC system. Such as system is shown in Figure 1.8.

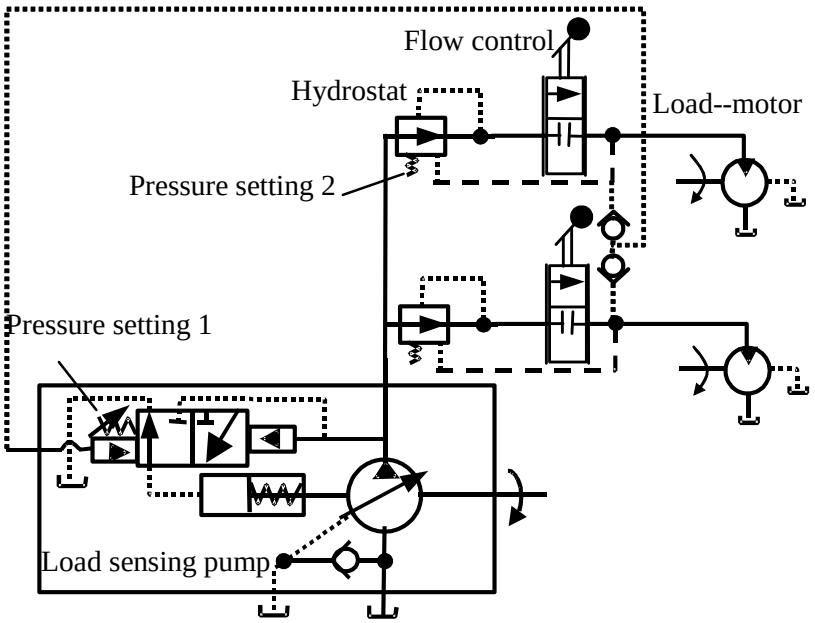

Figure 1.8 Circuit Diagram of a Simple LSPC System

The LS system acts to reduce the supply pressure P_s to the PC flow control valve reducing pressure losses across the valve. The PC flow control valves act to respond quickly to changes in the loads and to act as isolation valves for multiple loads. However, the resulting system is now much more complex and can give rise to controllability/stability problems.

1.2 Previous Research

Research into the controllability and stability problem of LS and LSPC systems can be traced back to the early 80's. Bitner and Burton [1984(1)] addressed the measurement technique of load sensing pump parameters for a LS system. It was found that special experimental measurements of pump parameters were essential for simulation and research into LS systems. This research indicated that two factors; fluid temperature and the operating point, greatly affected the flow gain and flow-pressure coefficient of the orifice, the leakage of the pump, and the frequency response. In 1984, Bitner developed a small signal model of a load-sensing pump. He developed a simplified model based on TF analysis which required linearization of non-linear equations. The correlation between experimental and theoretical results was poor. It was established that part of the problem was due to the choice of the operating point for the frequency responses.

Research by Palmberg, et al, [1985] provided a model of a particular pressure-control pump which is used in most LS or LSPC systems. The dynamic performance of the pressure-control pump was mainly influenced by the pump inductance L_p, but also by the break frequency and the leakage coefficient of the pump. The non-linearity associated with the hysteresis of the spool of the pilot valve was linked to system limit cycle oscillations.

Research by Ramachandran and Ukrainetz [1985] indicated that multiple loads could interact with LS systems. Pressure reducing valves included in the system in a meter-in configuration were found to improve the performance of multi-load systems. For the load with the highest inertia, the pressure-reducing valve decreased the load damping while increasing the damping of the system with a smaller inertial load. These

observations agreed with some of the findings reported by Ukrainetz, et al, [1985], Mai and Dransfield [1983], and Mai [1982].

Kim, et al, [1987(1) and 1987(2)] investigated the parameter sensitivity of a variable displacement axial piston pump. The results indicated that high-sensitivity parameters were the flow gain of the pressure compensator, the volumetric displacement of the yoke control cylinder, etc. The yoke inertia, the viscous friction coefficient, etc. are insensitive to the dynamics of the pressure pump. This helped reducing the model order of the pressure-compensated pump from the sixth to the second order system.

Zarotti and Nervegna [1988] addressed the "non-standard" operation of load sensing systems. Three-D plots of output flow, *Q*, of a LS system with a single load as a function of load pressure, *P*, and metering orifice area, *A*, showed the operation range which would be expected and which would be favored. In order to reduce saturation effects, a PC system with hydrostat downstream of the fixed orifice was shown to be able to handle saturation automatically at different degrees of effectiveness when compared to a PC system with hydrostat upstream to the fixed orifice.

Lin and Akers [1988] presented a detailed mathematical model of an axial piston pump controlled by a two-stage servo valve. The 8^{th} order state space model indicated that the open-loop system was unstable. In the model, the input was the current in the coil of flapper valve and the output was the pump pressure in the pump chamber. A closed loop optimal control was developed which proved to be stable. A comparison of models indicated that the performance of an axial piston pump controlled by a single-stage valve was superior to that controlled by a two-stage valve, since the single-stage valve demonstrated a faster frequency response. This research was relevant in the implementation of a LS system with an electrical-hydraulic load sensing structure.

Kim, et al, [1988] presented a stability analysis in the frequency domain which included linearizing models and then applying Routh-Hurwitz criterion. This model did not consider the damping of the load sensing line and the LS pump was simply considered as a standard 2nd order system. Based on their research, they concluded that

- Increasing the throttle opening of the flow orifice, x_v, and the pressure differential setting, P_d, of pump compensator increased the effect of the positive feedback loop, thus making the load sensing system unstable.
- The load inertia, the line volumes, and the volumetric displacement of the motor were closely related to a resonance phenomenon. When these parameters were chosen close to the resonance region, the system tended to be unstable.

Krus [1988] provided a detailed description and model of a LS system. A general transfer function was presented, which consisted of the transfer functions of three subsystems (the pump and pump regulator, valve systems, and loads). For a simple inertia load, a stability criterion was established. Two main instabilities (pump high-frequency instability at small valve openings and pump-load low-frequency instability at large valve openings) were described qualitatively. In addition, two other instabilities (load low-frequency instability at small valve openings and pump-load high-frequency instability at large valve openings) were also mentioned. His research proposed six possible ways to avoid an instability in an LS system.

- Increase the pressure drop over the flow control orifice (meter-in) which would be at the expense of energy loss.
- Increase the pressure drop over a meter-out orifice if one exists (also at the expense of energy loss).

- Use a PC system. The system could be highly underdamped but would not be unstable.
- Incorporate a pump-regulator with a high gain. This would have to be done with care in order to avoid high frequency instabilities.
- Design a "low pass filter" on the load sensing line hydraulically.
- Dampen the load so that any resonance peaks are removed.

Zhang and Hou [1989] examined a load sensing axial piston pump that used two pump-adjusted valves (one for increasing swash plate angle and the other for decreasing the angle). The use of two valves created separated pressure settings which could be used to find favorable states of the pump.

Mai and Dransfield [1989] found that the response time and quality of LS systems depend significantly on small differences in the cross-sectional areas of the regulator's spools.

Friedrichsen [1989] applied a LS system in the hydrostat steering of mobile vehicle as a LS hydrostatic steering system. The experiments for ramp and step responses were done to investigate the acceleration and speed of the steering wheel at different driving situations in order to obtain optimal values of adjustable parameters.

Lantto, et al, [1990] analyzed static and dynamic performance of LSPC systems with two different types of PC subsystem configurations. Her static analysis showed that, when the pump pressure decreased to a value less than the sum of the pump component setting and the highest load pressure, the load flow in the system with a "conventional" PC configuration (that is, where the hydrostat spool is controlled by the pressure drop across the fixed orifice) would decrease sequentially starting with the highest load. But,

for the system with a “relocated” PC configuration (that is, where the hydrostat spool is manipulated by the pressure drop cross the hydrostat orifice), all load flows would reduce proportionally. Even though the pump flow was saturated, interaction between loads did not occur, as long as the hydrostats would operate.

In another study by Lantto, et al, [1991] and indeed others [Bitner 1986; Kim and Cho 1988], the whole LS system has been observed to enter into limit cycle conditions—an instability problem. Three causes of instabilities were defined. The most common cause was due to the feedback of the pump pressure and the highest load pressure controlling the active pump regulator. The second was a result of “flow feedback” (pump flow minus load flow). A rapid change in the flow control valve orifice area can result in a sudden change in the load flow. If the system is “stiff”, this load flow change can result in a large pressure transient. This condition has been shown to lead to instability, but only under certain conditions (which are seldom met). Hence, this instability rarely occurs. The third cause of instability was attributed to the interaction of loads (for example, several loads controlling the same mechanical structure i.e. a crane arm). This instability was found to be highly dependent on the geometry of the mechanical structure; therefore, a proper design of the structure would eliminate this problem. The method of eliminating the problem in hydraulic systems was to use pressure compensation or by incorporating pressure feedback via a transducer to an electrical controller (using a low pass filter to stabilize the response).

Kim and Cho [1991] presented a design method using simulation techniques to simultaneously determine the optimal controller gains of a servo- flow control valve and the optimal setting pressure of the LS pump. The investigation indicated that the setting

pressure should be determined at the controller design stage, since it greatly affects both control performance and energy efficiency of LS systems.

Backe [1993] described a LS system with electrical-hydraulic LS mode for improving the dynamic behavior of a LS system. In this system, the LS regulator was an electro-hydraulic valve. There were two factors to motivate this research. On the one hand, the signals could be transmitted faster electronically. On the other hand, more complex controllers could be configured than it is possible by hydro-mechanical means.

Pizon and Sikora [1993] simulated four types of hydraulic circuits: constant source pressure and a simple orifice; constant flow source and a simple orifice; constant flow source and a PC valve with exit port; and a LS system. This study indicated that the energy-saving feature of the LS system was very apparent in the transient state.

Zarotti and Paoluzzi [1993] compared the steady state and dynamic behavior of a LS system for different types of LS controllers of a pressure control pump. These LS controllers included two 3-way valves which acted as the LS regulator (or flow compensator) and the pressure limiter (or pressure compensator). This study configured the LS regulator and the pressure limiter in the forms of tandem, parallel, two-stage, and other variations. The experimental results indicated that the tandem and parallel form were better than others.

Zheng and Guan [1993] investigated a digital control pressure pump. The spool of the pressure compensator or the LS regulator was actuated by a stepper motor. The experiments proved the feasibility of this electro-hydraulic control of the pressure pump.

Pettersson, et al, [1996] showed how the dynamic behavior of a PC-valve affects the system where it is incorporated. The flow-pressure coefficient, K_{cpc} of the orifice and natural frequency of the hydrostat have a significant influence on the effective flow-

flow-pressure coefficient, K_c, of PC systems, as well as the static and dynamic properties of the whole system. Pettersson showed that an increase of the flow-pressure coefficient, K_{cpc}, of the hydrostat will decrease the effective K_c of PC systems (destabilizing). An increase of the opening x_v of the flow control valve was shown to increase the effective K_c of PC systems (stabilizing effect).

Maiti, et al, [1996] analyzed the operation of a load sensing flow control valve with a bypass exit (i.e. PC system with bypass port) at five different conditions: (1) the fixed orifice was closed, (2) the fixed orifice was opened but no load flow demanded (when setting the directional valve following the PC valve to the closed center position), (3) the hydrostat spool was not in motion and the bypass orifice was closed (4) the hydrostat spool was controlled and the control behavior of the bypass orifice was activated, and (5) the hydrostat spool was controlled and the control behavior of the fixed orifice was activated. The simulation result would help in better understanding the functions, design and selection of such a valve. This research also indicated that the flow force had not much effect on spool equilibrium.

Andersson and Ayres [1997] compared steady state performances, energy efficiency and damping for different LS directional valves with open-center and closed-center configurations. The research indicated that, by adding load pressure feedback, closed-center load sensing valves could have the same favorable damping as open-center valve.

Sakurai and Takahashi [1997; 2000] used a bond-graph model of the LS system to investigate its overall efficiency taking into consideration the dynamic characteristics of the system. It was found that there was a maximum point of overall efficiency. This research displayed a curve of overall efficiency with respect to the steady-state ratio defined as the ratio of the oscillation period and one duty cycle of the cylinder load.

Simulation by Book and Goering [1997] verified that instabilities caused by the inertia load could be eliminated with the addition of damping in the feedback line. This was accomplished in the simulation by adding a transportation delay in the simulation model. No experimental work was done in this study.

Erkkila [1999] provided a block diagram of a LS system which could assist in the understanding of the dynamic analysis of LS systems. An analogue-mechanical model and an analogue-electrical model for a LS system were also provided.

Li [1999] described a generalized procedure for experimentally investigating LSPC systems with multi-loads based on state space models. No experimental results were provided.

Luomaranta [1999] implemented one type of an electrohydraulic LS system on a log loader application. The LS mode was accomplished using pressure transducers, electrical filters and electronically controlled pressure pump (Note: the control pressure was provided by a pressure divider which consisted of a restriction orifice and an electronically controlled relief valve.). Comparison of experimental results in the laboratory indicated that the electrohydraulic LS system was a competitive alternative.

Zhang, et al, [1999] compared three different power-matching energy-saving hydraulic systems: the hydro-mechanical LS system, the electric-hydraulic LS system with the programmable logic control (PLC) and the electrical LS system with a stepper motor controlled pump. The last two had the best efficiency but the first one was superior in term of the cost, maintenance and reliability.

Kappl [2001] used experimental methods to obtain a semi-empirical model for the variable displacement pump with load sensing regulator and power restrictor. The pump and LS line were both modeled as first order systems. Kappl's model was found to be

too simple, but was helpful in understanding the identification of the damping coefficient in a LS line.

One of the common objectives of many of the aforementioned research projects was to fully understand the relationship between hydraulic circuit parameters (components' structure parameters and setting parameters) and the expected operating state of the LS or LSPC systems and to then design a LSPC system with demonstrated controllability and energy saving. As an example, it is essential that an LSPC system must be stable for the expected range of opening, x_v, of the flow control valve. However, the complexity of LS or LSPC systems makes relationships between the type of hydraulic components and their design parameters very difficult to find. Two common methods of establishing such relationships are to use linearization and frequency response analysis, and time domain simulation techniques. Frequency response techniques were used by Bitner and Burton [1984], Palmberg, et al, [1985], Lin and Akers [1988], Krus [1988], Zhang and Hou [1989], Lantto, et al, [1990], Lantto, et al, [1991], and Pettersson, et al, [1996]. The time domain approaches were used by Mai and Dransfield [1989], Kim and Cho [1991], and Book and Goering [1997] and by some of the first group who used the first method as well for comparison or verification.

Users of the linearization approach experienced several problems which affect the universal application of their techniques. The first one was the "operating point" problem. Bitner and Burton [1984] was one of the first groups to encounter this problem in their research. Although they (and others) discovered that the operating point greatly affects the theoretical results, no attempt was made to establish how the operating point changed with changes in operating condition. Most researchers who used the linearization and TF analysis did not deal with this "crucial" problem. The transfer

function of LSPC systems and the stability criterion so developed included the flow-pressure coefficient, K_c, which is strongly affected by the operating point. In reality, the main parameters that were used in the stability analysis (flow gain, K_q, and flow-pressure coefficient, K_c, of valves) were a function of state variables of the system, such as the spool displacement and system pressures. Thus, any stability criterion developed from transfer functions could only be considered meaningful if all linearization parameters (K_c, K_q) had "reasonable" values.

To illustrate this, a value of K_c and K_q could be evaluated about an operating point x_{v0}, P_0 etc. When a stability criterion has been established, it can be said that the LSPC system is stable at this operating point. Thus small perturbation will eventually converge to this operating point. However, if x_v, the spool opening, is changed for the purpose of controlling load speed, the operating point is no longer x_{v0} and P_0. Thus, it is necessary to evaluate another new operating point corresponding to the new parameter x_v, establish new linearization parameters (K_c, K_q) and then repeat the stability analysis. To date, a systematic approach to this problem has not been done.

In order to further demonstrate this, consider the transfer function (Equation (1.1)) and the stability criterion for LSPC system established by Krus [1988], Lantto, et al, [1990, 1991], and Pettersson, et al, [1996].

$$G_0(s) = \frac{\dfrac{1}{L_p K_{cv}}\left(\dfrac{s^2}{\omega_L^2} + 2\dfrac{\delta_L}{\omega_L}s + 1\right)}{s\left(\dfrac{C_s s^3}{K_{cv}\omega_L^2} + \left\{\kappa + 2\dfrac{\delta_L \omega_L C_s}{K_{cv}}\right\}\dfrac{s^2}{\omega_L^2} + \left\{\dfrac{C_s}{K_{cv}} + 2\dfrac{\delta_L}{\omega_L}\kappa\right\}s + 1\right)} \tag{1.1}$$

where the criteria for stable operation were established as:

$$criterion\,1: \qquad \frac{1}{L_p C_s} \prec \frac{1}{\kappa}\omega_L^2 + 2\delta_L \omega_L \frac{K_{cv}}{C_s(1-1/\kappa)} \tag{1.2}$$

$$criterion\,2: \qquad C_s \prec\prec C_L \tag{1.3}$$

$$criterion\,3: \qquad \frac{K_{cv}}{C_s} \prec \frac{\omega_L}{\kappa} \tag{1.4}$$

$$criterion\ 4: \qquad \frac{2\delta_L}{K_{cv} L_p \kappa \omega_L} \succ 1 \tag{1.5}$$

In these equations, $\kappa = 1 + \frac{C_L}{C_S}$, L_p and C_s are the inductance and capacitance of the load-sensing pump respectively. C_L is the capacitance of the load. ω_L and δ_L are the natural frequency and damping ratio of the load respectively. K_{cv} is the equivalent flow-pressure coefficient of the PC subsystem (hydrostat and flow control valve combination).

K_{cv} is closely related to the operating point (such as P_{s0}, P_{L0}, x_{pc0} etc.) of the LSPC system. A LSPC system designed by criterion 1, 2, 3, or 4 for a particular operating point does not mean that it always is stable at other operating points. This is because K_{cv} would be different at different operating points.

In applying the stability criteria, a value of K_{cv} must be defined. In the literature, values of K_{cv} were defined but not justified. Further, the research did not demonstrate that K_{cv} (which is known to be operating point dependent) in fact would be valid at the operating point about which the system actually operated. Therefore, it cannot be concluded that these chosen values were, in fact, valid for their chosen operating condition.

Techniques which would validate the choice of the state dependent parameters (K_c,

K_q etc) as a function of the resulting state parameters, are necessary. In 1997, Scholz and Engelhardt examined a simple hydraulic system (not load sensing). They applied a linearization technique to the nonlinear flow equation and then attempted to calculate the operating point and choice of parameters for steady state condition only (static analysis). This study was limited in its application but did acknowledge that the problem did exist.

A second concern which arose from the literature search was that many simplifying assumptions were used in the development of the models. As an example, when developing the model of pressure-control (PC) pumps, Palmberg, et al, [1985] indicated that a simple two-parameter model described by Equation (1.6) was usually sufficient to describe the dynamic behavior of the pump.

$$Q_p = \frac{1 + s/\omega_{p1}}{R_p + L_p s}\left(P_{ref} - P_s\right) - K_{cp} P_s \tag{1.6}$$

where

$$K_{cp} = K_{c\eta} + K_{c1}\left(1 - \frac{A_{se}}{A_c}\right) + \kappa K_{cr} \tag{1.7}$$

L_p was the inductance, R_p the resistance, ω_{p1} a characteristic break frequency, K_{cp} a pressure gain of the PC pump, P_s the pressure, P_{ref} a reference pressure, which the pressure P_s is expected to be, $K_{c\eta}$ the leakage coefficient of the PC pump, K_{c1} the flow-pressure coefficient of the regulator's orifice, $\frac{A_{se}}{A_c}$ the ratio of the piston area of the stroke mechanism. κ and K_{cr} are the parameters of the regulator's pilot respectively. For a direct-operated regulator, K_{cr} was zero.

It should be noted that the model defined by Equation (1.6) has been adopted by many researchers in modeling load sensing system. Palmberg, et al, suggested that this

model could be further simplified by assuming that the pump resistance R_p and flow-pressure coefficient K_{cp} are negligible resulting in Equation (1.8).

$$Q_p = \frac{1 + s/\omega_{p1}}{L_p s}\left(P_{ref} - P_s\right) \tag{1.8}$$

It should be noted that this model is valid between the pump cut-off pressure and the dead head pressure (P_{dhp}). For pressures less than $P_{cut\text{-}off}$, the flow from the pump is constant and independent of P_s.

If these PC pump models are to be integrated in LSPC systems, it is questionable whether the pump resistance R_p and flow-pressure coefficient K_{cp} can be ignored. This is because the small change of the pump performance caused by varying K_{cp} may affect the dynamic performance of the whole system. Thus, the validity of using Equation (1.8) in simulation studies must be carefully established by considering the actual loads and operating points of the remaining system.

Even though the model of a PC pump as developed by Palmberg, et al, [1985] could be consider “detailed” (see Equation (1.6)), it was still not a complete model of the pressure-control pump. This is because Equation (1.6) ignores the dynamic factors (mass and damping) of the pump-regulator's spool, does not consider the effect of the fluid compressibility in the pump compensator chambers, and simplifies the local pressure feedback factor (the second item of Equation (1.6)) as a constant gain, K_{cp} (which, in fact, is a dynamic factor (transfer function) affected by the operating frequency).

A dynamic model of the PC system (Figure 1.7) was presented by Pettersson, et al, [1996]. For the PC system and nomenclature shown in Figure 1.7, his linear model was expressed as

$$Q_L = K_{cpc}(P_s - P_m) + G_{v0}(s)\left(P_m - P_L - P_{cpc}\right) \tag{1.9}$$

where

$$G_{v0}(s) = \frac{K_{cx}}{\frac{s}{\omega_3} + 1} \tag{1.10}$$

P_s, P_m, P_L and P_{cpc} were defined in Figure 1.7.

Petterson, et al, [1996] gave a value of K_{cx}, but the physical concept of K_{cx} was not explained and the value of K_{cx} used was not justified.

The dynamic models of pressure-control pumps and PC systems reviewed above are essential in developing the dynamic model of LS and LSPC systems. Krus [1988] developed a transfer function of an LS system with single inertia load given by Equation (1.1). The pump was regarded as a pure inductance L_p; hence the ω_{pl} was considered infinite in Equation (1.8). The stability criteria presented in Equations (1.2) to (1.5)) were derived from the simplified pump model. As a result, the stability deduction from the simplified model could only be considered approximate.

A comprehensive model of LS systems and especially models of LSPC systems have not been published. A comprehensive model of LS systems should take into account "more details" than that presented by Palmberg, et al, [1985]. A model of LSPC systems should include dynamic models of both the two subsystems (pressure-control pump and PC systems).

Although most of conclusions drawn by previous researchers were in agreement, some conclusions presented by researchers, such as Kim, et al, [1988] and Krus [1988], were in conflict.

In summary, the literature indicates that the operating point problem for linearized models, the "complexity" of the individual component models, and a complete model of LS or LSPC systems remain areas which require much further study. For a designed LS system or LSPC system, it is necessary to further investigate how the parameter variation of an LSPC system causes the change of the operating point and hence affects the change of the linearization parameters that are used for stability analysis. In order to develop and justify the comprehensive model of LS and LSPC systems, it is also essential to establish more detailed models of hydraulic components (pressure-control pump, PC systems etc.).

1.3 Objectives

The objectives of this thesis are

- To investigate the steady state operating condition and the steady state operation points (SSOP's) of a LS system with a critically lapped LS regulator spool in the LS pump,
- Based on the knowledge about the SSOP of the LS system, to develop the stability models of the LS system under different steady state operating conditions using the linearization method,
- To determine the dependence of the system stability on the SSOP of the LS system,
- To analyze the steady state and dynamic performances of a typical PC system,
- And finally, to investigate the stability of the LSPC system which consists of the LS system and the PC system.

In additions, this thesis is also to experimentally verify all models developed for

determining the SSOP's and stabilities of the LS, PC and LSPC systems.

1.4 Outline of Thesis

This thesis is organized in the sequence of the LS system, PC system and then the LSPC system.

The LS system is first investigated. The non-linear dynamic models are presented in Chapter 2. The steady state operating conditions are identified in Chapter 3, under which the system models are developed. These models are experimentally verified in Chapter 4. The frequency response models based on the linearization approach are developed in Chapter 5. These frequency response models are experimentally validated in Chapter 6. These frequency response models are used to analyze the stability of the LS system in Chapter 7.

Similar to the procedure for investigating the LS system, the PC system is then studied in Chapters 8 through Chapter 11. The non-linear dynamic model of the PC system is presented in Chapters 8. The steady state operating conditions is analyzed and the model for solving for the operating point is developed in Chapter 9. The comparison between the predicted and experimental results of the steady state operating point is given in Chapter 10. The frequency response model of the PC system based on the linearization approach is developed in Chapter 11.

The LSPC system is further investigated by applying the results for the LS system (Chapters 2 through 7) and for the PC system (Chapters 8 through 11). The steady state models used to solve for the SSOP's are developed in Chapter 12. The frequency response models are then presented in Chapter 13, which are used to carry out the stability analysis in Chapter 14. The analysis result is experimentally verified in Chapter 15. Finally, the conclusion and recommendation are given in Chapter 16.

Chapter 2 Modeling of Load Sensing Systems

Frequency domain analysis and time domain simulation are two common approaches to designing and analyzing a dynamic system of any kind (electrical, hydraulical, mechanical, etc.). The frequency response analysis is popular because it can give more information about the relationship between the parameters and the dynamic characteristics of a system than time domain simulations. However, the frequency domain (transfer function) analysis has the precondition that the system be linear. This limits the application of the frequency domain method in most hydraulic systems because of their high degree of non-linearity. In order to take advantage of the frequency domain analysis, linearization techniques are often applied. Typically, the non-linear system is linearized about a point of interest and the frequency domain method is applied for small excursions about this steady state operating point. Actually, so are the time domain methods. It is assumed that the system is approximately linear within a small region about the steady state operating point.

The objectives of this chapter are to introduce a mathematical model of the LS system which consists of non-linear differential equations and non-linear algebraic equations. The linearization forms of these equations are also provided. The non-linear model will be used in Chapters 3 & 4 for investigating the steady state operating conditions and solving for the SSOP of the LS system. The linearized model of the LS system will be used to develop the TF (transfer function) of the LS system in Chapter 5.

2.1 Linearization of a Load Sensing System

The mathematical foundations for linearization for a nonlinear function is presented in Appendix A. Consider the LS system shown in Figure 2.1. The system consists of a LS pump with a LS regulator (1), a control piston (2) and a pressure control pump (3), an adjustable orifice (4), a LS line with a damping orifice (5), and a motor load (6).

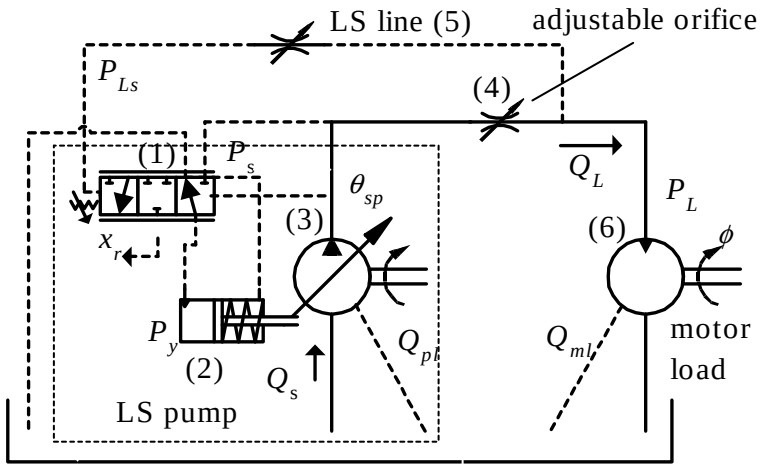

Figure 2.1 Schematic of the Load Sensing System

2.1.1 Load Sensing Pump

The LS pump system consists of three main hydraulic components as shown in Figure 2.2; pressure control pump, LS regulator (three-position three-way valve with critical center spool), and a control piston (the control piston makes contact with the yoke upon which the swash plate is fixed). From energy saving considerations, the spool of the LS regulator is most often selected to be critically centered [Ford 60 Series Gemini Tractors; Volvo Champion Motor Graders; Brueninghaus Hydromatik Variable Displacement Pump AA11VO; Vickers PVH Piston Pumps; Caterpiller 160H Motor Grader; Newholland Series 60 tractors etc.]. In a few other applications, [Newholland

Series 60 tractors with gear pumps], an underlapped spool is used. In this study, a critically lapped spool is considered.

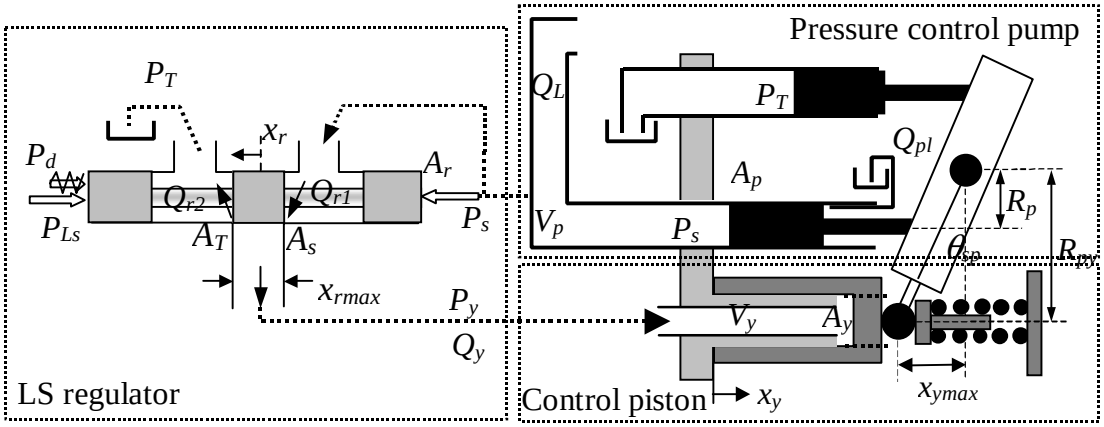

Figure 2.2 Schematic of the Load Sensing Pump System

The dynamic mathematical model consists of two equations of mechanical movement and one flow continuity equation.

- Force Equilibrium Equation for the LS Regulator Spool

The equation of motion for the spool of the LS regulator (Figure 2.2) can be described as

$$\ddot{x}_r = \frac{1}{m_r}\left(-B_r\dot{x}_r - k_r x_r + A_r\left(\left(P_s - P_{Ls}\right) - P_d\right)\right) \tag{2.1}$$

where x_r is the spool displacement. m_r, B_r, and k_r are spool mass, damping coefficient, and preset spring coefficient respectively. A_r is the cross sectional area of the spool. P_s, P_{Ls} and P_d are the pump pressure, the load pressure at the end of LS line, and the pressure differential setting respectively. It is noted that P_d is not a true "physical" pressure but an equivalent pressure term caused by the pre-compression force of the spring ($P = \frac{F}{A}$). P_d controls the pressure drop across an adjustable orifice and is a

designed value of pressure differential, P_s - P_L. P_d will be further discussed when its value is determined in Section 4.2.2.1 of Chapter 4.

It is also noted that Equation (2.1) does not include the steady state flow force and the transient flow force exerted on the spool of the LS regulator. This is because the flow rate (i.e. the leakage for the critically lapped LS spool) through orifices around the spool sleeve is small resulting in a flow force that is very small compared to the force produced by ($P_s - P_{Ls}$ - P_d). A dynamic simulation in which the steady state flow force and the transient flow force were considered has been conducted to verify that the flow forces are negligible for the LS regulator in this study.

- Dynamic Equation of the Yoke Control Cylinder and Swash Plate

Referring to the control piston (Figure 2.2), the relationship between the swash plate angle, $\theta_{sp,}$ and the yoke displacement, x_y, is

$$\tan\theta_{sp} = \frac{x_{y\max} - x_y}{R_{py}} \tag{2.2}$$

The pre-compression spring normally pushes the yoke piston back and maintains the displacement, $x_{y,}$ of the yoke at the original position (x_y = 0 in Figure 2.2). That is, the pre-compression spring value is such that the pump is at full displacement before the pump operates. When the yoke chamber pressure, P_y, increases, the yoke piston does not move until the yoke chamber pressure overcomes the pre-compression pressure P_{ys}. When P_y increases beyond P_{ys}, the yoke piston begins to move forward and the swash plate angle begins to decrease correspondingly. When x_y increases to the maximum, the pump swash plate angle decreases to zero. In this case, the pump is “destroked” and pump flow is zero.

In order to describe the dynamic behavior of the swash plate and the control yoke, the displacement of the control piston, x_y, or the swash plate angle, θ_{sp}, can be assigned as the state variable. The swash plate angle, θ_{sp}, is usually used as the variable in modeling because (1) the non-linearity of the pump is mainly caused by the pressure control pump, rather than the control piston, and (2) measuring θ_{sp} is easier than measuring x_y. The dynamic model of the swash plate angle depends on the structure of the variable displacement axial piston pump. Depending on the eccentricity of the swash plate axis, the external active torque on the swash plate assembly is dictated by both the yoke control pressure, P_y, and the pumping piston pressure, P_s.

Numerous models for axial displacement pump have been developed. Dobchuk, et al, [1999, 2000] developed a mathematical model of a variable displacement axial piston pump and investigated the effect of internal pump dynamics on control piston pressure ripple. However, this model was too complex to consider in the LS system-level models. Another model, which reflects the "back pressure" on the pump due to the pump pressure acting on the pistons, was developed by Kavanagh [1987]. The non-linear dynamic equation was developed to be

$$J_{sp}\ddot{\theta}_{sp} = -B_{sp}\dot{\theta}_{sp} - K_{sp}\theta_{sp} + T_{sp} + K_{pr2}P_s - K_{pr3}P_s\theta_{sp} - R_{py}A_yP_y \qquad (2.3)$$

where J_{sp} = Average total moment of inertia of swash plate, yoke and piston assembly, Nms^2.

B_{sp} = Simplified constant (damp coefficient) of the control piston and swash plate assembly, Nms.

K_{sp} = Angular effective spring coefficient, $Nm \cdot rad^{-1}$.

T_{sp} = Angular effective spring pretension, Nm.

K_{pr2} = Pressure torque constant, Nm·Pa^{-1}.

K_{pr3} = Pressure torque constant, Nm·Pa^{-1}·rad^{-1}.

R_{py} = The distance between the centerline of the control piston guide and the swash plate pivot (Figure 2.2), m.

A_y = Effective control piston area (Figure 2.2), m^2.

It is noted that P_s in Equation (2.3) was ΔP_p (the differential pressure, P_s - P_T) in the original model by Kavanagh [1987]. However because the pressure, P_T, in the suction piston chambers is small, ΔP_p can be considered as the pump pressure which is represented by P_s here.

This equation is nonlinear because the $K_{pr3}P_s\theta_{sp}$ term includes the product of two variables, P_s and θ_{sp}. Thus, this equation is linearized which results in:

$$J_{sp}\Delta\ddot{\theta}_{sp} = -B_{sp}\Delta\dot{\theta}_{sp} - (K_{sp} + K_{pr3}P_{s0})\Delta\theta_{sp} - R_{py}A_y\Delta P_y + (K_{pr2} - K_{pr3}\theta_{sp0})\Delta P_s \qquad (2.4)$$

The linearized Equation (2.4) does not include the constant T_{sp}. This indicates that the constant T_{sp} affects the steady state operating point and does not relate to the dynamic performance.

- Flow Continuity Equations of Chamber Volume of the Pump Swash-Plate Control Cylinder

Consider the chamber between the LS regulator and the control piston in Figure 2.2. For the adjusting valve with a critically lapped spool, the flow continuity equations can be described as

$$\dot{P}_y = \frac{\beta}{V_y}\left(Q_{r1} - A_y \dot{x}_y - Q_{r2}\right) \tag{2.5}$$

where β is the bulk modulus of hydraulic oil, V_y is the volume of yoke chamber which is given in Equation (2.6), Q_{r1} is the flow through the "charging" orifice on the right side (in the LS regulator of Figure 2.2), and Q_{r2} is the flow through the "discharging" orifice on the left side.

$$V_y = V_{y0} + A_y x_y \tag{2.6}$$

The control piston position is defined such that an increase in x_y will cause an increase in the volume, V_y, of the yoke chamber.

With reference to Figure 2.2, flow through the "charge" orifice (A_s) and "discharge" orifice (A_T) (depending on which orifice is opened) is given by

$$Q_{r1} = C_d A_s(x_r)\sqrt{\frac{2}{\rho}\left(P_s - P_y\right)} \qquad x_r \geq 0 \tag{2.7}$$

$$Q_{r2} = C_d A_T(x_r)\sqrt{\frac{2}{\rho}P_y} \qquad x_r < 0 \tag{2.8}$$

where C_d is the discharge coefficient of the valve orifice and ρ is the density.

For a rectangular-shaped orifice with a critically lapped spool, the orifice areas $A_s(x_r)$ and $A_T(x_r)$ can be represented by a piecewise linear relationship given as

$$A_s\left(x_r\right) = \begin{cases} w_r x_{r\max} & x_r \geq x_{r\max} \\ w_r x_r & 0 < x_r < x_{r\max} \\ 0 & x_r < 0 \end{cases} \tag{2.9}$$

$$A_T(x_r) = \begin{cases} w_r x_{r\max} & x_r \le -x_{r\max} \\ w_r |x_r| & -x_{r\max} < x_r \le 0 \\ 0 & x_r > 0 \end{cases} \tag{2.10}$$

w_r is the width of the rectangular-shaped orifice. $x_{r\max}$ is the largest width of the regulator orifice. The coordinate of x_r is defined such that when $x_r \le 0$, the orifice on the right hand side is closed ($Q_{r1} = 0$) and when $x_r \ge 0$, the orifice on the left hand side is closed (Q_{r2}=0).

In Kim and Cho [1991], the metering orifices of the LS regulator were assumed to be rectangular. In practice, the orifices in LS systems are usually round-shaped. The round-shaped orifice makes the LS system model more non-linear than rectangular-shaped orifices. For a round-shaped orifice with a critically lapped spool (Figure 2.2), the orifice areas $A_s(x_r)$ and $A_T(x_r)$ are piecewise non-linear and are given as

$$A_s(x_r) = \begin{cases} 0 & x_r \le 0 \\ R_r^2 \cos^{-1}\left(\frac{R_r - x_r}{R_r}\right) - (R_r - x_r)\sqrt{2R_r x_r - x_r^2} & 0 < x_r < 2R_r \\ R_r^2 \pi & x_r \ge 2R_r \end{cases} \tag{2.11}$$

$$A_T(x_r) = \begin{cases} 0 & x_r \ge 0 \\ R_r^2 \cos^{-1}\left(\frac{R_r + x_r}{R_r}\right) - (R_r + x_r)\sqrt{-2R_r x_r - x_r^2} & -2R_r < x_r < 0 \\ R_r^2 \pi & x_r \le -2R_r \end{cases} \tag{2.12}$$

where R_r is the radius of the round orifice (R_r replaces $\frac{x_{r\max}}{2}$ in order to distinguish the rectangular orifice in Figure 2.2. The top view of the round-shaped orifice is shown in Figure 2.3).

Linearization of Equations (2.7) and (2.8) gives

$$\Delta Q_{r1} = K_{qr1}\Delta x_r + K_{cr1}(\Delta P_s - \Delta P_y) \tag{2.13}$$

and $\Delta Q_{r2} = K_{qr2}\Delta x_r + K_{cr2}\Delta P_y$ (2.14)

where $K_{qr1} = C_d \cdot \frac{dA_s(x_{r0})}{dx_r} \cdot \sqrt{\frac{2}{\rho}(P_{s0} - P_{y0})}$, (2.15)

$$K_{cr1} = \frac{C_d A_s(x_{r0})}{\sqrt{2\rho(P_{s0} - P_{y0})}}, \quad (2.16)$$

$$K_{qr2} = C_d \cdot \frac{dA_T(x_{r0})}{dx_r} \cdot \sqrt{\frac{2}{\rho} P_{y0}}\ , \quad (2.17)$$

$$K_{cr2} = \frac{C_d A_T(x_{r0})}{\sqrt{2\rho P_{y0}}} \quad (2.18)$$

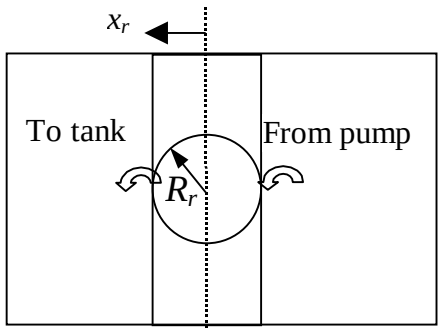

Figure 2.3 "Charge" Orifice and "Discharge" Orifice
of the Load Sensing Spool

The opening rates of orifice area, $\frac{dA_s(x_r)}{dx_r}$ and $\frac{dA_T(x_r)}{dx_r}$, for rectangular-shaped orifices are constant (w_r and -w_r depending on which orifice is opened). For the round-shaped orifice, the gradients $\frac{dA}{dx_r}$ are nonlinear.

Linearization of Equation (2.5) can be expressed as

$$\Delta\dot{P}_y = \frac{\beta}{V_y}(\Delta Q_{r1} - A_y\Delta\dot{x}_y - \Delta Q_{r2})$$

or $$\Delta\dot{P}_y = -K_{xy}\Delta x_y - K_{dxy}\Delta\dot{x}_y + K_{xr}\Delta x_r - K_{py}\Delta P_y + K_{ps}\Delta P_s \tag{2.19}$$

where

$$K_{xy} = \frac{\beta A_y}{\left(V_{y0} + A_y x_{y0}\right)^2}\left(Q_{r10} - A_y\dot{x}_{y0} - Q_{r20}\right) \tag{2.20}$$

$$K_{dxy} = \frac{\beta A_y}{V_{y0} + A_y x_{y0}} \tag{2.21}$$

$$K_{xr} = \frac{\beta}{V_{y0} + A_y x_{y0}}\left(K_{qr1} - K_{qr2}\right) \tag{2.22}$$

$$K_{py} = \frac{\beta}{V_{y0} + A_y x_{y0}}\left(K_{cr1} + K_{cr2}\right) \tag{2.23}$$

$$K_{ps} = \frac{\beta K_{cr1}}{V_{y0} + A_y x_{y0}} \tag{2.24}$$

Equation (2.19) involves two time derivatives ($\dot{P}_y$ and $\dot{x}_y$) of the state variables. The effect of piston velocity, $\dot{x}_y$, on the pressure, P_y, of the control piston chamber is not negligible due to the small volume of the control piston chamber.

Δx_y and $\Delta\dot{x}_y$ in Equation (2.19) must be expressed in term of $\Delta\theta_{sp}$ and $\Delta\dot{\theta}_{sp}$ because θ_{sp} is assigned as the state variable of the swash plate and control piston assembly. Rearranging Equation (2.2) and differentiating x_y give

$$x_y = x_{y\max} - R_{py}\cdot\tan\left(\theta_{sp}\right) \tag{2.25}$$

$$\dot{x}_y = -\frac{R_{py}}{\cos^2\left(\theta_{sp}\right)}\cdot\dot{\theta}_{sp} \tag{2.26}$$

Linearization of Equations (2.25) and (2.26) gives

$$\Delta x_y = -\frac{R_{py}}{\cos^2\left(\theta_{sp0}\right)} \cdot \Delta\theta_{sp} \tag{2.27}$$

$$\Delta \dot{x}_y = -\frac{R_{py}}{\cos^2\left(\theta_{sp0}\right)} \cdot \Delta\dot{\theta}_{sp} - \frac{2R_{py} \cdot \sin\left(\theta_{sp0}\right)\dot{\theta}_{sp0}}{\cos^3\left(\theta_{sp0}\right)}\Delta\theta_{sp} \tag{2.28}$$

Substituting Equations (2.27) and (2.28) into Equation (2.19) can give

$$\Delta \dot{P}_y = K_\theta \Delta\theta_{sp} + K_{d\theta}\Delta\dot{\theta}_{sp} + K_{xr}\Delta x_r - K_{py}\Delta P_y + K_{ps}\Delta P_s \tag{2.29}$$

where

$$K_\theta = \frac{R_{py}\left(K_{xy} + 2\tan\left(\theta_{sp0}\right)\dot{\theta}_{sp0}K_{dxy}\right)}{\cos^2\left(\theta_{sp0}\right)} \tag{2.30}$$

$$K_{d\theta} = \frac{R_{py}K_{dxy}}{\cos^2\left(\theta_{sp0}\right)} \tag{2.31}$$

- Flow Supply of the LS Pump

Figure 2.4 shows schematically the flow through the LS pump. Consider the control volume defined as illustrated by the dashed line. Three flows are illustrated; the flow ($D_p\omega$) from the tank, the flow (Q_{r1}) to the regulator, and Q_s, the flow to the load (commonly referred to as the pump flow)

From the flow continuity consideration of the pump outlet volume,

$$Q_s = D_p\omega - Q_{r1} \tag{2.32}$$

D_p is the "displacement" of the pump and is linearly related to the tangent of the swash plate angle, that is

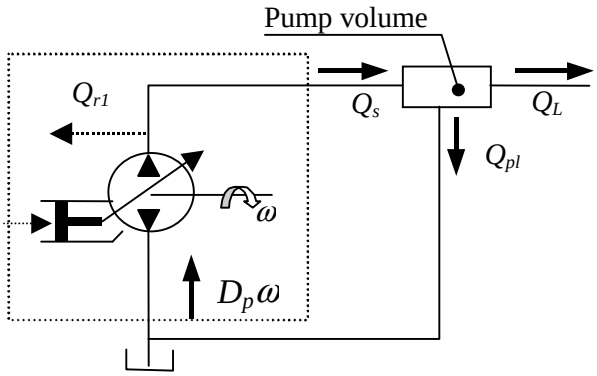

Figure 2.4 Flow Diagram of the LS Pump

$$D_p = f(\theta_{sp}) = \frac{NA_p R_p \tan\theta_{sp}}{\pi} \tag{2.33}$$

Substituting Equation (2.33) into Equation (2.32) gives

$$Q_s = \frac{NA_p R_p \omega \tan\theta_{sp}}{\pi} - Q_{r1} \tag{2.34}$$

Both terms of Equation (2.34) on the right hand side include non-linear functions. Linearization of Equation (2.34) can be expressed by

$$\Delta Q_s = C_p \Delta\theta_{sp} - K_{qr1}\Delta x_r - K_{cr1}(\Delta P_s - \Delta P_y) \tag{2.35}$$

where the K_{qr1} and K_{cr1} were defined in Equation (2.13), and

$$C_p = \frac{NA_p R_p \omega}{\pi \cdot \cos^2(\theta_{sp0})} \tag{2.36}$$

2.1.2 Pump Volume

Consider Figure 2.4. The pump pressure is dictated by the pump flow Q_s, the leakage flow Q_{pl}, and the load flow, Q_L. The pump pressure in the outlet volume is thus given as

$$\dot{P}_s = \frac{\beta}{V_p}((Q_s - Q_L) - Q_{pl}) \tag{2.37}$$

where $Q_{pl} = c_{pl} P_s$. c_{pl} is the leakage coefficient of the pump. V_p is the pump outlet volume which includes the volume of pipeline. The load flow, $Q_{L,}$, will be discussed in the next section. It should be noted that if the pump volume is small and the leakage is negligible, then the pump pressure is dictated by the loading condition and thus the causality of all the relationships do change. In most applications, the pipeline volume between the pump and valves is larger than the effective volume of pump pistons. The effect of long pipelines on the dynamic behavior of the pump is significant [Kauranne, et al, 1999].

2.1.3 Flow Adjusted Orifice without Pressure Compensation

The well-known equation of the volumetric flow rate through the adjustable orifice shown in Figure 2.1 is derived from Bernoulli's equation by assuming (1) an incompressible fluid, (2) turbulent flow and (3) rectangular type orifice [Merritt, 1967] as

$$Q = C_d w x \sqrt{\frac{2}{\rho}(P_s - P_L)} \tag{2.38}$$

where C_d is the discharge coefficient. w and x are the width and opening of the rectangular type orifice respectively. ρ is the fluid density. P_s is the pump pressure at the orifice upstream. P_L is the load pressure at the orifice downstream.

Because the flow through an orifice is assumed to be turbulent, the discharge coefficient, C_d, is commonly considered as a constant, typically, 0.61 for sharp edged orifice.

Linearization of Equation (2.38) can be expressed by

$$\Delta Q_L = K_q \Delta x + K_c (\Delta P_s - \Delta P_L) \tag{2.39}$$

where

$$K_q = C_d w \sqrt{\frac{2}{\rho}(P_{s0} - P_{L0})} \tag{2.40}$$

$$K_c = \frac{C_d w x}{\sqrt{2\rho(P_{s0} - P_{L0})}} \tag{2.41}$$

2.1.4 Motor Load

The mathematical model of the motor load in Figure 2.5 consists of a flow continuity Equation (2.42) of the inlet volume and the dynamic torque Equation (2.43) on the motor axis.

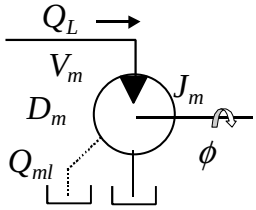

Figure 2.5 Diagram of a Hydraulic Motor

$$\dot{P}_L = \frac{\beta}{V_m}(-D_m\phi + Q_L - Q_{ml}) \tag{2.42}$$

$$\dot{\phi} = \frac{1}{J_m}\left(-B_m\phi + D_m P_L - T_{mf}\right) \tag{2.43}$$

where $Q_{ml} = c_{ml} P_L$. c_{ml} is the leakage coefficient of the motor. V_m is the inlet volume of motor, J_m is the total inertia of motor and load, B_m is the damping coefficient of the load, and D_m is the volumetric displacement of the motor. ϕ is the rotary speed of the motor. T_{mf} is the resistant torque of the load. The resistant torque cannot be neglected because it does exist due to many factors such as gravity, stiction, friction, etc. It directly affects the SSOP of the LS system.

Equations (2.42) and (2.43) can be linearized as

$$\Delta\dot{P}_L = \frac{\beta}{V_m}\left(-D_m\Delta\phi + \Delta Q_L - c_{pl}\Delta P_L\right) \tag{2.44}$$

$$\Delta\dot{\phi} = \frac{1}{J_m}\left(-B_m\Delta\phi + D_m\Delta P_L\right) \tag{2.45}$$

It can be seen that the constant resistant torque, T_{mf}, is absent in Equation (2.45) unless it depends on any state variable or it is an independent variable.

2.1.5 Feedback Line

It is difficult to build a precise mathematical model of the load sensing line. A lumped parameter model, however, can approximately describe the dynamic behavior of the load sensing line. Figure 2.6 shows a two-parameter model of load sensing line with hose volume, V_{Ls}, and hose flow resistance, R_{Ls}. Q_{Ls} represents the flow of load sensing line at the left end of pump compensator. This flow is linearly related to the speed, $\dot{x}_r$, of the compensator piston. Q_{Lsss} represents the flow that considers the presence of hose resistance and hose capacitance. Actually, in the limit, Q_{Lsss} can be regarded as the steady state value of $Q_{Ls.}$ Therefore,

$$Q_{Ls} = -A_r\dot{x}_r \tag{2.46}$$

$$Q_{Lsss} = \frac{\left(P_L - P_{Ls}\right)}{R_{Ls}} \tag{2.47}$$

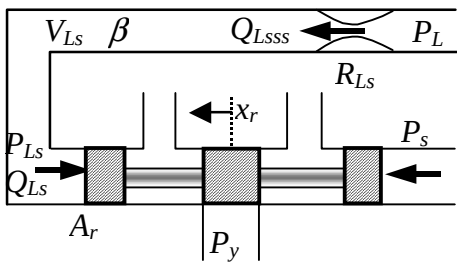

Figure 2.6 Model of Load Sensing Line

$$\dot{P}_{Ls} = \frac{\beta}{V_{Ls}}\left(Q_{Lsss} - Q_{Ls}\right) \tag{2.48}$$

Substituting Equations (2.46) and (2.47) into (2.48), the dynamic behavior of the load sensing line can be expressed by

$$\dot{P}_{Ls} = \frac{\beta}{V_{Ls}}\left(\frac{\left(P_L - P_{Ls}\right)}{R_{Ls}} + A_r \dot{x}_r\right) \tag{2.49}$$

Usually, $A_r \dot{x}_r$ is negligible. Equation (2.49) can be simplified into a simple first order system as

$$\dot{P}_{Ls} = \omega_{Ls}\left(P_L - P_{Ls}\right) \tag{2.50}$$

where $\omega_{Ls} = \frac{\beta}{V_{Ls} R_{Ls}}$. ω_{Ls} represents the break frequency of the "damping" system due to the effect of both the flow resistance and the hose capacitance. (Note, in the literature, ω_{Ls} is used rather than τ_{Ls}; as such, ω_{Ls} will be adopted in this work.)

2.2 Methodology—Design and Analysis of the Load Sensing System

The non-linearity and complexity of LS systems makes system analysis and design very complicated. The stability of linear systems is uniquely determined by the system parameters which are time invariant, independent of steady state operating points, and independent of the amplitude of the input signals. Unlike a linear system, however, the dynamic characteristics of non-linear systems are dependent on steady state operating points and input signals. Therefore, the approaches to analyzing these systems are different.

2.2.1 Examples

Two simple examples shown in Figures 2.7 and Figure 2.8 are used to explain the difference in the analytical methods. Consider a linear system with mass, *m*, and linear damping, *B*, shown in Figure 2.7. For an arbitrary step input, F, the final velocity of the block will converge to $v_f = \frac{F}{B}$ uniquely. It can be said that the system is always stable. However, for the case of a single pendulum shown in Figure 2.8, the situation is different.

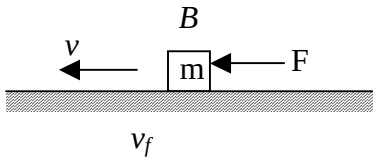

Figure 2.7 An Example of Linear Systems

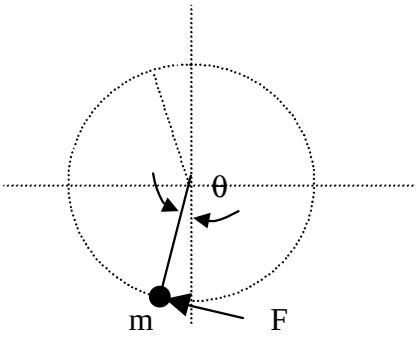

Figure 2.8 An Example of Non-Linear Systems—Single Pendulum

Assume that a step input in *F* is in the tangential direction. The equation of motion is given as

$$ml^2\ddot{\theta} + \eta\dot{\theta} + mgl\sin(\theta) = lF_0U(t) \tag{2.51}$$

where *m* is the mass of the block suspended, η is the angle damping coefficient, *l* is the length of the pendulum, and *g* is the gravitation acceleration, *U(t)* is a unit step input and

F_0 is the magnitude of this step input. For a particular range of F_0, the single pendulum will be eventually stabilized at a particular steady state operating point, θ_0 (<90^0). In order to analyze the stability of the single pendulum mathematically, there are two aspects that must be considered.

All possible operating points at steady state must be determined. From Equation (2.51), the steady state angle of the pendulum is given by

$$\theta_0 = \begin{cases} \begin{cases} \arcsin\left(\dfrac{F}{mg}\right) \\ 180^0 - \arcsin\left(\dfrac{F}{mg}\right) \end{cases} & |F| \le mg \\ \text{no operating point exists} & |F| > mg \end{cases} \tag{2.52}$$

Equation (2.52) indicates that, for $|F|>mg$, no steady state operating point exists. For $|F| \le mg$, there are two steady state operating points.

Secondly, it is necessary to establish if each steady state operating point is a "realizable" steady state operating point. In order to do this, linearization of Equation (2.51) is necessary.

$$a_2 \Delta\ddot{\theta} + a_1 \Delta\dot{\theta} + a_0 \Delta\theta = \Delta F \tag{2.53}$$

where $a_2 = ml$, $a_1 = \eta / l$, and $a_0 = mg \cdot \cos(\theta_0)$. The transfer function corresponding to linearization Equation (2.53) is

$$f(s) = \frac{\Delta\theta(s)}{\Delta F(s)} = \frac{1}{a_2 s^2 + a_1 s + a_0} \tag{2.54}$$

According to the theory of dynamic analysis of linear systems, the single pendulum is stable only if the three coefficients (a_i i=0,1,2) are of the same sign. Substituting the

two possible steady state points for Equation (2.52) into the linearized Equation (2.43), it is observed that, for $\theta_0 = \arcsin\left(\frac{F}{mg}\right)$, all three coefficients of Equation (2.52) are positive. Therefore, the single pendulum is stable. For $\theta_0 = 180^0 - \arcsin\left(\frac{F}{mg}\right)$, a_0 is negative. Therefore, under these conditions, the single pendulum is unstable. This example illustrates that, for a non-linear system, it is necessary to find the steady state operating points before the dynamic analysis can be done.

2.2.2 Summary of Linearization Approach

The lineariztion approach of the LS system is defined in the thesis as the method of small signal analysis of a non-linear LS system using linear theory. The method includes "steady state analysis" and "dynamic analysis". The former is defined as the procedure for finding all possible steady state operating conditions and steady state operating points. The latter is defined as the procedure using frequency response modeling and analysis, or alternatively a small signal simulation, based on the linearized equations of the non-linear LS system.

For the steady state analysis, it is impossible to give an analytical expression for all possible steady state operating points at all possible operating conditions. First, finding all possible operating conditions requires the complete analysis for components which demonstrate the significant non-linearities. The regions in which the LS system cannot be described by the same dynamic equations set, can be separated into several different operating conditions. Second, for each operating condition, finding all possible steady state operating points requires all possible solutions to a very large set of nonlinear system equations for the case where all the derivatives are set equal to zero. For

example, Equation (2.52) is the solution of Equation (2.51) with $\ddot{\theta} = \dot{\theta} = 0$. Usually, a LS system is required to operate about operating points at steady state in such a way that derivatives of pressures (pump pressure and load pressure) and spool position (LS regulator spool) are zero. As such, the very large set of non-linear system equations become a set of non-linear algebraic equations involving several unknown variables. Solving for these unknown variables needs an iteration computation in most cases.

Dynamic analysis, or small signal analysis of the linearized dynamic equations often involves frequency response modeling approach and analysis. The objective is to find the stability of the LS system at SSOP's. The detailed explanation about the method of the frequency response modeling and analysis is presented in Section A.3 of Appendix A.

A linearization approach can also be used for the design of a LS system, such as the one shown Figure 2.1, which involves choosing the hydraulic components and setting parameters of some components to meet required specifications. Primarily, these components can be "pre-chosen" by the power and/or flow requirements of the load(s). The feasibility of these choices of components must be subsequently validated by steady state and dynamic analysis. If they cannot meet the specifications, the original component choice must be re-examined.

Usually, the design inputs include the pressure differential setting, P_d, to control the pressure drop across the orifice in the non-compensated valve which is the pump-regulator setting. For a specific opening, x_v, of the orifice within the range ($0 \sim x_{vmax}$), it is necessary to first do the steady state analysis and then its dynamic analysis. If the result of the steady state analysis indicates that no steady state operating point exists within a

specified range, then it is not necessary to proceed with stability analysis. In this case, it may be that the component(s) is chosen improperly, or the design inputs P_d is unreasonable. For example, suppose the steady state operating point of the spool displacement of the LS regulator was calculated to be x_{rmax} which is the maximum opening of LS regulator orifice. This would be an unacceptable steady state operating point because it is at saturation.

If the steady state operating point(s) are within a specified range, dynamic analysis, using tools such as the Bode diagram of the linearized system, help assess the stability at the steady state operating point(s) for the specific opening, x_v, of the flow control valve. For all expected openings, x_v, of the adjustable orifice, if the LS system is stable, the system meets the required design constraints and is considered stable.

Chapter 3 Steady State Analysis of the Load Sensing system

3.1 Introduction

As indicated in Chapter 2, a "steady state analysis" procedure for a dynamic system must be developed to determine all possible SSOP's. Finding these operating points requires all possible solutions to a set of nonlinear system equations in which all the derivatives are set equal to zero. For some simple non-linear systems, such as a single pendulum, it is possible to develop an analytical solution of the corresponding steady state equations. However, for many actual hydraulic systems, such as LS systems, it is not possible to develop an analytical expression for all possible operating points. Fortunately, numerical methods and powerful computers have provided alternate approaches for solving all possible solutions to a non-linear equation.

This chapter will develop a set of causal relationships which will facilitate the steady state analysis of LS systems. A numerical method for solving non-linear equations will be provided. The "piece-wise model" problem which surfaces from these equations will also be discussed. Finally, a procedure of solving for the SSOP's of the LS system is forwarded.

3.2 Non-linear Models for Steady State Analysis of a Typical Load Sensing System

In order to understand the procedure of solving for the operating point of general LS systems, it is necessary to consider a set of nonlinear algebraic equations resulting from the non-linear dynamic models developed in Chapter 2, and to use these equations to illustrate the steady state analysis of a typical LS system.

3.2.1 Non-linear Equation Set

For the LS system under steady state conditions, the time derivatives of the state variables (x_r, θ_{sp}, ϕ, P_s, P_y, P_L, and P_{Ls}) are zero. Therefore, setting $\dot{x}_r, \ddot{x}_r, \dot{\theta}_{sp}, \ddot{\theta}_{sp}$, $\dot{\phi}$, $\dot{P}_s$, $\dot{P}_y$, $\dot{P}_L$, and $\dot{P}_{Ls}$ to zero in Equations (2.1), (2.3), (2.43), (2.37), (2.5), (2.42), and (2.50) yields seven algebraic equations having seven unknown variables (x_r, θ_{sp}, ϕ, P_s, P_y, P_L, and P_{Ls}). These equations are listed in Table 3.1.

Equation (3.4) indicates that the flow rates, Q_{r10} and Q_{r20}, are zero due to the critically lapped condition. This will give rise to the different operating conditions discussed in the next section.

Table 3.1 Generic Steady State Models of the LS system

$x_r = \frac{A_r}{k_r}\left(\left(P_s - P_{Ls}\right) - P_d\right)$	(3.1)
$-K_{sp}\theta_{sp} + T_{sp} + K_{pr2}P_s - K_{pr3}P_s\theta_{sp} - R_{py}A_yP_y = 0$	(3.2)
$\phi = \frac{D_mP_L - T_{mf}}{B_m}$	(3.3)
$Q_{r1}\left(x_{r01}, P_{s01}, P_{y01}\right) = Q_{r2}\left(x_{r02}, P_{y02}\right) = 0$ (For critically lapped spool)	(3.4)
$Q_s - Q_L - c_{pl}P_s = 0$	(3.5)
$Q_L - c_{ml}P_L - D_m\phi = 0$	(3.6)
$P_{Ls} = P_L$	(3.7)

Equation (3.2) can be re-expressed as

$$P_y = \frac{T_{sp}}{R_{py} A_y} + \frac{K_{pr2}}{R_{py} A_y} P_s - \frac{K_{sp}}{R_{py} A_y} \theta_{sp} - \frac{K_{pr3}}{R_{py} A_y} \theta_{sp} P_s \qquad (3.8)$$

Define:

$$T_{sp}^{'} = \frac{T_{sp}}{R_{py} A_y} \qquad \text{N·m}^{-2} \qquad (3.9)$$

$$K_{pr2}^{'} = \frac{K_{pr2}}{R_{py} A_y} \qquad \text{dimensionless} \qquad (3.10)$$

$$K_{sp}^{'} = \frac{K_{sp}}{R_{py} A_y} \qquad \text{N·m}^{-2}\text{·rad}^{-1} \qquad (3.11)$$

$$K_{pr3}^{'} = \frac{K_{pr3}}{R_{py} A_y} \qquad \text{rad}^{-1} \qquad (3.12)$$

Equation (3.8) can be now expressed

$$P_y = T_{sp}^{'} + K_{pr2}^{'} P_s - K_{sp}^{'} \theta_{sp} - K_{pr3}^{'} \theta_{sp} P_s \qquad 0 < \theta_{sp} < \theta_{sp\max} \qquad (3.13)$$

The particular form of Equation (3.13) is preferred here because the values of parameters $T_{sp}^{'}$, $K_{sp}^{'}$, $K_{pr2}^{'}$ and $K_{pr3}^{'}$ have been experimentally evaluated for the particular pump used in this study.

3.2.2 Steady State Operating Condition of the Load Sensing Regulator

The critically lapped spool design of the LS regulator necessitates a special consideration when solving the equation set. Equation (3.4) indicates that under steady state conditions, Q_{r1} and Q_{r2} are equal to zero for critically lapped spool design. This condition occurs when $x_r = 0$ or $x_r = x_{r0}$ (with other conditions attached). This gives rise to the identities

$$Q_{r1}\left(x_{r01}, P_{s01}, P_{y01}\right) = 0 \tag{3.14}$$

$$Q_{r2}\left(x_{r02}, P_{y02}\right) = 0 \tag{3.15}$$

where the subscript "$_{01}$" in Equation (3.14) represents the operating point with $x_{r0} > 0$ (i.e. the "charge" orifice is open) (see Figure 3.1). The subscript "$_{02}$" in Equation (3.15) represents the operating point with $x_{r0} < 0$ (i.e. the "discharge" orifice is open). It is now necessary to consider the condition under which these identities can occur.

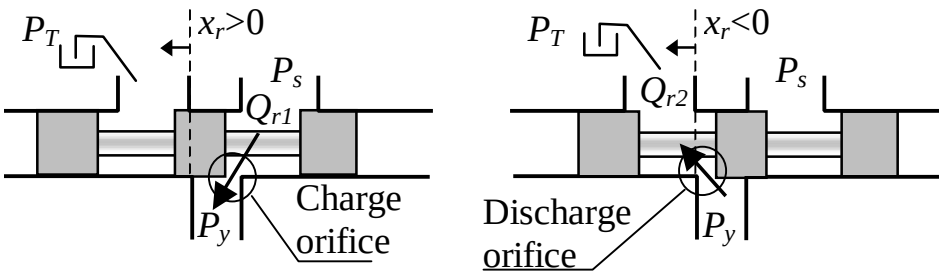

(a) (b)

Figure 3.1 LS Regulator: (a) the Control Chamber Charged
(b) the Control Chamber Discharged

Equations (2.11) and (2.12) shows that $A_s(x_r)$ is zero for $x_r \le 0$ (and hence $Q_{r1}(x_r)$ is zero), and $A_T(x_r)$ is zero for $x_r \ge 0$ (hence $Q_{r2}(x_r)$ is zero). Further, $A_s(x_r)$ and $A_T(x_r)$ are also zero at $x_r = 0$ (hence $Q_{r1}(0)$ and $Q_{r2}(0)$ are zero). With respect to Figure 2.2, the

flow to the control piston ($x_r > 0$), or the flow to the tank ($x_r < 0$) must be zero for steady state conditions; that is

$$\begin{cases} C_d A_s(x_{r0})\sqrt{\frac{2}{\rho}(P_{s0} - P_{y0})} = 0 & x_{r0} \geq 0 \\ Q_{r2} = 0 & \text{(blocked)} \end{cases} \tag{3.16}$$

and

$$\begin{cases} C_d A_T(x_{r0})\sqrt{\frac{2}{\rho}P_{y0}} = 0 & x_{r0} \leq 0 \\ Q_{r1} = 0 & \text{(blocked)} \end{cases} \tag{3.17}$$

The above analysis gives rise to the following conditions in which Q_{r1} or Q_{r2} are zero or both.

Condition I: $x_{r0} = 0$. (Q_{r1}= 0 and Q_{r2} = 0). This condition is obvious because the valve is critically lapped.

Condition II: $x_{r0} > 0$ (Q_{r1} = 0). This only occurs if $P_{s0} = P_{y0}$ (see Equation (3.16)).

Condition III: $x_{r0} < 0$ (Q_{r2} = 0). This can only occur if $P_{y0} = 0$ and $P_T = 0$ (see Equation (3.17)).

The aforementioned three conditions describe “possible” scenarios of the LS regulator with a critically lapped spool under steady state conditions in which the flow rates are zero. Whether the operating point exists or is stable for each condition depends upon control equations of other parts of the LS system shown (i.e. the control piston and pressure control pump in Figure 2.2 and the load in Figure 2.5), in particular, the steady state control characteristic of the pressure control pump. To assist in explaining the relationship between the above three conditions and the steady state control

characteristics of the pressure control pump, consider Figure 3.2 in which the control pressure, P_y, is plotted as a function of the pump pressure, P_s, and swash plate angle, θ_{sp} (see Equation (3.13)). The minimum swash plate angle, $\theta_{sp\min}$, is zero and the maximum, $\theta_{sp\max}$, is 0.32 radians for the pump studied. The regions or lines which reflect two of the three conditions are also labeled in Figure 3.2.

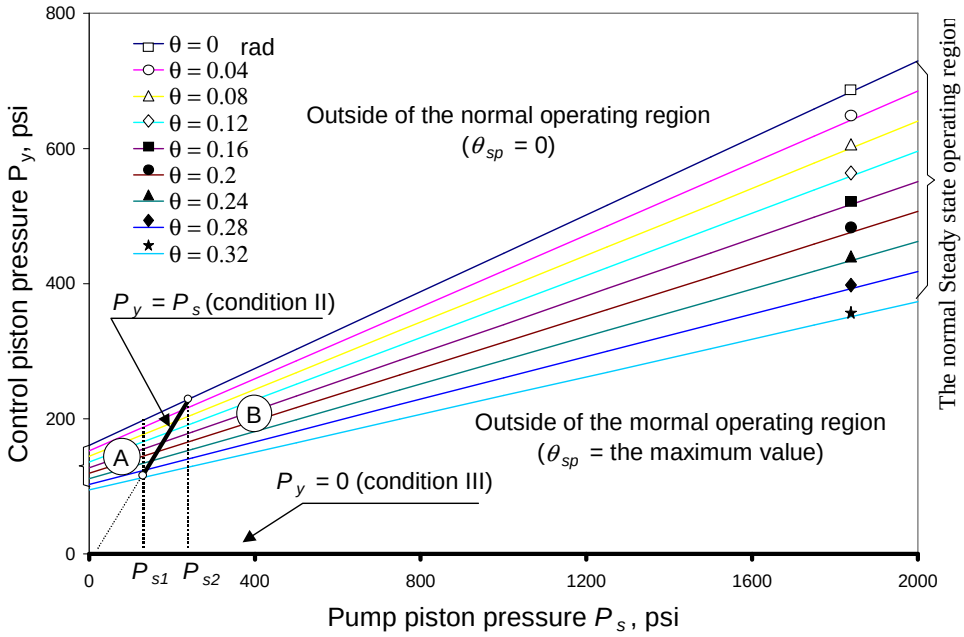

Figure 3.2 Steady State Characteristic of the Pressure Pump

Consider condition I. Condition I cannot be shown in Figure 3.2. This is because there is no explicit relationship between P_y and P_s for $x_r = 0$. Thus, P_{y0} and P_{s0} must be mathematically derived from other steady state equations. It is reasonable to expect that the solution may be any point in regions (A) and (B) which represent steady state operating regions permitted by the pressure control pump. However, any solution in region (A) does not make physical sense in the LS mode because, physically, P_y cannot

be greater than P_s under steady state condition. Therefore, only solutions in region (B) can be considered for $x_r = 0$.

Consider condition II. This condition requires that the control pressure, P_y, be equal to the pump pressure, P_s (see Figure 3.2). Possible operating points under condition II must be on the line ($P_y = P_s$) and within Q_{spmin} and Q_{spmax}; this line is also the boundary between regions (A) and (B). Pressures, P_s and P_y, at two terminal points can be determined by applying Condition II to Equation (3.13) to give

$$P_{s1} = \frac{T_{sp}^{'} - \theta_{sp\max} K_{sp}^{'}}{\theta_{sp\max} K_{pr3}^{'} + 1 - K_{pr2}^{'}} \tag{3.18}$$

and

$$P_{s2} = \frac{T_{sp}^{'}}{1 - K_{pr2}^{'}} \tag{3.19}$$

The specific operating point under condition II must also be mathematically determined.

Consider condition III. This condition requires that the control pressure, P_y, be zero. However, Figure 3.2 indicates that Condition III ($P_y = 0$) is outside the normal steady state operating region (B) of the pressure control pump. In fact, condition III represents the "fully stroked" status of the pressure control pump where the swash plate angle is limited to the maximum value. This often occurs if the pressure setting (such as P_d) of the LS system or the opening of the orifice (x_v) is very large, or the load is overrunning and theoretically would require more flow than the pump could deliver.

In order to solve for the operating point at each condition, the steady state equation sets with a critically lapped spool need to be expressed in a different way, as presented in the following section.

3.2.3 Steady State Equations Set

As a first step, ϕ (Equation (3.3)) is substituted into Equation (3.6). Further P_{Ls} (Equation (3.7)) is substituted into Equation (3.1). Thus the algebraic Equations (3.1), (3.13), (3.3) through (3.7) can be simplified into a set of four nonlinear equations and one assumed condition which can be one of Conditions I, II or III.

Substituting Equation (3.7) into (3.1) gives

$$\begin{cases} (P_{s0} - P_{L0}) = P_d & \text{for } x_{r0} = 0 \text{ (condition I)} \\ (P_{s0} - P_{L0}) > P_d & \text{for } x_{r0} > 0 \text{ and } P_y = P_s \text{ (condition II)} \\ (P_{s0} - P_{L0}) < P_d & \text{for } x_{r0} < 0 \text{ and } P_y = 0 \text{ (condition III)} \end{cases} \tag{3.20}$$

Equation (3.20) is expressed as an inequality because the discussion in this chapter is more interested in the sign of x_{r0} than the magnitude of x_{r0}. (See Equation (3. 28))

In order to reflect Condition III in the relationship between the swash plate angle, θ_{sp}, P_s, and P_y, Equation (3.13) is expressed as

$$\begin{cases} P_y = T'_{sp} + K'_{pr2} P_s - K'_{sp} \theta_{sp} - K'_{pr3} \theta_{sp} P_s & 0 < \theta_{sp} < \theta_{sp\max} \\ \theta_{sp} = \theta_{sp\max} & P_y = 0 \end{cases} \tag{3.21}$$

Substituting Equations (2.34) and (2.38) into Equation (3.5) in Table 3.1 results in

$$\frac{NA_p R_p \omega \tan\theta_{sp}}{\pi} - C_d w x \sqrt{\frac{2}{\rho}(P_s - P_L)} - c_{pl} P_s = 0 \tag{3.22}$$

It must be noted that Q_{r1} is equal to zero (steady state) in the expression for Q_s.

In a similar fashion, Equation (3.6) can be expressed as

$$C_d w x \sqrt{\frac{2}{\rho}(P_s - P_L)} - \left(c_{ml} + \frac{D_m^2}{B_m} \right) P_L + \frac{D_m T_{mf}}{B_m} = 0 \tag{3.23}$$

Equations (3.20), (3.21), (3.22) and (3.23) are the four equations to be used to solve for operating points (x_{r0}, θ_{sp0}, P_{s0}, P_{l0}, P_{y0}). It is apparent that there are five variables and four non-linear equations. To solve these equations, one parameter value must be assumed; for example, x_{r0} is zero for condition I, P_{y0} equals to P_{s0} for condition II, and P_{y0} is zero for condition III. Using one of these conditions, all other parameters can be solved. Because P_{Ls0} and ϕ_0 are uniquely determined by P_{L0} (see Equations (3.3) and (3.7)), solving for these variables is straight forward and will not be considered in subsequent sections.

3.3 Solving for the Steady State Operating Point

In this section, the solutions of the steady state equation sets for the three conditions are discussed separately. For each condition, the general solution of the operating point is developed associated with x_{r0}, θ_{sp0}, P_{s0}, P_{L0}, P_{y0}.

3.3.1 Solution of the Steady State Equation Sets under Condition I ($x_{r0} = 0$)

Consider the load pressure P_{L0}. Substituting Equation (3.20) into Equation (3.23) and then re-organizing the equation results in

$$P_{L0} = \frac{1}{\left(c_{ml} + \frac{D_m^2}{B_m}\right)}\left[C_d w x \sqrt{\frac{2P_d}{\rho}} + \frac{D_m T_{mf}}{B_m}\right] \tag{3.24}$$

Again, it must be noted that P_d is not a true physical pressure but an equivalent pressure term. Recall that the value of P_d is equal to the designed external pressure differential, $\left(P_{s0} - P_{L0}\right)$, which, under the steady state condition, forces the spool to its null position (refer to Figure 2.2). The load pressure, P_{L0}, of the operating point under steady state conditions can been directly computed via Equation (3.24). Equation (3.24) indicates

that the larger the motor leakage, the smaller the load pressure is. There are two terms in the square bracket of Equation (3.24). The first term is the load flow and the second term is a flow which is proportional to the resistant torque on the axle of the motor with the load. Therefore, the larger the flow rate entering the motor and the higher the load resistant torque, the higher the load pressure is.

To calculate the pump pressure P_{s0}, it is necessary to substitute Equation (3.24) back into Equation (3.20) to give

$$P_{s0} = P_d + P_{L0} \tag{3.25}$$

To find the swash plate angle, θ_{sp0}, Equation (3.20) is substituted into Equation (3.22) and re-organized to give

$$\theta_{sp0} = \tan^{-1}\left[\frac{\pi}{NA_p R_p \omega}\left(C_d wx\sqrt{\frac{2P_d}{\rho}} + c_{pl}P_{s0}\right)\right] \tag{3.26}$$

where P_{s0} is determined using Equation (3.25).

To determine the control pressure P_{y0}, it is necessary to substitute the values of Equations (3.25) and (3.26) into Equation (3.21) to give the control pressure under the steady state condition as

$$P_{y0} = T_{sp}^{'} + K_{pr2}^{'}P_{s0} - \left(K_{sp}^{'} + K_{pr3}^{'}P_{s0}\right)\theta_{sp0} \tag{3.27}$$

Equations (3.24), (3.25), (3.26) and (3.27) can now be sequentially solved to give the value of four variables under the steady state condition $x_{r0} = 0$ (condition I). However, it should be noted that the operating points calculated from the above equations, may not always exist in the operating region. It is necessary to check if the solution of each variable is in the normal operating region. This approach is now explained.

Whether the operating point with condition I exists or not is determined by checking two requirements. First, the swash plate angle, θ_{sp0}, calculated by the flow continuity Equation (3.26) must be smaller than the maximum angle, θ_{spmax}. Then, the control pressure, P_{y0}, computed by Equation (3.27) must be smaller than the pump pressure, P_{s0}, by Equation (3.25).

The above two requirements have a physical interpretation. The first requirement ($\theta_{sp} < \theta_{sp\max}$) implies that the flow demanded by the load plus the pump leakage which corresponds to the swash plate angle, θ_{sp0}, must be smaller than the maximum flow delivered at the maximum swash plate angle, θ_{spmax}. If this is not true, the LS pump must be in the "fully stroked" status (i.e. condition III). The second requirement means that, if the control pressure, P_{y0}, computed by Equation (3.27) is larger than the pump pressure, P_{s0}, then this situation results in a physically unrealizable condition under steady state conditions.

3.3.2 Solution of the Steady State Equation Sets under Condition II ($P_{s0} = P_{y0}$)

Figure 3.2 shows that the pump pressure under condition II must be in region [P_{s1}, P_{s2}]; that is, the pump pressure must be less than P_{s2} in Figure 3.2.

$$P_{s0} < P_{s2} \tag{3.28}$$

Now from Equation (3.20), P_s must satisfy the relationship

$$P_{s0} > P_d + P_{L0} \tag{3.29}$$

Combining inequalities (3.28) and (3.29) results in

$$P_{L0} < P_{s2} - P_d \tag{3.30}$$

This indicates that the operating point with condition II may only exist when $P_{L0} < P_{s2} - P_d$. If P_d is set to a larger value than P_{s2}, the inequality would never be

established because pressures P_{L0} is always positive unless a runaway load exists. This implies that no operating point exists with condition II and $P_d > P_{s2}$. Therefore, the operating point with condition II can exist only when P_d is smaller than P_{s2}. Again, because P_d is always positive and P_{s2} usually is small (e.g. for the pump studied, P_{s2} = 1.55 MPa), the operating point with condition II exists when P_d is smaller than P_{s2} and P_{L0} is small.

Condition II of Equation (3.20) gives the equality relationship between the control pressure, P_{y0}, and the pump pressure, P_{s0}, but does not give the value of x_r like condition I. This results in a different method of solving the non-linear equation sets.

For the convenience of iteratively solving for the SSOP, Equation (3.22) can be rearranged as

$$\frac{NA_p R_p \omega \tan(\theta_{sp})}{\pi} = C_d w x \sqrt{\frac{2}{\rho}(P_s - P_L)} - c_{pl} P_s \tag{3.31}$$

Equation (3.31) involves three unknown variables, θ_{sp}, P_s and P_L. In order to solve for the SSOP of the LS system under Condition II, Equations (3.21) and (3.23) have to be used.

Equation (3.21) can be rearranged to reflect condition II as

$$\theta_{sp}(P_s) = \frac{T'_{sp} + (K'_{pr2} - 1)P_s}{K'_{sp} + K'_{pr3} P_s} \qquad 0 \le \theta_{sp} \le \theta_{sp\max} \text{ and } P_y = P_s \tag{3.32}$$

It is noted that the pump pressure, P_s, in Equation (3.32) is not labeled with the subscript '$_0$' because at this point P_s is not known. Indeed, all subsequent equations will not bear the "$_0$" subscript until P_s can be solved.

Equation (3.23) can be rearranged to express P_L as a function of the P_s as

$$P_L = \frac{-b_2 + \sqrt{b_2^2 - 4b_1 b_3}}{2b_1} \tag{3.33}$$

where $b_1 = a_1^2$, $b_2 = a_3 - 2a_1 a_2$, and $b_3 = a_2^2 - a_3 P_s$. The coefficients, a_1, a_2, and a_3, can be further expressed as $a_1 = c_{ml} + \frac{D_m^2}{B_m}$, $a_2 = \frac{D_m T_{mf}}{B_m}$, and $a_3 = \frac{2C_d^2 w^2 x^2}{\rho}$. Substituting Equations (3.32) and (3.33) into Equation (3.31) yields a non-linear algebraic equation to solve for P_{s0} (and P_{y0} due to $P_{s0} = P_{y0}$ under Condition II) under steady state conditions. Then, substituting P_{s0} into Equations (3.32) and (3.33) obtains θ_{sp0} and P_{L0} respectively.

Similar to the approach of Section 3.3.1, it is necessary to check if the operating point calculated above is on the line ($P_{s0} = P_{y0}$) of Figure 3.2. Firstly, the pump pressure, P_{s0}, must satisfy $P_{s1} \le P_{s0} \le P_{s2}$. Then, the basic relationship of condition II ($P_{s0} - P_{L0} > P_d$) must be met.

3.3.3 Solution of the Steady State Equations Set under Condition III ($\theta_{sp0} = \theta_{sp0max}$; $P_y = 0$)

It was mentioned that condition III represented the "fully stroked" status of the pressure control pump in which the swash plate angle, θ_{sp}, was limited to its maximum value, θ_{spmax}. In order to avoid this operating condition when designing a LS system, or to diagnose what causes this operating condition, it is necessary to develop the mathematic solution of the operating point at this operating condition.

If condition III exists, $\theta_{sp0} = \theta_{sp\max}$ (Equation (3.21)) and $P_{y0} = 0$ (Equation (3.20)). Because the leakage flow is very small relative to the delivered pump flow and the load flow rate when the pump is fully stroked, the leakage term in Equation (3.31) can be

neglected, and as a consequence, the first term in Equation (3.23) is constant and approximately equals to the maximum pump flow delivery. Therefore, the load pressure can be directly obtained from Equation (3.23), that is,

$$P_{L0} = \frac{1}{\left(c_{ml} + \frac{D_m^2}{B_m} \right)} \left[\frac{NA_p R_p \omega \tan \theta_{sp\max}}{\pi} + \frac{D_m T_{mf}}{B_m} \right] \tag{3.34}$$

Neglecting pump leakage (the third term) of Equation (3.31) and rearranging Equation (3.31) gives

$$P_{s0} = P_{L0} + \frac{\rho}{2} \left(\frac{NA_p R_p \omega \tan \theta_{sp\max}}{\pi C_d A_v} \right)^2 \tag{3.35}$$

Again, the method of checking the operating point presented in Section 3.3.2 is used. First, the numeric solution, P_{s0}, of Equation (3.35) can be substituted into Equation (3.33) to obtain the load pressure, P_{L0}, and to further check the basic condition of condition III ($P_{s0} - P_{L0} < P_d$).

To summarize, the method of finding the operating point of the LS system is to solve each non-linear algebraic equation with three possible operating conditions and to check if the operating point exists in each condition. There is at most one operating point among the three conditions.

3.4 Procedure for Solving for the Steady State Operating Point

This section presents the flow chart for solving for the SSOP of the LS system (Figure 3.3). Because, before the steady state analysis process begins, there is no obvious knowledge of the operating condition in which the LS system operates, an operating condition must be assumed — for example — the normal operating Condition I (Step (1) in Figure 3.3). Calculating Equations (3.24), (3.25), (3.26) and (3.27) gives

the SSOP directly (Step (2)). Then, Steps (3) and (4) determine if the result satisfies the essential conditions.

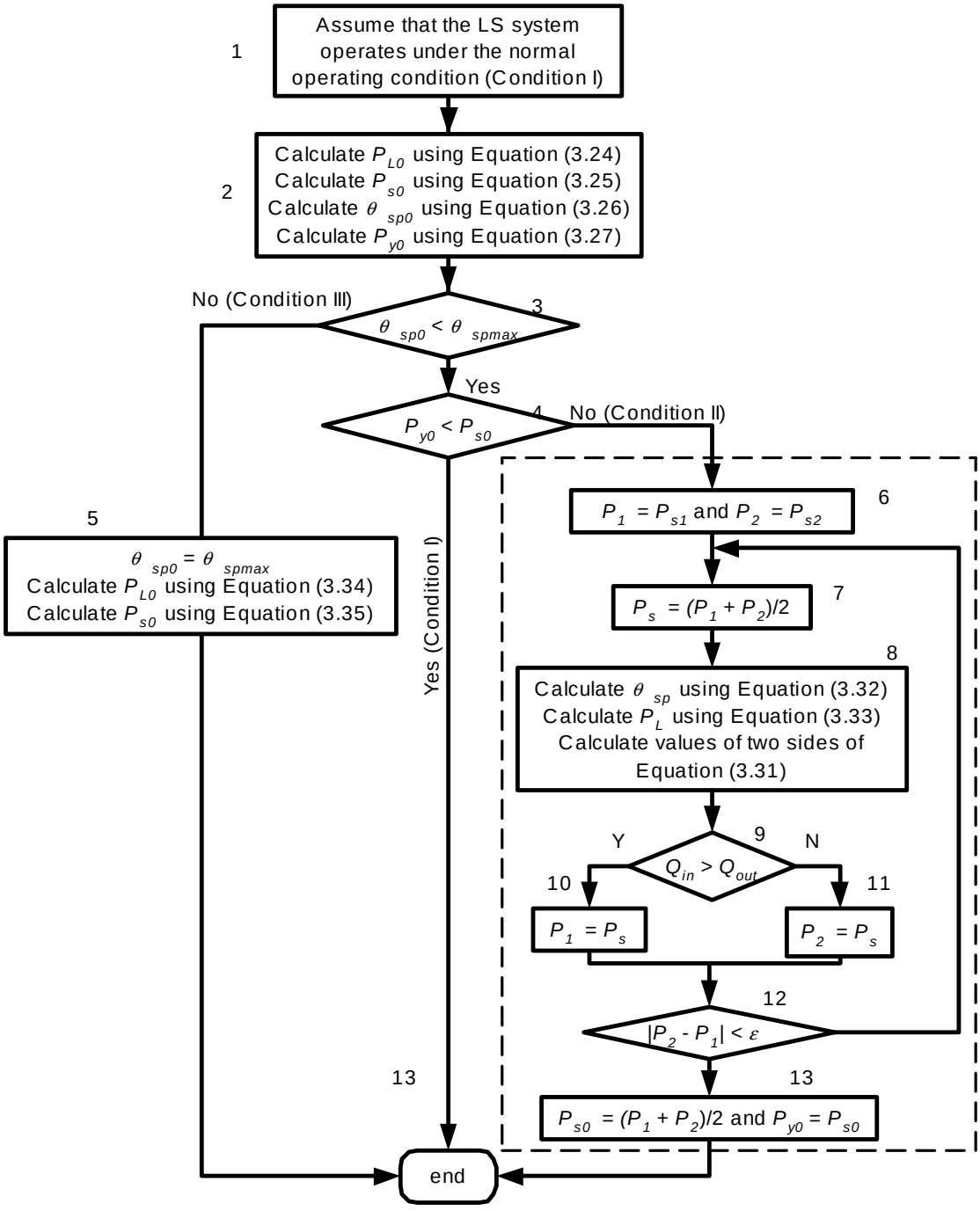

Figure 3.3 Flow chart of solving for the SSOP of the LS system

It is impossible in practice for the swash plate angle to be larger than the maximum value. If the calculation result gives this result, this indicates that the LS system could not operate under Condition I. In this case, the LS system must operate under Condition III. Therefore, the SSOP should be calculated by Equations (3.34) and (3.35). It is noted that the solutions under Conditions I and III do not require the iteration calculation.

If the control pressure, P_{y0}, computed by Equation (3.27) in Step (2) is larger than the pump pressure, P_{s0}, then this situation results in a physically unrealizable condition under steady state conditions. In this case, the LS system must operate under Condition II. The dashed line box in Figure 3.3 is the flow chart of the iteration for computing the SSOP of the LS system for this condition, because substituting Equations (3.32) and (3.33) into Equation (3.31) cannot give a direct expression of P_{s0}.

The method of iteration is as follows: a region [P_1, P_2] of the pump pressure, P_s, in which the solution of SSOP is located, is first selected. Because the pump pressure, P_{s0}, and the control pressure, P_{y0}, are equal and must be a value between P_{s1} and P_{s2} (see Figure 3.2), the first region is selected to be [P_1, P_2] =[P_{s1}, P_{s2}] (Step (6)). A pump and control pressure is assumed to be $0.5(P_1 + P_2)$, at the mid-point in the region (step (7)). The swash plate angle, θ_{sp}, and the load pressure, P_L, are then determined using $0.5(P_1 + P_2)$ via Equations (3.32) and (3.33) and are substituted into both sides of Equation (3.31). The value of the left hand side is the pump flow, i.e. the input flow rate of the pump chamber (here defined as Q_{in}), while the value of the right hand side represents the output flow rate of the pump chamber (here defined as Q_{out}). If $Q_{in} > Q_{out}$ (step (9)), the pump volumetric flow rate has to be reduced. According to Figure 3.2, reducing Q_{in} along the straight line ($P_s = P_y$) implies increasing pump pressure. In other

words, the solution of the pump pressure, P_s, must be larger than the pressure, $0.5(P_1 + P_2)$. Therefore, the new region becomes [P_1, P_2] = [$0.5(P_1 + P_2)$, P_2] (Step (11)), otherwise, this region becomes [P_1, P_2] = [P_1, $0.5(P_1 + P_2)$] (Step (12)). 20 iterations is about all that is required to reduce the length of the region from the initial value of 0.79 MPa to 0.75 Pa. The final result for Condition II is given by Step (13). The calculation based on the flow chart shown in Figure 3.3 can give the operating condition (I, II, or III) under which the LS system is operating, as well as the SSOP of the LS system.

3.5 Summary

This chapter has demonstrated that the operating point of the LS system with a critical center spool of the LS regulator is determined by three conditions. As condition I, the LS regulator spool displacement of the operating point under steady state conditions, x_{r0}, is always at the null position for the LS regulator with a critically lapped spool. In this case, the value of all state variables can be obtained directly.

Under condition II, the control pressure and the pump pressure are the same. This would occur when the system pressure differential setting, P_d, is small. Condition III represents the "fully stroked" status of the pump. When the opening of the flow control valve is quite large (which results in a small pressure differential, $P_{s0} - P_{L0}$), this condition could occur. This chapter also gives a flow chart which summarizes the procedure for solving for the SSOP of the LS system.

Chapter 4 Experimental Verification of the Steady State Operating Point of the Load Sensing System

4.1 Introduction

In Chapter 3, the mathematical model for solving for the SSOP of the LS system was developed. The objective of this chapter is to experimentally verify the theoretical solution of the SSOP.

In the steady state analysis of the LS system, the load pressure is assumed to be a controlled input. Therefore, in this part of the study, the steady state load pressure, P_{L0}, is established using a relief valve, instead of using a motor load. Adjusting the load pressure, P_{L0}, the opening of the flow control valve, A_v, or the pressure differential setting, P_d, can all cover changes in the SSOP.

In the subsequent sections, the experimental platform and the measurement system are discussed first. Finally a comparison of the experimental and theoretical SSOP's is presented.

4.2 Experimental System

Because the main interest of this chapter is the experimental verification of the SSOP, and not the dynamic response, a simple relief valve was used to replace the hydraulic motor as the load.

The schematic of the experimental system is shown in Figure 4.1. Six variables, the pump pressure, P_s, the control pressure, P_y, the load pressure, P_L, the swash plate angle, θ_{sp}, the LS spool displacement, x_r, and the fluid temperature, T, were measured. The relief valve located directly after the pump was used to protect the system in case of a

failure in the pressure compensator. A relief valve located down stream of the flow control valve was used to create a constant pressure load.

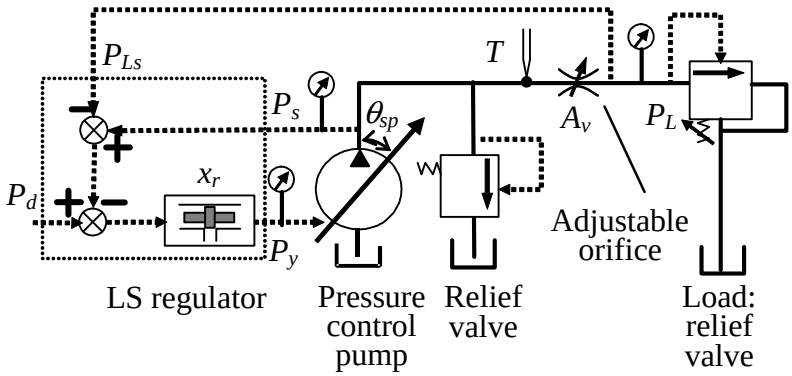

Figure 4.1 Schematic of Load Sensing (LS) System

In order to verify the theoretical model developed in Chapter 3, it is necessary to compare the experimental results to those obtained from theoretical computations. It is noted that the coefficients or constants used in the theoretical model must be consistent with those of their experimental counterparts. Some of these coefficients can be found from manufacturer specifications (pump volumetric displacement, for example); others need to be obtained from experimental results (leakage coefficient, for example). This chapter, then, considers the calibration of all transducers, the characteristics of certain components and the identification of certain system parameters that cannot be obtained directly.

4.2.1 Measurement System

There are four types of physical quantities to be measured; pressure (the pump pressure, P_s, the control pressure, P_y, and the load pressure, P_L), the swash plate angle, θ_{sp}, the spool displacement of the LS regulator, x_r, and the fluid temperature, T. Figure 4.2 shows a schematic of the instrumentation and the Data Acquisition system (DAQ)

used in the experimental system. Each channel includes a transducer, a signal conditioning circuit and an A/D converter. All signals are converted into DC voltage signals which can be monitored visually by multimeters. This setup facilitated the "zeroing" of appropriate transducer outputs for all tests.

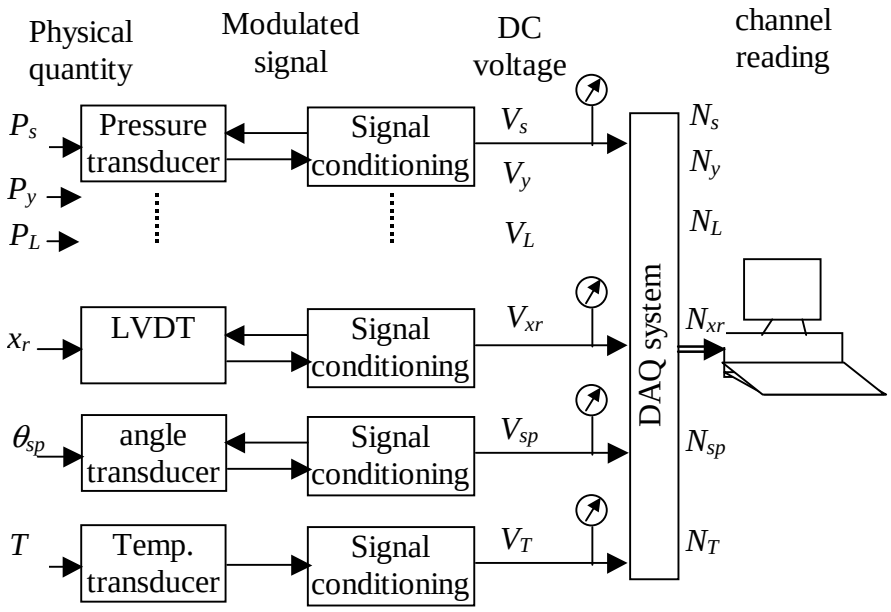

Figure 4.2 Transducers, Signal Conditioners and the DAQ of the LS System

The purpose of the measurement system calibration was to determine the relationships between channel readings (output from the DAQ) and physical quantities such as pressures and displacements. These relationships reflect the gain of transducers and include the measurement error. The measurement system can be considered as a cascade of two subsystems: the sensing system and the DAQ system. The gains and measurement error of the DAQ system are the same for all channels. The error associated with the DAQ is mainly introduced by the limitation of the "word length". For this study, the DAQ system uses a multifunction interface board (model: CIO-DAS16) with 16 channels of A/D converters and 4 channels of D/A converters. The

word length of the DAQ system's A/D and D/A converters is 12 bits. For the specific setting (range = [-5, 5]; gain = 1), the resolution of the A/D and D/A converters is 2.44 mv. The bias error is measured to be –3.3 mv when each channel is set to 0 volt. The bias error can be removed through the use of an appropriate software algorithm.

The gain and the measurement error of the transducers and signal conditioners depend on the gain and sensing error of each measurement system. Calibration procedures are necessary in order to determine the gain relationship and sensing error between the physical quantities and the DC voltage outputs. According to experimentation and uncertainty theory, measurement error or uncertainty of transducers is expressed as the square root of the sum of the squares of the random error and bias error [Coleman and Steele, 1999]. As previously discussed, the bias error of the A/D converter can be readily compensated. The bias error of the sensing system is mainly caused by a slow zero drift of the signal conditioning circuit. This can be minimized by "re-zeroing" each system before each test. Therefore, the following section will focus on the calibration of the sensing system via the transducer gain and the random measurement error.

Because the sensing error of the transducers and the signal conditioner and the A/D converter error are independent, the overall random error can be calculated by

$$e = \sqrt{(Ke_s)^2 + e_c^2} \tag{4.1}$$

where e_s is the sensing random error, e_c is the A/D converting error, and K is the gain of the A/D converter. In this case, the A/D converter gain is set to equal to 1.

The calibration of pressure sensors for the measurements of LS pump, control piston and the load pressure, angle position sensor for the measurement of the swash plate angle, and Proximator for the measurement of the displacement of the LS spool are given in Appendix B.

4.2.2 Determination of Relevant Parameters for the Load Sensing System

4.2.2.1 Load Sensing Regulator

A schematic of the LS regulator used in this study is shown in Figure 4.3. The regulator consists of the body, the LS spool, an end cap, the balance spring, an adjustable screw and a spring guide. The spring and spool are separated by a spring end cap. Adjusting the screw moves the spring guide, the spring, the end cap and the spool.

Parameters of the LS regulator associated with SSOP theoretical models are the pressure differential setting, P_d, the cross-sectional area of the spool, A_r, and the spring coefficient, k_r. A_r and k_r were measured to be 31.7 mm^2 and 61.1 N/mm respectively. The P_d has to be determined through the value of setting x_{ri} (see Figure 4.3). This is now considered.

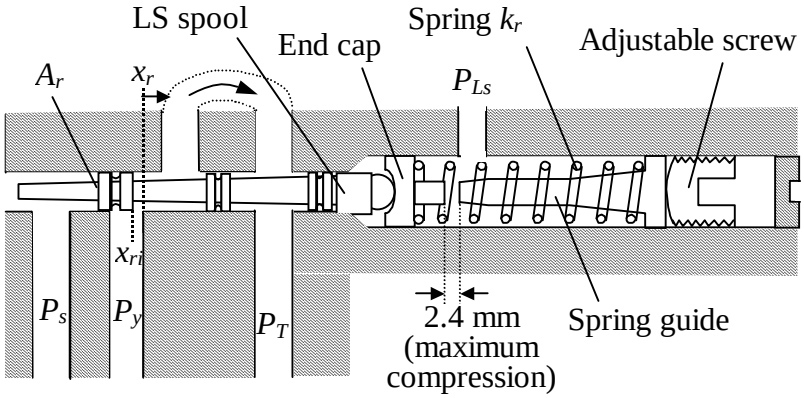

Figure 4.3 LS Regulator of the Pressure Control Pump

It has been mentioned that P_d is not a true physical pressure but an equivalent pressure term. The value of P_d is equal to the external pressure differential which forces the spool to its null position (refer to Figure 4.3). In order to calculate P_d, the schematic of the LS regulator related to the pressure differential setting, P_d, is shown in Figure 4.4.

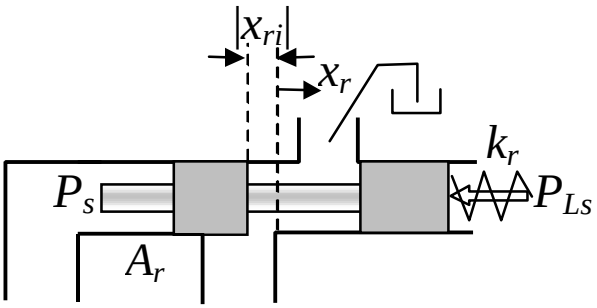

Figure 4.4 Coordinate Definition of the LS Regulator Spool Displacement

Under steady state condition, the spring force, F_{sp}, can be expressed as

$$F_{sp} = k_r \left(x_r - x_{ri} \right) \tag{4.2}$$

where x_r is the displacement of the LS regulator spool and whose direction is defined opposite to the direction of the spring force exerted on the spool. x_{ri} is the initial displacement of spool. k_r is the spring coefficient. When x_r is equal to x_{ri}, the spring force is zero. When x_r is forced to zero by an external force under steady state, the external force will balance the spring force which can be determined by

$$F_{ext} = F_{sp} = -k_r x_{ri} \tag{4.3}$$

When the LS regulator operates in the LS system, the external force is determined by the product of the pressure differential on the spool and the sectional area of the spool, that is

$$F_{ext} = A_r \left(P_s - P_{Ls} \right) \tag{4.4}$$

The pressure differential, $(P_s - P_{Ls})$, under the condition $x_r = 0$ (i.e. the system pressure differential setting P_d according to the definition) can thus be determined by combining Equation (4.3) and Equation (4.4) as

$$P_d \triangleq (P_s - P_{Ls})\big|_{x_r=0} = -\frac{k_r}{A_r} x_{ri} \tag{4.5}$$

The subscript '$_{ri}$' is used to distinguish the initial position from the operating point '$_{r0}$'. It is noted that x_{ri} must be negative, that is, the "discharge" orifice of the LS regulator is always open before the system starts operation (see Figure 4.4). For the LS regulator study, the manufacture setting of initial displacement is –1.27 mm. The derived parameter, P_d, is thus calculated to be 2.45 MPa. P_d can be decreased by adjusting the spring pretension screw (via an adjustable screw) out so as to reduce the absolute value of x_{ri}. In contrast, P_d can be increased by tightening the adjustable screw (i.e. increasing the absolute value of x_{ri}).

4.2.2.2 Pressure Compensated Pump

Figure 4.5 shows the schematic of the pressure compensated pump (Model: Vickers PVE 10) with its control piston (note there are two types of pistons: pumping pistons and a control piston). The theoretical delivery at maximum RPM (1800 rpm) and maximum swash plate angle (18 degree) is 73.44 lpm (19.4 US gpm). When the pump shaft rotates, each pump piston rotates around the pump shaft as well as translates along the piston sleeve. The displacement of each piston changes in the cylinder sleeve as the piston and sleeve assembly rotate along the swash plate. Each piston draws flow from the tank for half the rotary cycle and discharges fluid for the other half of the cycle. Leakage in the pump can follow three paths: through the clearance between this piston and its sleeve,

between the piston assembly and the valve plate and between the piston shoe slipper assembly and the swash plate.

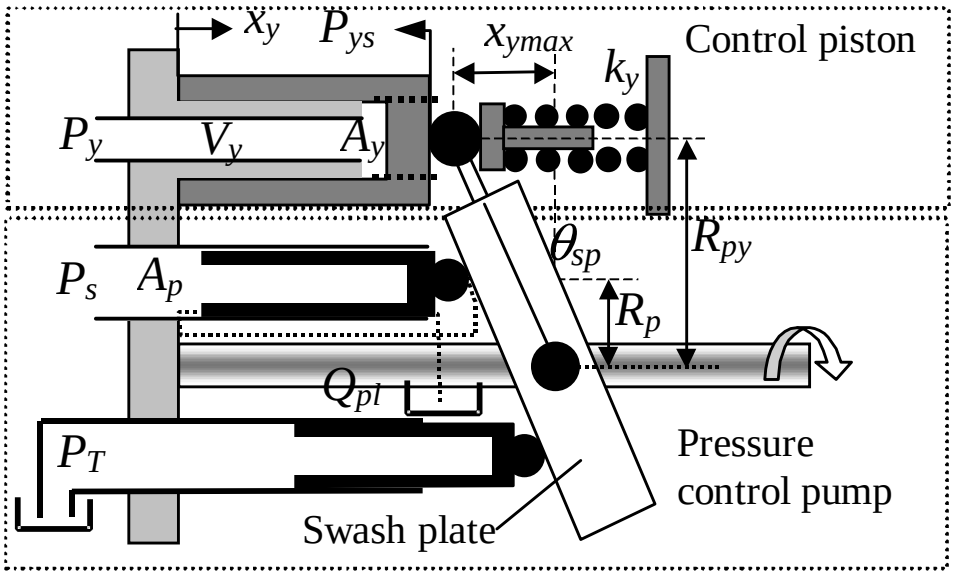

Figure 4.5 Pressure Control Pump with Control Piston

Many pump parameters must be determined; these can be divided into three types. The first type is defined as structure parameters which are used to determine the pump effective gain, C_{pss} (which relates the pump flow to the swash plate angle). Mathematically, this was given in Section 2.1.1 as

$$C_{pss} = \frac{Q_p}{\theta_{sp}} = \frac{D_p \omega}{\theta_{sp}} = \frac{NA_p R_p \omega \tan(\theta_{sp})}{\pi \theta_{sp}} \tag{4.6}$$

For the pressure compensated pump in this study, the pump gain varies from 3.96 lpm/deg. (1.04 gpm/degree) at θ_{sp} = 18° to 4.09 lpm/deg. (1.08 gpm/degree) at θ_{sp} =0 and at a rotary speed of 1800 rpm. It is noted that C_{pss} represents the steady state gain of the pump while C_p (see Equation (2.37)) is the linearization gain of the pump. C_{pss} is

used to calculate the SSOP of the LS system and C_p is used for the linearization and dynamic analysis of the LS system.

The second type is made up of the torque balance parameters which describe the relationships between the pump pressure, P_s, the control pressure, P_y, and the swash plate angle, θ_{sp}. These parameters are $T_{sp}^{'}$, $K_{sp}^{'}$, $K_{pr2}^{'}$ and $K_{pr3}^{'}$ (refer to Equation (3.34)).

The third type is the hydraulic parameters, for example, the leakage coefficient, c_{pl}. The parameters of the first type are known because they are measurable or specified by the manufacturer. The second type of parameters for this specific pump was determined by Bitner [1996] and Huh et al [2000]. The third type, however, was unknown and had to be measured. The procedures involved in making these measurements of the third type are now considered.

Consider a situation where the load ports are blocked (no flow condition). The second term of Equation (3.35) is zero giving,

$$c_{pl} = \frac{NA_p R_p \omega \tan\theta_{sp}}{\pi P_s} \tag{4.7}$$

Equation (4.7) can be expressed as

$$c_{pl} = \frac{NA_p R_p \omega \tan\theta_{sp}}{\pi \theta_{sp}} \frac{\theta_{sp}}{P_s} = C_{pss} \frac{\theta_{sp}}{P_s} \tag{4.8}$$

The only fluid that the pump is delivering is due to leakage. Therefore, the swash plate angle is very small and $\tan(\theta_{sp}) \approx \theta_{sp}$. C_{pss} is a known constant, $\frac{NA_p R_p \omega}{\pi}$, and θ_{sp} and P_s are measurable; then c_{pl} can be calculated from the slope of a plot of $C_{pss}\theta_{sp}$ versus P_s.

In order to obtain the slope of a plot of $C_{pss}\theta_{sp}$ versus P_s by measuring θ_{sp} and P_s (without load flow), it is essential to measure many points ([P_{si} ,θ_{spi}], i = 1, 2,. …). The pump pressure, P_s, must be variable. The regulator shown in Figure 4.6 is used to explain the method of varying P_s. The LS regulator (lower part) and a pressure compensator (upper part) are normal components in a commercial pressure regulator. The pressure compensator is used to limit the pump pressure for safety. The pump pressure, P_s, can be adjusted using the adjustable screw of the LS spool (i.e. changing pressure differential setting, P_d), or by the adjustable screw of the pressure compensator spool (see Figure 4.6). If the pressure, P_s, was adjusted by changing P_d (i.e. by adjusting the LS spring adjustable screw), P_s would only reach the maximum design value of P_d (4.6 MPa) because the load pressure was zero in this experiment (note $P_s - P_L = P_d$) and the adjustable screw could only be moved a limited amount, Δx_{rmax}. But the pump pressure under normal operating conditions would be higher than this value due to the presence of the load pressure. Thus, a wide pressure range could not be created. The other way to adjust P_s was by keeping LS orifice open by completely tightening the LS adjustable screw ($x_r < 0$) and then adjusting the screw of the pressure compensator of the LS regulator assembly in order to vary the pump pressure P_s. Under these operating conditions (i.e. No load flow with the “discharge” orifice of the LS regulator opened), the pump pressure was almost equal to the pressure of the compensator spool spring (i.e. deadhead pressure) due to the very small flow rate (i.e. the pump leakage).

Figure 4.7 shows a typical test result at a fluid temperature of 41°C in which $C_{pss}\theta_p$ is plotted as a function of P_s. This result indicates that the relationship between the flow leakage ($C_{pss}\theta_p$) and the pump pressure approximates a linear relationship. The leakage

coefficient at 41°C is calculated to be 0.13 lpm/MPa (or, 2.17×10^{-12} m^3/s/Pa). Figure 4.8 is the plot of the leakage coefficients as a function of the fluid temperature. The position of the temperature transducer was close to the drain port of the pump casing to the tank. The curve shown in Figure 4.8 indicates that the pump leakage increases as the fluid temperature increases. This is as expected since pump leakage is laminar and the viscosity which is significantly affected by fluid temperature is related to the flow rate. Theoretically, the relationship between the flow rate and viscosity is the reverse ratio for laminar flow conditions.

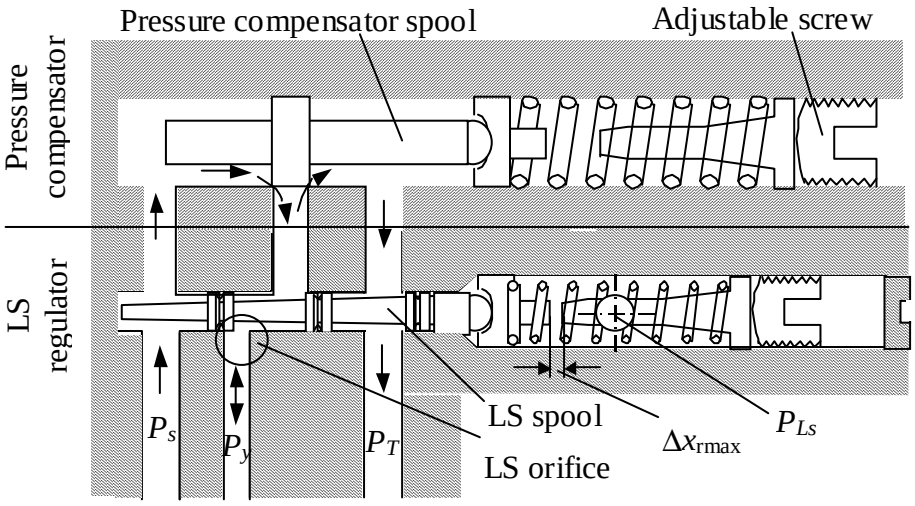

Figure 4.6 Pressure Regulator Assembly

This section has discussed the estimation or measurement of the pump parameters; the pump gain, C_{pss}, the torque equivalent parameters ($T_{sp}^{'}$, $K_{sp}^{'}$, $K_{pr2}^{'}$ and $K_{pr3}^{'}$) and the pump leakage coefficient, c_{pl}, which are essential to calculate SSOP of LS systems. These parameters will be used in the subsequent sections.

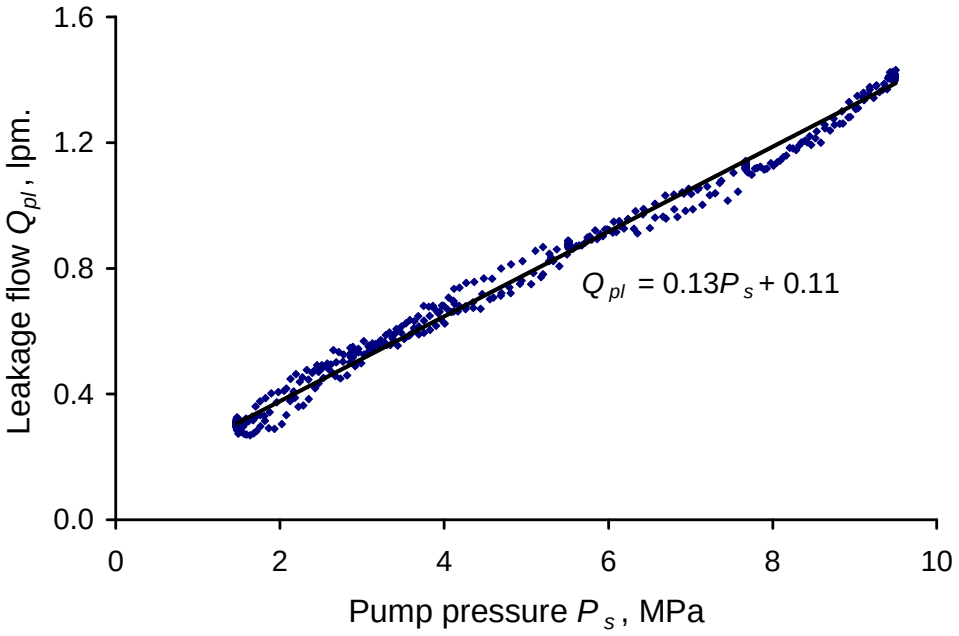

Figure 4.7 Estimation of the Pump Leakage Coefficient

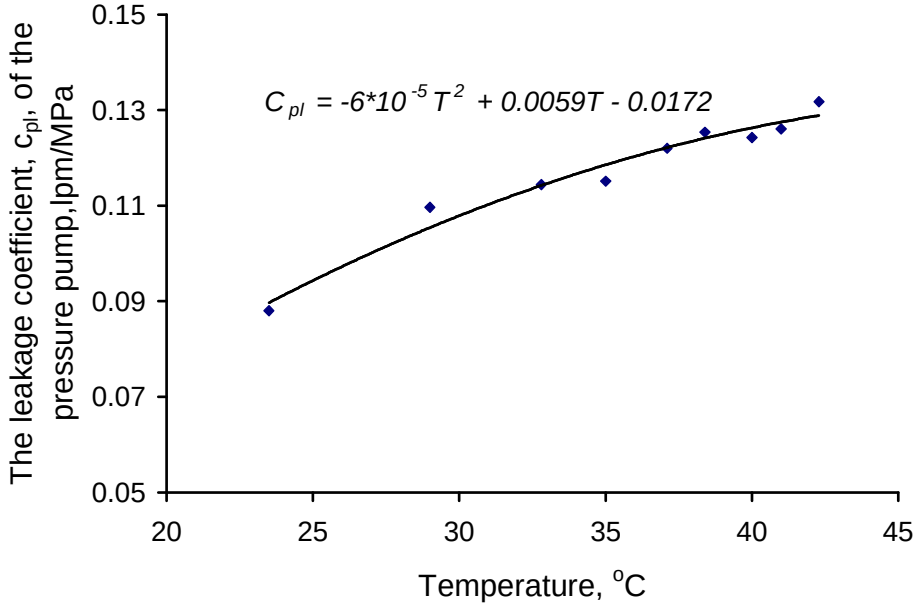

Figure 4.8 Leakage Coefficient as a Function of the Fluid Temperature

4.2.2.3 Parameters of the Needle Valve

In this study, a needle valve was used (See A_v in Figure 4.1) to create the "fixed" orifice for the LS system. In order to predict SSOP of the LS system, two parameters, the flow cross sectional area, A_v, and the discharge coefficient, C_d, of the adjustable orifice must be known. A_v is a function of the displacement, x_v, of the spool of needle valve (or in this case the "turn number" of the valve knob). For the studied needle valve, the relationship was determined by Huh et al [2000] and can be presented as a piece-wise linear function as

$$A_v = \begin{cases} 2.4N_{xv} & 0 \le N_{xv} \le 2.5 \\ 16N_{xv} - 34 & 2.5 \le N_{xv} \le 4 \end{cases} \tag{4.9}$$

where N_{xv} is the number of turns on the needle valve.

Another important parameter which was needed to describe the uncompensated needle valve was C_d. C_d is a function of the Reynolds number, *Re*, which can be experimentally determined. The experimental method and result of the discharge coefficient, C_d, are presented in Appendix C, (Wu, et al [2002]). For the studied needle valve, the empirical model of C_d is re-written as

$$C_d = 0.75 - 2.47e^{-0.22\sqrt{\mathrm{Re}}} + 1.72e^{-0.28\sqrt{\mathrm{Re}}} \tag{4.10}$$

4.2.3 Discussion of Experimental Procedures

The hydraulic components and the measurement system associated with the SSOP of the LS system have been discussed in the previous sections. This section provides information pertaining to the experimental procedures to be followed.

It should be recalled that the objective of the experiments was to verify all three models associated with Conditions I, II and III. These conditions were excited by adjusting the system pressure differential setting, P_d, the opening of the flow control orifice, x_v, and the load pressure, P_L. Methods of setting the system pressure differential, P_d, and the flow orifice area of the needle valve were described in Sections 4.2.2.1 and 4.2.2.3 respectively. The load pressure, P_L, was adjusted manually using the relief valve.

The first procedure to be considered is that associated with the DAQ, in particular, the determination of the sampling frequency. The pump has nine pistons which are evenly distributed around the shaft. For one rotation, each piston delivers one pulse of fluid. Thus, the period between each pulse is $\frac{1}{9\omega}$ where ω is the rotary speed of the shaft. This translates to pulses every 0.0037 seconds at 1800 RPM. A pressure and flow ripple will appear at the output of the pump at a frequency of 270 Hz. In addition, other frequency components due to the structural design of the valve plate are present. For a LS system, this pressure ripple can have a significant effect on the performance of the components. A typical pressure trace of the output pump pressure, control pressure and load pressure ripple is shown in Figure 4.9. A spectrum analysis of the control pressure indicates that frequency spikes occur at a fundamental frequency (270 Hz) and a second-order harmonic frequency (540 Hz). Higher order frequency components are not present because the signals are filtered with an analog anti-alias filter with cut-off frequency of 750 Hz.

The sampling frequency should be five to ten times the maximum significant signal frequency [Thaler, 1989]. Therefore, the sampling frequency in this experiment was selected to be 5000 Hz.

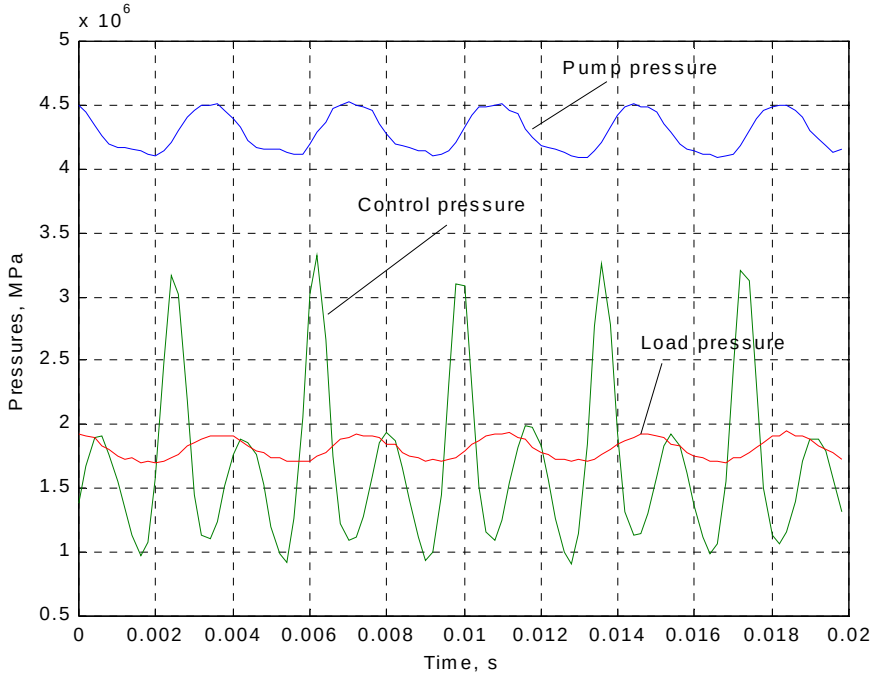

Figure 4.9 System Pressures of the LS System

For steady state experiments, the valve opening and the load pressure had to be set at fixed values. Although all variables will demonstrate some small oscillations at 270 Hz and higher order harmonic frequencies, it is the steady state components which represent the SSOP. To accommodate collection of data at several operating points, the DAQ was programmed to sequentially adjust the load pressure via the solenoid pressure relief valve. Another signal was a slow ramp load pressure profile (2.5MPa change in 10 seconds, for example). With this slow ramp, the change in the operating conditions would not excite system transients; thus a steady state relationship could be deduced at any point in the trace. The collected data had to be filtered to obtain the result for all the SSOP's.

4.3 Comparison of the Experimental and Theoretical Results

Section 4.2 presented the experimental system, hydraulic components, and measurement system which were used to determine the SSOP of the LS system with controlled load. This section compares the experimental and theoretical results for Conditions I, II and III. The theoretical results are obtained through the calculation procedure presented in Figure 3.5 of Chapter 3. It is noted that, because P_{L0} is a controlled input in this experimental study, it is unnecessary to calculate P_{L0} in Step (2), (5) or (8) in Figure 3.5.

4.3.1 Condition I

When the pressure differential across the needle valve was set to 2.5 MPa via the LS regulator and the needle valve opening was set to less than 3.5 turns, the LS system operated in Condition I. Figures 4.10 through 4.13 compare the predicted and measured SSOP's as a function of load pressure with the needle valve opening at 2.75 turns. Figure 4.10 shows the pump pressure and the control pressure. The actual pump pressure correlated very well with the experimental results but the control pressure does show some small error at large load pressures. This deviation may be due to the assumption of neglecting the leakage in the clearance between the LS spool land and the LS sleeve. Another reason may be a consequence of error in the pump parameters found by Huh et al [2000].

Figure 4.11 shows the measurement of the system pressure differential, P_s - P_L. All of experimental points lie within a band of 0.06 MPa. The "scatter" band of the pressure measurement system itself is 0.04MPa (±0.02MPa). This indicates that some amount of scatter exists in the quantity P_s - P_L and is approximately 0.04 MPa ($\sqrt{0.06^2 - 0.04^2}$).

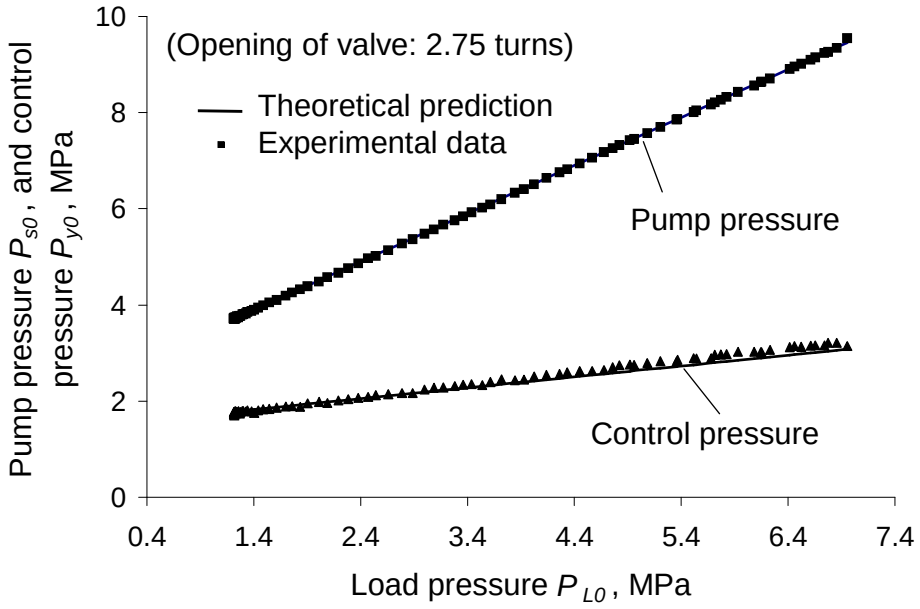

Figure 4.10 Pressure Relationship of LS System SSOPs

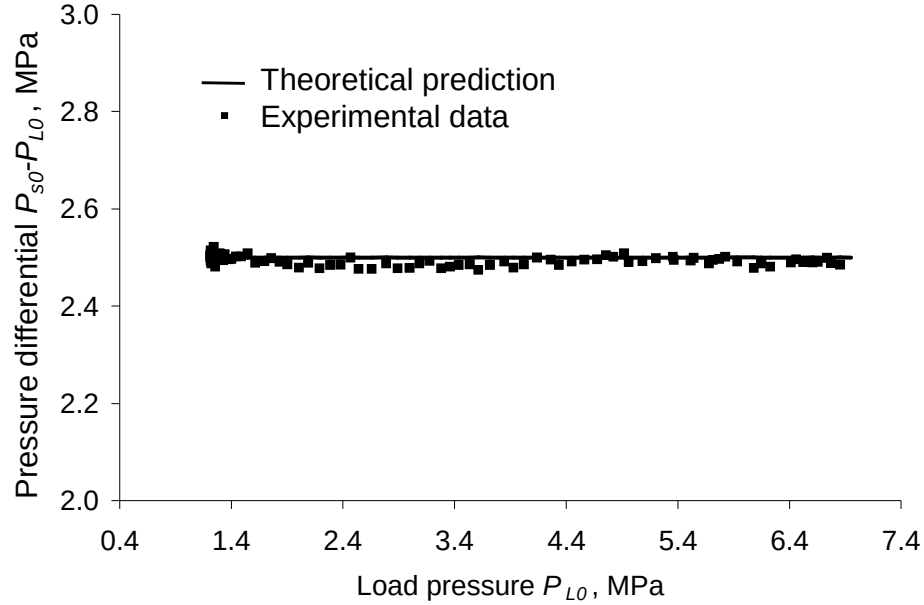

Figure 4.11 Pressure Differential (P_s - P_L) of LS System SSOPs

Figure 4.12 shows the swash plate angle as a function of P_{L0}. The scatter of experimental data is within the band of 0.002 radians which is about 0.6% of the full swash plate angle. This scatter is less than that of the measurement system (0.003 radians at $\theta_{sp0} \approx 0.12$ radian or 6.9 degree (reference to Figure B.2 in Appendix B). Therefore, the measured result of the swash plate angle is considered valid. In addition to the random error of the measurement system, the fluid temperature also affects the scatter of the resulting error. It can be further observed that when the load pressure is less than about 4.4 MPa, the prediction has an excellent agreement with the experiments. But the agreement decreases for load pressures larger than 4.4 MPa. This may be a result of two factors related to the pump leakage and the load flow rate (note: $\theta_{sp0} = \frac{Q_{s0}}{C_{pss}} = \frac{Q_{pl} + Q_{L0}}{C_{pss}}$). On one hand, it was assumed that the pump leakage is

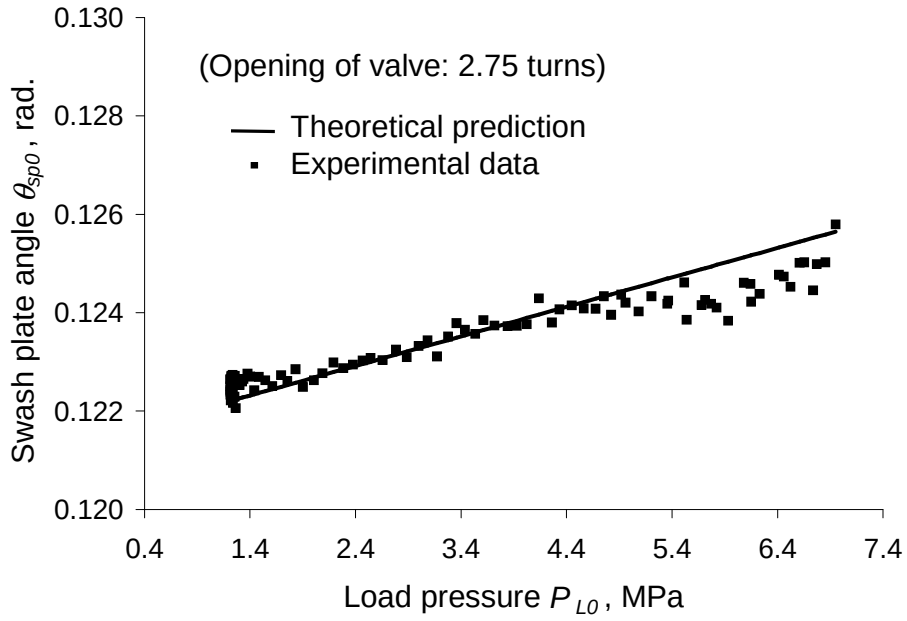

Figure 4.12 Swash Plate Angle of LS System SSOPs

proportional to the pump pressure ($Q_{pl} = c_{pl}P_s$). In fact, when using this linear leakage model, model error also exists. On the other hand, in practice, the pressure drop across the orifice is not exactly P_d ($P_d = P_{s0} - P_{L0}$ under Condition I). When the P_{L0} increases, the pressure drop, $P_{s0} - P_{L0}$, would change by a small amount.

Figure 4.13 shows the LS spool displacement. Theoretically, the spool should be at the null position $x_{r0} = 0$ for Condition I. The SSOP of experiments, however, are distributed within a band of width 0.04 mm with a bias of –0.012 mm. This scatter value is related to the data processing method. It was mentioned that with a slow ramp load pressure profile, the change in the operating conditions would not excite system transients. But the collected data included a fundamental frequency of 270 Hz and its high order harmonic frequencies. The SSOP's were measured by filtering out these high frequency signals with a Chebyshev type II digital filter (cut-off frequency: 250Hz). In spite of this, the signal still included some noise components less than 250 Hz.

It is noted that the centerline of the scatter band is 0.015 mm lower than the null position ($x_r = 0$). The tiny difference is negligible compared to the error caused by visually identifying the null position when the calibration of the proximitor measurement system was processed.

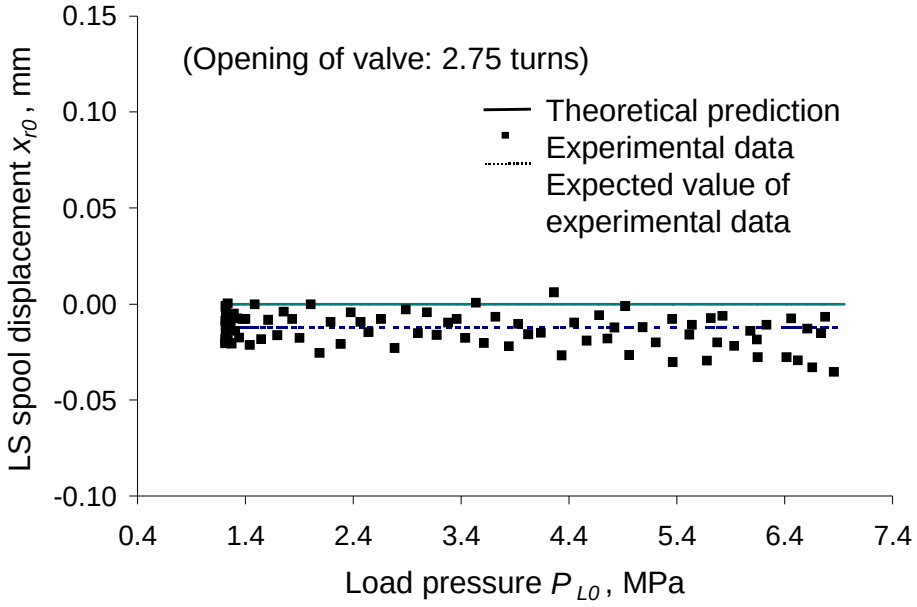

Figure 4.13 LS Spool Displacement of LS System SSOPs

4.3.2 Condition II

When the system pressure differential setting, P_d, was set to 0.58 MPa (84 psi) and when the load pressure was less than 0.8 MPa ($P_{s2} - P_d$), operating Condition II occurred. Figures 4.14 through 4.17 show the comparisons of the theoretical and experimental results with a valve opening of 2.75 turns. Figure 4.14 shows the SSOP for P_{s0} and P_{y0} as functions of P_{L0}. If the load pressure is less than 0.8 MPa (116 psi), the theoretical calculation indicates that the LS system operates in the range Condition II. The pump pressure, P_{s0}, approaches the control pressure, P_{y0}. In reality, P_{s0} is always larger than P_{y0} under any circumstances due to the leakage in the control chamber.

Figure 4.15 shows the measurement of the system pressure differential, $P_{s0} - P_{L0}$ as a function of P_{L0}. The experimental pressure differential is larger than the theoretical pressure differential setting P_d under Condition II. When the system operating condition transfers from Condition II to I, the pressure differential approaches P_d. Figure 4.16

shows that the LS spool displacement is larger than zero. This is a necessary condition for the existence of Condition II (Equation (3.28)).

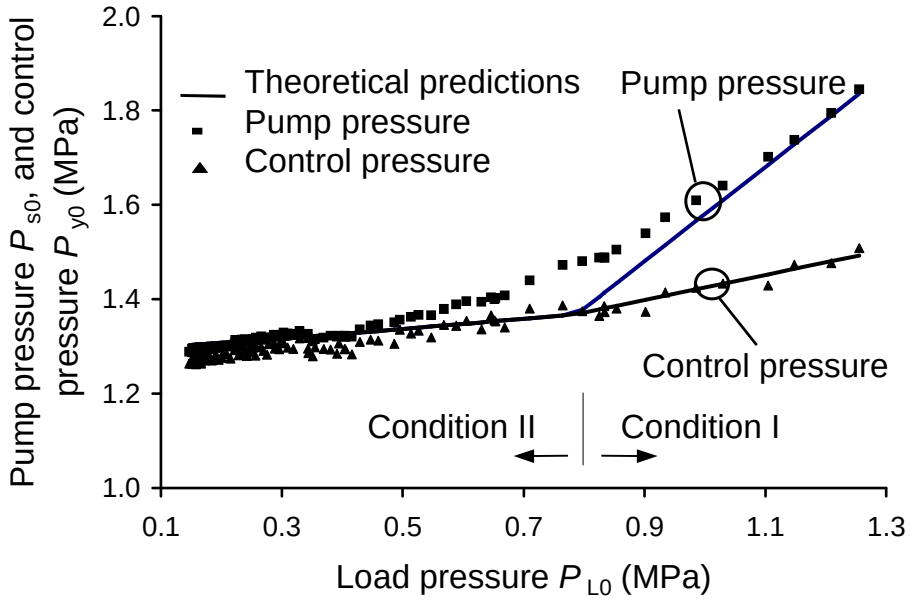

Figure 4.14 Pressure Relationship of LS System SSOPs

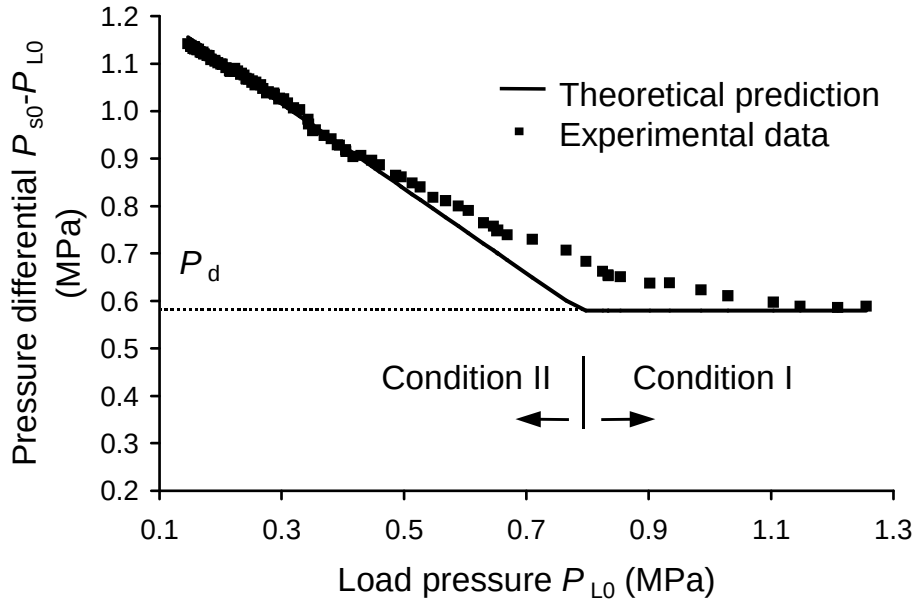

Figure 4.15 Pressure Differential (P_s - P_L) of LS System SSOPs

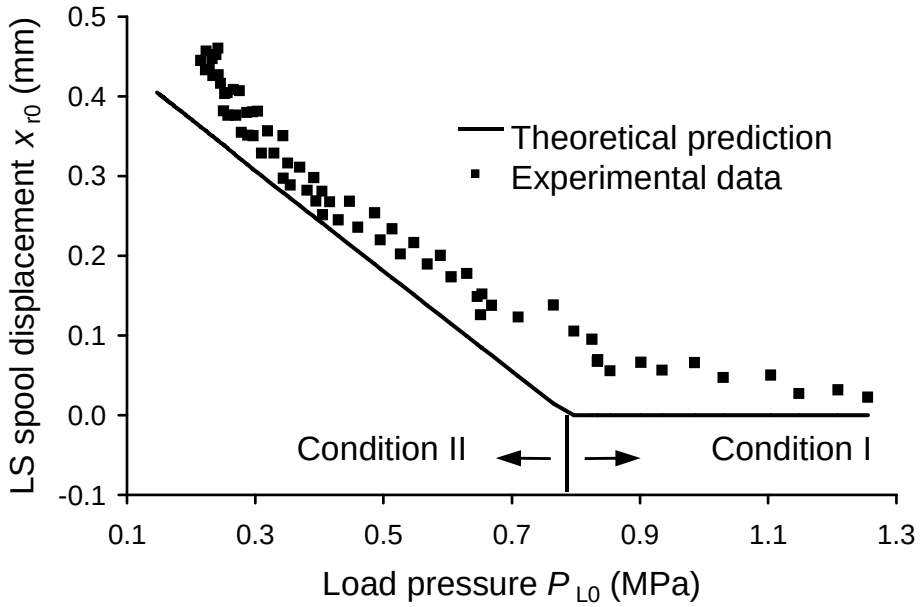

Figure 4.16 LS Spool Displacement of LS System SSOPs

Figure 4.17 shows the swash plate angle as a function of P_{L0}. It is observed that the swash plate angle decreases as the load pressure increases. In Condition II, the flow through the valve orifice decreases as the pressure differential ($P_{s0} - P_{L0}$) decreases (note: the orifice opening is fixed to 2.75 turns). This can be true only if the swash plate angle decreases. In Condition I, although the pump leakage increases slightly as P_{s0} increases, (due to the load pressure increase, P_{L0}), the load flow decreases as the pressure differential ($P_{s0} - P_{L0}$), continuously decreases. The overall flow being delivered from the pump pistons decreases as the load pressure increases. This can be true only if the swash plate angle decreases.

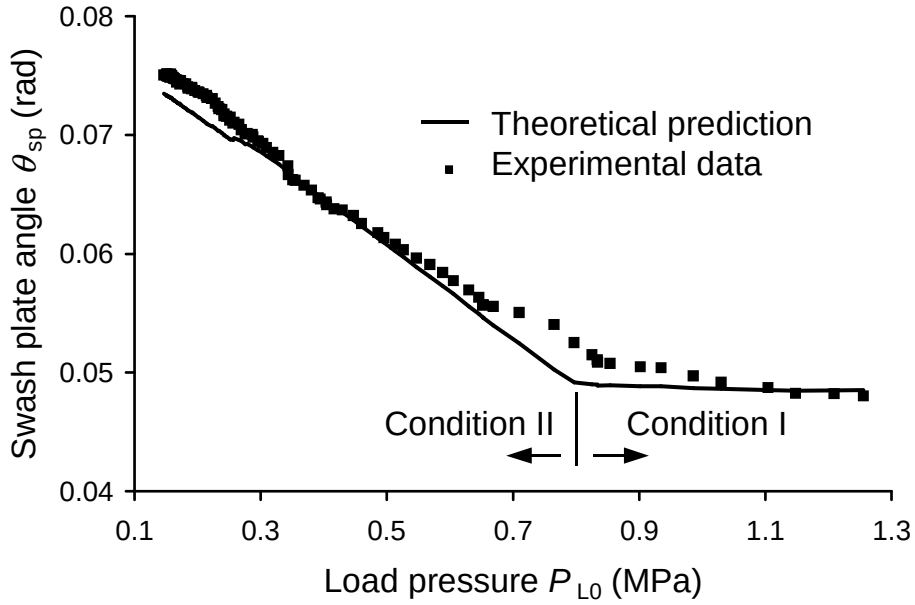

Figure 4.17 Swash Plate Angle of LS System SSOPs

It is also observed from Figures 4.14 through 4.17 that the theoretical calculations yield a distinct boundary between Conditions II and I, This is not true for the experimental results which show a smooth transition from Condition I to Condition II. This is because the practical LS hydraulic system is very complex which no theoretical model can exactly represent. The theoretical model was based on several assumptions; the leakage through the clearance between the LS spool land and the sleeve was neglected, and the non-linearities of the LS spring and the Coulomb friction of the LS spool were neglected. Finally, small chamfers at the edge of the needle valve orifice were not considered in the model. Regardless, the results are considered to be sufficiently close for practical SSOP predictions.

In Figure 4.17 the results for Condition II are presented for small swash plate angles. This corresponds to the short upper segment of the oblique line given by the equation $P_y = P_s$ (Condition II) in Figure 3.5 of Chapter 3. Experiments at large swash plate angles

could not be conducted because the relief valve could not produce the small load pressure required for Condition II with the large opening of the flow control valve.

4.3.3 Condition III

Condition III will occur if the opening of the flow control valve increases beyond a certain value. Therefore, an experiment to create Condition III requires the valve opening to be the controlled variable. This is different from the experiments for Condition I and Condition II in which the opening of the valve was fixed and the load pressure varied independently. Figure 4.18 shows the pump pressure P_s as a function of the opening of valve. In this test, the load pressure was not adjusted via the relief valve (the load pressure would increase as the opening of the needle valve increases). The sectional area of the valve orifice increased to 2.5 mm^2 (3.5 turns). When the LS system passed from operating Condition I to operating Condition III, the control pressure, P_y, suddenly drops to zero (refer to Figure 4.19). Because this experiment did not adjust the relief valve which simulates the load, the load pressure will increase when the load flow increases under Condition I. Soon after the system reaches Condition III, the load flow is a maximum and the load pressure tends to be constant. This can be seen in Figure 4.20.

Figure 4.21 shows the pressure differential, $P_s - P_{L0}$ as a function of A_v. In Condition I, the pressure differential, P_s-P_L, is controlled to the design value, P_d, which is 2.5 MPa. When the system passes through Condition III, the pressure differential decreases due to the constant load flow (pump stroked) and the increasing needle valve opening. A decrease of the pressure differential causes the LS spool to move to the left (Figures 4.3 and 4.22). When $x_r < 0$, the control piston chamber is exposed to the return line. The control pressure, P_y, decreases to zero. The swash plate continues to stroke until it reaches maximum position (Figure 4.23).

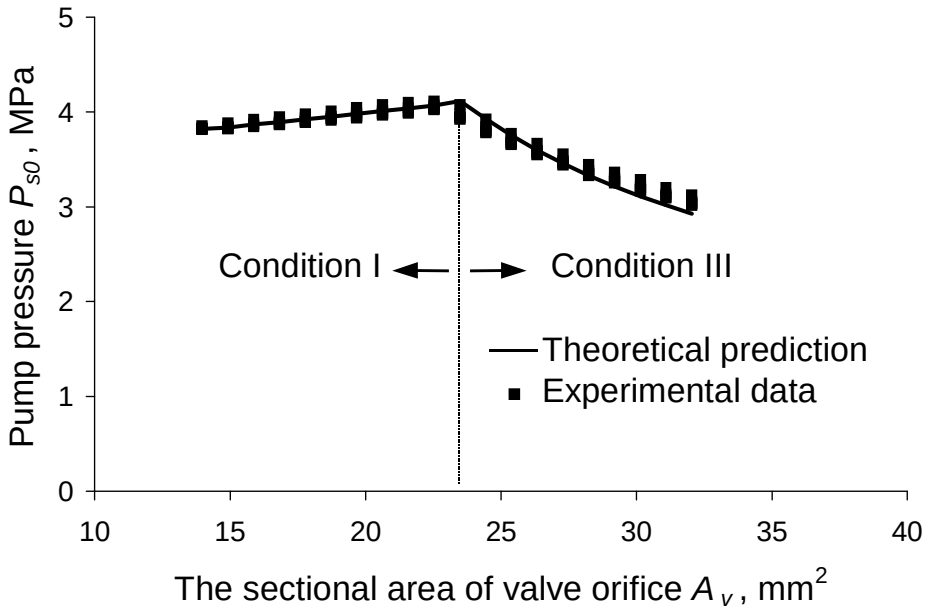

Figure 4.18 Pump Pressure of SSOPs under Condition III

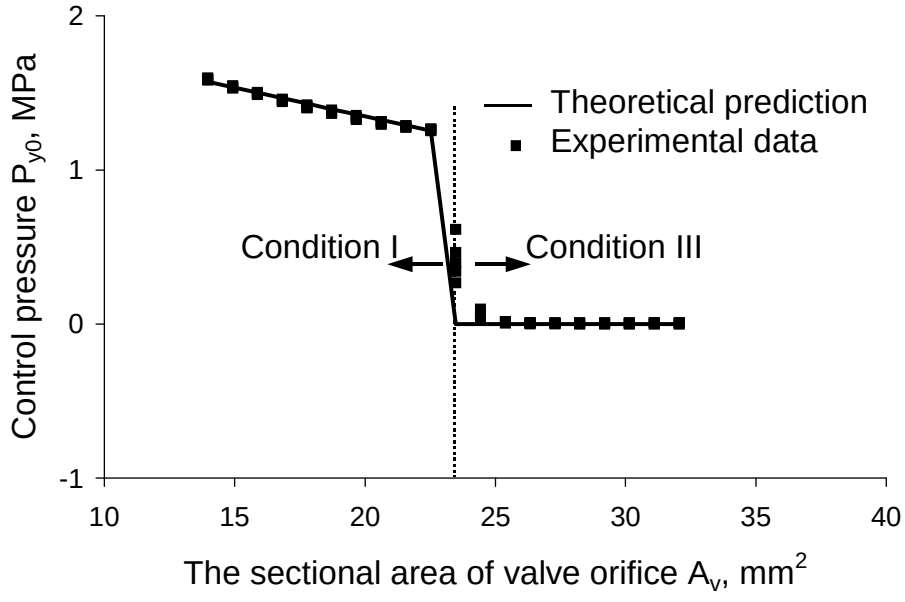

Figure 4.19 Control Pressure of SSOPs under Condition III

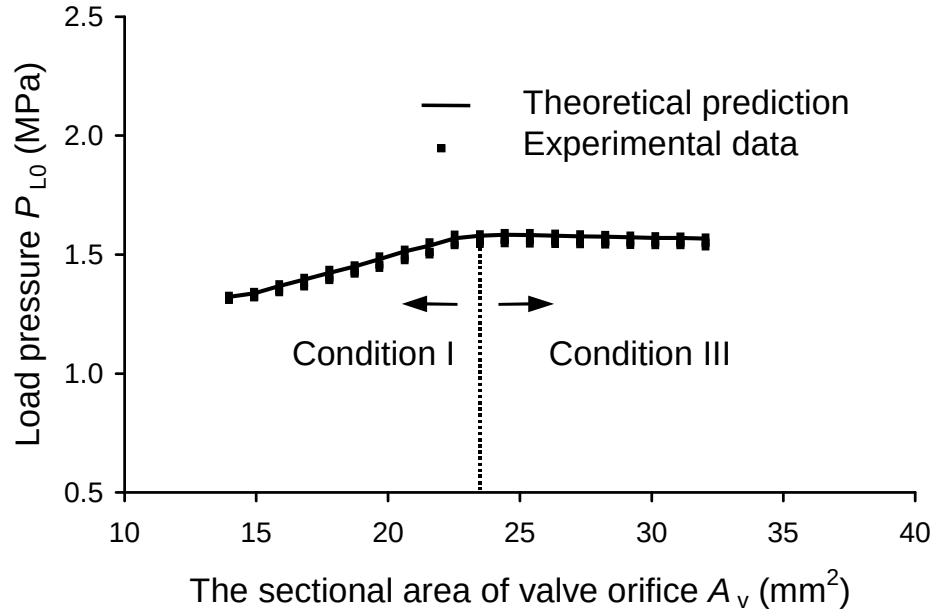

Figure 4.20 Load Pressure of SSOPs under Condition III

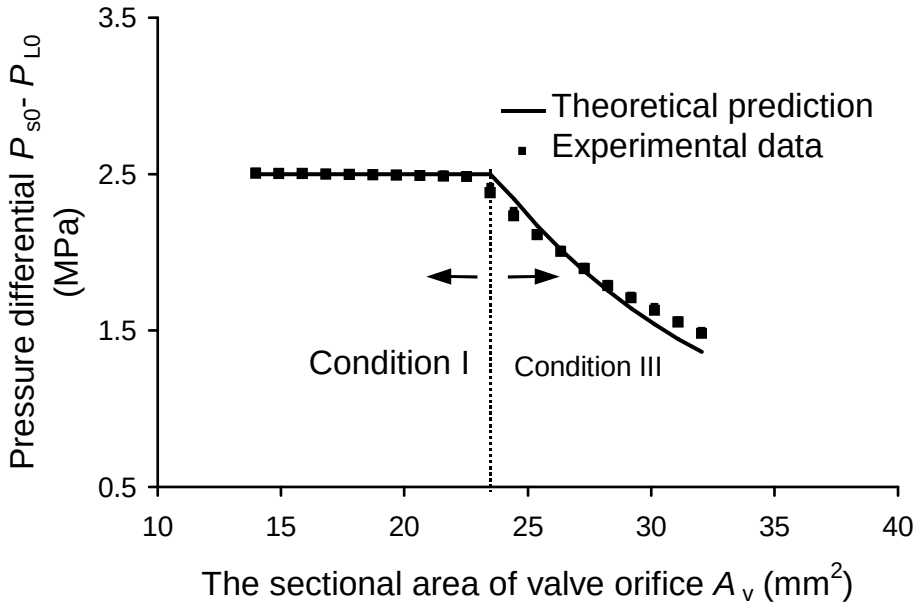

Figure 4.21 Pressure Differential of SSOPs under Condition III

Figure 4.22 shows a significant difference between the theoretical and experimental results. Even though the trends of the measurement and theoretical prediction are same, an offset of 0.1 mm exists. This is due to neglecting the leakage in its LS spool which can generate a steady state flow force. A mathematical simulation which considered the leakage and the steady state flow force has illustrated the offset of about 0.12 mm. Figures 4.13 and 4.16 also indicate that the measurement is lower than the theoretical prediction. In the experimental system, the leakage across the LS spool perimeter results in the pressure, P_s, decreasing at the end next to the proximitor sensor; subsequently, the LS spool moves in a negative direction (refer to Figure 4.5). Another possible reason for this effect is a consequence of the null position error caused by visually identifying the null position when the calibration of the proximitor measure system was processed.

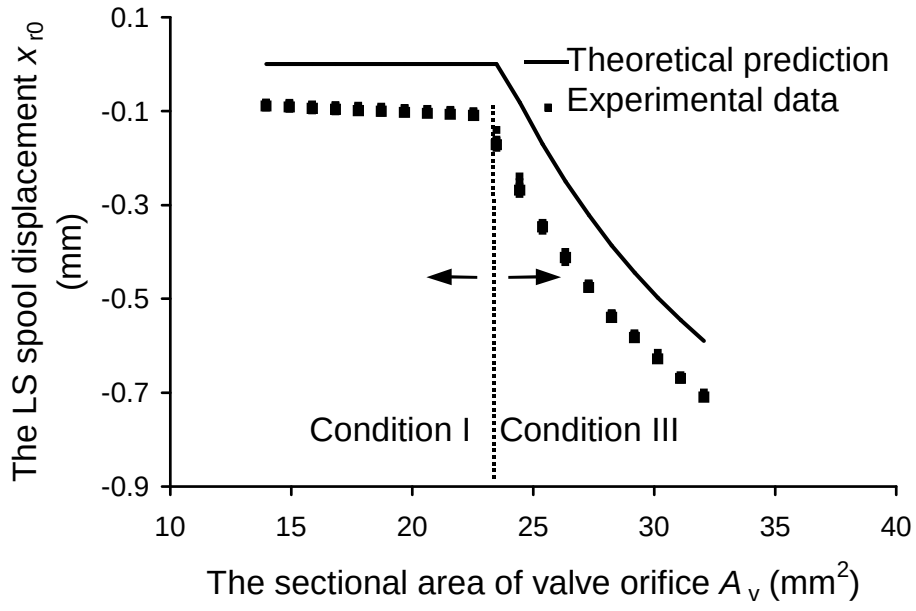

Figure 4.22 LS Spool Displacement of SSOP's under Condition III

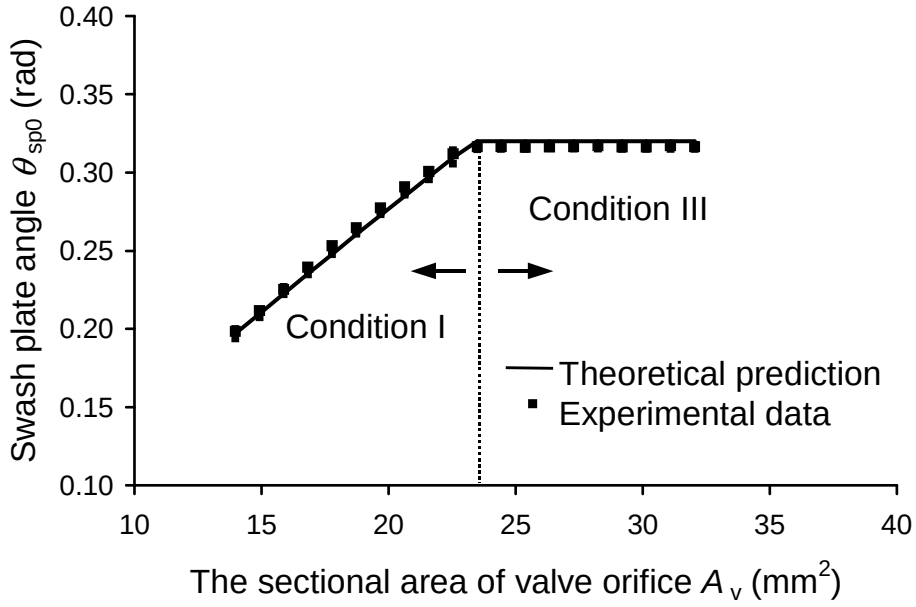

Figure 4.23 Swash Plate Angle of SSOPs under Condition III

4.4 Summary

For the LS pump and non-compensated valve, the following conclusions can be made:

1. Three theoretical conditions of SSOP of a LS system do exist in a practical LS system with a critically lapped LS regulator.
2. For each condition, the experimental results show acceptable repeatability and are consistent with the theoretical predictions.
3. The experiments show a smooth transition between the three conditions which is different from the abrupt transition predicted.
4. Condition I is the “normal” operation condition. Conditions II and III should be avoided in practice.

5. The condition of the SSOP of the LS system depends on the system pressure differential setting, P_d, the load pressure, P_L, and the opening of the flow control valve, A_v. When both P_d and P_L are small, Condition II occurs. When the demand flow is larger than the supply flow by the LS pump (i.e. the opening of the valve, A_v, is larger than the critical value), Condition III occurs.

Chapter 5 Dynamic Analysis of the Load Sensing System

5.1 Introduction

It is well known that LS systems have a high energy-savings potential, but stability problems do exist. Some researchers [Bitner and Burton, 1984(2); Krus, 1988; Lantto, et al, 1990; and Lantto, et al, 1991] have investigated the stability problem of some LS systems. However, their studies were limited in scope and as such, there is room for further investigation of the stability associated with the non-linearities in the LS system. Before approaching the stability issue, it is necessary to define what is the "dynamic problem" of the LS system from a flow control point of view.

Fig.5.1 is the schematic circuit of a basic LS system which consists of the LS pump, a variable adjusting orifice (1), the motor load (2) and the LS line (3). As stated in Chapter 1, when an increase in the orifice opening, x, occurs (in order to increase the load rotary speed), P_s is temporally reduced. Since P_s acts on the LS pump spool (4), the spool

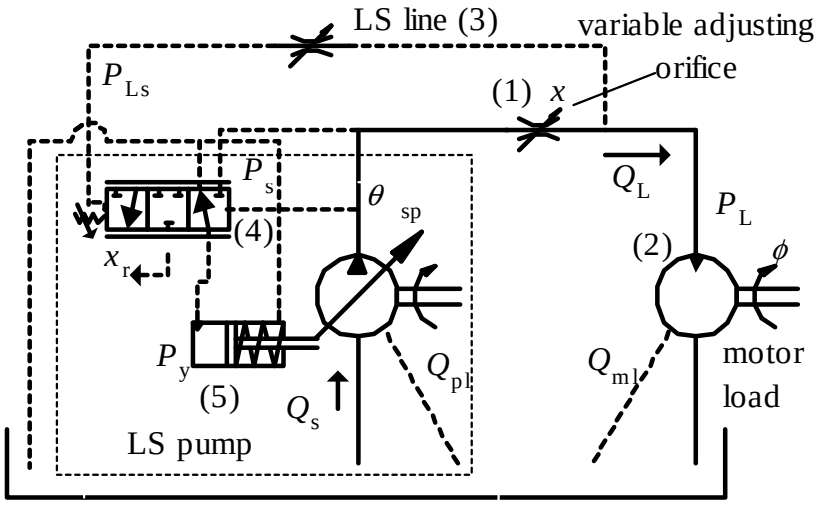

Figure 5.1 A Basic Load Sensing Circuit

moves to the right in Figure 5.1. As such, fluid in the control port area on the compensator pump piston side (5) is ported to tank reducing the pressure, P_y, in the control piston chamber. As a consequence, the pump swash plate angle, θ_{sp}, increases and the flow from the pump also increases. This causes P_s to increase, which in turn, increases in the load flow until the pump pressure establishes a new balanced operating point.

Fig.5.2 is a simplified block diagram of the LS system (which is to be developed in this section). K_q and K_c, represent the flow gain and flow-pressure coefficient of the adjustable orifice. The rest of the block transfer functions are defined as follows.

$G_\phi = \dfrac{\phi(s)}{Q_L(s)}$ —— Output transfer function.

$H_L = \dfrac{P_L(s)}{Q_L(s)}$ —— Load transfer function.

$G_p = \dfrac{Q_s(s)}{\delta P(s)}$ —— LS pump transfer function (note*: $\delta P(s) = P_s^*(s) - P_{Ls}(s)$).

$H_p = \dfrac{P_s^*(s)}{P_s(s)}$ —— Overall pressure feedback gain of the LS pump.

$G_s = \dfrac{P_s(s)}{\delta Q(s)}$ —— Pump volume transfer function (note: $\delta Q(s) = Q_s(s) - Q_L(s)$).

$G_{Ls} = \dfrac{P_{Ls}(s)}{P_L(s)}$ —— Damping of the LS line.

This chapter will show the development of the block diagram of Figure 5.2 but it is first desirable to explain how this transfer function is to be used from a physical point of view.

* δ is used to emphasize that the input is a differential signal.

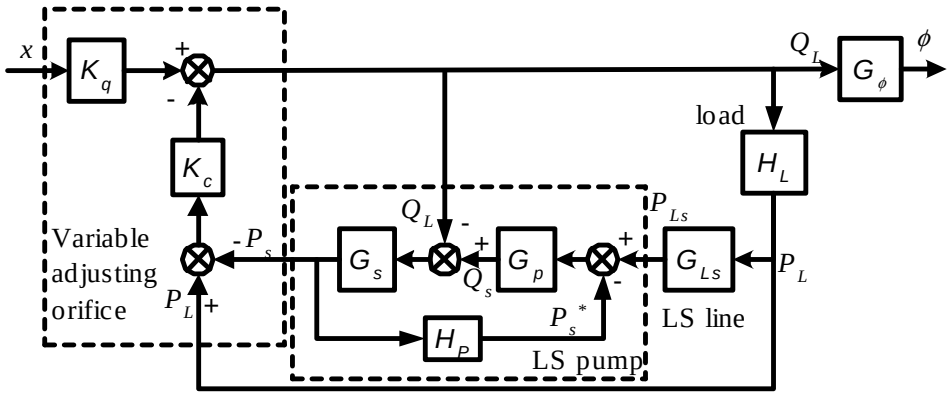

Figure 5.2 Block Diagram of the Basic Load Sensing Circuit

As illustrated in Figure 5.2, the flow rate, Q_L, can be manipulated directly by the opening, x, of the adjustable orifice and indirectly by the feedback path via K_c. The system includes one "positive" feedback loop ($H_L \rightarrow G_{Ls} \rightarrow G_p \rightarrow G_s \rightarrow K_c$ path), in addition to many negative feedback loops. It is the "positive" feedback loop that, under certain conditions, could cause the system to become unstable. This is defined as the "dynamic problem" of flow control in the LS system.

The method of solving the dynamic problem is to find out these "certain conditions" which cause the instabilities, and to avoid these regions without compromising the energy saving of the LS system (i.e. by increasing the allowable pressure across the adjustable orifice, as an example). Other researchers have considered this problem but only in a marginal sense. These studies were unable to demonstrate that instabilities are related to the SSOP and operating conditions (Conditions I, II, & III which were identified in Chapter 3). The SSOP's were shown to have a significant influence on the values of the linearized coefficients in the models (K_q, K_c etc.). The operating conditions do affect the stability at different operating modes (Condition I, II, or III). In other words, the system TF parameters and order are very much a function of the operating conditions. The objective of this chapter is to develop the system TF at different

operating conditions (I, II, & III) and to further analyze how changes in the SSOP and operating conditions affect the stability of LS system.

The procedure includes building dynamic models of all components for the LS system, expressing them in TF form, giving a complete block diagram of the LS system, analyzing and simplifying the block diagram for different operating conditions (I, II & III), and developing the TF, $\frac{\phi(s)}{X(s)}$, of the LS system for Conditions I, II and III. These TF's are validated in Chapter 6.

5.2 Modeling of the Dynamic System

This section is to use the linearized models in Section 2.1 in Chapter 2 in order to develop the TF of individual component. It is noted that the "Δ" prior to each variable in linearized Equations (2.4), (2.13), (2.14), (2.29), and (2.35) will now be dropped for simplicity. But it should be emphasized that all variables represent their "dynamic component". When the steady state operating point (SSOP) occurs in any equation, the subscript "$_0$" is added to distinguish the parameters/state from the dynamic component of variables. For convenience, the schematic of the LS system is redrawn in Figure 5.3.

5.2.1 Dynamic Model of the Load Sensing Spool

Equation (2.1) represents the dynamic model of the LS spool. Because the pressure differential setting, $P_{d,}$ is neither a state variable nor the input variable, P_d is absent in the linearized equation of Equation (2.1). P_d affects the stability of the LS system only through the SSOP. The dynamic equation is given as

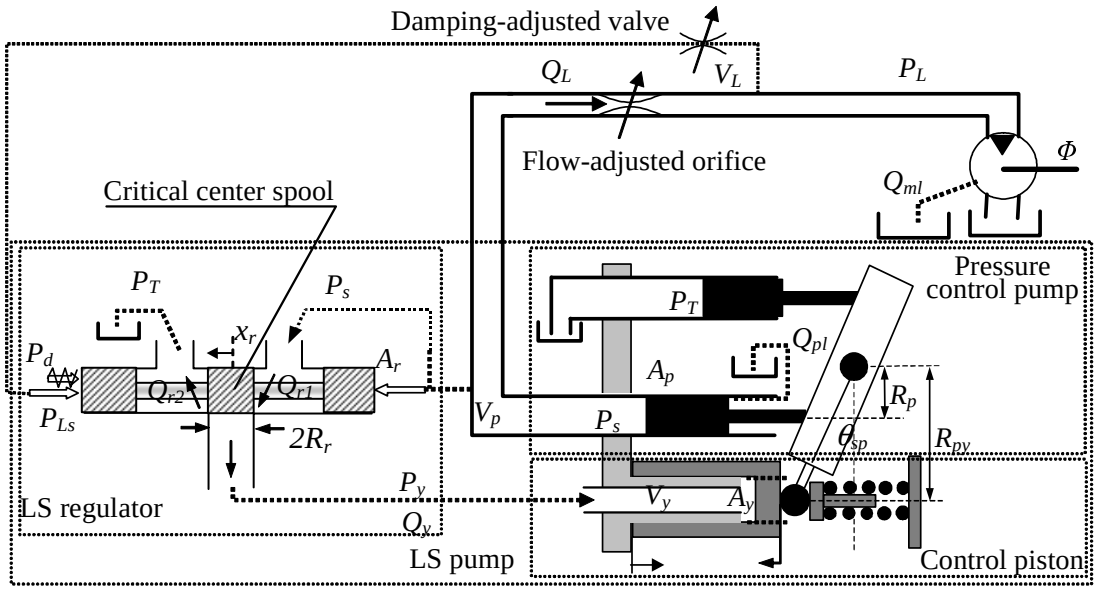

Figure 5.3 Schematic of the Load Sensing System

$$\ddot{x}_r = \tfrac{1}{M_r}\left(-B_r\dot{x}_r - k_r x_r + A_r\left(P_s - P_{Ls}\right)\right) \tag{5.1}$$

Taking the Laplace transform of Equation (5.1) yields the TF relating $X_r(s)$ to $P_s(s) - P_{Ls}(s)$ as

$$G_r(s) = \frac{X_r(s)}{P_s(s) - P_{Ls}(s)} = \frac{K_r}{\frac{s^2}{\omega_r^2} + \frac{2\zeta_r s}{\omega_r} + 1} \tag{5.2}$$

where

$$K_r = \frac{A_r}{k_r} \tag{5.3}$$

$$\omega_r = \sqrt{\frac{k_r}{M_r}} \tag{5.4}$$

$$\zeta_r = \frac{B_r}{2\sqrt{M_r k_r}} \tag{5.5}$$

Equation (5.2) can be represented in block diagram form as shown in Figure 5.4.

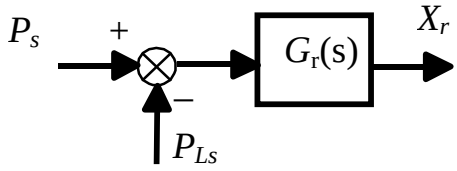

Figure 5.4 TF of the LS Spool

5.2.2 Dynamic Model of the Swash Plate

Equation (2.4) is re-written as

$$J_{sp}\ddot{\theta}_{sp} = -B_{sp}\dot{\theta}_{sp} - (K_{sp} + K_{pr3}P_{s0})\theta_{sp} - R_{py}A_y P_y + (K_{pr2} - K_{pr3}\theta_{sp0})P_s \tag{5.6}$$

Taking the Laplace transform of Equation (5.6) yields the TF of θ_{sp} with respect to P_s and P_y in the frequency domain as

$$\theta_{sp}(s) = G_{sp}(s)\left(K_{sps}P_s(s) - K_{spy}P_y(s)\right) \tag{5.7}$$

where

$$G_{sp}(s) = \frac{1}{\frac{s^2}{\omega_{sp}^2} + \frac{2\zeta_{sp}s}{\omega_{sp}} + 1} \tag{5.8}$$

$$\omega_{sp} = \sqrt{\frac{K_{sp} + K_{pr3}P_{s0}}{J_{sp}}} \tag{5.9}$$

$$\zeta_{sp} = \frac{B_{sp}}{2\sqrt{J_{sp}\left(K_{sp} + K_{pr3}P_{s0}\right)}} \tag{5.10}$$

$$K_{sps} = \frac{K_{pr2} - K_{pr3}\theta_{sp0}}{K_{sp} + K_{pr3}P_{s0}} \tag{5.11}$$

$$K_{spy} = \frac{R_{py}A_y}{K_{sp} + K_{pr3}P_{s0}} \tag{5.12}$$

Equation (5.6) can be represented in block diagram form as in Figure 5.5.

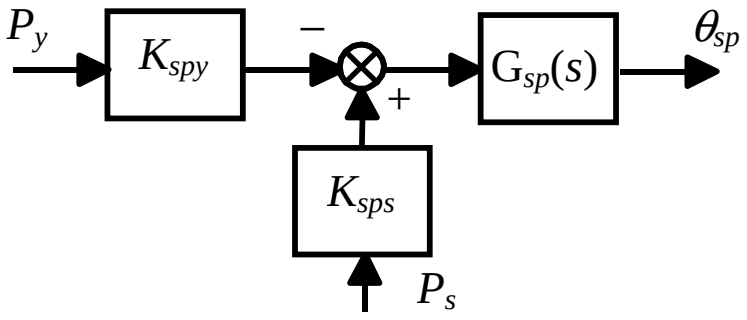

Figure 5.5 TF of the Swash Plate

5.2.3 Flow Continuity Equation for the Pressure Control Chamber

Consider Equation (2.29).

$$\dot{P}_y = K_\theta\theta_{sp} + K_{d\theta}\dot{\theta}_{sp} + K_{xr}x_r - K_{py}P_y + K_{ps}P_s \tag{5.13}$$

It will now be shown that the linearization coefficient, K_θ, equals zero. In order to prove this, Equation (2.30) is re-written as

$$K_\theta = \frac{-R_{py}\left(K_{xy} + 2\tan\left(\theta_{sp0}\right)\dot{\theta}_{sp0}K_{dxy}\right)}{\cos^2\left(\theta_{sp0}\right)} \tag{5.14}$$

where K_{xy} was defined in Equation (2.20) as

$$K_{xy} = \frac{\beta A_y}{\left(V_{y0} + A_y x_{y0}\right)^2}\left(Q_{r10} - A_y \dot{x}_{y0} - Q_{r20}\right) \tag{5.15}$$

Under steady state conditions, the sum of the three terms in the bracket of Equation (5.15) are always zero no matter in which condition (I, II, or III) the LS system operates ($Q_{r10} = Q_{r20},\ \dot{x}_{y0} = 0$). Therefore K_{xy} is always equal to zero. Further, $\dot{\theta}_{sp0}$ in Equation (5.14) is zero under steady state conditions; therefore, K_θ is also always zero.

Consider the linearized coefficient, $K_{d\theta}$, in Equation (5.13). Substituting Equation (2.25) into Equation (2.21) and then substituting the result into Equation (2.31) gives

$$K_{d\theta} = \frac{R_{py}\beta A_y}{\cos^2\theta_{sp0}\left(V_{y\max} - A_y R_{py}\cdot\tan\left(\theta_{sp0}\right)\right)} \tag{5.16}$$

where V_{ymax} is the maximum volume of the control piston chamber.

Consider the linearized coefficients K_r, K_{ps}, and K_{py} in Equation (5.13). Substituting Equation (2.25) into Equations (2.22) through (2.24) gives

$$K_{xr} = \frac{\beta\left(K_{qr1} - K_{qr2}\right)}{V_{y\max} - A_y R_{py}\cdot\tan\left(\theta_{sp0}\right)} \tag{5.17}$$

$$K_{py} = \frac{\beta\left(K_{cr1} + K_{cr2}\right)}{V_{y\max} - A_y R_{py}\cdot\tan\left(\theta_{sp0}\right)} \tag{5.18}$$

$$K_{ps} = \frac{\beta K_{cr1}}{V_{y\max} - A_y R_{py} \cdot \tan\left(\theta_{sp0}\right)} \tag{5.19}$$

Equations (5.17) through (5.19) indicate that linearized coefficients K_{xr}, K_{ps}, and K_{py} mainly depend on flow gains, K_{qr1} and K_{qr2}, and flow-pressure coefficients, K_{cr1} and K_{cr2}. Recall that these coefficients are the partial differentials of flow rates, Q_{r1} and Q_{r2} with respect to displacement, x_r, and the pressure drop across orifice, δP (reference to Figure 5.3), that is,

$$Q_{r1} = K_{qr1} x_r + K_{cr1}\left(P_s - P_y\right) \tag{5.20}$$

$$Q_{r2} = K_{qr2} x_r + K_{cr2} P_y \tag{5.21}$$

where $K_{qr1} = \frac{\partial Q_{r1}}{\partial x_r}$, $K_{cr1} = \frac{\partial Q_{r1}}{\partial \delta P}$ (Note $\delta P = P_s - P_y$), $K_{qr2} = \frac{\partial Q_{r2}}{\partial x_r}$, $K_{cr2} = \frac{\partial Q_{r2}}{\partial P_y}$.

In order to theoretically estimate these four coefficients, the flow rate equations of the two orifices in the pressure regulator (Q_{r1}, Q_{r2}) must be considered. Because the normal operation of the LS regulator with a critically lapped spool occurs at the null position, the application of the general flow rate equation ($Q = C_d A(x)\sqrt{\frac{2}{\rho}\Delta P}$) would introduce significant uncertainty. There are two reasons for this: (1) C_d may not be equal to 0.61 due to laminar flow conditions and (2) the precise value of $A(x)$ cannot be obtained (small chamfers could exist which would be very difficult to measure). Therefore, the flow rate equation must be modified to reflect this physical reality. Appendix C provides an empirical model of the discharge coefficient, C_d, which can be applied to both turbulent and laminar flow. Using the results of Appendix C, Appendix D modifies the orifice area, $A(x)$, as a function of the orifice opening. A comprehensive flow rate model which has been shown to be valid around the null point is given as (zero lap)

$$Q = C_{d\infty}\left(1 + ae^{-\frac{\delta_1}{C_{d\infty}}\sqrt{\mathrm{Re}}} + be^{-\frac{\delta_2}{C_{d\infty}}\sqrt{\mathrm{Re}}}\right)\frac{wx}{1-e^{-\frac{x}{d}}}\sqrt{\frac{2}{\rho}\Delta P} \tag{5.22}$$

The "charge" (Q_{r1}) and "discharge" (Q_{r2}) orifices of the LS regulator can be considered to be approximately symmetric about the null position; the flow rate equations are therefore,

$$Q_{r1} = C_{d\infty}\left(1 + ae^{-\frac{\delta_1}{C_{d\infty}}\sqrt{\mathrm{Re}_1}} + be^{-\frac{\delta_2}{C_{d\infty}}\sqrt{\mathrm{Re}_1}}\right)\frac{wx_r}{1-e^{-\frac{x_r}{d}}}\sqrt{\frac{2}{\rho}\left(P_s - P_y\right)} \tag{5.23}$$

and

$$Q_{r2} = C_{d\infty}\left(1 + ae^{-\frac{\delta_1}{C_{d\infty}}\sqrt{\mathrm{Re}_2}} + be^{-\frac{\delta_2}{C_{d\infty}}\sqrt{\mathrm{Re}_2}}\right)\frac{wx_r}{e^{\frac{x_r}{d}}-1}\sqrt{\frac{2}{\rho}P_y} \tag{5.24}$$

The corresponding flow gains and the flow-pressure coefficients for the "charge" and "discharge" orifices are given as

$$K_{qr1} = \frac{\partial Q_{r1}}{\partial x_r} = \frac{C_d w\left(1-\left(1+X\right)e^{-X}\right)}{\left(1-\varepsilon\right)\left(1-e^{-X}\right)^2}\sqrt{\tfrac{2}{\rho}\left(P_s - P_y\right)} \tag{5.25}$$

where $C_d = C_{d\infty}\left(1 + ae^{-\frac{\delta_1}{C_{d\infty}}\sqrt{\mathrm{Re}}} + be^{-\frac{\delta_2}{C_{d\infty}}\sqrt{\mathrm{Re}}}\right)$

$$X = \frac{x_r}{d}$$

$$\varepsilon = \frac{\left(-a\delta_1 e^{-\frac{\delta_1}{C_{d\infty}}\sqrt{\mathrm{Re}}} - b\delta_2 e^{-\frac{\delta_2}{C_{d\infty}}\sqrt{\mathrm{Re}}}\right)\sqrt{\mathrm{Re}}}{2C_d}$$

$$K_{qr2} = \frac{\partial Q_{r2}}{\partial x_r} = \frac{C_d w\left(\left(1-X\right)e^{X}-1\right)}{\left(1-\varepsilon\right)\left(e^{X}-1\right)^2}\sqrt{\tfrac{2}{\rho}P_y} \tag{5.26}$$

$$K_{cr1} = \frac{\partial Q_{r1}}{\partial \Delta P} = \frac{C_d w x_r}{(1-\varepsilon)(1-e^{-X})\sqrt{2\rho(P_s - P_y)}} \tag{5.27}$$

$$K_{cr2} = \frac{\partial Q_{r2}}{\partial P_y} = \frac{C_d w x_r}{(1-\varepsilon)(e^{X} - 1)\sqrt{2\rho P_y}} \tag{5.28}$$

With empirical Equations (5.25) through (5.28), the value of $K_{d\theta}$ (Equation (5.16)), K_{xr} (Equation (5.17)), K_{py} (Equation (5.18)), and K_{ps} (Equation (5.19)) now can be calculated. It was mentioned earlier that K_{θ} equals zero. Now it is possible to further develop the TF for the linearized Equation (5.13).

Taking the Laplace transform of Equation (5.13) can give the TF of the pressure P_y with respect to three inputs, x_r, P_s, and θ_{sp} in the frequency domain as

$$P_y(s) = G_y(s)\left(K_{yr} X_r(s) + K_{ys} P_s(s) + K_{ysp} s\theta_{sp}(s)\right) \tag{5.29}$$

where

$$G_y(s) = \frac{1}{\frac{s}{\omega_y} + 1} \tag{5.30}$$

$$\omega_y = K_{py} = \frac{\beta(K_{cr1} + K_{cr2})}{V_{y\max} - A_y R_{py} \cdot \tan(\theta_{sp0})} \tag{5.31}$$

$$K_{yr} = \frac{K_{qr1} - K_{qr2}}{K_{cr1} + K_{cr2}} \tag{5.32}$$

It is noted that K_{qr2} as calculated by Equation (5.26), is always negative due to the "discharge" flow. In order to avoid any possible misinterpretation, Equation (5.32) is rewritten as

$$K_{yr} = \frac{K_{qr1} + |K_{qr2}|}{K_{cr1} + K_{cr2}} \tag{5.33}$$

$$K_{ysp} = \frac{R_{py} A_y}{\cos^2 \theta_{sp0} \left(K_{cr1} + K_{cr2} \right)} \tag{5.34}$$

$$K_{ys} = \frac{K_{cr1}}{K_{cr1} + K_{cr2}} \tag{5.35}$$

Equation (5.29) can be represented in block diagram form as shown in Figure 5.6.

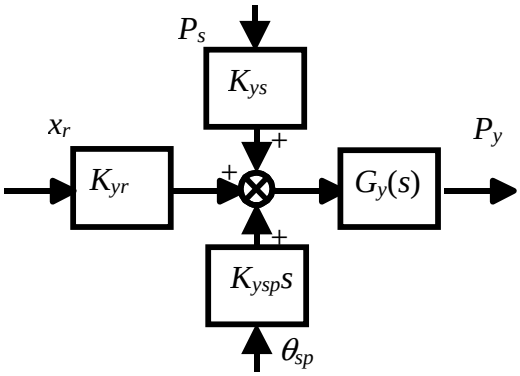

Figure 5.6 TF of the Pressure Control Chamber

5.2.4 Swash Plate-Flow Gain of the Pump

Equation (2.35) represents the flow equation of the LS pump. It is re-written as

$$Q_s = C_p \theta_{sp} - K_{qr1} x_r - K_{cr1} \left(P_s - P_y \right) \tag{5.36}$$

where C_p was given by Equation (2.36) and repeated here for clarity: $C_p = \frac{N A_p R_p \omega}{\pi \cdot \cos^2 \left(\theta_{sp0} \right)}$.

K_{qr1} and K_{cr1} are determined by Equations (5.25) and (5.26) respectively.

Equation (5.36) is an algebraic equation. The first term of the right hand side is the ideal flow rate from the pump pistons. The other two terms represent the flow rate entering the LS regulator via its charge orifice. Although the steady state value of the pump flow delivery, Q_{s0}, at large swash plate angles is many orders of magnitude larger than Q_{r10}, this does not imply that the dynamic component must also satisfy $Q_s >> Q_{r1}$.

When the swash plate angle is very small, the effect of Q_{r1} on the system is significant. Therefore, the other two terms in Equation (5.36) cannot be neglected.

5.2.5 Flow Continuity Equation of the Pump Chamber

Equation (2.37) is the dynamic equation of the pump pressure, P_s, with respect to two flow inputs; Q_s and Q_L. It is re-written as

$$\dot{P}_s = \frac{\beta}{V_p}\left((Q_s - Q_L) - c_{pl}P_s\right) \tag{5.37}$$

where c_{pl} is the leakage coefficient of the pump. Substituting Equation (5.36) into Equation (5.37) gives

$$\dot{P}_s = \frac{\beta}{V_p}\left(-\left(c_{pl} + K_{cr1}\right)P_s + C_p\theta_{sp} - K_{qr1}x_r + K_{cr1}P_y - Q_L\right) \tag{5.38}$$

Taking Laplace transform of Equation (5.38) can give the TF of the pump pressure, P_s, with respect to four input variables, swash plate angle, θ_{sp}, the LS spool charge orifice opening, x_r, the control piston pressure, P_y, and the load flow rate, Q_L, to yield

$$P_s(s) = G_s(s)\left(C_p\theta_{sp}(s) - K_{qr1}X_r(s) + K_{cr1}P_y(s) - Q_L(s)\right) \tag{5.39}$$

where

$$G_s(s) = \frac{K_s}{\frac{s}{\omega_s} + 1} \tag{5.40}$$

$$\omega_s = \frac{\beta\left(K_{cr1} + c_{pl}\right)}{V_p} \tag{5.41}$$

$$K_s = \frac{1}{K_{cr1} + c_{pl}} \tag{5.42}$$

Equation (5.39) can be represented in block diagram form as shown in Figure 5.7.

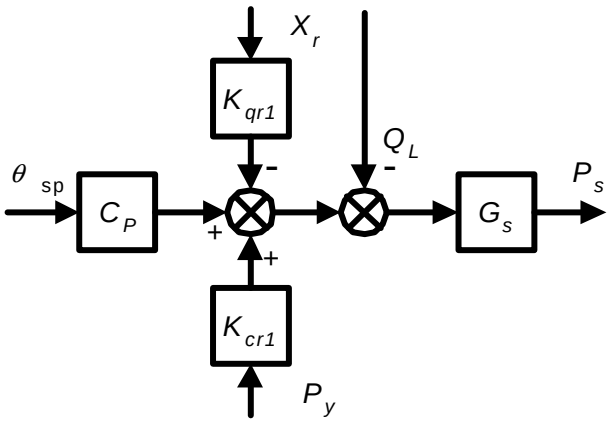

Figure 5.7 TF of the Pump Volume

5.2.6 Model of the LS Line

Equation (2.49) is the dynamic model of the LS line. Since $\dot{x}_r$ is very small under all operating conditions, $A_r \dot{x}_r$ is negligible. Thus,

$$\dot{P}_{Ls} = \frac{\beta(P_L - P_{Ls})}{V_{Ls} R_{Ls}} \tag{5.43}$$

Taking the Laplace transform of Equation (5.43) can give the TF of the LS pressure P_{Ls} with respect to the load pressure, P_L, in frequency domain as

$$G_{Ls}(s) = \frac{P_{Ls}(s)}{P_L(s)} = \frac{1}{\frac{s}{\omega_{Ls}} + 1} \tag{5.44}$$

where $\omega_{Ls} = \frac{\beta}{V_{Ls} R_{Ls}}$. The diagram is shown in Figure 5.8.

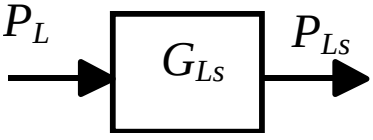

Figure 5.8 TF of the LS Line

5.2.7 Model of the Flow Adjusted Orifice without Pressure Compensation

The linearized flow equation of the adjustable orifice (Equation (2.39)) can be expressed in the frequency domain as

$$Q_L(s) = K_q X(s) + K_c\left(P_s(s) - P_L(s)\right) \tag{5.45}$$

where

$$K_q = C_d w\sqrt{\frac{2}{\rho}\left(P_{s0} - P_{L0}\right)} \tag{5.46}$$

$$K_c = \frac{C_d w x}{\sqrt{2\rho\left(P_{s0} - P_{L0}\right)}} \tag{5.47}$$

The block diagram of this equation was shown in Figure 5.1.

5.2.8 Load Model

The load model is defined as the TF of the load pressure, $P_L(s)$, with respect to the load flow rate, $Q_L(s)$. Equations (2.42) and (2.43) can be rewritten as.

$$\dot{P}_L = \frac{\beta}{V_m}\left(-D_m\phi + Q_L - c_{ml}P_L\right) \tag{5.48}$$

$$\dot{\phi} = \frac{1}{J_m}\left(-B_m\phi + D_m P_L\right) \tag{5.49}$$

Taking the Laplace transform of Equations (5.48) and (5.49) and then eliminating $\phi(s)$ can give the TF of the load as

$$H_L(s) = \frac{P_L(s)}{Q_L(s)} = K_L\frac{\frac{s}{\omega_{L0}} + 1}{\frac{s^2}{\omega_L^2} + \frac{2\zeta_L s}{\omega_L} + 1} \tag{5.50}$$

where

$$K_L = \frac{B_m}{c_{ml} B_m + D_m^2} \tag{5.51}$$

$$\omega_L = \sqrt{\frac{\beta\left(c_{ml} B_m + D_m^2\right)}{V_m J_m}} \tag{5.52}$$

$$\zeta_L = \frac{V_m B_m + c_{ml} J_m \beta}{2\sqrt{J_m V_m \beta\left(c_{ml} B_m + D_m^2\right)}} \tag{5.53}$$

$$\omega_{L0} = \frac{B_m}{J_m} \tag{5.54}$$

In order to obtain the TF of system output, ϕ_L, with respect to the load flow, Q_L, taking the Laplace transform of Equations (5.48) and (5.49) and then eliminating $P_L(s)$ can give the TF of the system output as

$$G_\phi(s) = \frac{\phi(s)}{Q_L(s)} = \frac{K_\phi}{\frac{s^2}{\omega_L^2} + \frac{2\zeta_L s}{\omega_L} + 1} \tag{5.55}$$

where

$$K_\phi = \frac{1}{D_m + \frac{c_{ml} B_m}{D_m}} \tag{5.56}$$

If the leakage of motor is negligible (i.e. $c_{ml} = 0$), the model parameters are simplified as

$$K_L = \frac{B_m}{D_m^2} \tag{5.57}$$

$$\omega_L = D_m \sqrt{\frac{\beta}{V_m J_m}} \tag{5.58}$$

$$\zeta_L = \frac{B_m}{2D_m} \sqrt{\frac{V_m}{J_m \beta}} \tag{5.59}$$

$$\omega_{L0} = \frac{B_m}{J_m} = 2\zeta_L \omega_L \tag{5.60}$$

$$K_\phi = \frac{1}{D_m} \tag{5.61}$$

Equations (5.50) and (5.55) can be represented in block diagrams as shown in Figure 5.9(a) and 5.9(b).

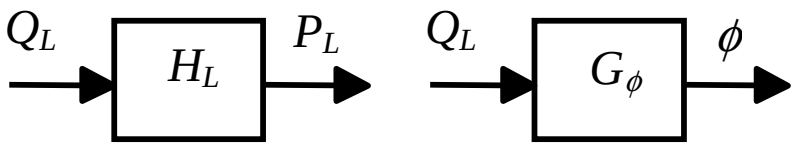

(a) Motor load TF (b) System output TF

Figure 5.9 TF's of Motor Load

This section has developed the required TF's of all hydraulic components and has shown the appropriate block diagrams. The following section will combine all block diagrams and then show appropriate simplification for operating conditions I, II & III.

5.3 Development of the Transfer Function of the Load Sensing System for each Operating Condition

The objective of this section is to develop the TF of the LS system for each operating condition (I, II & III). When the LS system operates at different loading conditions, parameters of the dynamic model change due to the variation of the SSOP. If the variation of SSOP is so large that the operating condition of the LS system shifts from one condition to another, the system dynamic model would have to change, reflecting the different forms of the TF's for different operating conditions. In order to obtain the simplified TF at each operating condition, the complete block diagram of the LS system must be considered (essentially combining all the block diagrams developed in the chapter).

Combining the transfer functions given in Figures 5.4 through Figure 5.9 provides a complete TF of the LS system as shown in Figure 5.10. This block diagram is too complex to directly obtain the TF, because there are as many as 24 terms in the determinant of the graph if Mason's gain formula is applied [Ogata, 1970]. Even if the TF could be obtained, the TF would not readily reveal the information about which terms dominate the poles of the TF at specific operating conditions (I, II or III). Therefore, the block diagram must be simplified for each operating condition (I, II, and III).

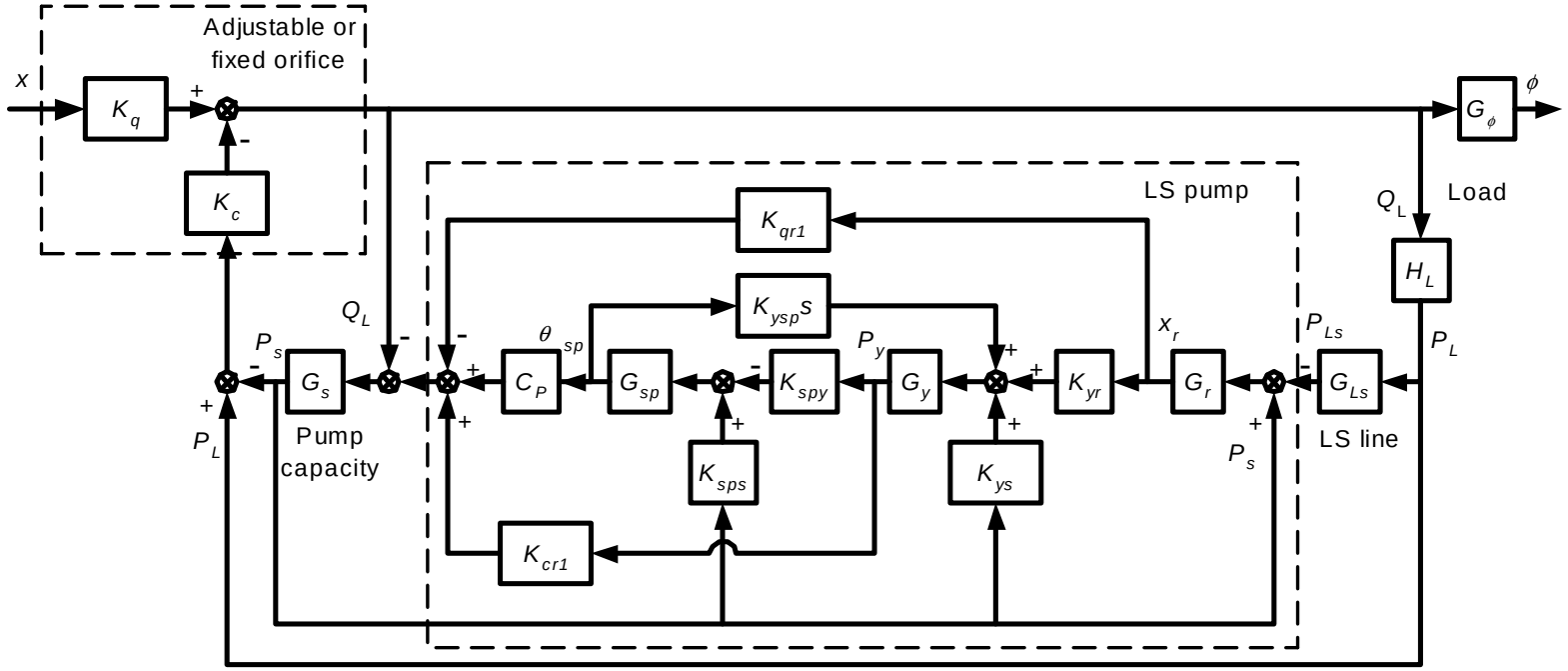

Figure 5.10 Complete Block Diagram of the LS System

5.3.1 System Transfer Function at Condition I

In order to obtain the TF of the LS system at operating Condition I, it is necessary to simplify the block diagram (Figure 5.10). It is very difficult to simplify it using the "rules of block diagram algebra" (Ogata, 1970) due to the fact that the summing points and branch points come into contact with the main path from P_L to P_s.

Consider the block diagram in the dashed line box of Figure 5.10. The block diagram of the load sensing pump is redrawn in Figure 5.11 to reflect a more common form in which the input variable is on the left side and the output is on the right side.

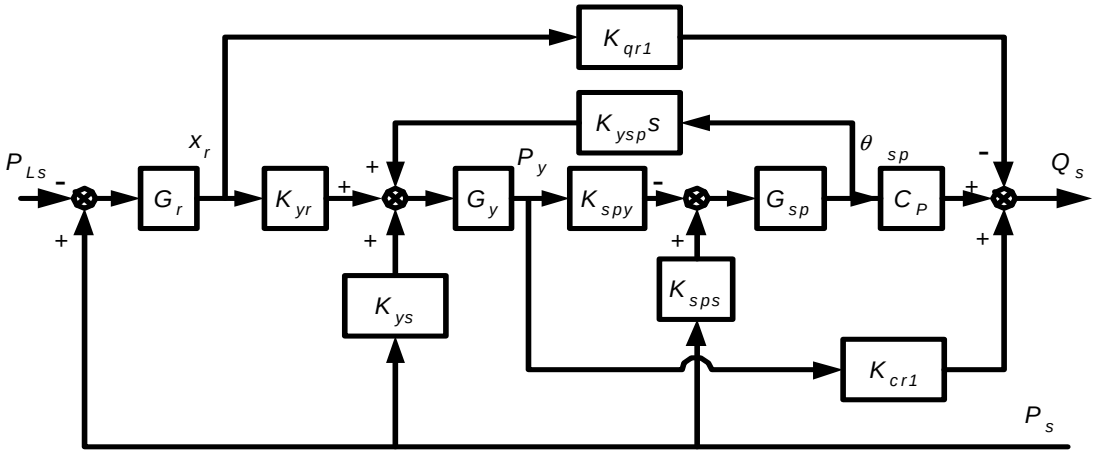

Figure 5.11 Block Diagram of the LS Pump

As a result of the complex nature of the block diagram shown in Figure 5.11, it is desirable to make the model simpler and make it user-friendlier. In order to simplify the block diagram, it is necessary to analyze it and then make some assumption. This block diagram includes one inner loop ($G_y \rightarrow K_{spy} \rightarrow G_{sp} \rightarrow K_{ysp}s$), three feedback paths of the pump pressure (unit feedback, K_{ys} and K_{sps} – the first one is the dominant term) and three feedforward paths (the main feedforward path, K_{qr1} and K_{c1}– the first one is the dominant term). When the operating point is within the operating boundaries of Condition I, certain assumptions can be made to simplify the transfer function and still maintain its validity.

When the operating point approaches the boundaries of Condition II or Condition III the assumptions may not be valid. In the literature, (Bitner and Burton [1984], Erkkila [1999], Kim and Cho [1988], Krus [1988], Lantto, et al, [1990], etc), excluded the non-dominant blocks from their models (feedback: K_{ys} and K_{sps}, and feedforward: K_{qr1} and K_{cr1}). This simplification in the normal operating region, does not affect the model accuracy significantly. However, when the LS system operates in the transition region between Condition I and Condition II or III, the accuracy of the models presented by the aforementioned authors is questionable.

In this study, the non-dominant terms are considered. However, it is very difficult to simplify the block diagram on basis of the rules of the block diagram reduction [Ogata, 1970]. A capitulated assumption was made such that the feedback path can be simplified by neglecting the non-dominant feedforward paths (K_{qr1} and K_{c1}). The feedforward path can be simplified by neglecting the non-dominant feedback paths (K_{ys} and K_{sps}). Even though the non-dominant paths are neglected, the terms K_{qr1} and K_{cr1} are included in the feedforward gain and terms K_{ys} and K_{sps} are included in the feedback gain. With this assumption, Figure 5.11 can be simplified into Figure 5.12.

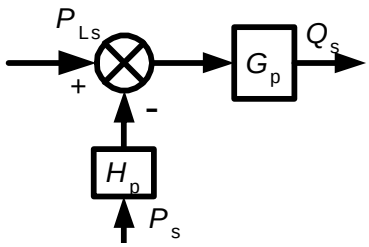

Figure 5.12 Simplified TF of the LS Pump

♦ **Equivalent pressure feedback gain of the LS pump, H_p**

In order to obtain the equivalent pressure feedback gain, H_p, it is necessary to move the second and third addition points of P_s forward until the first addition point (Figure

5.11). Because it was assumed that K_{qr1} and K_{cr1} were negligible, it is feasible to move the second and third addition points to the first addition point.

H_p considers all effect of the three inner feedbacks of the pump pressure, P_s (refer to Figure 5.10). The first inner feedback of the pump pressure relates to the force, A_rP_s, exerted on the LS spool. The second inner feedback reflects the effects of the pump pressure to the control pressure, P_y, via the flow pressure sensitivity, K_{cr1}, on the "charge" orifice, and the third corresponds to the "back pressure" on the swash plate. H_p can be derived on the basis of the rule of the block diagram algebra to give

$$\begin{aligned} H_p(s) &= 1 + \frac{K_{ys}}{K_{yr}G_r(s)} - \frac{K_{sps}}{K_{yr}K_{spy}G_r(s)G_y(s)} \\ &= 1 + \frac{1}{K_{yr}K_r}\left(\frac{s^2}{\omega_r^2} + \frac{2\zeta_r s}{\omega_r} + 1\right)\left(K_{ys} - \frac{K_{sps}}{K_{spy}}\left(\frac{s}{\omega_y} + 1\right)\right) \end{aligned} \tag{5.62}$$

Equation (5.62) can be simplified for the low frequency regions as

$$H_p = 1 + \frac{K_{ys}}{K_{yr}K_r}\left(1 - \frac{K_{sps}}{K_{spy}K_{ys}}\right) \tag{5.63}$$

Substituting equations (5.3), (5.11), (5.12), (5.33) and (5.35) into above equation gives

$$H_p = 1 + \frac{K_{cr1}k_r}{A_r\left(K_{qr1} + \left|K_{qr2}\right|\right)}\left(1 - \frac{\left(1 + \frac{K_{cr2}}{K_{cr1}}\right)\left(K_{pr2} - K_{pr3}\theta_{sp0}\right)}{R_{py}A_y}\right) \tag{5.64}$$

♦ **Equivalent feedforward gain of the LS pump, G_p**

Because it was assumed that K_{ys} and K_{sps} were negligible, it is feasible to combine the non-dominant feedforward term, K_{cr1}, into the pump gain term, C_p, to give an equivalent C_p^* as

$$C_p^* = C_p\left(1-\frac{K_{cr1}}{C_p K_{spy}}\left(\frac{s^2}{\omega_{sp}^2}+\frac{2\zeta_{sp}s}{\omega_{sp}}+1\right)\right) \tag{5.65}$$

Considering the fact that the term, $\frac{K_{cr1}}{C_p K_{spy}}$, is usually less than 0.01 at Condition I, less than 0.1 in the transition region between Conditions I and II, and ω_{sp} = 78 ~ 190 rad/s, the effect of the dynamics term, $\frac{s^2}{\omega_{sp}^2}+\frac{2\zeta_{sp}s}{\omega_{sp}}+1$, on C_p^* is negligible. Therefore,

$$C_p^* = C_p\left(1-\frac{K_{cr1}}{C_p K_{spy}}\right) = C_p\left(1-\frac{K_{cr1}\left(K_{sp}+K_{pr3}P_{s0}\right)}{C_p R_{py} A_y}\right) \tag{5.66}$$

In order to derive the equivalent feedforward gain of the LS pump, G_p, Figure 5.11 is redrawn into Figure 5.13 in which an inner loop shown in the dashed line box relates to the velocity feedback of the control piston. The TF of the inner loop is

$$\begin{aligned} G_{pinloop} &= \frac{-K_{spy}G_y(s)G_{sp}(s)}{1+K_{spy}G_y(s)G_{sp}(s)K_{ysp}s} \\ &= \frac{\dfrac{-K_{spy}}{\left(\dfrac{s^2}{\omega_{sp}^2}+\dfrac{2\zeta_{sp}s}{\omega_{sp}}+1\right)\left(\dfrac{s}{\omega_y}+1\right)}}{1+\dfrac{\dfrac{s}{\omega_{ysp}}}{\left(\dfrac{s^2}{\omega_{sp}^2}+\dfrac{2\zeta_{sp}s}{\omega_{sp}}+1\right)\left(\dfrac{s}{\omega_y}+1\right)}} = \frac{-K_{spy}}{\left(\dfrac{s^2}{\omega_{sp}^2}+\dfrac{2\zeta_{sp}s}{\omega_{sp}}+1\right)\left(\dfrac{s}{\omega_y}+1\right)+\dfrac{s}{\omega_{ysp}}} \end{aligned} \tag{5.67}$$

where

$$\omega_{ysp} = \frac{1}{K_{spy}K_{ysp}} = \frac{\cos^2\theta_{sp0}\left(K_{cr1}+K_{cr2}\right)\left(K_{sp}+K_{pr3}P_{s0}\right)}{R_{py}^2 A_y^2} \tag{5.68}$$

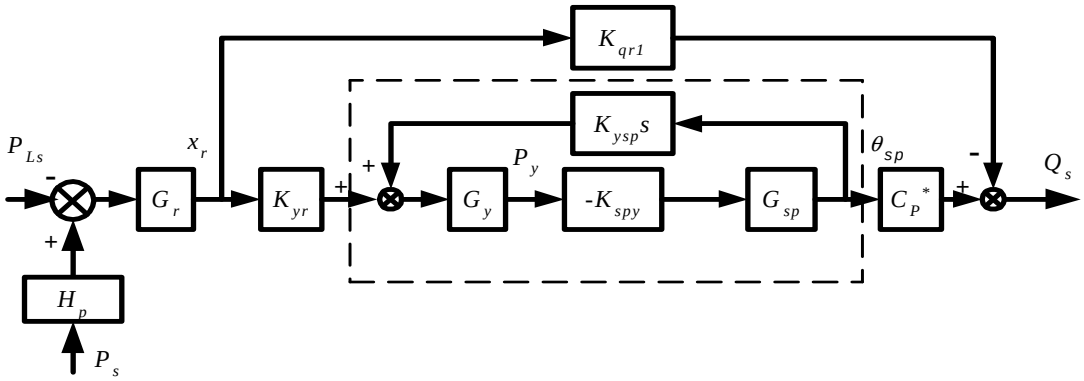

Figure 5.13 Block Diagram of the LS Pump at Condition I

For the pump and valve examined, ω_{ysp} = 0.19 ~ 1.23 rad/s, ω_{sp} = 78 ~ 190 rad/s and $\omega_{sp} < \omega_y$ (see Table 5.1). Therefore, Equation (5.67) can be reduced to

$$G_{pinloop} = \frac{-K_{spy}}{\left(\frac{s}{\omega_{ysp}}+1\right)\left(\frac{s^2}{\omega_{Lsp}^2}+\frac{2\zeta_{Lsp}s}{\omega_{Lsp}}+1\right)} \tag{5.69}$$

where $\omega_{Lsp} = \omega_{sp}\sqrt{\frac{\omega_y}{\omega_{ysp}}}$ (5.70)

$$\zeta_{Lsp} = \left(\zeta_{sp} + \frac{\omega_y}{2\omega_{sp}}\right)\sqrt{\frac{\omega_{ysp}}{\omega_y}} \tag{5.71}$$

Table 5.1 Frequency Parameters of the LS Pump's Dynamics Characteristics (Condition I)

Range	ω_{ysp} (rad/sec)	ω_{sp} (rad/sec)	ω_y (rad/sec)
Min	0.19 (θ_{sp0} = 18°; P_{s0} = 0.76MPa)	78 (P_{s0} = 0.76Mpa)	407 (θ_{sp0} = 0°)
Max	1.23 (θ_{sp0} = 0°; P_{s0} = 20MPa)	190 (P_{s0} = 20Mpa)	2200 (θ_{sp0} = 18°)

In additions, when ω < 1000 rad/s, Equation (5.67) can be further approximated as

$$G_{pinloop} = \frac{-K_{spy}}{\frac{s}{\omega_{ysp}} + 1} \tag{5.72}$$

Figure 5.14 is the simplified block diagram of the studies LS pump which can be further reduced. The TF of the LS pump, $G_p(s)$, can be obtained from Figure 5.14 as

$$G_p(s) = \frac{K_p\left(\frac{s}{\omega_{p0}} + 1\right)}{\left(\frac{s}{\omega_{ysp}} + 1\right)\left(\frac{s^2}{\omega_r^2} + \frac{2\zeta_r s}{\omega_r} + 1\right)} \tag{5.73}$$

where $K_p = K_r K_{yr} K_{spy} C_p^* (1+\gamma)$ (5.74)

$$\omega_{p0} = \frac{\omega_{ysp}}{\gamma}(1+\gamma) \tag{5.75}$$

$$\gamma = \frac{K_{qr1}}{K_{yr} K_{spy} C_p^*} \tag{5.76}$$

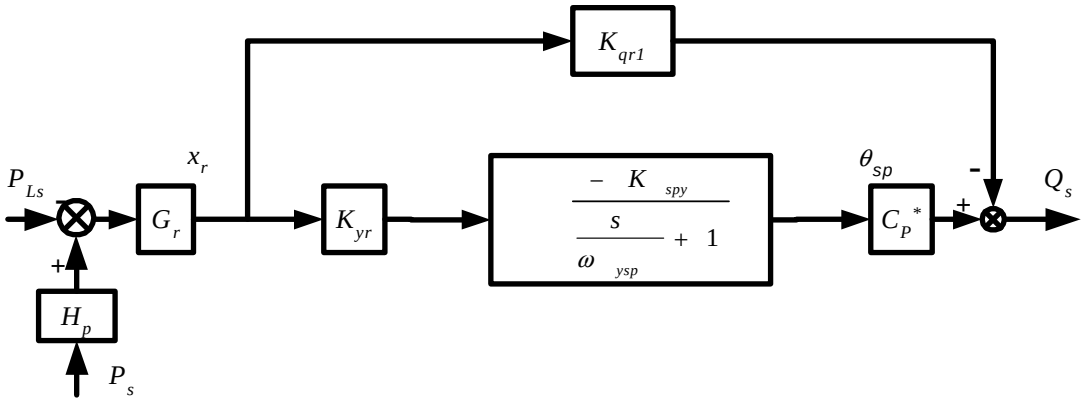

Figure 5.14 Simplified Block Diagram of the LS Pump

Substituting Equations (5.33), (5.12), (5.37) and (5.66) into Equation (5.76) gives

$$\gamma = \frac{(K_{cr1} + K_{cr2})(K_{sp} + K_{pr3} P_{s0})}{C_p R_{py} A_y \left(1 + \frac{|K_{qr2}|}{K_{qr1}}\right)\left(1 - \frac{K_{cr1}(K_{sp} + K_{pr3} P_{s0})}{C_p R_{py} A_y}\right)} \tag{5.77}$$

Substituting Equations (5.3), (5.33), (5.12), (5.37) and (5.66) into Equation (5.74) gives

$$K_p = \frac{A_r}{k_r} \frac{C_p R_{py} A_y \left(K_{qr1} + \left|K_{qr2}\right|\right)\left(1 - \dfrac{K_{cr1}\left(K_{sp} + K_{pr3} P_{s0}\right)}{C_p R_{py} A_y}\right)}{\left(K_{cr1} + K_{cr2}\right)\left(K_{sp} + K_{pr3} P_{s0}\right)} (1+\gamma)$$

$$\text{or } K_p = \frac{A_r}{k_r}\left(\frac{C_p R_{py} A_y \left(K_{qr1} + \left|K_{qr2}\right|\right)\left(1 - \dfrac{K_{cr1}\left(K_{sp} + K_{pr3} P_{s0}\right)}{C_p R_{py} A_y}\right)}{\left(K_{cr1} + K_{cr2}\right)\left(K_{sp} + K_{pr3} P_{s0}\right)} + K_{qr1} \right) \tag{5.78}$$

γ in Equation (5.76) represents the ratio of leakage flow gain (via the LS regulator), $K_{qr1} = \dfrac{\partial Q_{r1}}{\partial x_r}$, and the control gain, $C_p^* \dfrac{\Delta\theta_{sp}}{\Delta x_r}$ [1], in the main path. From the point of view of energy saving, γ is expected to be small because physically this reflects the orifice's leakage. However, a very small K_{qr1} (hence K_{qr2} because symmetry about the null position was assumed in the model) results in a very small equivalent gain of the LS pump (see Equation (5.78)).

Substituting Equations (5.68) and (5.77) into Equation (5.75) gives

$$\omega_{p0} = \frac{N R_p A_p \omega}{\pi R_{py} A_y}\left(1 + \frac{\left|K_{qr2}\right|}{K_{qr1}}\right)\left(1 - \frac{K_{cr1}\left(K_{sp} + K_{pr3} P_{s0}\right)}{C_p R_{py} A_y}\right)(1+\gamma) \tag{5.79}$$

It is noted that $G_p(s)$ accommodates a change in sign of P_{Ls} and P_s at the summing point in Figure 5.14. It should be noted that the input signal in Figures 5.14 is ($H_p P_s - P_{Ls}$) while the input signal in Figure 5.12 is ($P_{Ls} - H_p P_s$).

[1] Δ represents the small signal analysis

Because the undamped natural frequency, ω_r, of the LS spool is very high (in this study, ω_r = 1954 rad/s) compared to ω_{ysp} (in this study, ω_{ysp} < 1.23 rad/s), Equation (5.73) can be further simplified as

$$G_p(s) = \frac{K_p\left(\frac{s}{\omega_{p0}}+1\right)}{\left(\frac{s}{\omega_{ysp}}+1\right)} \tag{5.80}$$

Consequently, the dashed line box in Figure 5.10 is simplified into a single block in Figure 5.12 which represents the TF of the LS pump (refer to Equations (5.64) and (5.80)) at operating Condition I. As a result of the simplification, the block diagram shown in Figure 5.10 now becomes the block diagram originally shown in Figure 5.2 at operating Condition I.

The TF of the overall LS system can be obtained from the Mason's gain formula as

$$F(s) = \frac{K_q\left(1+G_pG_sH_p\right)G_\phi}{1+K_cH_L+K_cG_s+G_pG_sH_p+K_cH_LG_pG_s\left(H_p-G_{Ls}\right)}$$

$$= \frac{K_q\left(1+\frac{K_pK_sH_p\left(\frac{s}{\omega_{p0}}+1\right)}{\left(\frac{s}{\omega_{ysp}}+1\right)\left(\frac{s}{\omega_s}+1\right)}\right)\frac{K_\phi}{\left(\frac{s^2}{\omega_L^2}+\frac{2\zeta_Ls}{\omega_L}+1\right)}}{1+\frac{K_cK_L\left(\frac{s}{\omega_{L0}}+1\right)}{\left(\frac{s^2}{\omega_L^2}+\frac{2\zeta_Ls}{\omega_L}+1\right)}+\frac{K_sK_c}{\left(\frac{s}{\omega_s}+1\right)}+\frac{K_pK_sH_p\left(\frac{s}{\omega_{p0}}+1\right)}{\left(\frac{s}{\omega_{ysp}}+1\right)\left(\frac{s}{\omega_s}+1\right)}+\frac{K_pK_sK_cK_L\left(H_p-1\right)\left(\frac{s}{\omega_{Lp0}}+1\right)\left(\frac{s}{\omega_{L0}}+1\right)\left(\frac{s}{\omega_{p0}}+1\right)}{\left(\frac{s}{\omega_{ysp}}+1\right)\left(\frac{s^2}{\omega_L^2}+\frac{2\zeta_Ls}{\omega_L}+1\right)\left(\frac{s}{\omega_s}+1\right)\left(\frac{s}{\omega_{Ls}}+1\right)}} \tag{5.81}$$

Equation (5.81) can be presented in a more general form as

$$F(s) = \frac{b_3s^3+b_2s^2+b_1s+b_0}{a_5s^5+a_4s^4+a_3s^3+a_2s^2+a_1s+a_0} \tag{5.82}$$

where all coefficients, a_i and b_i, of the s polynomials in the numerator and the denominator are given in Appendix E.

Equation (5.82) can be compared to Bitner's model [1986]. Bitner [1986] derived a 7th order TF which considered the LS spool dynamics (ω_r = 1954 rad/s). Equation (5.82) neglects effects of system characteristic frequencies higher than 1000 rad/s (refer to the derivation of Equation (5.80)). The reason for doing so can be explained as follows. The system presented by Figure 5.10 has a pair of dominant conjugate poles in which the undamped natural frequency is usually small ($\leq \omega_L$). This pair of dominant conjugate poles can be estimated by Ding's method [1989]. At a frequency of 1000 rad/s, the magnitude of the TF is attenuated by about 40 dB. In other words, the high frequency components in the motor's rotary speed are difficult to identify. It is recognized that if the focus of study is such that high frequency behavior is of concern, the simplifications (Equation (5.67) to Equation (5.72) and Equation (5.73) to Equation (5.80)) made in this section cannot be applied. In this case, a TF or a state space model has to be directly derived from Figure 5.10. This would result in a 9th order model. Although this derivation is not developed in this thesis, the 9th order TF has been developed and programmed for the purpose of comparison to a simplified 5th model. A comparison of the frequency response for the 5th and 9th order transfer functions with four different operating conditions is given in Figure 5.15. The comparison indicates that simplifying the pump's transfer function to that given by Equation (5.80) would not affect the outcome of any analysis of the LS system in the frequency regions of interest in this study. The trivial difference between the 5th and 9th order models at resonant peak can be observed when the flow orifice has a small opening and the LS line has a small damping.

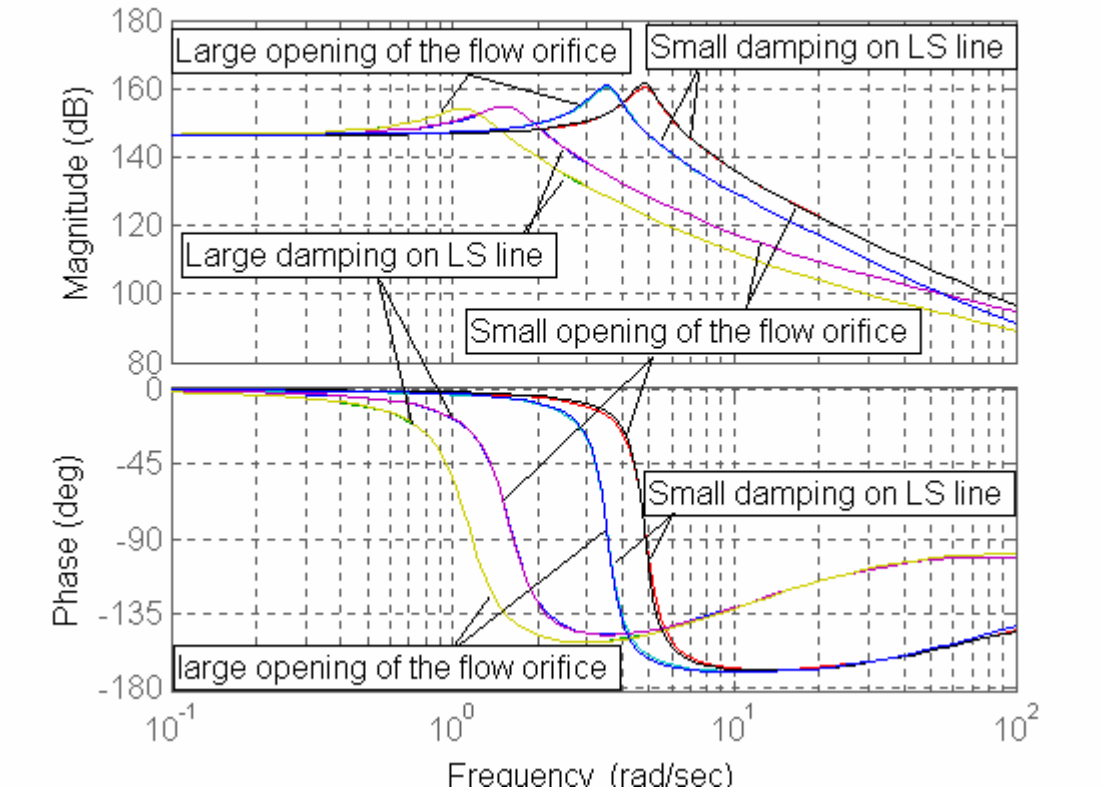

Figure 5.15 Comparison between 9th and 5th models for four different conditions

5.3.2 System Transfer Function at Condition II

When the LS system operates in Condition II, the LS spool does not operate about the null position (see Figure 5.3). Instead, the LS spool moves to the side in which the load pressure is exerted. In this condition, $x_{r0} > 0$, $P_{s0} = P_{y0}$. In order to explain the simplification at Condition II, the LS regulator and the control piston are illustrated as Figure 5.16.

The charge orifice usually is open at Condition II though it may sometimes be closed during the dynamic oscillation. The average opening, x_{r0}, is significant for the small control piston volume, V_y, under Condition II ($P_{y0} = P_{s0}$).

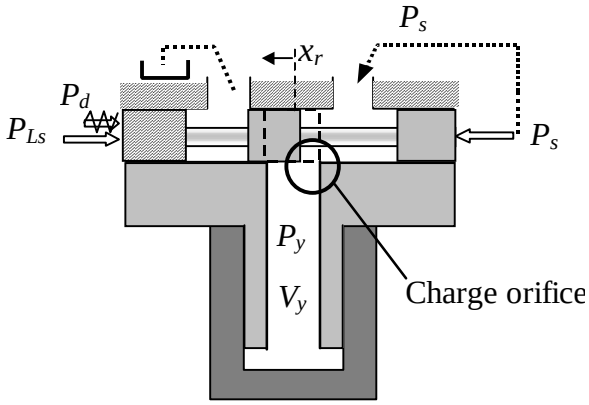

Figure 5.16 Schematic of the LS Regulator and Control Piston at Operating Condition II

The block diagram in Figure 5.10 can be simplified to that shown in Figure 5.17. It is noted that block K_{cr1} in Figure 5.10 does not exist because the two terms which contained K_{cr1} in Equation (5.38) cancel due to $P_{s0} = P_{y0}$. It is further noted that ω_s is independent of K_{cr1} due to this cancellation at Condition II. It can be observed from Figure 5.17 that one positive feedback loop ($G_s \rightarrow K_{sps} \rightarrow G_{sp} \rightarrow C_p$) still exists and hence there is a potential risk of instability.

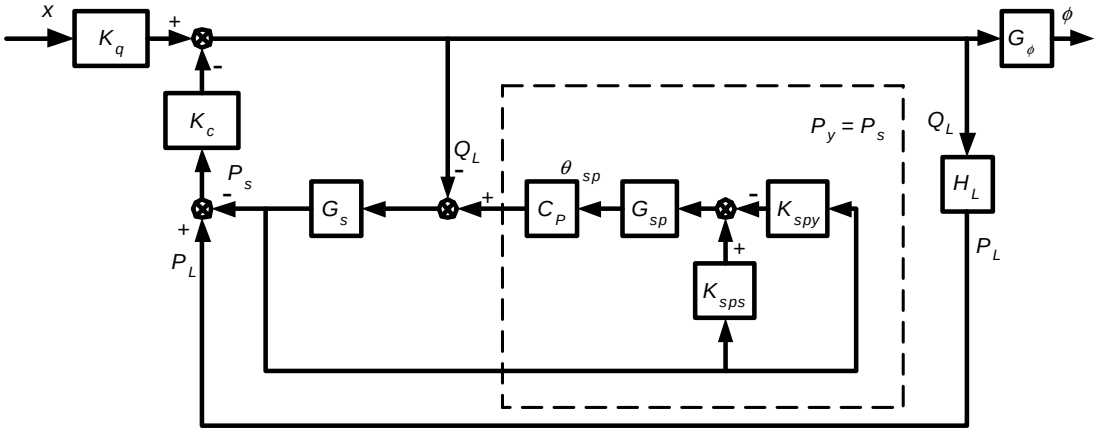

Figure 5.17 Block Diagram of the LS Pump at Condition II

The block diagram is further simplified into Figure 5.18 in which the pressure feedback of the LS pump, H_p, can be written as:

$$H_p = \frac{K_p^*}{\dfrac{s^2}{\omega_{sp}^2} + \dfrac{2\zeta_{sp} s}{\omega_{sp}} + 1} \tag{5.83}$$

$$\text{where } K_p^* = C_P\left(K_{spy} - K_{sps}\right) = \frac{C_p\left(R_{py}A_y - K_{pr2} + K_{pr3}\theta_{sp0}\right)}{K_{sp} + K_{pr3}P_{s0}} \tag{5.84}$$

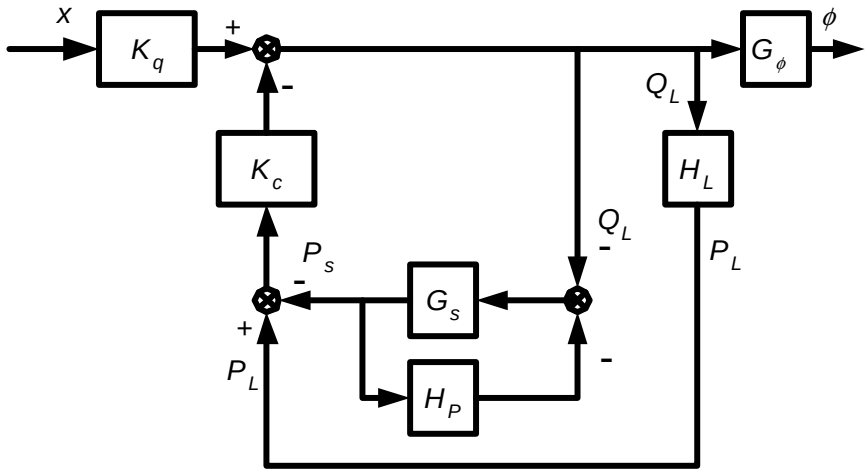

Figure 5.18 Simplified Block Diagram of the LS Pump at Condition II

Equation (5.84) indicates that the coefficients, K_{pr2} and K_{pr3}, of the swash plate's "backpressure" terms in Equation (2.3) (see Chapter 2) affect the pressure feedback gain, K_p^*, under operating Condition II.

The TF of the overall LS system can be obtained from the Mason's gain formula as

$$\begin{aligned} F(s) &= \frac{K_q\left(1 + G_s H_p\right)G_\phi}{1 + K_c H_L + K_c G_s + G_s H_p + K_c H_L G_s H_p} \\ &= \frac{K_q\left(1 + \dfrac{K_p^* K_s}{\left(\dfrac{s^2}{\omega_{sp}^2} + \dfrac{2\zeta_{sp}s}{\omega_{sp}} + 1\right)\left(\dfrac{s}{\omega_s} + 1\right)}\right)\dfrac{K_\phi}{\left(\dfrac{s^2}{\omega_L^2} + \dfrac{2\zeta_L s}{\omega_L} + 1\right)}}{1 + \dfrac{K_c K_L\left(\dfrac{s}{\omega_{L0}} + 1\right)}{\left(\dfrac{s^2}{\omega_L^2} + \dfrac{2\zeta_L s}{\omega_L} + 1\right)} + \dfrac{K_s K_c}{\left(\dfrac{s}{\omega_s} + 1\right)} + \dfrac{K_p^* K_s}{\left(\dfrac{s^2}{\omega_{sp}^2} + \dfrac{2\zeta_{sp}s}{\omega_{sp}} + 1\right)\left(\dfrac{s}{\omega_s} + 1\right)} + \dfrac{K_p^* K_s K_c K_L\left(\dfrac{s}{\omega_{L0}} + 1\right)}{\left(\dfrac{s^2}{\omega_{sp}^2} + \dfrac{2\zeta_{sp}s}{\omega_{sp}} + 1\right)\left(\dfrac{s^2}{\omega_L^2} + \dfrac{2\zeta_L s}{\omega_L} + 1\right)\left(\dfrac{s}{\omega_s} + 1\right)}} \end{aligned} \tag{5.85}$$

Equation (5.85) can expressed in a more general form as

$$F(s) = \frac{b_3 s^3 + b_2 s^2 + b_1 s + b_0}{a_5 s^5 + a_4 s^4 + a_3 s^3 + a_2 s^2 + a_1 s + a_0} \tag{5.86}$$

where all coefficients, a_i and b_i, of s polynomials in the numerator and the denominator are given in Appendix F.

5.3.3 System Transfer Function at Condition III

When the LS system operates in Condition III, the flow control function of the LS pump does not exist. The situation can be observed from Figure 5.10 in which the dashed line box does not exist because $Q_s(s) = 0$ (i.e. the flow delivered is a constant when the pump is fully stroked). Recall that $Q_s(s)$ is actually $\Delta Q_s(s)$ which is zero because the pump swash plate does not move. The block diagram of the LS system is reduced to that shown in Figure 5.19.

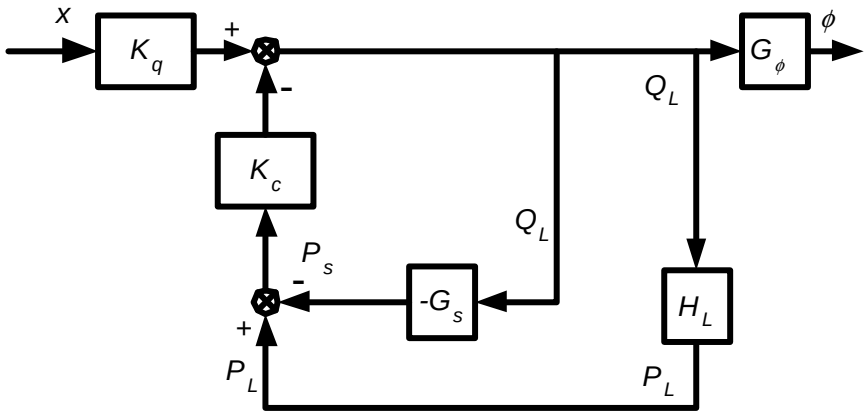

Figure 5.19 Block Diagram of the LS Pump at Condition III

It is noted that no positive feedback loop exists in the block diagram (Figure 5.19). The TF of the overall LS system can be obtained from the Mason's gain formula as

$$F(s)=\frac{K_q\left(\dfrac{K_\phi}{\dfrac{s^2}{\omega_L^2}+\dfrac{2\zeta_L s}{\omega_L}+1}\right)}{1+\dfrac{K_c K_L\left(\dfrac{s}{\omega_{L0}}+1\right)}{\dfrac{s^2}{\omega_L^2}+\dfrac{2\zeta_L s}{\omega_L}+1}+\dfrac{K_s K_c}{\dfrac{s}{\omega_s}+1}} \tag{5.87}$$

Equation (5.87) can be expressed as a more general form as

$$F(s)=\frac{b_1 s+b_0}{a_3 s^3+a_2 s^2+a_1 s+a_0} \tag{5.88}$$

The coefficients of s polynomials in Equation (5.87) are obtained in Appendix G. It can be verified by Routh's stability criterion that the LS system is always stable at condition III (see Appendix G).

This section has developed the TFs of the LS system for conditions I, II, and III. The TF's for conditions I and II are approximated as 5th order and for condition III, the TF is 3rd order.

5.4 Procedure to Calculate the Load Sensing System Stability

This section discusses how to compute the stability of the LS system for the three conditions (I, II, III). For the LS system with the given LS pump (Vickers PVE19Q), most of the model parameters are unchangeable such as the dimension parameters. However, the setting parameters (such as the system pressure differential setting in the LS regulator, P_d), the control input (such as the opening of the flow adjustable orifice area, A_v) and the load parameters (such as the volume of pump's outlet chamber, V_p, the volume of motor's inlet chamber, V_m, the motor damping, B_m, the inertia of motor and the load, J_m, and the resistant torque of the load, T_{mf}) are changeable. The system stability can

be usually described in terms of its "absolute" stability (i.e. conditions in which the system is either "stable" or "unstable") and its relative stability in terms of its undamped natural frequency, ω_n, and its damping ratio, ξ, associated with the dominant poles.

Table 5.2 shows the process that was used to establish the stability for the LS system. The calculations are broken into five steps. The first step is to establish the operating point with the method introduced in Chapter 3. The second step is to estimate the flow gains and the flow-pressure coefficients of the LS regulator orifices and the adjustable orifice. The third step computes the coefficient of the TF's for each functional subsystem based on the models introduced in Sections 5.3. The fourth step calculates the coefficients of the s-polynomial in the denominator and numerator for the TF of the LS system in Section 5.4. Only roots of the denominator determine the stability of the LS system. However, in order to check if there is a "zero-pole cancellation" or a situation in which a zero and a pole on the right half of the s plane are very close each other, it is necessary to know all the zeros determined by numerator. Finally, applying the "root" function of Matlab®, all the poles of the TF of the LS system can be calculated. In the following chapter, the procedure using the models introduced in previous sections will be used to calculate the stability of a specific LS system. The results will be compared to their experimental counterparts.

5.5 Summary

This chapter has established comprehensive frequency-domain models of the LS system for Conditions I, II, & III. A summary of the procedure to evaluate the zero's and pole's is given in Table 5.2. These models relate to the steady state operating points via the flow gains, K_q, the flow-pressure coefficients, K_c, and the non-linear dynamic

Table 5.2 Procedure of Stability Analysis for the LS System

Calculation steps	Parameters
Input parameters	P_d V_p A_v V_m J_m B_m T_{mf} ω_{Ls}
⇩	
Operating point	P_{s0} P_{y0} P_{L0} x_{r0} (Figure 3.3)
⇩	
linearization parameters	K_{qr1} K_{qr2} K_{c1} K_{c2} K_q K_c (Eqs.5.25 through 5.28, Eqs.5.46 and 5.47**)
⇩	
Coefficients of subsystem TFs	K_p K_p^* K_s K_L ω_s ω_L ω_{sp} ω_r ω_y ω_{ysp} ω_{L0} ω_{p0} ζ_L ζ_r ζ_{sp}
⇩	
Coefficients of closed loop TF	a_i b_i (Appendix E, F, and G)
⇩	
Poles and zeros of loop TF	$\sigma_{pi} + j\omega_{pi}$ (i = 1, 2, …9) and $\sigma_{zi} + j\omega_{zi}$ (i = 1, 2, …7) (Matlab programming)

** —— The flow rate, Q_L, through the adjustable orifice usually is turbulent. Therefore, it is unnecessary to use the more accurate flow rate model in Appendix D

equation of the pump swash plate. In order to obtain a precise model of the flow gain and flow-pressure coefficient for the LS regulator orifices, the empirical flow model of an orifice developed in Appendices C & D was used.

These models are experimentally verified in Chapter 6 and are used in Chapter 7 to investigate the relationship between the stability of the LS system and the SSOP's under a variety of operating conditions.

Chapter 6 Validation of Dynamic Models of the Load Sensing System

Chapter 5 has developed the transfer functions of the LS system under Conditions I, II and III. The purpose of this chapter is to experimentally validate these models. The procedure for the validation experiments includes (1) setting up a proper experimental system, (2) determining all parameters of the LS system for the models, (3) the description of the experimental method and (4) a comparison between the theoretical and experimental results.

6.1 Experimental System

Figure 6.1 shows the experimental platform for testing the LS system. The LS system is same as that studied in previous chapters, except that (a) a servo valve acts as the

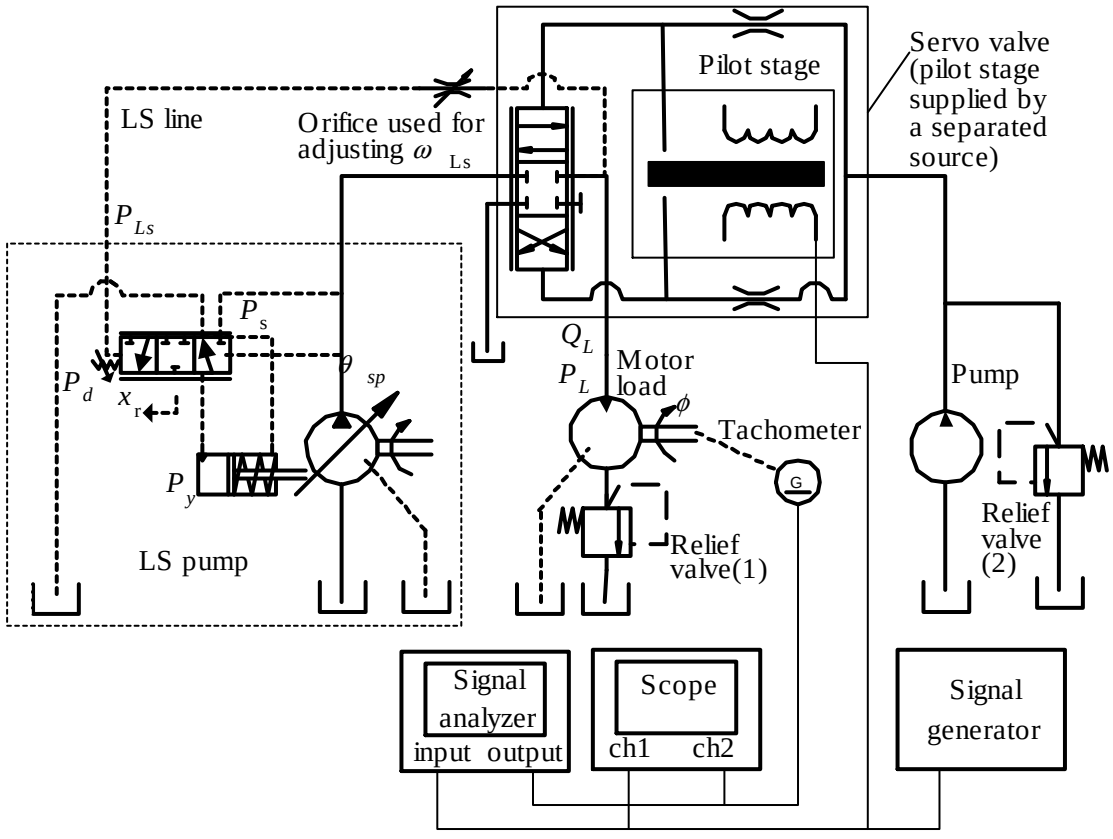

Figure 6.1 Experimental System of frequency response of the LS System

adjusting orifice (compare to Figure 6.1) and (b) a relief valve (1) in Figure 6.1 is positioned downstream of the motor to simulate a constant resistance torque for the load. The experimental setup included a signal generator, a tachometer, a signal analyzer, and a scope.

The servo valve (model: MOOG 72-102) has a pilot stage which was supplied by a separate hydraulic pump and adjustable relief valve (2). For comparative frequency response experiments, it is essential to generate an input signal (the opening of the adjustable orifice, *x*) within a certain bandwidth. A servo valve with suitable frequency response characteristics was selected for this purpose. An additional requirement was that the servo valve had a separate pilot stage source port. The pilot stage of most servo valves uses the same source pressure as the main stage. For this type of servo valve, there are two problems: (a) the dynamic response is poor when the source pressure is lower than the specified operating pressure (usually 3000 psi for a high frequency response servo valve and 1000 psi for the low frequency response servo valve), and (b) the bypass flow through the pilot stage is significant compared to the flow rate through the main stage when the orifice opening of the main stage is small. Therefore, a servo valve with a separated pilot stage source was used. This servo valve (MOOG 72-102) had a response time of 10 ms at 3000 psi pilot pressure.

The relief valve (1) creates a backpressure on the motor load which was used to adjust the operating point. In order to explain the relationship between the relief valve pressure in the experimental circuit and the simulated load torque, the dynamic model of the motor is provided as (refer to Figure 6.1)

$$\dot{\phi} = \frac{1}{J_m}\left(-B_m\phi + D_m\left(P_L - P_{mb}\right) - T_{mf}^{*}\right) \tag{6.1}$$

where P_{mb} is the pressure setting of the relief valve (2) in Figure 6.1. T_{mf}^{*} is the measured value of the motor torque (see Appendix I). Comparing Equation (6.1) to Equation (2.43) gives

$$T_{mf} = T_{mf}^{*} + D_m P_{mb} \tag{6.2}$$

T_{mf}^{*} and D_m are known. Adjusting P_{mb} can change the simulated T_{mf} in Equation (2.43).

A tachometer (model: KEARFOTT CM-09608007) was used to measure the rotary speed of the motor load of the LS system. Appropriate transducers for measuring the operating points, P_{s0}, P_{y0}, P_{L0}, x_{r0}, θ_{sp0} and Q_{L0}, were installed. These were the same transducers used for the operating point determinations described in Chapter 4.

The signal generator provided a pseudo random input signal to control the orifice opening. A signal analyzer was employed to directly obtain the experimental Bode plot.

6.2 Model Parameters

In order to predict stability regions of the LS system (based on the model developed in Chapter 5) the model parameters must be known. Appendix H lists all parameters with a "*****" representing adjustable parameters. A_v is the cross sectional area which is proportional to the adjustable orifice opening, x, as an input variable of the system (Note: the orifice of the servo valve is rectangular type). The pressure differential setting, P_d, the damping frequency in the LS line, ω_{Ls}, and the resistant torque of the load, T_{mf}, are settable. It is noted that the damping frequency in the LS line, ω_{Ls}, does not affect the SSOP. When the back pressure is set to zero, T_{mf} is minimum and represents the motor's Coulomb friction torque.

The values of these parameters were obtained from four sources:

(1) Direct measurement (k_r, m_r, A_y, V_{ymin}, V_p, V_m, J_m),

(2) An internal research report provided by Bitner [1996] (A_r, B_r, R_{py}, R_p, A_p, ω, K_{sp}, T_{sp}, K_{pr2}, K_{pr3}, B_{sp}, J_{sp},),

(3) Manufacturer specifications (β, ρ, μ, θ_{spmax}, c_{ml}, D_m) and

(4) Experimental methods (d_r, w_r, c_{pl}, C_d, B_m, T_{mf}, ω_{Ls}).

Some explanatory comments are required regarding the parameters determined by experimental methods. The equivalent height, d_r, and the width, w_r, of the LS regulator orifice at the null point are two important parameters which affect the gain of the LS pump. The description of how they were measured is presented in Appendix D. The procedure for determining the leakage coefficient of the LS pump, c_{pl}, was described in Chapter 4. The method for determining the servovalve discharge coefficient, C_d, is contained in Appendix C. The damping coefficient, B_m, and the Coulomb resistant torque, T_{mf}, of the motor with an inertia load (flywheel) were experimentally determined according to the procedure described in Appendix I. The method for finding the damping break frequency, ω_{Ls}, of the LS line can be found in Appendix J.

6.3 Comparison of the Model Predictions and Experimental Results

This section will provide a frequency domain comparison between the theoretical predictions and experimental results for the dynamic models of the LS system under operating Conditions I, II and III. A comparison can only be conducted for the dominant poles of the LS system due to the finite band width (<20Hz) of the servo valve and the limited resolution of the tachometer.

For the frequency response experiments, it is necessary to explain the method of setting an operating point and the dynamic excitation signal. The input signal applied on the servo-valve has a carrier signal (i.e. a DC voltage plus a small pseudo random). The

DC voltage bias sets the operating point. The small pseudo random signal is a dynamic excitation signal about the operating point. The magnitude of the pseudo random signal must be small. Otherwise, the linarization procedure is invalid. From an experimental point of view, however, the very small magnitude of the pseudo random signal results in a poor SNR (signal to noise ratio) and consequently poor precision in experimental results. In this study, the magnitude of the pseudo random signal is 10 mv which results in small excursions (amplitude of about 1 lpm) in the flow rate about the operating point.

6.3.1 Condition I

The objective of this section is to provide comparisons of the theoretical and experimental frequency response results of the LS system at a small opening and at a large opening (operating points).

For the experiment using a large opening in the valve area, the adjustable parameters were fixed at the values shown in Table 6.1 by setting the relief valve (1) at 500 psi. The linearized parameters, model parameters and the coefficients of the system TF were also determined. Finally, the poles of the TF which related motor rotary speed, $\phi(s)$, to the adjustable orifice opening, $X(s)$, were obtained.

Figures 6.2 and 6.3 show a comparison of Bode diagrams between the model prediction and measured values. Figure 6.2 indicates that the model is an accurate representation particularly at lower frequencies. There is a resonance peak about 6 rad/s. This is a result of a pair of dominant conjugate poles ($s_{1,2}$ = -0.6 ±6j) which yield a small damping ratio (ζ = 0.1).

Table 6.1 An example of Determining Parameters for the Stability Analysis

Adjustable parameters	A_v			Settable parameters	P_d	T_{mf}	ω_{Ls}
	11 mm^2				0.3 MPa	13.7 Nm	450 s^{-1}
Operating point	P_{s0}	P_{y0}	P_{L0}	x_{r0}	θ_{sp0}	Q_{L0}	ϕ_0
	7.6 MPa	3 MPa	7.3 MPa	-0.006 mm	0.055 rad	13 l/min	53 rad/s
Lineaized parameters	K_{q1}	K_{q2}	K_{c1}	K_{c2}	K_c		
	0.099 m^2s^{-1}	-0.092 m^2s^{-1}	$0.5x10^{-12}$ $m^5s^{-1}N^{-1}$	0.8x10-12 $m^5s^{-1}N^{-1}$	$3.6x10^{-12}$ $m^5s^{-1}N^{-1}$		
Model parameters	K_p	K_s	K_L	ω_s	ω_L	ω_{sp}	ω_r
	$2x10^{-8}$ $m^5s^{-1}N^{-1}$	$5x10^{11}$ $m^{-5}sN$	$9.8x10^9$ $m^{-5}sN$	13.8 s^{-1}	18.6 s^{-1}	130 s^{-1}	1954 s^{-1}
	ω_y	ω_{L0}	ω_{p0}	ζ_r	ζ_L	ζ_{sp}	
	290 s^{-1}	0.34 s^{-1}	405 s^{-1}	0.0353	0.06	0.4	
Coefficients of TF	numerator			b_3	b_2	b_1	b_0
				$4.69x10^{-4}$	0.384	143	$2.95x10^4$
	Denominator	a_5	a_4	a_3	a_2	a_1	a_0
		$1.36x10^{-6}$	$0.94x10^{-2}$	5.96	803	1127	$2.95x10^4$
Poles of TF	s_1	s_2	s_3	s_4	s_5		
	-0.6+j6	-0.6-j6	-188	-499	-6248		

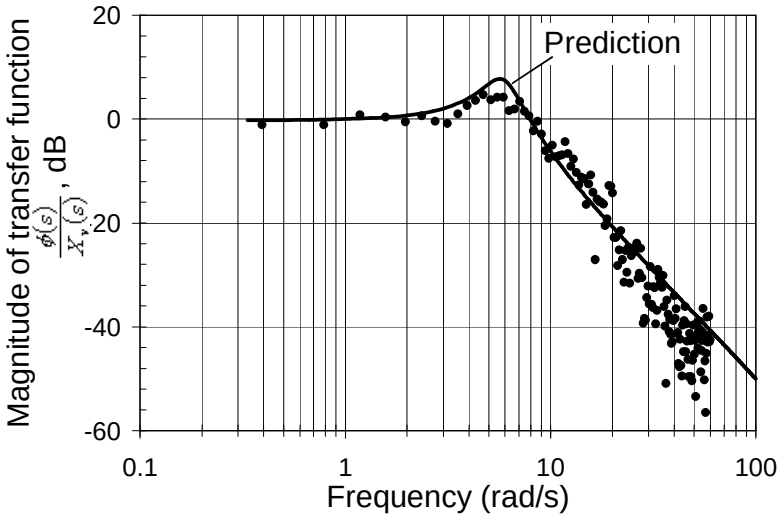

Figure 6.2 Comparison of Magnitudes between the Measured and Predicted Results Using Equation (5.81)

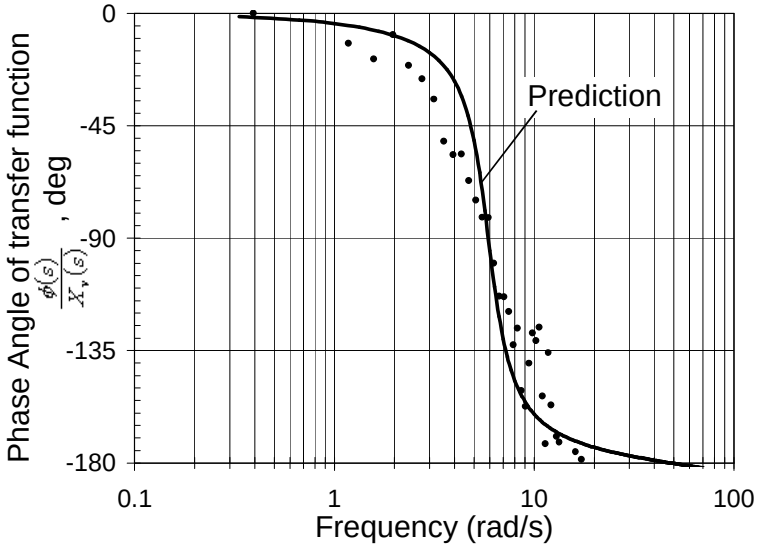

Figure 6.3 Comparison of the Phases between the Measured and Predicted Results Using Equation (5.81)

In order to verify that the relative stability shifts with operating points, another frequency response was measured and calculated at a small orifice opening, *x*. The input parameters, the operating point and the poles of the LS system at the condition of a small orifice opening, *x*, are given in Table 6.2. The comparisons of the magnitudes and phases are shown in Figures 6.4 and 6.5. A resonant peak exists at about 7 rad/s. This is again a consequence of a pair of the dominant conjugated poles ($s_{1,2}$ = -0.5 ± j7.3) with a small damping ratio (ζ = 0.07).

Table 6.2 Another example of Determining Parameters for the Stability Analysis

Adjustable parameters	A_v			Settable parameters	P_d	T_{mf}	ω_{Ls}
	4 mm^2				0.3 MPa	6.1 Nm	250 s^{-1}
Operating point	P_{s0}	P_{y0}	P_{L0}	x_{r0}	θ_{sp0}	Q_{L0}	ϕ_0
	7.2 MPa	3 MPa	6.9 MPa	-0.004 mm	0.025 rad	4.8 l/min	33 rad/s
Poles of TF	s_1	s_2	s_3	s_4	s_5		
	-0.5+j7.3	-0.5-j7.3	-247+j177	-247-j177	-2336		

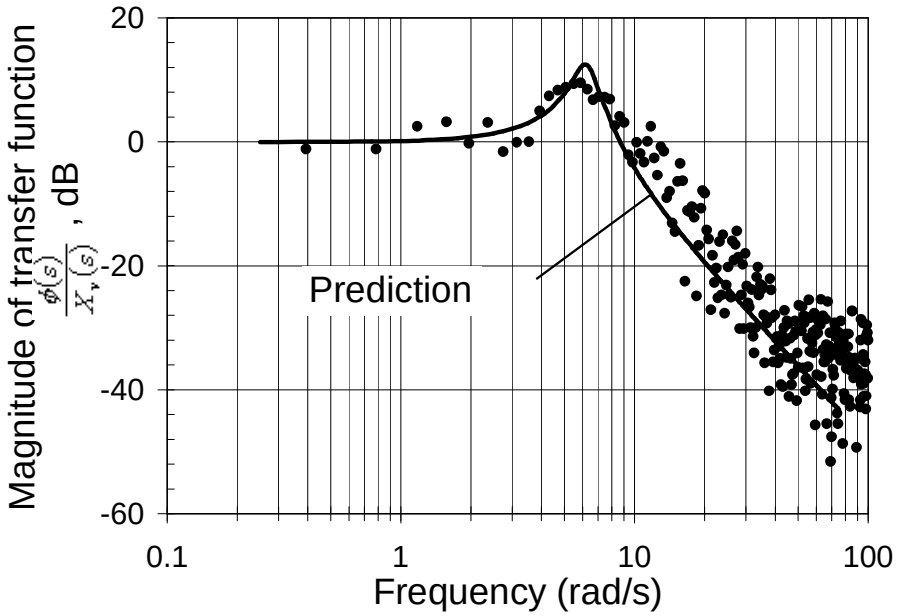

Figure 6.4 Comparison of the Magnitudes between the Measured and Predicted Results Using Equation (5.81) with Small Opening of the Adjustable Orifice

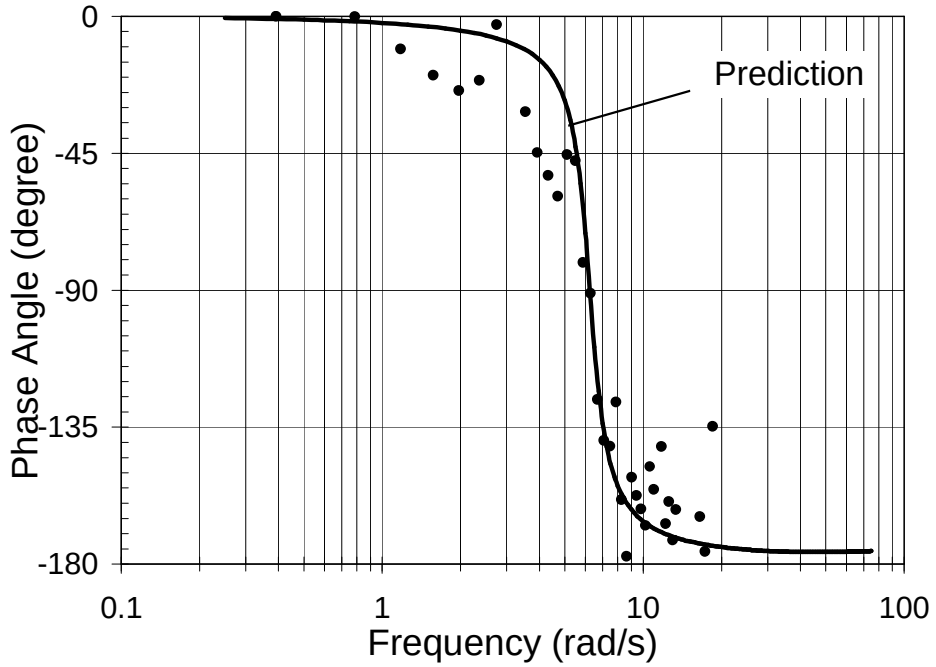

Figure 6.5 Comparison of the Phase between the Measured and Predicted Results Using Equation (5.81) with Small Opening of the Adjustable Orifice

Comparing Figures 6.2 and 6.4 indicates that at the smaller orifice opening, *x*, a higher resonant peak in the magnitude occurred. It can also be observed that the experimental plot in Figure 6.4 has the larger scatter than that in Figure 6.2. This is because SNR at the small opening in the valve area is larger than that at the large opening.

6.3.2 Condition II

In order to validate the model for the operating Condition II, it is necessary to predict the locus of the pair of the dominant poles as the opening, *x*, of the adjustable orifice increases (see Figure 6.6). The purpose of the prediction is to determine a proper operating point for the experiments. Based on model predictions, this pair of the dominant poles is sensitive to the operating points. For example, when the opening of the adjustable orifice begins to increase from zero, the dominant poles of the LS system are a pair of conjugate poles. The corresponding undamped natural frequency is 18 rad/s at a

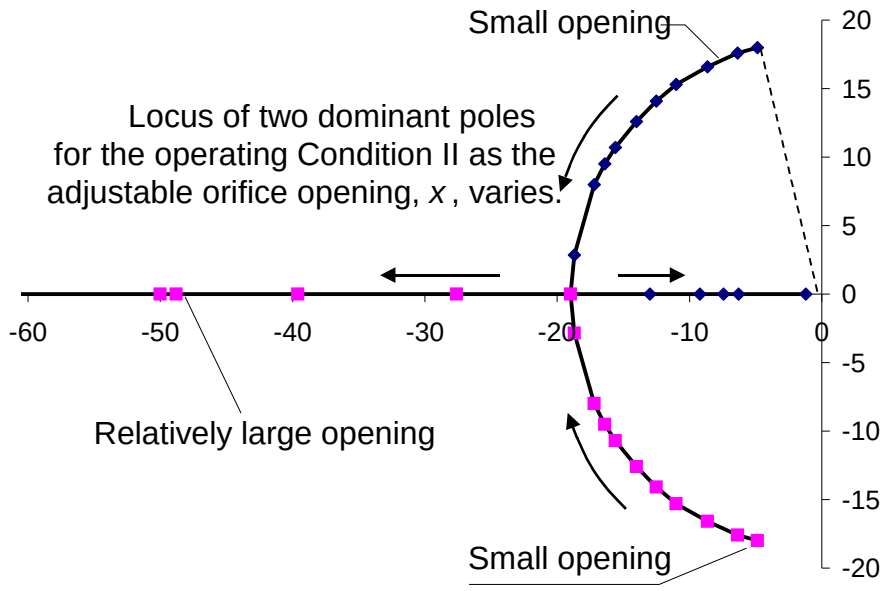

Figure 6.6 Root Locus of the LS system for Condition II

small opening, x. The smaller the opening is set at, the smaller the damping ratio becomes. When the opening reaches a specific value (flow rate about 0.87 litre/min), the damping ratio is larger than 0.7 and hence the large oscillations disappear. The model prediction also indicates that in the high frequency regions, another pair of conjugate poles with positive real parts (about 100 ~ 300 rad/s) may exist when the opening, x, is large depending on the operating point. However, this pair of poles is approximately cancelled by a pair of zeros which are very close to them. Therefore, experimentally, this pair of poles in the region of 100 ~ 300 rad/s was seldom detectable.

For the low frequency region of Condition II which requires a small opening of the adjustable orifice, it was difficult to obtain an accurate Bode plot from the signal analyzer due to the low signal-noise-ratio. In order to check if an undamped natural frequency of about 3 Hz (18 rad/s) existed in the experimental system, the orifice opening, x, was set to a very small value (but not zero). Although a pseudo random signal was not applied, the noise in the LS system served the same purpose. A spectral analysis of the output signal can provide this information.

Figure 6.7 shows the spectrum of the measured pump pressure, P_s. In addition to the frequency components of 30 Hz and its harmonic frequencies (caused by the pump rotational speed), a frequency component of 3 Hz in the pressure signal exists. This signal indicates a dominant frequency of about 3 Hz. Therefore, it was concluded that the model could predict the main dynamic characteristics of the actual LS system.

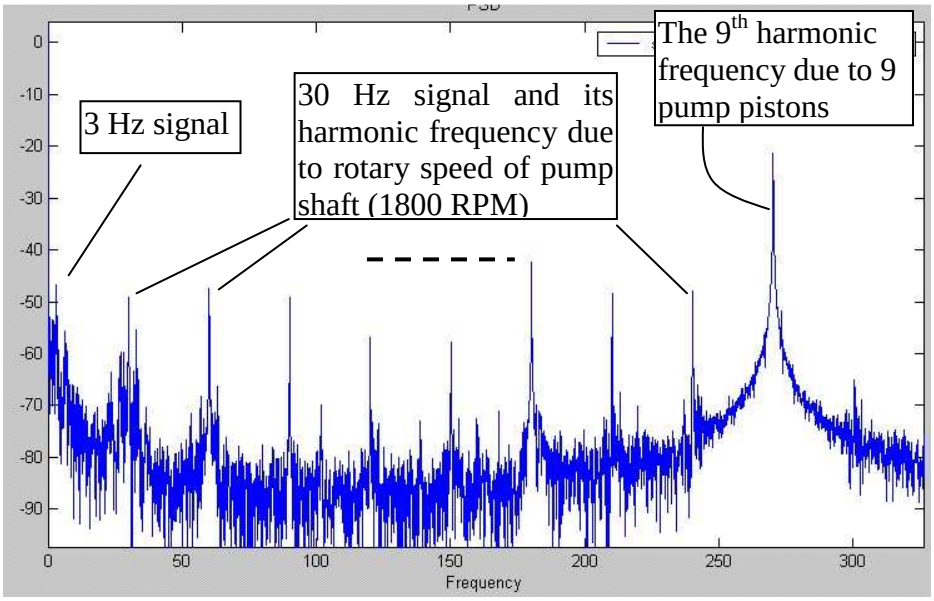

Figure 6.7 Power Spectrum of the Pump Pressure at Condition II

6.3.3 Condition III

When the LS system operates at Condition III, the LS pump acts as a fixed displacement pump since it is fully stroked. The circuit thus becomes a simple fixed displacement pump/valve/motor configuration. For the experimental LS system, the model is given in the normalized form as

$$G(s) = \frac{0.000288(s+3)}{(s+30)(s^2+3.4s+38.54)} \tag{6.3}$$

Equation (6.3) indicates that the system is stable because the TF has a zero (s_z = -3 rad/s), a pair of dominant conjugate poles ($s_{p1,2}$ = -1.7 ± j 6 rad/s), and the other pole (s_{p3} = 30 rad/s). Figures 6.8 and 6.9 show a comparison of the model prediction and the experimental result in the form of Bode plots. It can be observed that the resonant frequency occurs at about 6 rad/s (i.e. 1 Hz). The comparison indicates that the

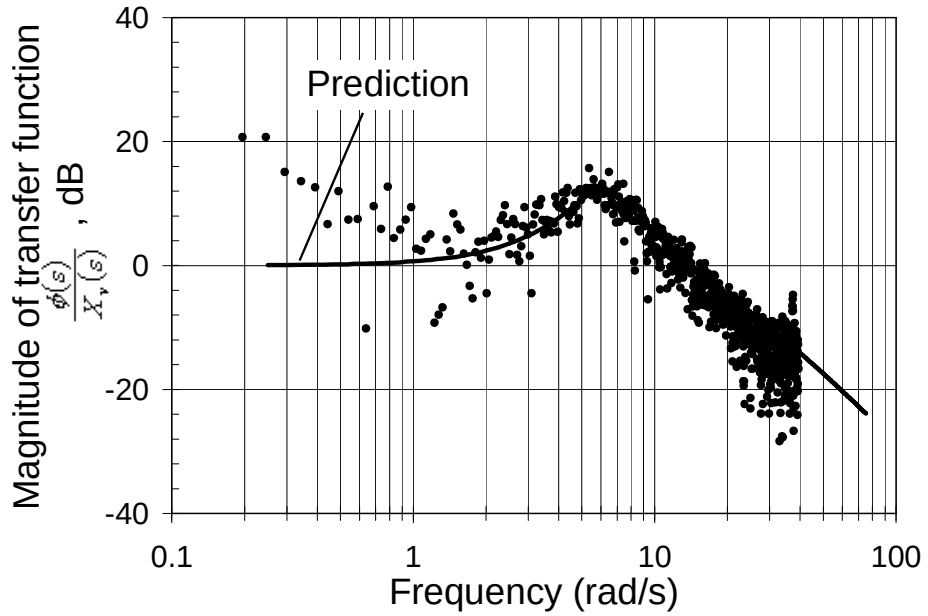

Figure 6.8 Comparison of the Magnitude between the Model and Experimental Results under Operation Condition III

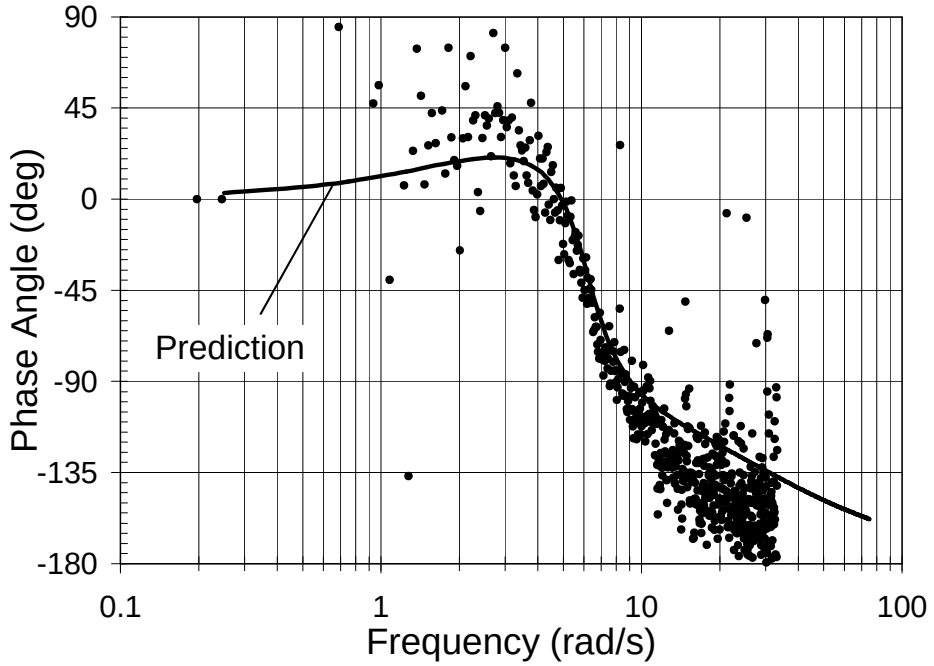

Figure 6.9 Comparison of the Phase between the Model and Experimental Results under Operation Condition III

experimental results show a significant scatter (frequencies less than 2 rad/s) and the predicted results did not agree with their experimental counterpart in this frequency range.

6.4 Summary

This chapter has attempted to experimentally validated the dynamic models of the LS system under operating Conditions I, II and III developed in Chapter 5. A servo valve acts as an adjustable orifice. The opening, x, of adjustable orifice can be proportionally manipulated by DC bias plus a pseudo random signal. The bias sets the operating point and the pseudo signal provides the signal necessary to determine the dynamic response of the LS system. This carrier signal was also fed into a signal analyzer as the input signal of the LS system. The rotary speed of the motor measured by a tachometer was connected to the signal analyzer as the output of the LS system. The experimental result in the form of the Bode plot can be used to compare to the model prediction. The comparisons indicated that the models of the LS system for Condition I, II and III are satisfied for most conditions, the exception being the lower frequency region for Condition III.

Chapter 7 Stability Analysis of the Load Sensing System

Chapter 5 provided a comprehensive block diagram (Figure 5.10) of the LS system and developed the simplified TFs for three different operating conditions. Chapter 6 experimentally verified the dynamic models (i.e. TF's for operating Conditions I, II and III) in the low frequency regions. This chapter uses the stability model developed in Chapter 5 to analyze the stability of the LS system at a variety of operating points as a function of the opening of the adjustable orifice.

When the aforementioned opening varies from zero to its maximum, the operating points associated with the appropriate variables move and form "trajectories". In addition for the same opening but under different load conditions, the trajectory is different. Before the stability of the LS system is discussed, it is necessary to first illustrate some common SSOP trajectories when the orifice is adjusted in a practical LS system. The stability is then calculated at each operating point along these common SSOP trajectories. It must be noted that initially the damping-adjustable orifice in Figure 5.3 is fully opened. The effect of the damping orifice in the LS line on stability at a specific SSOP is then discussed.

7.1 Trajectory of Steady State Operating Points for the Load Sensing System

In order to investigate how the stability varies as the operating point shifts, it is necessary to know some common trajectories during operation. In practice, it is necessary to determine flow control of the LS system by changing the opening, x_v, of the flow orifice at certain load conditions such as J_m, B_m c_{ml}, D_m and T_{mf}. In this study, it is assumed that J_m, B_m, c_{ml} and D_m are constant. The load resistance, T_{mf}, however, can be different. Such is an application when, for example, a crane or an excavator lifts its load;

T_{mf} is a large positive value. When unloaded, T_{mf} is a small positive value or can even become negative (i.e. runaway load: $T_{mf} < 0$). For different T_{mf}, the trajectory of the SSOP of the LS system can be quite different when varying x_v. To assist in this discussion, two types of trajectories are defined. Before proceeding, it is necessary to know the pump's initial status (the pump is almost destroked even though the orifice has not been opened). Assume that the load pressure, P_{L0}, is zero initially. According to Equation (3.20) in Chapter 3, the pump's initial pressure is determined by

$$P_{si} = \begin{cases} P_d & P_d \geq P_{s2} \quad \text{(Condition I)} \\ P_{s2} & P_d < P_{s2} \quad \text{(Condition II)} \end{cases} \tag{7.1}$$

It is necessary to further explain Equation (7.1). First, Condition III is not possible because the pump is destroked (zero flow). When P_d is set to be larger than P_{s2}, the assumption behind Condition II (that is, $P_{s0} > P_d$ due to $P_{L0} = 0$, — refer to Equation (3.20)) would result in a prediction that $P_{s0} > P_{s2}$ (refer to Figure 3.2) which is not physically possible. Therefore, the pump pressure, P_{si}, can only be P_d for condition $P_d > P_{s2}$. When P_d is set to be smaller than P_{s2}, the pump pressure, P_{si}, would no longer be equal to P_d, but, equal to P_{s2}, otherwise, the pump flow would not be zero in the initial condition.

Trajectory I:

Trajectory I is a consequence of plotting the SSOP's of the LS system for Condition I or Conditions I & III as a function of the orifice opening. These SSOP's are evaluated using the procedure presented in Figure 3.3 of Chapter 3. However, it is first necessary to determine the actual conditions for Trajectory I. It is known that for certain load conditions (i.e. T_{mf}, B_m, c_{ml} and D_m, constant) the pump pressure always increases as the

flow orifice opening, x_v, increases. Therefore, as long as the pump pressure, P_{s0}, satisfies $P_{s0} > P_{s2}$ (see Figure 3.2) at the zero opening ($x_v = 0$), the LS system would not operate in the region of Condition II. Based on Equation (3.25), $P_{s0} > P_{s2}$ is true if the following condition is satisfied, that is,

$$P_d + \frac{D_m T_{mf}}{\left(c_{ml} B_m + D_m^2\right)} > P_{s2} \tag{7.2}$$

Trajectory I is shown in Figure 7.1, When the orifice has a small opening, the load pressure is soon established (limited by the compressibility of the fluid) and the pump pressure would jump from point x_0 to x_{10}. The trajectory starts from the initial opening ($x_{10} \approx 0$). According to Equation (3.25), the pump pressure, P_{s0}, is equal to $P_d + \frac{D_m T_{mf}}{\left(c_{ml} B_m + D_m^2\right)}$ at x_{10}. The swash plate angle, θ_{sp0}, is not zero, but very small due to

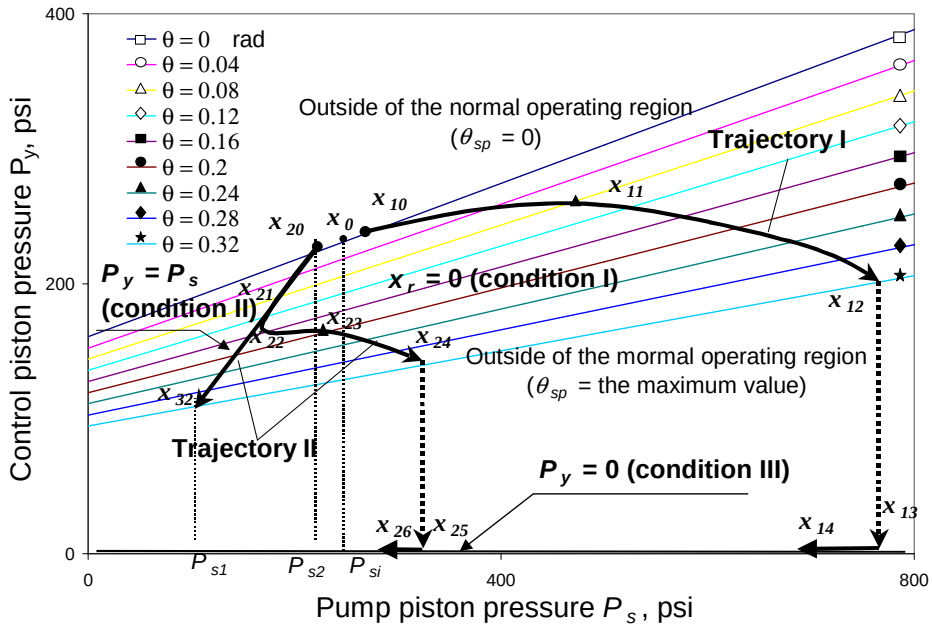

Figure 7.1 Operating Point Trajectories of the LS system

leakage in the pump. As the orifice opening increases, the control piston pressure, P_{y0}, and the pump pressure, P_{s0}, increase until the point x_{11} where the control pressure reaches a maximum value. Beyond x_{11}, the control pressure decreases until the point x_{12} where the pump is fully stroked. At point x_{12}, the pump flow delivery reaches the maximum. Neglecting the leakage in the pump ($c_{pl}P_s$), the flow orifice opening can be approximated by the relationship

$$x_{12} = \frac{NA_p R_p \omega \tan\theta_{sp\max}}{\pi C_d w \sqrt{\frac{2}{\rho} P_d}} \qquad \text{(See Equation (3.31))} \qquad (7.3)$$

As x continues to increase (x_{13}), the control pressure suddenly drops to zero. This is because the flow rate through the orifice now becomes constant (Q_{pmax}) and an increase in the orifice opening, x, must result in a decrease in the pressure drop across the orifice, ($P_s - P_L$). The decrease in ($P_s - P_L$) moves the LS spool such that the discharge orifice is fully opened and as a consequence, the control pressure, P_y, becomes zero. As the orifice opening further increases, the pump pressure decreases (x_{14}) due to the fact that the pump is fully stroked (maximum flow rate, Q_{pmax}).

Trajectory II

Trajectory II is considered as the "trace" of the SSOP's of the LS system starting under Conditions II, as the adjustable orifice is opened gradually. Again, it is noted that these SSOP's are evaluated using the procedure presented in Figure 3.3 of Chapter 3. When Inequality (7.2) cannot be satisfied, the operating point must start from point (x_{20}) at the zero opening (see Figure 7.1). As the opening of the adjustable orifice increases, the operating point moves along a straight line $P_{s0} = P_{y0}$ (x_{21} in Figure 7.1) until a critical point, x_{22}, in which P_{L0} and P_{s0} as solved by Equations (3.37) and (3.38) can no longer

satisfy the essential condition for operating Condition II (i.e. $P_{s0} - P_{L0} > P_d$). In this case, the operating point enters the region of Condition I. As the adjustable orifice opening increases, the remaining segment of Trajectory II is similar to Trajectory I which passes through x_{23}, x_{24}, x_{25} and x_{26}, etc.

If the SSOP cannot reach the break point (x_{22}) on Trajectory II before the swash plate angle increases to the maximum, θ_{spmax}, (point x_{32}), the operating point can only move in the region defined by Conditions II and III. This trajectory usually occurs in the case of a significant runaway load. As the opening of the adjustable orifice increases, the runaway load decreases the resistance as seen by the pump and subsequently, the pressure decreases. In order to determine the condition under which the SSOP would not enter the region of Condition I, consider a typical SSOP ($P_{s0} = P_{y0} = P_{s1}$, $\theta_{sp0} = \theta_{spmax}$) which is the boundary between Condition I, II & III (refer to Figure 7.1). Substituting Equation (3.34) into Equation (3.20) gives

$$P_{s1} - \frac{1}{\left(c_{ml} + \frac{D_m^2}{B_m}\right)}\left[\frac{NA_p R_p \omega \tan\theta_{sp\,max}}{\pi} + \frac{D_m T_{mf}}{B_m}\right] = P_d$$

$$\text{or } T_{mf} = (P_{s1} - P_d)\left(\frac{B_m c_{ml}}{D_m} + D_m\right) - \frac{B_m NA_p R_p \omega \tan\theta_{sp\,max}}{\pi D_m} \qquad (7.4)$$

When the load torque, T_{mf}, is less than the critical value expressed by Equation (7.4), the SSOP moves along the region at Condition II and directly runs into the region at Condition III without entering the region at Condition I (x_{32} in Figure 7.1).

7.2 Stability of the Load Sensing System on Trajectories of Steady State Operating Points

It is well known that stability of a non-linear system depends on its SSOP. This

dependence, in particular in the LS system, is significant. Previous researchers have not adequately addressed this problem. The objective of this section is to investigate the dependence of the LS system on its SSOP's. The stability along the trajectories defined in Section 7.1 is first examined. The absolute and relative stability [Ogata, 1970] of the LS system are graphically presented as a function of the SSOP.

7.2.1 Trajectory I

Figure 7.2 shows an example of Trajectory I for the model parameters defined in Appendix H in which certains variable parameters (pressure differential setting, P_d, resistant torque of the motor load, T_{mf}, and the damping frequency in the LS line, ω_{Ls}), are set to be equal to 2.5MPa, 0.21Nm and 450 s^{-1} respectively. Parameter, A_v, is chosen to be 2.4×10^{-3}, 16.2, 20.9^-, 20.9^+, and 30 mm^2 by setting the needle valve opening, x_v, to an initial start's point (very small value), and then 3.1, 3.4^-, 3.4^+ and 4 turns (see Equation (4.9)). The procedure for determining stability was given in Table 5.2. The results indicated that **in the region of Condition I, the dominant conjugate poles with frequencies less than ω_L (the undamped natural frequency of the motor load), and a second pair of "non dominant" poles with frequencies very close to ω_t (the undamped natural frequency of the LS spool), are those that influence the stability of the LS system.**

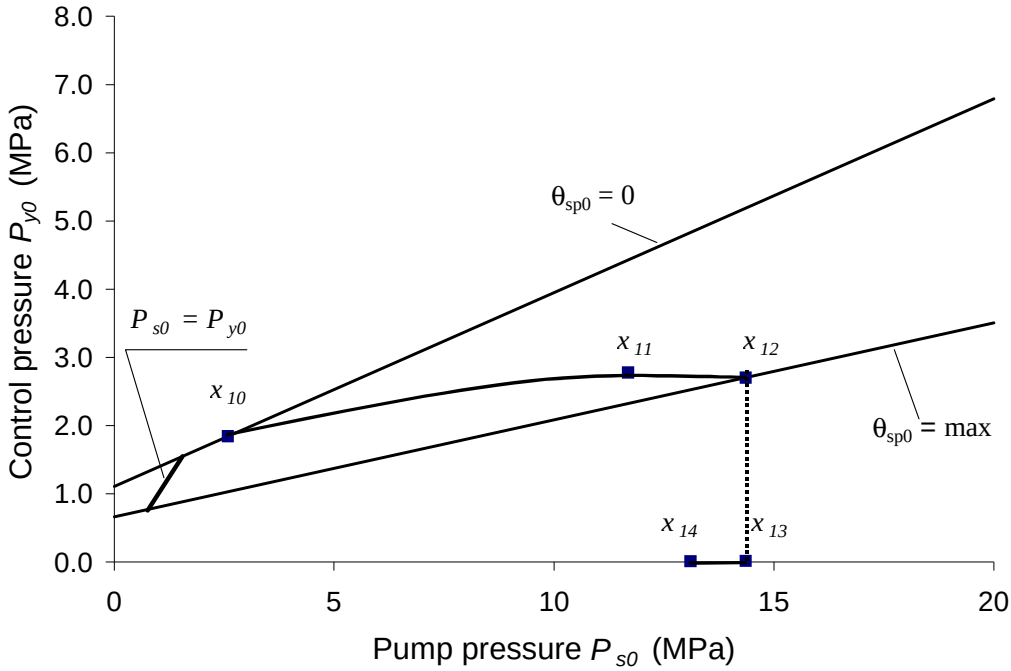

Figure 7.2 Operating point trajectory I of the LS system

Figure 7.3 shows that for Trajectory I, in the region dictated by Condition I, the non-dominant poles (x_{10}, x_{11} and x_{12}) are in the right half of the s plane. The system is unstable in this region. The magnitude of complex part of these poles are close to the undamped natural frequency of the LS regulator spool, ω_r. It can be observed that when the orifice opening is small (x_{10}, x_{11}) the poles and zeros of the LS system transfer function at these frequency points exactly cancel (x_{10}) or approximately cancel (x_{11}).

In a practical LS system, however, instabilities which result from these particular poles are not readily observed in the output flow of the LS system. This is because the poles and zeros cancel. When the dynamic signal becomes large enough, the non-linearity of the LS system results in a limit cycle oscillation. In the presence of a load with a relative large inertia, the high frequency oscillation of about 2000 rad/s are filtered. In other word, the high frequency oscillation in the motor rotary speed cannot be identified. It is noted that the high frequency oscillation might be observable in other

parameters, such as the system pressures, (P_s, P_y and P_L) and the displacement of the LS regulator spool, x_r.

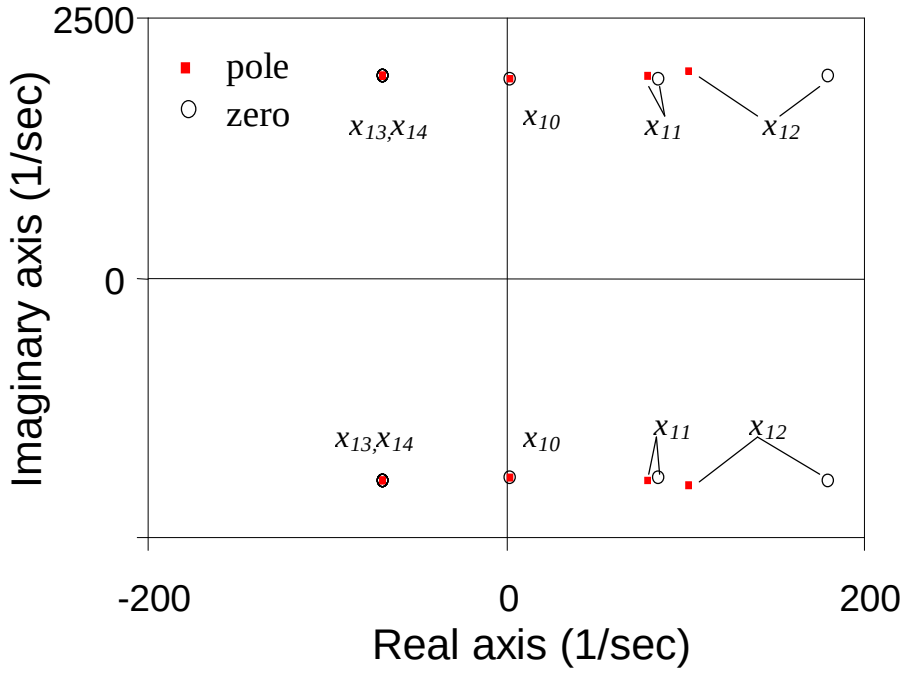

Figure 7.3 Relative stability of the non dominant poles on trajectory I

It is necessary to note that if the lines, which connect the LS pump, the flow control valve, and the load, are soft hoses, the equivalent bulk module of the fluid is much smaller than that of pipes and hence these poles and zeros would occur in the left half of the s plane.

From a more practical perspective, the relative stability of the dominant conjugate poles is of more concern than non-dominant poles described above because of possible low frequency "hunting". This pair of dominant conjugate poles has their frequency component less than ω_L (in this study, ω_L = 18.6 s^{-1}). It can be observed that as the operating point moves along the trajectory shown in Figure 7.2, the damping ratio, ζ, of the dominant conjugate poles shown in Figure 7.4 is approximately constant

($\zeta = cos^{-1}\phi$) but the undamped natural frequency, ω_n, decreases. It can also be observed that when the operating point enters the region of Condition III (pump fully stroked) from Condition I (the normal LS operation), the dominant poles no longer vary (x_{13} and x_{14} in Figure 7.4). The LS system shows more significant oscillations in Condition I than in Condition III, because the damping ratio of the dominant poles (x_{10}, x_{11} and x_{12}) in Condition I is less than that in Condition III (x_{13} and x_{14}).

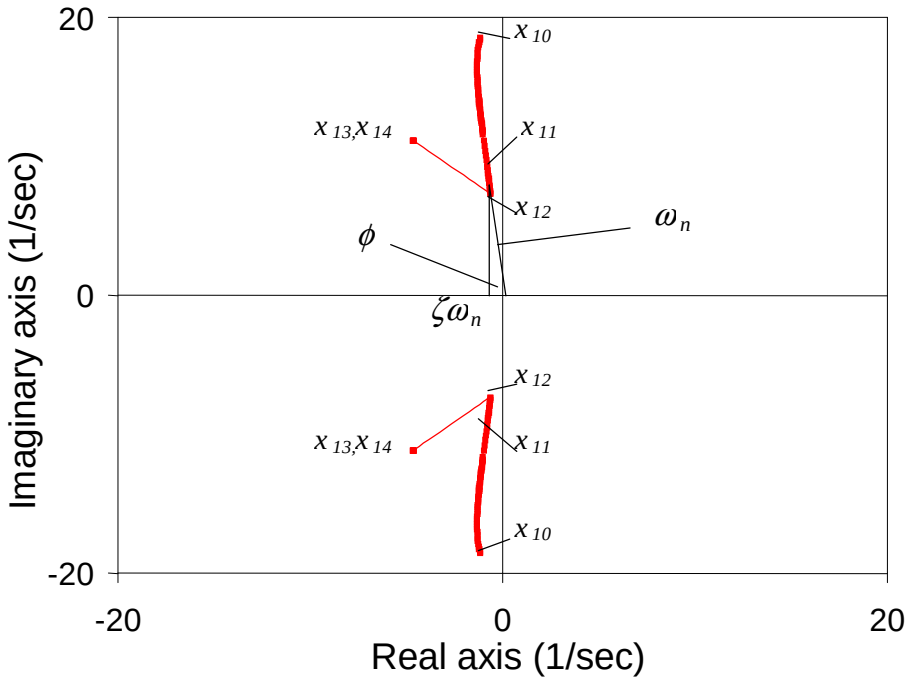

Figure 7.4 Relative stability of the dominant poles on trajectory I

7.2.2 Trajectory II

Figure 7.5 shows Trajectory II. In this example, it is assumed that a "runaway" load with a negative torque of 6.94 Nm is applied to the rotary shaft. When the opening of the adjustable orifice is set to x_{20} (very small value), x_{21} (0.15), x_{22} (0.25), x_{23} (1.34), x_{24} (1.47), x_{25} (1.5), x_{26} (2.4), x_{27} (3.33), x_{28} (3.44^-), x_{29} (3.44^+) and x_{2a} (4), the operating

point moves along the trajectory shown in Figure 7.5. Points, x_{20}, x_{21} and x_{22} are in the region of Condition II. x_{23} is a boundary operating point between Conditions II and I. Points, x_{24}, x_{25}, x_{26} and x_{27} are in the region of Condition I. x_{28} and x_{29} are boundary operating points between Conditions I and III. x_{2a} is in the region of Condition III.

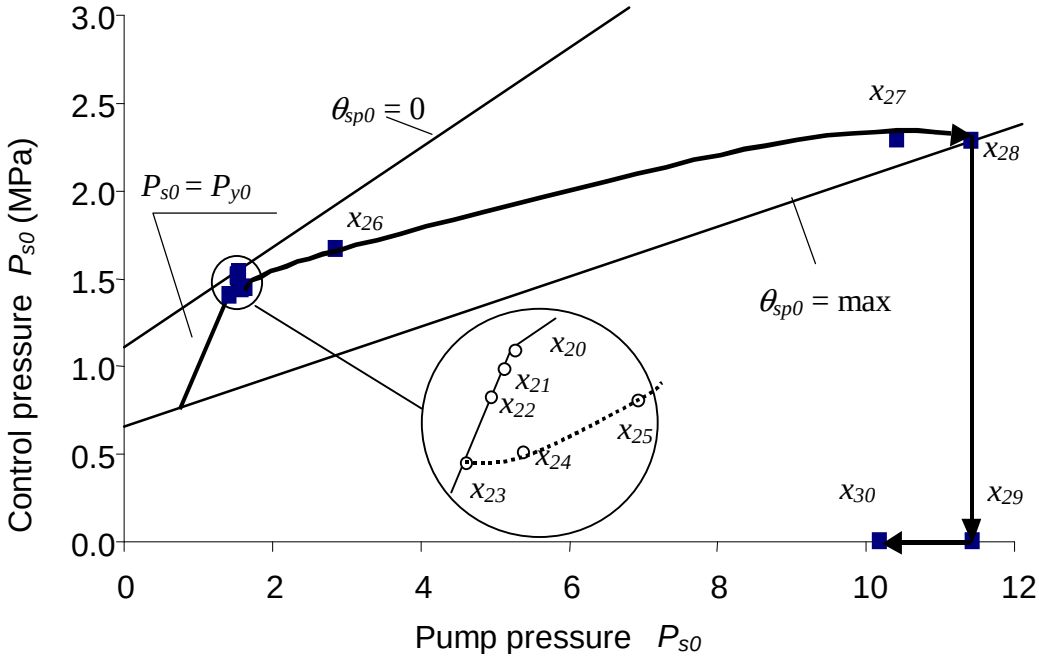

Figure 7.5 Operating point trajectory II of the LS system

Figure 7.6 shows the locus of the dominant poles. The calculation indicates **that, when the system operates in the region of Condition II, at least one pole with a positive real part exists. Therefore, the system is theoretically unstable in the region of Condition II**. **However, for each pole with the positive real part, one zero with a positive real part always exists. These zeros have a value very close to the positive pole and hence can be considered as canceling out.**

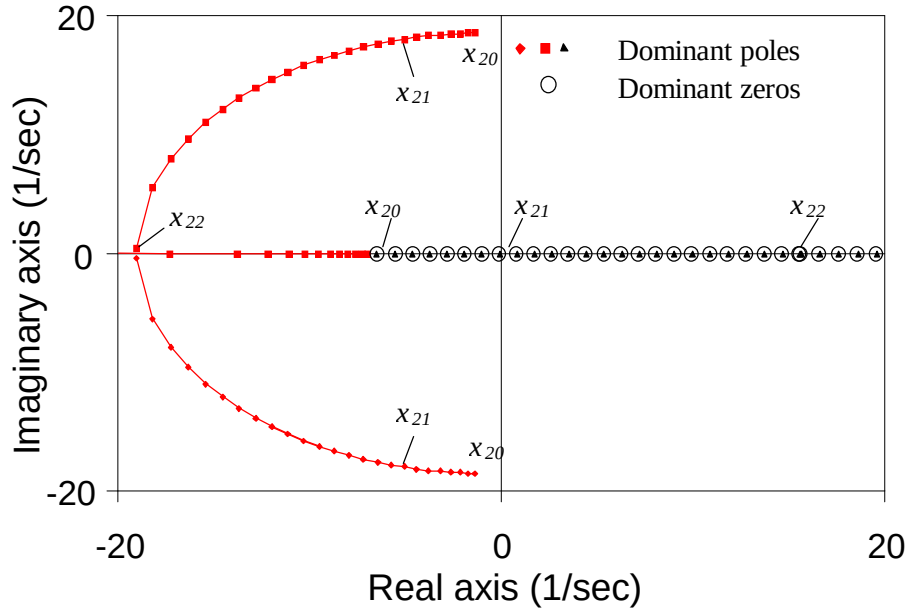

Figure 7.6 Dominant poles on trajectory II in the region of Condition II

When the orifice opening is very small (x_{20} → x_{21}), there are three dominant poles (a real pole and a pair of conjugate poles). The real pole and a real zero in the left half of s plane cancel (see Figure 7.6). The conjugate poles have a small damping ratio. The dominant conjugate poles are very close to the imaginary axis with their frequency component very close to ω_L. As the orifice opening increases (from x_{21} to x_{22}), the damping ratio of the dominant conjugate poles increases due to an increasing of the phase angle of the poles. However, the dominant real pole in this region (from x_{21} to x_{22}) lies in the right half of s plane so that the LS system becomes unstable. At operating point x_{22}, the dominant conjugate poles now become two negative real poles. As the orifice opening continues to increase (x_{23}), the operating point enters the region of Condition I (Figure 7.7). The LS system becomes stable. At the operating point (x_{24}), the two dominant poles become a pair of dominant conjugate poles (Figure 7.7). However, as the operating point shifts from x_{25} to x_{26}, then a pair of non-dominant conjugate poles

shifts to the right half of s plane (shown in Figure 7.8) and the LS system becomes unstable. When the operating point reaches x_{28}, the pump is fully stroked. The operating condition of the LS system suddenly changes from Condition I (x_{28}) to Condition III (x_{29}) in Figure 7.7. In the region of Condition III, the poles no longer vary with increasing x (comparing x_{29} and x_{30} in Figures 7.7 and 7.8). The locus plot of dominant and non-dominant poles indicates that on the trajectory the LS system experiences transitions from "unstable" (x_{20}, x_{21}, x_{22}, x_{23}) to "stable" (x_{24}, x_{25}, and x_{26}) to "unstable" (x_{26}, x_{27} and x_{28}) and then back to "stable" (x_{29} and x_{30}) operating regions.

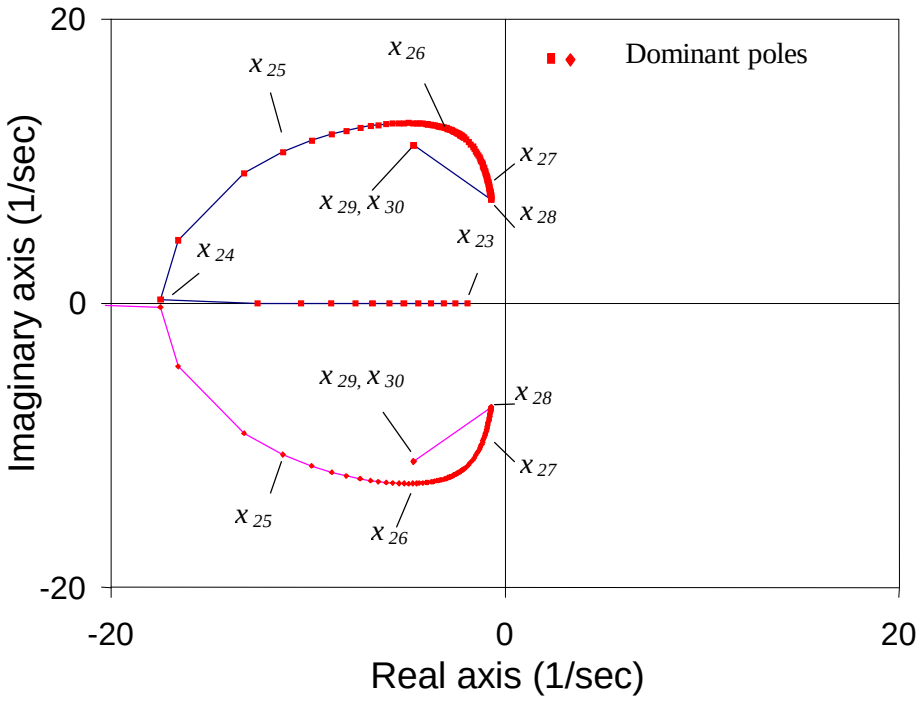

Figure 7.7 Dominant conjugate poles on trajectory II in the region of Condition I

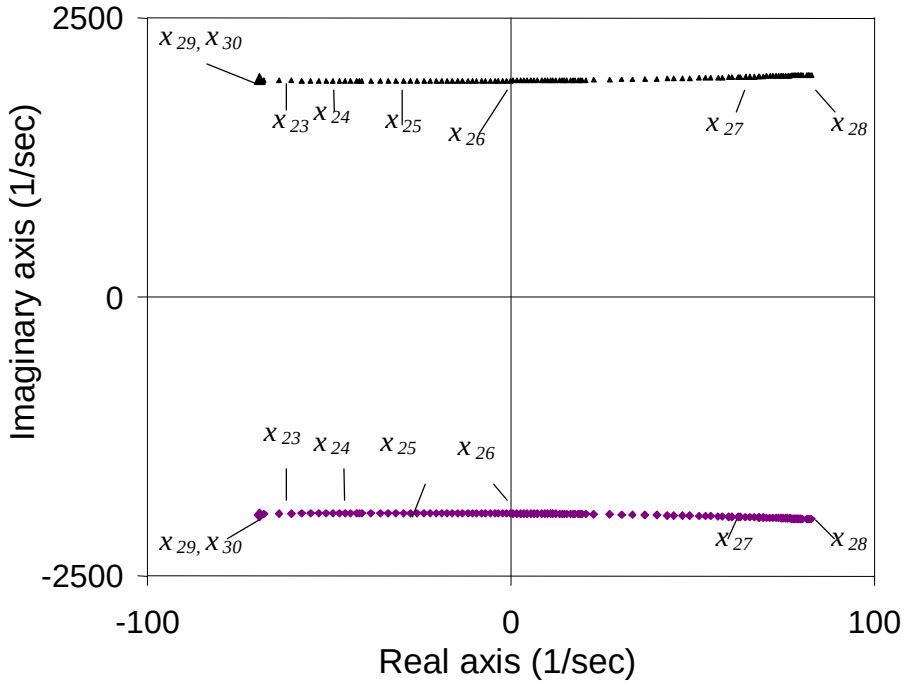

Figure 7.8 Non-dominant conjugate poles on trajectory II in the region of Condition I

7.2.3 Stability Presentation Based on Steady State Operating Points

The purpose of this section is to calculate the absolute and relative stability of the LS system for different openings of the adjustable orifice, x, and for different load conditions, T_{mf}, and to present the results in terms of the system pressures, P_{s0}, P_{y0} and θ_{sp0}.

Figure 7.9 shows the absolute stability perspective related to SSOP's. In this stability analysis (Chapters 3 through 5), the load torque, T_{mf}, is allowed to vary from –33 Nm (runaway load) to 14 Nm and the orifice opening, x_v, varies in the region of zero through 4 "turns". The stable region is labeled with "O" and the unstable region is represented by "×".

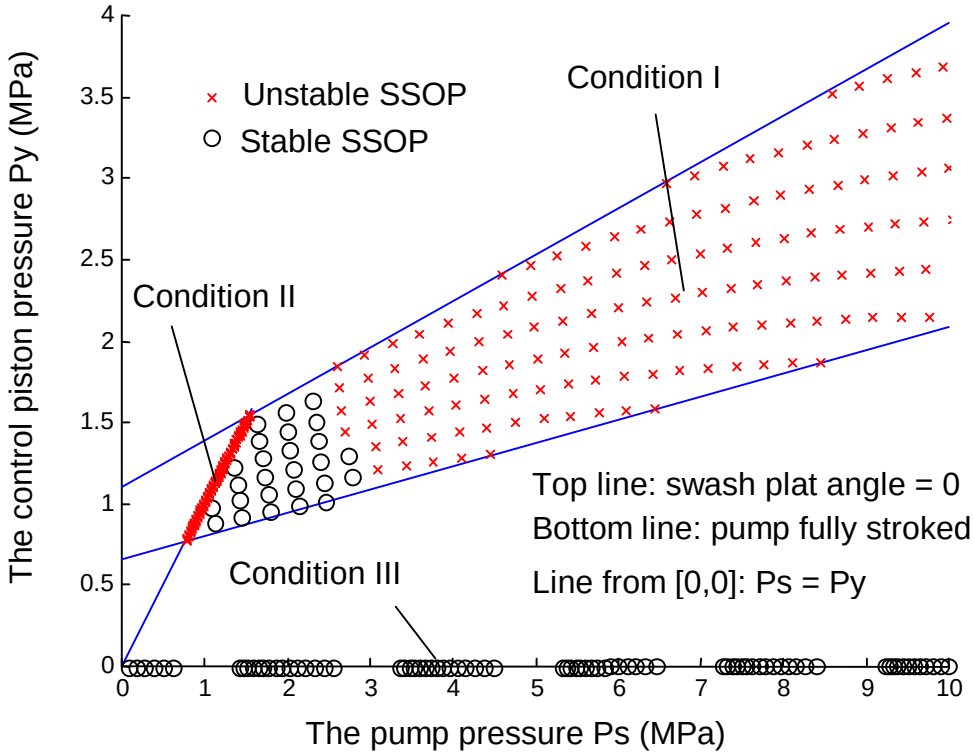

Figure 7.9 Stability of the LS system

In the region of Condition I, when the pump pressure, P_{s0}, is large, the system becomes "locally" unstable (Note: the term "locally" implies small excursions from the operating point). The result is a consequence of the dynamics of the LS regulator spool, because the magnitude of the frequency component of the conjugate poles is very close to the undamped natural frequency of the LS regulator spool, ω_r. The boundary between the unstable region and stable region may change depending on the parameters of the LS pump and the load. In the region of Condition II, the LS system is always unstable. In the region of Condition III, the LS system is always stable.

Figure 7.10 illustrates the damping ratio of the dominant poles of the LS system in the normal operation condition (Condition I). It can be observed that the damping ratio is less than 0.1 in all normal operation regions and lies in the range (0.06 ~0.08). Hence ζ is approximately constant.

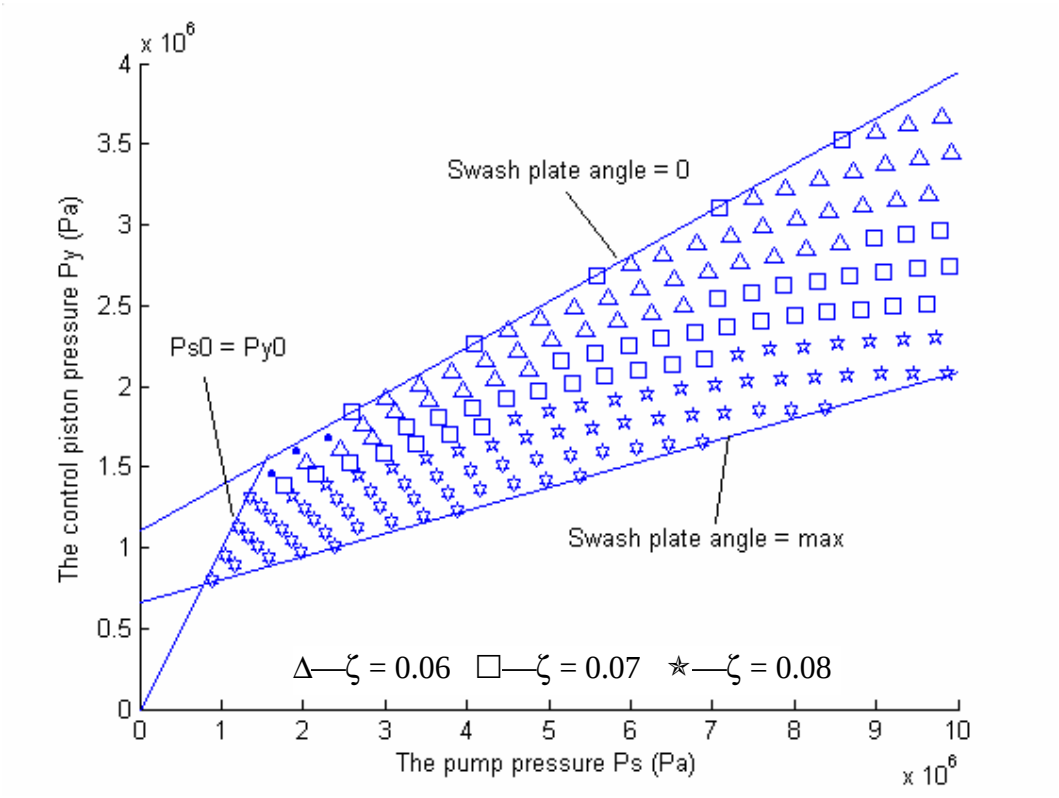

Figure 7.10 Damping ratio of the dominant poles of the LS system

Figure 7.11 illustrates that the undamped natural frequency (i.e. the bandwidth) of the dominant poles of the LS system reduces as the opening of the adjustable orifice increases (hence the swash plate angle and the pump flow delivery increase). When the orifice opening is very small, the system bandwidth approaches the undamped natural frequency of the load, ω_L. In this study, ω_L was 18.6 rad/s.

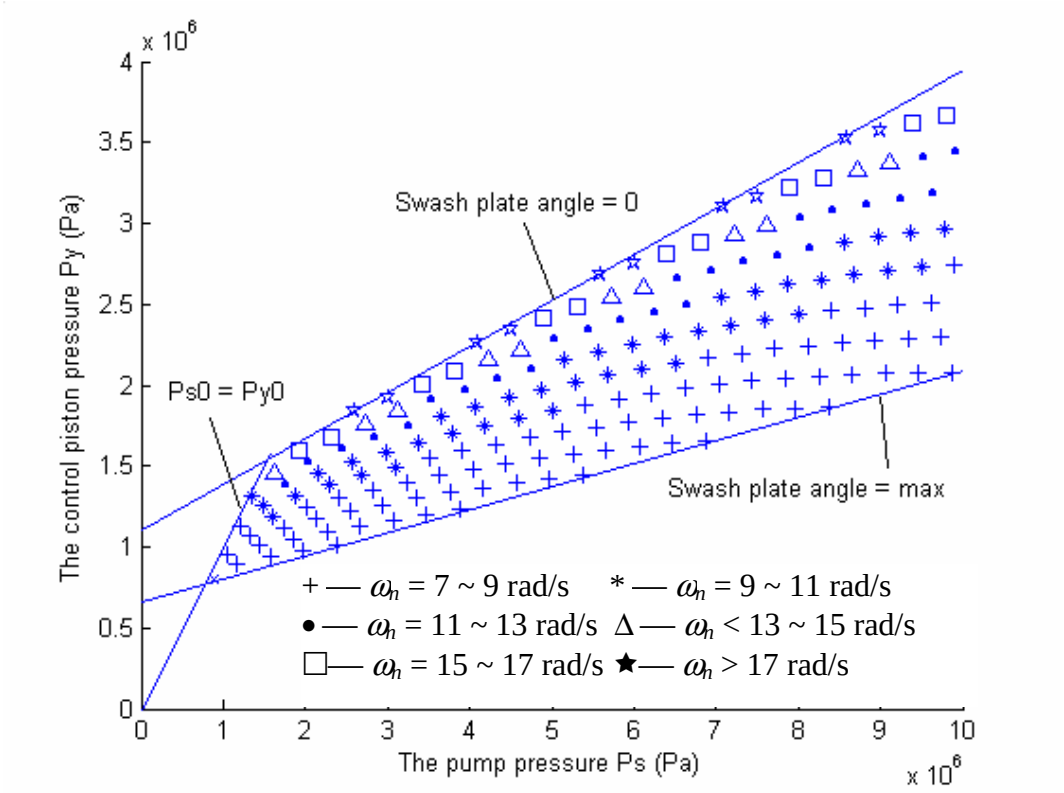

Figure 7.11 The undamped natural frequency of the dominant poles of the LS system

7.3 Effect of the pressure differential set, P_d

As an important parameter of the LS system, P_d can affect both the steady state and dynamic performance of the LS system. From an energy saving of point view, P_d is desired to be as small as possible. However, P_d directly affects the steady state operating condition (see Equation (7.2)). The LS system with small P_d tends to enter the region of Condition II where the LS system is unstable. In addition, decreasing P_d results in a decrease of the bandwidth because the magnitudes of dominant poles become small. Figure 7.12 compares the root locus of the dominant poles of the LS system for P_d = 0.5 MPa and 2.5 MPa under Condition I.

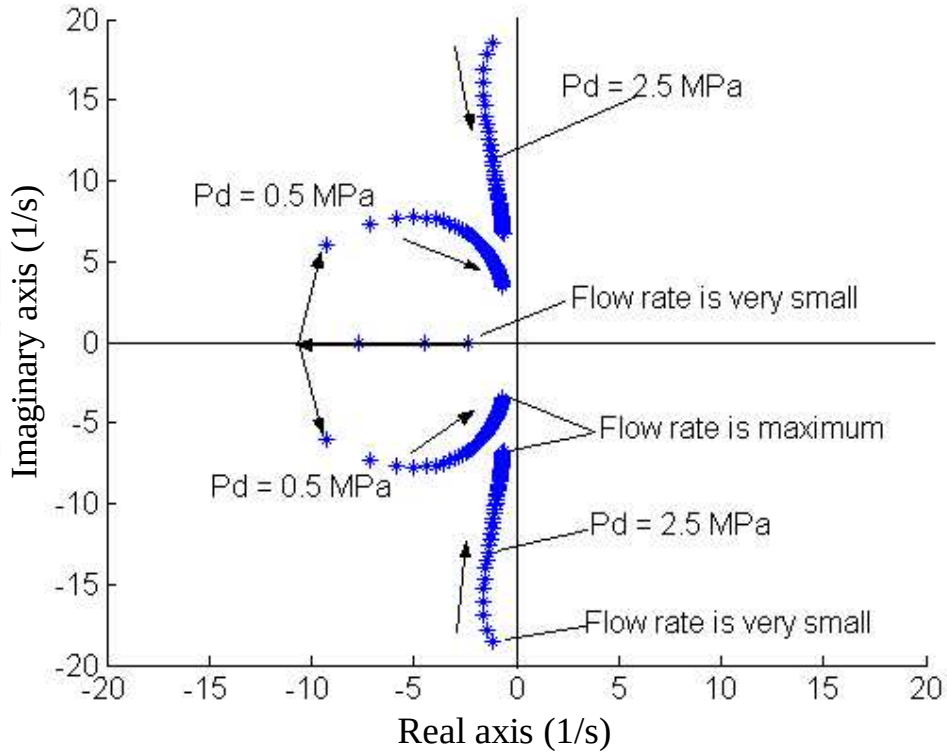

Figure 7.12 Dominant pole root locus comparison of the LS system between different pressure differential sets, P_d

7.4 Effect of the damping in the Load Sensing line, ω_{Ls}

It can be observed from Figure 7.4 that under normal conditions (Condition I) the dominant pole of the LS system is a pair of conjugate poles which are very close to the imaginary axis. Therefore, the damping of the LS system is very small (see Figure 7.10). A practical system would thus display a significant low frequency oscillation. In order to reduce this oscillation, one practical method is to increase the damping in the LS line (see Figure 5.3). The purpose of this section is to theoretically calculate the relative stability of the LS system when the damping in the LS line varies. The disadvantage of changing this parameter is also discussed.

Figure 7.13 shows comparisons of the theoretical frequency responses of the flow control TF (Equation (5.81)) as a function of different damping coefficients in the LS line. When the damping orifice in Figure 5.3 is fully opened, the damping in the LS line is minimum (ω_{Ls} = 500 rad/s in Figure 7.13). The magnitude of the flow control TF, $\frac{\phi(s)}{X(s)}$, of the LS system has a significant resonant peak of about 20 dB at 9.5 rad/s. When the damping orifice is gradually closed, the resonant peak decreases. This illustrates the stabilization process on the LS system by increasing the magnitude of the damping in the LS pilot line. However, this improvement is associated with a side effect in that the bandwidth of the control system decreases. Figure 7.13 indicates that the bandwidth of the LS system is about 0.6 rad/s for ω_{Ls} = 1 rad/s. Consequently, the LS system transient response decreases. Figure 7.14 shows a comparison of the

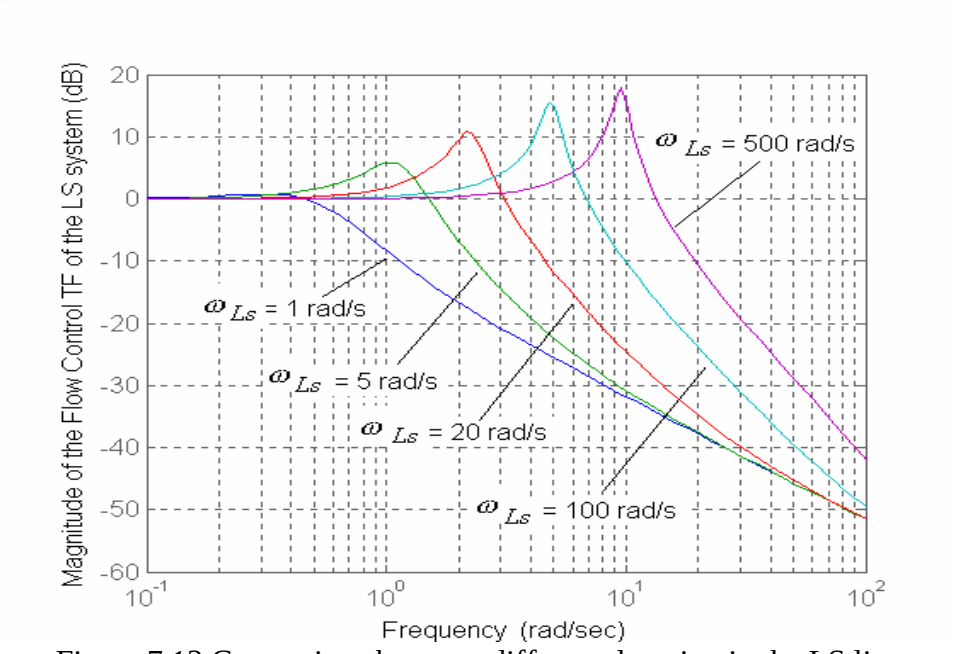

Figure 7.13 Comparison between different damping in the LS line

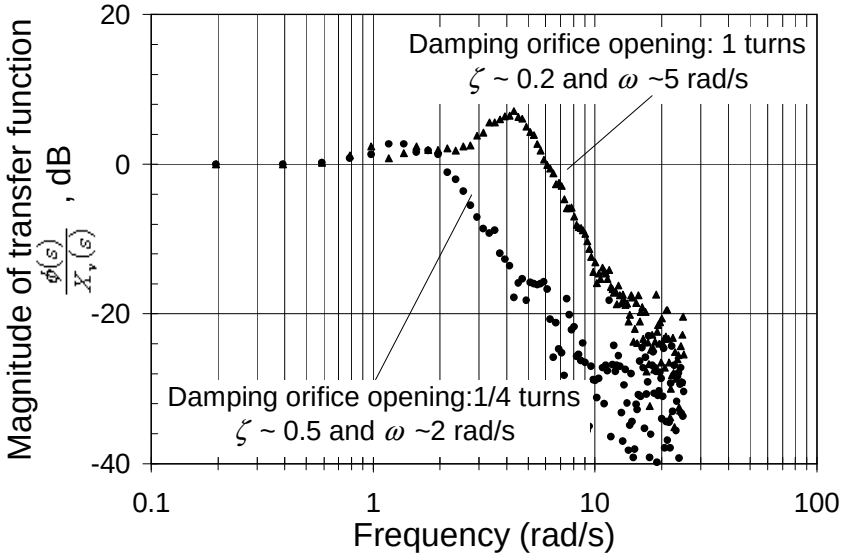

Figure 7.14 Comparison of experimental results for different damping in the LS line

experimental magnitude frequency response for different openings of the damping valve. When the opening of the damping valve decreases from 1 turn to 1/4 turn, the damping ratio of the LS system increases from 0.2 to 0.5 but the bandwidth decreases from 5 rad/s to 2 rad/s.

In summary, the LS system can be stabilized via the damping orifice in the LS pilot line but it results in a decrease in the transient performance.

7.5 Summary

The result of the dynamic analysis of the LS system in this chapter can be summarized as follows:

- When the system pressure setting, P_d, and the load, T_{mf}, satisfy Equation (7.2), the LS system always operates in Conditions I and III as the adjustable orifice is opened from zero to a large value. Otherwise, the operation of the LS system operates in Conditions II, I and III. When the runaway load, T_{mf} , is less than a critical value as

determined by Equation(7.4), the LS system can only operate in Conditions II and III.

- In the region of Condition I, the LS system is stable when the pump pressure, P_s, is small. When P_s is large, the LS system is "locally" unstable. A high frequency oscillation would be observable in the system pressures. In additions, a low frequency oscillation also occurs in all regions of Condition I, because the damping ratio of the dominant poles of the LS system is very small (<0.1) and hence the LS system has a poor relative stability.
- In the region of Condition II, the LS system is unstable.
- In the region of Condition III, the LS system is always stable.
- Decreasing P_d can improve the efficiency of the LS system. But a small P_d tends to force the LS system to enter the region of Condition II where the LS system is unstable. Under Condition I, a small P_d also makes the dynamic response of the LS system slower.
- The damping orifice in the LS line can be used to stabilize the system but the bandwidth of the LS system is compromised.

Chapter 8 Modeling of the Pressure Compensate Flow control Valve

8.1 Background

Chapters 2 through 7 have investigated the steady state and dynamic performance of a practical LS system with a critically lapped spool in the LS regulator. As illustrated in Chapter 7, a main problem in the LS system is the poor relative stability. In order to solve this problem, Krus [1988] suggested an increase in the damping in the LS line. Based on the theoretical results presented in Chapter 7, increasing damping in the LS line is not an ideal method, because the bandwidth is reduced.

It can be noticed from the literature review in Chapter 1, that other methods have been suggested to stabilize the LS system such as, (1) replacing the simple adjustable orifice (See Figure 2.1) with a PC valve (LSPC system [Lantto, et al, 1990 and 1991; Pettersson, et al, 1996; Li, 1999]); (2) replacing the hydraulic LS line with an electrohydraulic LS line [Backe, 1993; Luomaranta,1999; Zhang, et al, 1999]. The second approach required additional control valves and hence introduced additional sources of inefficiencies. It was also found that improved stabilization using the electrohydraulic valve was not evident. The first method using a PC valve is simple and practical but a comprehensive analysis of the LSPC system has not been attempted.

In this chapter, a comprehensive model and analysis of the PC valve is presented. A general non linear dynamic model of a typical PC valve and its linearized equations is developed. Chapter 9 develops the steady state model for solving for the SSOP of the PC valve. Chapter 10 experimentally verifies the steady state model developed in Chapter 9. Chapter 11 further develops the dynamic model of the PC valve and discusses the relationship between the dynamic performance and the design parameters of the PC

valve. Based on the knowledge of the LS system (Chapters 2 through 7) and the PC valve (Chapters 8 through 11), Chapters 12 and 13 present the steady state analysis and the dynamic analysis of the LSPC system respectively.

8.2 Introduction

As introduced in Chapter 1, the pressure compensated valve (PC system) is a flow control device which consists of a fixed or adjustable orifice and a compensator valve. The compensator valve modulates its opening in order to maintain a fixed pressure drop (P_s - P_m) across the fixed or adjustable orifice.

There usually are two configurations for PC systems[1]: (a) hydrostat upstream and (b) hydrostat downstream as shown in Figure 8.1. Their purpose for flow control are same, that is, to maintain a constant pressure drop across the fixed orifice independent of changes in load pressure, thus flow is maintained constant and is independent of changes in the load pressure. The hydrostat upstream, configuration (a), has been studied by many researchers [Lantto, et al, 1990; Li 1999; Pettersson, et al, 1996; Zarotti and Nervegna 1988]. From a practical viewpoint, in this study, it was very difficult to install transducers to measure the spool displacement, x_{pc}, and the intermediate pressure, P_m, for the hydrostat upstream due to the compact structure of these valves. However, PC systems with the hydrostat downstream can be fitted with appropriate transducers to measure x_{pc} and P_m. Therefore, only the hydrostat downstream configuration is studied in this thesis. There is no loss in generality here because if the model can be verified with the hydrostat downstream then the approach can be applied to the case of the upstream hydrostat with some confidence. For the duration of this thesis, a hydrostat

[1] The term PC system is synonymous with PC valve in the literature.

downstream will be assumed.

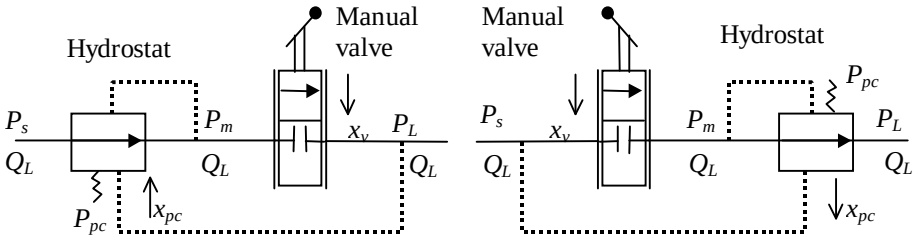

(a) Hydrostat upstream configuration (b) Hydrostat downstream configuration

Figure 8.1 Comparison of Two Types of PC Systems

The PC system investigated in this study was a PC flow control valve manufactured by Brand Hydraulics Inc (model: EFC12-10-12). The PC system shown in Figure 8.2 consists of the valve case, a hydrostat spool (automatically controlled) and an adjustable spool (manually or electrically). Its operation principle has been explained in Chapter 1 and is not repeated here. It is noted that the PC flow control valve was designed with a by-pass port (5). In order to investigate the performance of this valve without by-pass flow (See Figure 8.1b), the by-pass port was capped.

The state variables used to describe the dynamic behavior are the displacement, x_{pc}, of the hydrostat spool, the pressure, P_{sh}, in chamber (2) and the intermediate pressure, P_m (see Figure 8.2). The input variables include the upstream pressure, P_s, the downstream pressure, P_L, and the opening , x_v, of the adjustable orifice.

This chapter presents the non-linear dynamic model of this particular PC system and the process used to linearize the nonlinear relationships.

8.3 Non linear Dynamic Model of the Pressure Compensated system

Figure 8.2 shows the sectional drawing and its equivalent schematic of the PC system. The control equations associated with the PC system include the flow, Q_{Lv}, into the PC system through the fixed or adjustable orifice (1), the flow, Q_{Lpc}, out of the PC

system through the hydrostat orifice (4), the dynamic equation of the hydrostat spool, the flow continuity equation of the chamber (2), and the flow continuity equation of the intermediate chamber between orifices (1 & 4).

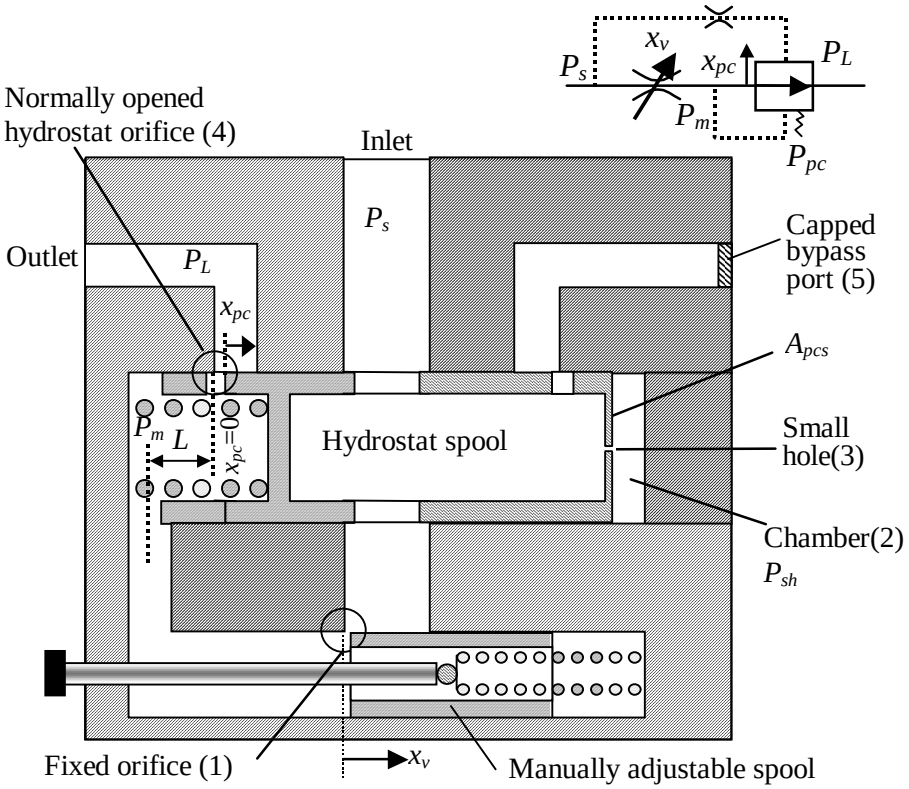

Figure 8.2 Sectional Drawing of the PC System

Preliminary studies have shown that the adjustable orifice is rectangular shape and the hydrostat orifice is crescent-type (such as Parker PC series and Brand FC series). Therefore, the flow equations of Q_{Lv} and Q_{Lpc} can be defined as [Merritt 1967]

$$Q_{Lv} = C_{dv} w_v x_v \sqrt{\frac{2}{\rho}(P_s - P_m)} \tag{8.1}$$

$$Q_{Lpc} = C_{dc} A_{pc}(x_{pc}) \sqrt{\frac{2}{\rho}(P_m - P_L)} \tag{8.2}$$

where

$$A_{pc}(x_{pc}) = \begin{cases} 0 & x_{pc} \le 0 \\ R_{pc}^2 \cos^{-1}\left(\frac{R_{pc} - x_{pc}}{R_{pc}}\right) - (R_{pc} - x_{pc})\sqrt{2R_{pc}x_{pc} - x_{pc}^2} & 0 < x_{pc} < 2R_{pc} \\ R_{pc}^2 \pi & x_r \ge 2R_{pc} \end{cases} \quad (8.3)$$

It must be noted that flow discharge coefficients, C_{dv} and C_{dc}, of Equations (8.1) and (8.2) were not the same. Although the flow rates through both orifices were the same, the flow status (that is, turbulent or laminar flow conditions) was different due to different pressure drops and different cross-sectional areas for each orifice, especially when the flow rate was small. This gives rise to different Reynolds numbers for the same flow rate.

Consider the dynamic equations of the PC system. The dynamic force balance across the hydrostat is considered first.

$$\ddot{x}_{pc} = \frac{1}{M_{pc}}\left(-B_{pc}\dot{x}_{pc} - k_{pc}x_{pc} - k_{ff}A_{pc}(x_{pc})(P_m - P_L) - \rho L\dot{Q}_{Lpc} + A_{pcs}\left(P_{pc} - (P_{sh} - P_m)\right)\right) \quad (8.4)$$

where x_{pc} is the opening of the hydrostat orifice (also the displacement of the hydrostat spool). M_{pc} is the spool mass. B_{pc} is the damping coefficient of the spool. k_{pc} is the coefficient of the pre-compression spring. The third term in the bracket represents the steady state flow force which is proportional to the flow orifice sectional area and the pressure drop across the hydrostat orifice. The constant of proportionality is defined by the coefficient, k_{ff}. The fourth term stands for the transient flow force in which the damping length, L, is equal to the axial length between the hydrostat orifice (i.e. outgoing port) and centerline of the conduit (i.e. incoming port) shown in Figure 8.2. The fifth term is the force which relates to the pressures differential across the ends of

the hydrostat spool. It is further noted that P_{pc} is not a true "physical" pressure but an equivalent pressure term caused by the pre-compression spring ($P = \frac{F}{A}$). P_{pc} controls the pressure drop across an adjustable or fixed orifice and is a design value which reflects the maximum pressure differential, P_s - P_m across the orifice. This will be discussed further in Chapter 10.

The flow continuity equation of the right hand side chamber (2) of the spool is

$$\frac{V_{sh}}{\beta}\dot{P}_{sh} = \frac{P_s - P_{sh}}{R_{sh}} + A_{pcs}\dot{x}_{pc} \tag{8.5}$$

where $V_{sh} = V_{sh0} - x_{pc}A_{pcs}$. V_{sh} represents the chamber volume in chamber (2) at the right hand side of the hydrostat spool which varies as the hydrostat spool moves. V_{sh0} is the value of V_{sh} at x_{pc} = 0. P_{sh} is the pressure in chamber (2). R_{sh} represents the resistance of the short slot type orifice (small hole (3)). It is noted that, because V_{sh} is very small and β is very large, the term at the left side of Equation (8.5) can approximate to zero. Therefore, Equation (8.5) is further simplified as

$$P_{sh} = P_s + A_{pcs}R_{sh}\dot{x}_{pc} \tag{8.6}$$

The flow continuity equation of the intermediate chamber between the adjustable orifice and the hydrostat orifice is

$$\frac{V_{pcm}}{\beta}\dot{P}_m = Q_{Lv} - Q_{Lpc} - A_{pcs}\dot{x}_{pc} \tag{8.7}$$

where $V_{pcm} = V_{pcm0} + x_{pc}A_{pcs}$. V_{pcm} represents the intermediate volume between the fixed orifice (1) and the hydrostat orifice (4) which varies as the hydrostat spool moves. V_{pcm0}

is the value of V_{pcm} at $x_{pc} = 0$. P_m is the intermediate pressure. Similarly, because V_{pcm} is very small and β is very large, the term at the left side of Equation (8.7) can approximate to zero. Therefore, Equation (8.7) can also be simplified as

$$Q_{Lv} - Q_{Lpc} - A_{pcs}\dot{x}_{pc} = 0 \tag{8.8}$$

8.4 Linearization of the Non-linear Dynamic Model of the Pressure Compensated System

Linearizing Equations (8.1) and (8.2) gives

$$\Delta Q_{Lv} = K_{qv}\Delta x_v + K_{cv}\left(\Delta P_s - \Delta P_m\right) \tag{8.9}$$

$$\Delta Q_{Lpc} = K_{qpc}\Delta x_{pc} + K_{cpc}\left(\Delta P_m - \Delta P_L\right) \tag{8.10}$$

where K_{qv} and K_{qpc} are flow gains of two orifices (1 & 4). K_{cv} and K_{cpc} are flow-pressure coefficients and are given by

$$K_{qv} = C_{dv} w_v \sqrt{\frac{2}{\rho}\left(P_s - P_{m0}\right)} \tag{8.11}$$

$$K_{cv} = \frac{C_{dv} w_v x}{\sqrt{2\rho\left(P_s - P_{m0}\right)}} \tag{8.12}$$

$$K_{qpc} = C_{dc}\sqrt{\frac{2}{\rho}\left(P_{m0} - P_L\right)} \cdot \frac{dA_{pc}\left(x_{pc}\right)}{dx_{pc}} \tag{8.13}$$

$$K_{cpc} = \frac{C_{dc} A_{pc}\left(x_{pc}\right)}{\sqrt{2\rho\left(P_{m0} - P_L\right)}} \tag{8.14}$$

When the flow rate through the PC valve is small so that the flow status is laminar or in the transition from the laminar to turbulent, these parameters must be determined using models presented in Appendix D.

Linearizing Equation (8.4) gives

$$\begin{aligned} M_{pc}\Delta\ddot{x}_{pc} + \left(B_{pc} + \rho LK_{qpc}\right)\Delta\dot{x}_{pc} + k^{*}_{pc}\Delta x_{pc} \\ = -k_{ff}A_{pc}\left(x_{pc0}\right)\left(\Delta P_m - \Delta P_L\right) - \rho LK_{cpc}\left(\Delta\dot{P}_m - \Delta\dot{P}_L\right) - A_{pcs}\left(\Delta P_{sh} - \Delta P_m\right) \end{aligned} \tag{8.15}$$

where $k^{*}_{pc} = k_{pc} + k_{ff}\dfrac{dA_{pc}\left(x_{pc0}\right)}{dx_{pc}}\left(P_{m0} - P_L\right)$ (8.16)

The term, $\rho LK_{cpc}\left(\Delta\dot{P}_m - \Delta\dot{P}_L\right)$, is usually neglected because there is little direct evidence to indicate that the pressure rate term contributes substantially to the valve dynamics [Merritt, 1967]. Linearizing Equation (8.5) gives

$$\Delta P_{sh} = \Delta P_s + A_{pcs}R_{sh}\Delta\dot{x}_{pc} \tag{8.17}$$

Substituting Equation (8.17) into Equation (8.15) and neglecting $\rho LK_{cpc}\left(\Delta\dot{P}_m - \Delta\dot{P}_L\right)$ give

$$\begin{aligned} M_{pc}\Delta\ddot{x}_{pc} + B^{*}_{pc}\Delta\dot{x}_{pc} + k^{*}_{pc}\Delta x_{pc} - \left(A_{pcs} - k_{ff}A_{pc}\left(x_{pc0}\right)\right)\Delta P_m \\ = -A_{pcs}\Delta P_s + k_{ff}A_{pc}\left(x_{pc0}\right)\Delta P_L \end{aligned} \tag{8.18}$$

where $B^{*}_{pc} = B_{pc} + \rho LK_{qpc} + A^{2}_{pcs}R_{sh}$ (8.19)

Equations (8.18) and (8.19) indicate that the hydraulic resistance, R_{sh}, associated with the small hole (3) in Figure 8.2 can be used to increase the damping coefficient of the hydrostat spool.

Linearizing Equation (8.8) gives

$$\Delta Q_{Lv} - \Delta Q_{Lpc} - A_{pcs}\Delta\dot{x}_{pc} = 0 \tag{8.20}$$

Substituting Equations (8.9) and (8.10) and then rearranging Equation (8.20) yields

$$K_{qpc}\Delta x_{pc} + A_{pcs}\Delta\dot{x}_{pc} + \left(K_{cv} + K_{cpc}\right)\Delta P_m = K_{qv}\Delta x_v + K_{cv}\Delta P_s + K_{cpc}\Delta P_L \tag{8.21}$$

Equations (8.10), (8.19) and (8.21) will be used to develop the TF of the PC system in Chapter11.

8.5 Summary

This chapter introduced two different configurations of PC systems (i.e. hydrostat upstream and hydrostat downstream configurations). The non-linear dynamic models of the PC system with hydrostat downstream were presented. These equations will be used to develop the SSOP model of the PC system in Chapter 9. Finally, these models are linearized and will be used to develop the TF of the PC system (Chapter 10).

Chapter 9 Steady State Analysis of the Pressure Compensated System

It is necessary to know the steady state operating point (SSOP) before the linearized models in Section 8.3 in Chapter 8 can be used to develop the transfer functions (TF) of the PC system. This chapter provides a set of non-linear algebraic equations and the procedure of solving for SSOP (x_{pc0} and P_{m0}).

9.1 Steady State Model of the PC System

Under steady state conditions, the derivatives of all variables in Equations (8.4), (8.6) and (8.8) are zero. A subscript "$_0$" is added to all variables (except for x_v, P_s and P_L because they are input variables for particular study of the PC system) of all non-linear equations to present the SSOP. In this situation, P_s is equal to P_{sh0} from Equation (8.6) and Q_{Lv0} is equal to Q_{Lpc0} from Equation (8.8). Equating the right hand sides of Equations (8.1) and (8.2), and expressing P_m as a function of the variables P_s and P_L, give

$$P_m = \frac{\eta^2 w_v^2 x_v^2 P_s + A_{pc}^2(x_{pc}) P_L}{\eta^2 w_v^2 x_v^2 + A_{pc}^2(x_{pc})} \tag{9.1}$$

where η is defined as $\eta = \frac{C_{dv}}{C_{dc}}$. Equation (9.1) indicates that the pressure, P_m, is a linear combination of pump pressure, P_s, and load pressure, P_L, with coefficients proportional to the ratio of the square of the orifice areas.

Substituting P_m into Equations (8.1) and (8.2), Q_{Lv} can be expressed in terms of P_s and P_L as

$$Q_{Lv} = Q_{Lpc} = \frac{C_{dv} w_v x_v A_{pc}(x_{pc})}{\sqrt{A_{pc}^2(x_{pc}) + \eta^2 w_v^2 x_v^2}} \sqrt{\frac{2}{\rho}(P_s - P_L)} \tag{9.2}$$

The steady state algebraic equation of Equation (8.4) is

$$A_{pcs}\left(P_{pc}-\left(P_s-P_m\right)\right)-k_{pc}x_{pc}-k_{ff}A_{pc}\left(x_{pc}\right)\left(P_m-P_L\right)=0 \tag{9.3}$$

It is noted that the transient flow force does not affect the steady state operating point because the transient flow force is proportional to the acceleration of the fluid elements, i.e. the derivation of the flow rate. At steady state, the flow rate can be considered as constant. Therefore, no term associated with the transient flow force exists in Equation (9.3).

Substituting Equation (9.1) into Equation (9.3) gives

$$A_{pcs}\left(P_{pc}-\frac{A_{pc}^2\left(x_{pc}\right)}{A_{pc}^2\left(x_{pc}\right)+\eta^2 w_v^2 x_v^2}\left(P_s-P_L\right)\right)-k_{pc}x_{pc}-\frac{k_{ff}\eta^2 A_{pc}\left(x_{pc}\right)w_v^2 x_v^2}{A_{pc}^2\left(x_{pc}\right)+\eta^2 w_v^2 x_v^2}\left(P_s-P_L\right)=0 \tag{9.4}$$

Equation (9.4) can be rewritten to give the pressure differential, P_s - P_L, as a function of the hydrostat spool displacement x_{pc}, that is,

$$P_s-P_L=\left(P_{pc}-\frac{k_{pc}}{A_{pcs}}x_{pc}\right)\lambda_2\left(x_{pc}\right) \tag{9.5}$$

where $\lambda_2\left(x_{pc}\right)=\dfrac{A_{pcs}\left(A_{pc}^2\left(x_{pc}\right)+\eta^2 w_v^2 x_v^2\right)}{k_{ff}\eta^2 A_{pc}\left(x_{pc}\right)w_v^2 x_v^2+A_{pc}^2\left(x_{pc}\right)A_{pcs}}$ (9.6)

Equation (9.6) can be further simplified. Assume that

$$k_{ff}\eta^2=0.7C_{dc}\left(\frac{C_{dv}}{C_{dc}}\right)^2=\frac{0.7C_{dv}^2}{C_{dc}}\approx 0.5$$

Usually, the hydrostat spool sectional area, A_{pcs}, is much larger than the flow area of two orifices, $w_v x_v$ and A_{pc}. Thus,

$$k_{ff}\eta^2 A_{pc}\left(x_{pc}\right)w_v^2 x_v^2+A_{pc}^2\left(x_{pc}\right)A_{pcs}\approx A_{pc}^2\left(x_{pc}\right)\left(\frac{0.5w_v^2 x_v^2}{A_{pc}\left(x_{pc}\right)}+A_{pcs}\right)\approx A_{pc}^2\left(x_{pc}\right)A_{pcs}.$$

Equation (9.6) can be approximated by

$$\lambda_2\left(x_{pc}\right)=1+\frac{\eta^2 w_v^2 x_v^2}{A_{pc}^2\left(x_{pc}\right)} \tag{9.7}$$

The method of solving Equation (9.5) for x_{pc0} will be discussed in Section 9.3. Substituting the solved x_{pc} into Equation (9.1) generates the intermediate pressure P_m.

It is necessary to discuss all possible operating conditions of the PC system shown in Figure 8.2 before introducing the procedure for solving Equation (9.5). This is because the solution of Equation (9.5) could be invalid under certain conditions, such as that associated with mechanical limitations.

9.2 Operating Conditions of the Pressure Compensated system

In order to find different operating conditions of the PC system, it is necessary to examine several scenarios of the operation of the PC system as a function of different upstream pressures, P_s, in Figure 9.1. The PC valve in Figure 9.1 represents the PC system shown in Figure 8.2.

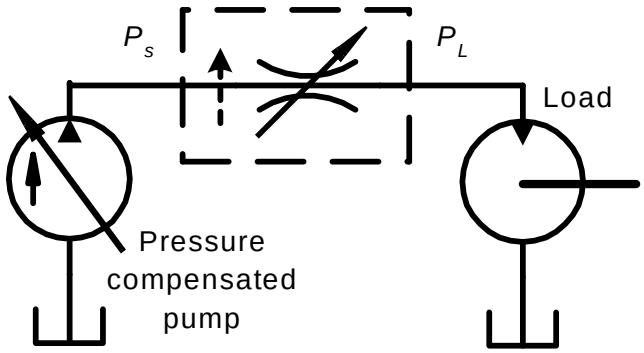

Figure 9.1 Investigation of the Operating Conditions of the PC system

If the deadhead pressure of the pump is set to be small (See Figure 9.1) and hence the upstream pressure, P_s, is small, the hydrostat spool does not move until the product of the pressure differential, $P_s - P_m$, and the hydrostat spool sectional area, A_{pcs}, is larger than the pre-compression force of the hydrostat spring (See Figure 8.2). In other words,

a critical value of the pressure drop across the PC system, $P_s - P_L$, must exist for a designed PC system. When the pressure drop, $P_s - P_L$, is larger than this critical value, the hydrostat spool is not limited. This condition is defined as Condition A. If the hydrostat is limited due to mechanical constraints, then this is defined as Condition B. Under Condition B, the PC system essentially becomes a cascade of two fixed orifices.

The critical value, δP_{pcc}, of the PC system pressure drop can be determined by

$$\delta P_{pcc} = P_s - P_L = \left(P_{pc} - \frac{k_{pc}}{A_{pcs}} x_{pc\max} \right) \lambda_2 \left(x_{pc\max} \right) \tag{9.8}$$

where x_{pcmax} is the maximum displacement of the hydrostat spool due to mechanical limitations. It is noted that because $\lambda_2(x_{pcmax})$ relates to x_v, the critical value, δP_{pcc} is a function of x_v, that is, $\delta P_{pcc}(x_v)$.Therefore, the non-linear algebraic Equation (9.5) about the operating point x_{pc0} is expressed as

$$\begin{cases} P_s - P_L = \left(P_{pc} - \dfrac{k_{pc}}{A_{pcs}} x_{pc} \right) \lambda_2 \left(x_{pc} \right) & P_s - P_L > \delta P_{pcc}\left(x_v \right) \quad \text{(Condition A)} \\ x_{pc0} = x_{pc\,max} & P_s - P_L \le \delta P_{pcc}\left(x_v \right) \quad \text{(Condition B)} \end{cases} \tag{9.9}$$

Equations (9.8) and (9.9) are used to define the operating status of the valve and to solve for the operating point, x_{pc}.

9.3 Numerical Procedure to Determine x_{pc0}

Figure 9.2 shows the procedure of solving for the operating point, x_{pc0}. With reference to this figure, the critical value is calculated (1). When the pressure drop across the PC system is not larger than the critical value (2), the hydrostat spool has a maximum displacement due to the spring pre-compression (3). When the pressure drop across the PC system is large enough to overcome the spring pre-compression, the PC system is at Condition A. It is necessary to use iteration for solving for x_{pc0} because Equation (9.9) is

an implicit non-linear algebraic equation (see the dashed line box in Figure 9.2). The flow chart of the iteration is similar to that shown in Figure 3.3.

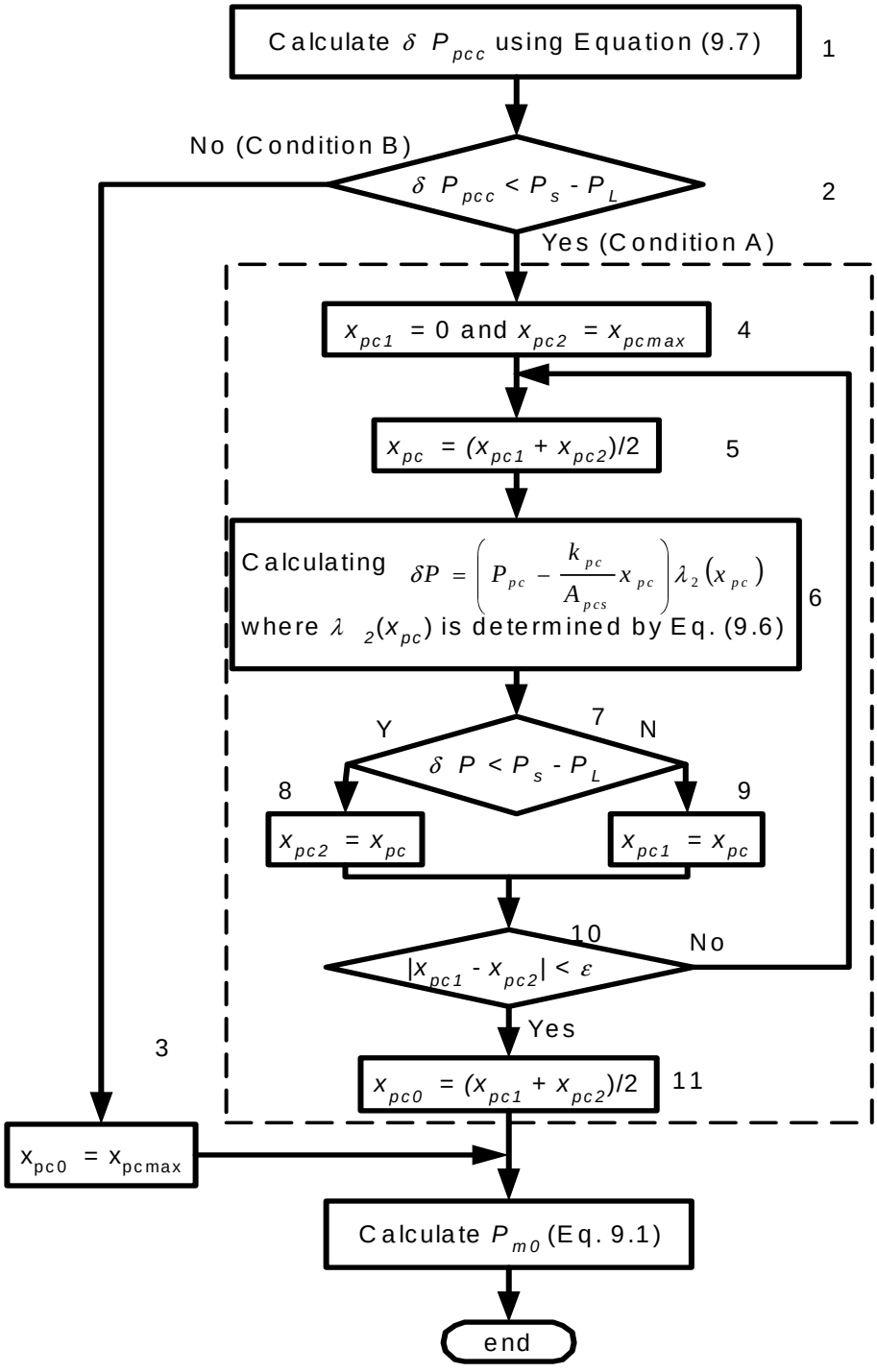

Figure 9.2 Procedure of Solving for Operating Points

Chapter 10 Experimental Verification of the Steady State Operating Points of the Pressure Compensated System

As explained in previous chapters, knowledge of the steady state operating point (SSOP) of a non-linear system is essential when using the linearization approach to determine stability boundaries. A pressure compensated (PC) flow control valve is a simple pressure feedback (or load sensing) system. It has three state variables; the hydrostat spool displacement, x_{pc}, the intermediate pressure, P_m, and the pressure, P_{sh} (See Chamber (2) in Figure 10.1). Therefore, their SSOP's must be determined using the non-linear equations presented in Chapter 8. From Chapter 9, the SSOP of the pressure, P_{sh}, is equal to the upstream pressure, P_s. But the hydrostat spool displacement operating point, x_{pc0}, and the intermediate pressure operating point, P_{m0}, must be determined by Equations (9.8) and (9.1). The objective of this chapter, then, is to experimentally verify the solution of Equation (9.8).

In order to solve for the SSOP of the PC system from Equation (9.8), the parameters P_{pc}, k_{pc}, A_{pcs}, k_{ff}, C_{dc} and C_{dv} must be known. The SSOP, x_{pc0}, of the hydrostat spool displacement can be uniquely determined as a function of the pressure drop across the PC system, $P_s - P_L$, and the cross-sectional area of fixed rectangular orifice, A_v. Measurement or estimation of these parameters is now considered.

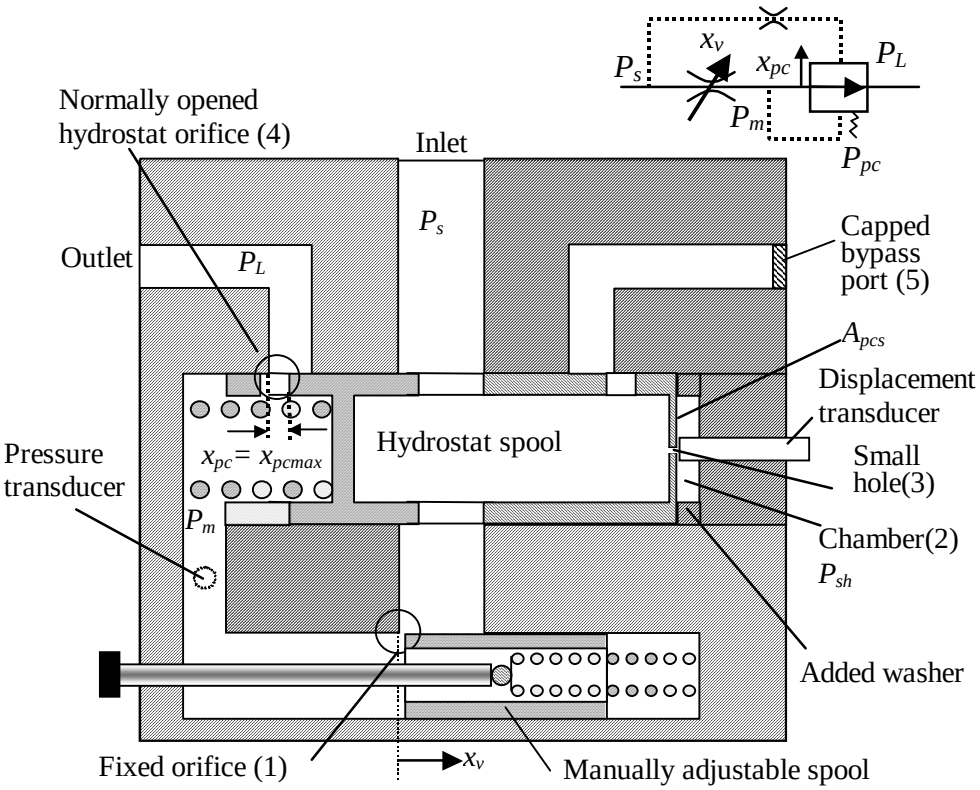

Figure 10.1 Sectional Drawing of the PC System

10.1 Parameters of Pressure Compensated System

The PC system investigated in this study was manufactured by Brand Hydraulics Inc (model: EFC12-10-12). To assist in describing how the remaining parameters are estimated, Figure 10.1 shows a cross sectional drawing of the PC system with installed transducers. A displacement transducer (Eddy current Proximator) was embedded into the end cap at the right hand side of the hydrostat spool. A pressure transducer was installed between the two orifices (orifices (1) and (4)). The fluid enters the system from the inlet and through orifice (1). The pressured fluid P_s is also fed to the chamber (2) via a small hole (3) at the end of spool. The fluid downstream of the fixed orifice (1) is at pressure P_m. Flow from the fixed orifice (1) must then pass through the hydrostat orifice (4). The area of the hydrostat orifice, $A_{pc}(x_{pc})$ (i.e. a function of the spool displacement,

x_{pc}) can be determined from the force balance equation between the hydraulic force, $A_{pcs}(P_s - P_m)$, the spring pre-compression, F_{pc}, the spring force, $k_{pc}x_{pc}$ and the steady state flow force, $k_{ff}A_{pc}(x_{pc})(P_m - P_L)$ (see Equation 8.4). It should be noted that orifice (1) is rectangular in shape and the hydrostat orifice (4) is round (to be precise, four crescent shaped orifices).

Measured and calculated parameters (those obtained indirectly from other known measurements are marked with a "*") are listed in Table 10.1. The spring coefficient, k_{pc}, and the spool cross-sectional area, A_{pcs}, can be directly measured. The spring pre-compression, F_{pc}, was calculated from the product of the spring coefficient, k_{pc}, and the initial deformation (15.63 mm) of the balance spring. In the initial condition, the hydrostat spool makes contact with the washer. Thus, the spool initial displacement, x_{pci}, is equal to the maximum, x_{pcmax}.

Table 10.1 Parameter of the PC System

Fixed rectangular orifice width	w_v	49.83	mm
Spool diameter	D_{pcs}	23.55	mm
Number of circular orifices	N_{pc}	4	
Diameter of circular orifice	D_{pc}	7.2	mm
Spring constant	k_{pc}	9.1	N/mm
Maximum opening of orifice	x_{pcmax}	2.62	mm
Pre-compression*	F_{pc}	142.3	N
Pressure setting of the PC system*	P_{pc}	0.38	MPa
Coefficient related to steady state force*	k_{ff}	$0.7C_{dc}$	

10.1.1 Pressure Differential Setting, P_{pc}, for Pressure Compensated System

As was the case for P_d for the LS system, P_{pc} is not a true physical pressure but equivalent pressure term. In order to understand its physical meaning for the PC system shown in Figure 10.1, consider Equation (9.3). Because x_{pc} is defined such that when the spool displacement, x_{pc}, equals 0, the hydrostat orifice area, A_{pc}, is also zero, the value of P_{pc} is equal to the external pressure differential ($P_s - P_m$) on the hydrostat spool of the PC system which forces the hydrostat orifice to close ($x_{pc} = 0$) (see Figure 10.1).

The initial displacement of the hydrostat spool is so designed that the hydrostat orifice is normally fully open (that is, $x_{pci} = x_{pcmax}$). The spring force, F_{sp}, under steady state condition can be expressed as

$$F_{sp} = F_{pc} + k_{pc}\left(x_{pc\max} - x_{pc}\right) \tag{10.1}$$

where F_{pc} is the pre-compression of the spool spring at the initial displacement. x_{pcmax} is the maximum opening of the hydrostat orifice (also the initial displacement of the hydrostat spool). k_{pc} is the spring coefficient of the hydrostat spool spring. x_{pc} is the displacement of the hydrostat spool whose sign is defined as positive in the same direction of the spring force exerted on the spool. When x_{pc} is equal to x_{pcmax}, the spring force is equal to the pre-compression, F_{pc}. When x_{pc} is forced to zero by an external force, the external force will balance the spring force which value can be determined by Equation (10.1)

$$F_{ext} = F_{sp} = F_{pc} + k_{pc} x_{pc\max} \tag{10.2}$$

During normal PC system operation, the external force on the spool is the sum of the steady state flow force and the product of the pressure differential across the spool ends and the sectional area of the spool. When x_{pc} is forced to zero, the steady state flow force

becomes zero. Therefore, the external force can be expressed as the product of an equivalent pressure differential and the spool sectional area, that is

$$F_{ext} = A_{pcs}\left(P_s - P_m\right) \tag{10.3}$$

The pressure differential $\left(P_s - P_m\right)$ under the condition $x_{pc} = 0$ (i.e. the pressure setting P_{pc} based on the definition) can thus be determined by combining Equation (10.2) and Equation (10.3) as

$$P_{pc} \triangleq \left(P_s - P_m\right)\Big|_{x_{pc}=0} = \frac{F_{pc} + k_{pc}x_{pc\,max}}{A_{pcs}} = \frac{k_{pc}x_{spring\_def}}{A_{pcs}} \tag{10.4}$$

The derived parameter, P_{pc}, is calculated to be 0.38 MPa using the parameters in Table 10.1. The pressure differential, (P_s - P_m), across the fixed orifice is ideally constant (P_{pc}); however, (P_s - P_m) decreases as the fixed orifice opening increases. (P_s - P_m) is, thus, always slightly less than P_{pc}. $\underline{x_{spring\_def}}$ represents the deformation (from free length) of the spring at $x_{pc} = 0$.

10.1.2 Determining the coefficient k_{ff}

As will be shown, the parameter k_{ff} in Equation (8.4) is a coefficient associated with steady state flow force. The steady state flow force exerted on the hydrostat spool cannot be neglected in this case. Simulation studies indicated that the steady state flow force was substantial when compared to the spring force on the spool. Mathematically, the steady state flow force on a spool is proportional to the discharge coefficient of the hydrostat orifice [Merritt, 1967] and is given by

$$F_{ff} = 2C_{dc}C_v \cos\theta A_{pc}\left(x_{pc}\right)\left(P_m - P_L\right) \tag{10.5}$$

where C_v = 0.98. θ = 69$^{\mathrm{o}}$. In Equation (8.4), the steady sate flow force, however, is represented by $k_{ff}A_{pc}\left(x_{pc}\right)\left(P_m - P_L\right)$. Thus, the coefficient, k_{ff}, can be expressed by

$$k_{ff} = 2C_{dc}C_v \cos\theta = 0.7C_{dc} \tag{10.6}$$

Therefore, k_{ff} becomes known if C_{dc} is determined.

All parameters, except the two discharge coefficients, C_{dv} and C_{dc}, are known or can be calculated. Determining these two coefficients, however, is a non-trivial process. Thus, a detailed discussion on the methodology used to determine these parameters is now considered.

10.2 Determination of the Discharge Coefficients

Methods of measuring and modeling the discharge coefficient of orifices in Appendix C were applied to both the fixed orifice (1) (rectangular shaped) and the hydrostat orifice (4) (crescent type) in the PC system. When changing the operating conditions of the PC system by adjusting $x_{v,}\Delta P_{sL}$ and T, variables Q_{pc}, P_s, P_m, P_L, and x_{pc} would change. C_{dv}, C_{dc}, Re_v and Re_c can be calculated using Equations (C16) and (C17) provided in Appendix C (Note, the subscript "$_v$" represents the fixed orifice and the subscript "$_c$" represents the hydrostat orifice).

10.2.1 Discharge Coefficient of the Fixed orifice (1) (Rectangular Type)

Figure 10.2 shows the experimental results for the fixed orifice (1) of the PC system. The experimental data demonstrates a slightly higher discharge coefficient than what has been generally accepted as a value for rectangular orifice (C_d = 0.61, Merritt, 1967) but generally behaves as expected. An analytical approximation to C_{dv} as a function of $\sqrt{\mathrm{Re}_v}$ was obtained using a statistical curve fit of the form $C_{d\infty}\left(1-e^{-\frac{\delta}{C_{d\infty}}\sqrt{\mathrm{Re}_v}}\right)$. $C_{d\infty}$ is the discharge coefficient when the flow becomes fully turbulent. δ represents the

laminar flow coefficient because, when $\sqrt{\mathrm{Re}_v}$ is less than $\frac{C_{d\infty}}{\delta}$, this formula can be further approximated by its 1st Taylor expansion $\delta\sqrt{\mathrm{Re}_v}$ which has the same form as

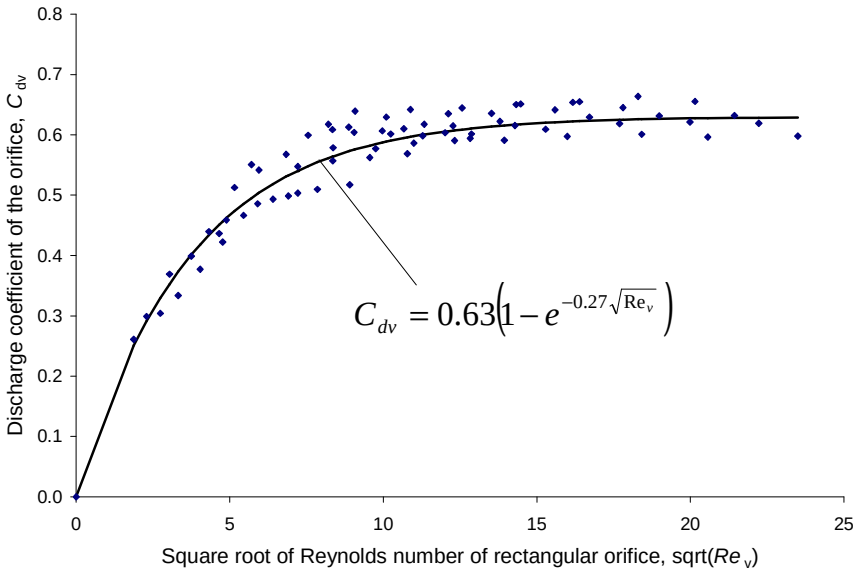

Figure 10.2 Discharge Coefficient of the Fixed Orifice (1) of the PC System

Merrit (1967) used. For this situation, $C_{d\infty} = 0.63$ and $\delta = 0.17$, that is,

$$C_{dv} = 0.63\left(1 - e^{-0.27\sqrt{\mathrm{Re}_v}}\right) \tag{10.7}$$

10.2.2 Discharge Coefficient of the Hydrostat Orifice (4) (Crescent Shaped)

Figure 10.3 shows the experimental result of the discharge coefficient of the hydrostat orifice (4) in the PC system. This curve indicates that there is considerable scatter in the results in the region of transition. Only when the Reynolds number is larger than 1000 ($\sqrt{\mathrm{Re}} = 31$), does the discharge coefficient begins to converge. Thus, a correlation equation of the form of Equation (10.7) is unacceptable.

In order to identify the source of the "too much scatter" problem in Figure 10.3, the flow through the hydrostat orifice (4) at a very small opening, x_{pc}, is considered, because

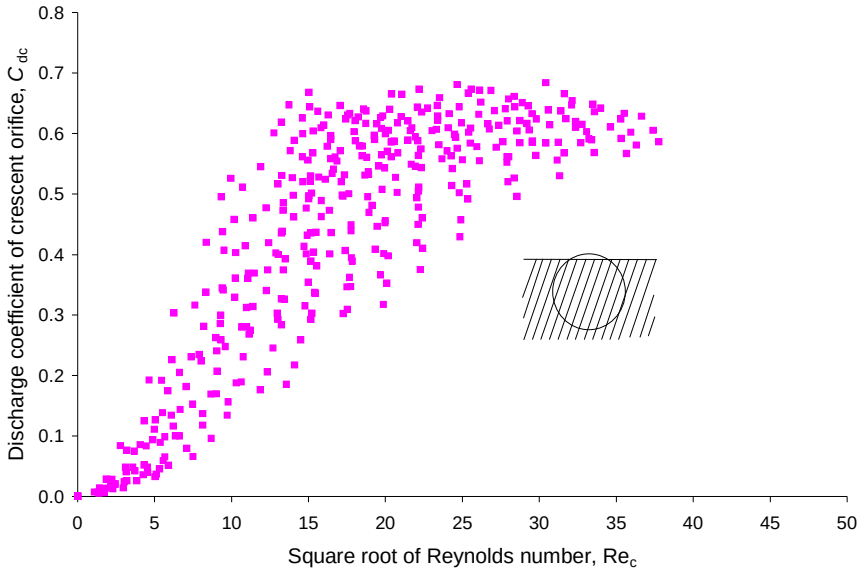

Figure 10.3 Discharge Coefficient of the Hydrostat Orifice (4) of the PC System

small Reynolds numbers occur when the opening of the crescent orifice is small. Figure 10.4 shows the geometry of the hydrostat orifice (4) for a very small opening. The experimental PC system has four crescent orifices along the perimeter of the hydrostat spool. The flow through each orifice consists of two components: the orifice flow, Q_1, and the leakage, Q_2. When the opening of these orifices, x_{pc}, is very small, the leakage, Q_2, becomes significant relative to the orifice flow, Q_1 (Figure 10.4). Under these circumstances, calculating Reynolds number, Re_c, and discharge coefficient, C_{dc}, using the overall measured flow rate ($Q = Q_1 + Q_2$) and flow cross sectional area of the crescent type orifice, in fact, is unreasonable. Theoretically, Re_c and C_{dc} should be calculated by Q_1 instead of overall flow rate ($Q_1 + Q_2$). Ruan, et al, [2002] developed a leakage model of Q_2. However, it is impossible to separate Q_1 and Q_2 from the measured value of Q. It is noted that Equations (10.6) and (10.7) cannot be used for a crescent orifice, because the leakage, Q_2, at $x_{pc} = 0$ is different from that at $x_{pc} \neq 0$. In this case, a

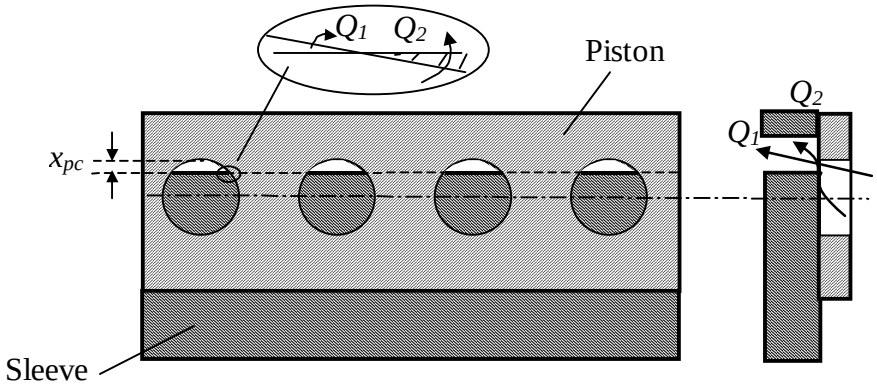

Figure 10.4 Geometry of Orifice (4) on Perimeter of the Hydrostat Spool

possible method to determine C_{dc} is to modify Re_c to reflect a dependency on fluid temperature, orifice opening and the pressure drop across the crescent orifices.

The modification coefficient, ε, is empirically selected as

$$\varepsilon = \left(\frac{T_0}{T}\right)^m \left(\frac{\Delta P_{mL0}}{\Delta P_{mL}}\right)^n \tag{10.8}$$

$$\text{such that } \mathrm{Re}_c = \frac{\varepsilon\rho\left(Q_{pc}/A_{pc}\right)D_h}{\mu(T)} \tag{10.9}$$

where coefficient m is equal to 2 and n is a function of x_{pc} as $n = \frac{x_{pc}}{x_{pc0}}$. T_0 is room temperature (23°C) for this experiment. ΔP_{mL0} is a specific value (here 2 MPa). x_{pc0} is 1 mm.

Applying this new modification to the *Re* calculated from the experimental data yields the plot of Figure 10.5. Also shown is the corresponding C_{dc} as a function of Re_c (See Appendix C). It is quite apparent that this modification reduces the scatter significantly.

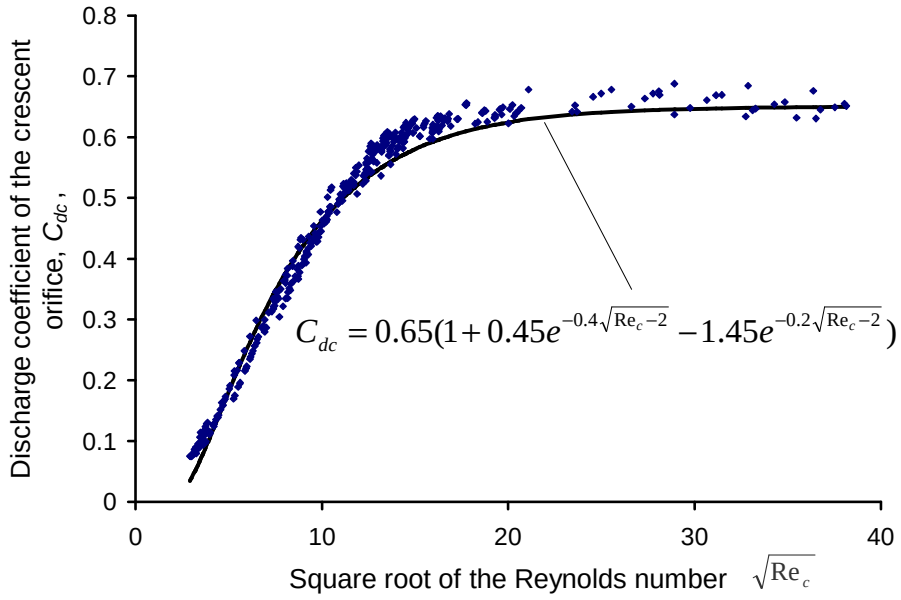

Figure 10.5 Discharge coefficient of the hydrostat orifice (4) of the PC system as a function of the modified Reynolds number

10.3 Comparison of Experimental and Theoretical Results of the Steady State Operating Points

A set of experiments was conducted to measure the displacement, x_{pc}, of the hydrostat spool as a function of x_v, P_s and P_L. The input conditions of each experiment (i.e. x_v, P_s, and P_L) are considered as the input to the nonlinear Equation (3.35) to predict the displacement, x_{pc}, of the hydrostat spool. The predicted and experimental results of x_{pc} are compared in Figures 10.6 through 10.9.

Figure 10.6 shows the comparison between the experimental and predicted results of x_{pc} as a function of x_v under the condition of a constant pressure drop of 1.6 MPa across the PC system. The region between the dashed lines contains all of the measured values for the hydrostat orifice opening, x_{pc}. The region between solid lines represents all of the predicted results of x_{pc}, which vary mainly due to changes in oil temperature (viscosity). When the opening of the fixed orifice, x_v, is small, the measured and predicted results

are almost identical. As the opening, x_v, increases, the measured value is gradually larger than the predicted results.

Figures 10.7 through 10.9 are comparisons between the experimental and predicted results of x_{pc} as a function of x_v under conditions of different pressure drops across the PC system, P_s - P_L. The agreement between predicted and measured results is generally very good. The higher the pressure drop, the more accurate predictions occur.

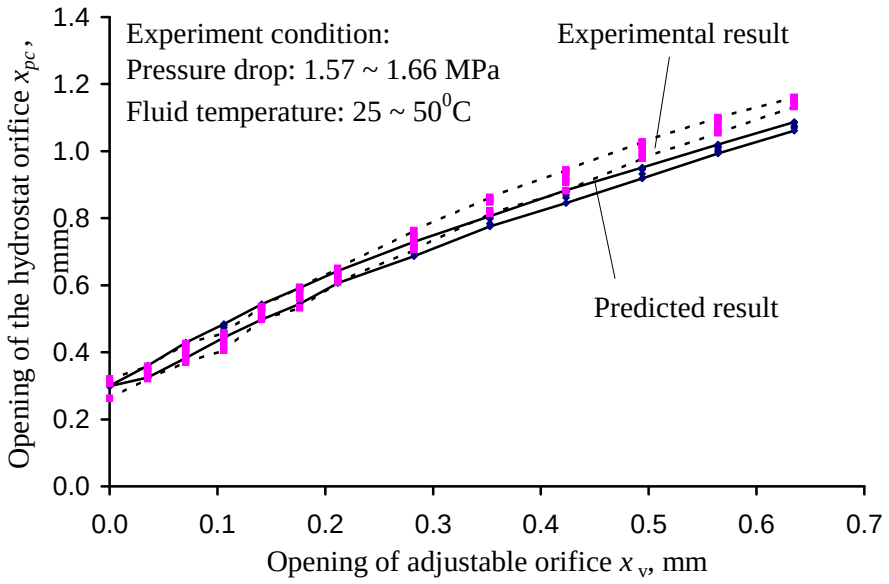

Figure 10.6 Comparison of the Experimental and Theoretical Results of the Hydrostat Orifice Opening, x_{pc} (ΔP_{sL} = 1.6 MPa)

10.4 Summary

The PC system has a fixed orifice and a hydrostat located orifice. The fixed orifice is used to manually, or electronically, adjust the flow rate of the PC system. The hydrostat orifice is automatically controlled by the pressure drop across the fixed orifice. Because the opening of the hydrostat orifice (i.e. the displacement of the hydrostat spool) directly affects the dynamic and steady state behavior of the flow, it is necessary to study the SSOP of the opening of the hydrostat orifice.

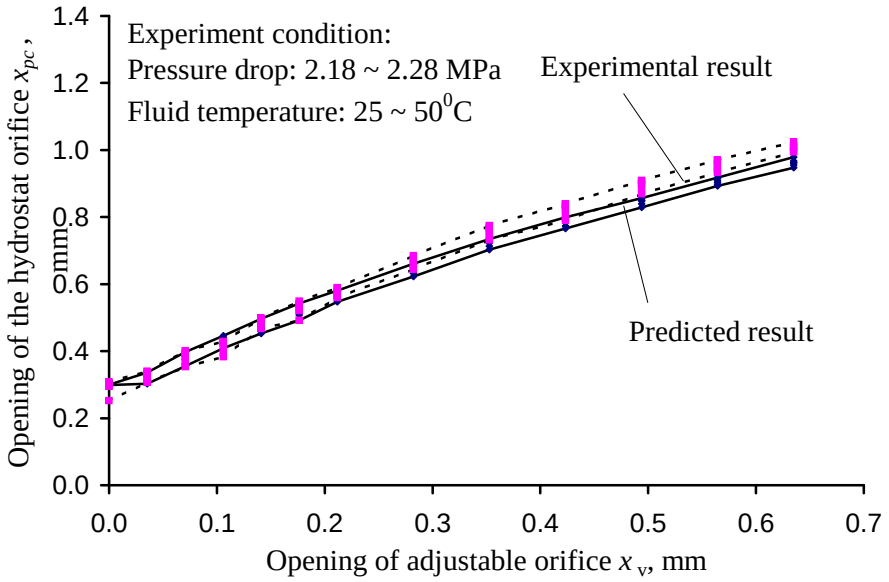

Figure 10.7 Comparison of the Experimental and Theoretical Results of the Hydrostat Orifice Opening, x_{pc} (ΔP_{sL} = 2.2 MPa)

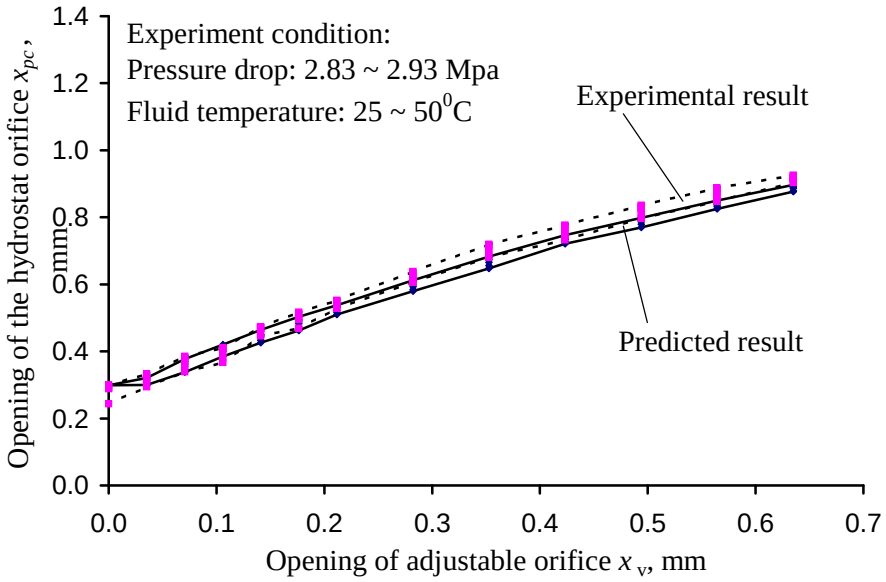

Figure 10.8 Comparison of the Experimental and Theoretical Results of the Hydrostat Orifice Opening, x_{pc} (ΔP_{sL} = 2.9 MPa)

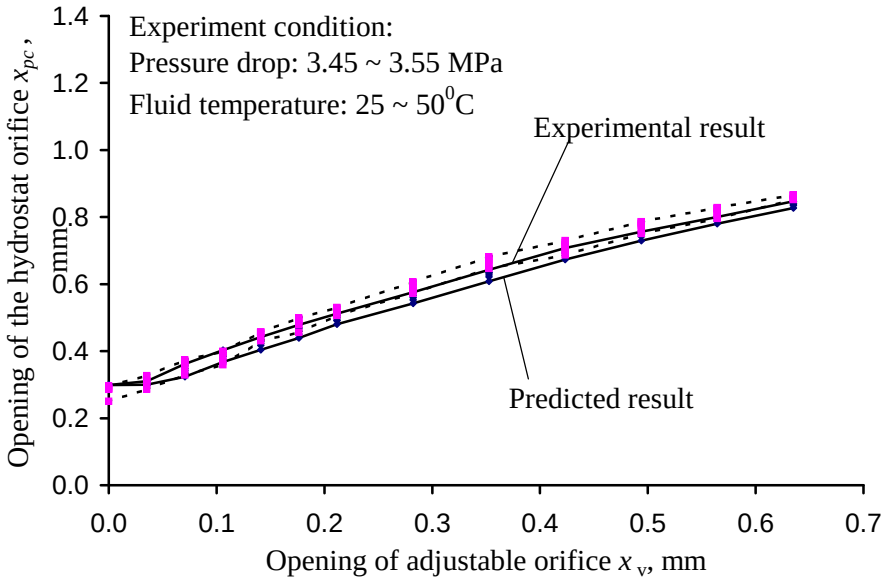

Figure 10.9 Comparison of the Experimental and Theoretical Results of the Hydrostat Orifice Opening, x_{pc} (ΔP_{sL} = 3.5 MPa)

This study establishes a nonlinear equation to solve the SSOP of the opening of the hydrostat orifice, x_{pc}. This nonlinear equation involves the discharge coefficients of two different types of orifices. For the fixed rectangular-type orifice, the discharge coefficient, C_{dv}, is indirectly measured and fitted as an exponential function of the square root of Reynolds number. For the hydrostat crescent-shaped orifice, however, the discharge coefficient, C_{dc}, has to be presented as a function of a modified Reynolds number due to significant leakage at small orifice openings. The discharge coefficient, C_{dc}, is also fitted as an exponential function of the square root of the modified Reynolds number.

Chapter 11 Dynamic Analysis of the Pressure Compensated System

The objective of this chapter is to develop the frequency response model of the PC system with the downstream hydrostat configuration. Similar to the methods used in Chapter 5, the linearization equations given in Chapter 9 are used to develop the appropriate transfer functions.

11.1 Dynamic Model of the Pressure Compensated System

This section develops the frequency response model of the PC system based on the linearized dynamic model in time domain. Condition A and B are considered separately.

11.1.1 Condition A (Normal condition)

Equation (8.4) represents the dynamic model of the hydrostat spool. Because the pressure setting, $P_{pc,}$ is neither a state variable nor an input variable, P_{pc} is absent in the linearized equation of Equation (8.18). P_{pc} affects the dynamic behavior of the PC system only through the SSOP. The dynamic Equation (8.18) is repeated (Again, note: "Δ" used for linearization is dropped)

$$\begin{aligned} M_{pc}\ddot{x}_{pc} + B^{*}_{pc}\dot{x}_{pc} + k^{*}_{pc}x_{pc} - \left(A_{pcs} - k_{ff}A_{pc}\left(x_{pc0}\right)\right)P_m \\ = -A_{pcs}P_s + k_{ff}A_{pc}\left(x_{pc0}\right)P_L \end{aligned} \tag{11.1}$$

Taking the Laplace transform of Equation (11.1) gives

$$A_{11}(s)X_{pc}(s) + A_{12}P_m(s) = -A_{pcs}P_s(s) + k_{ff}A_{pc}\left(x_{pc0}\right)P_L(s) \tag{11.2}$$

where $A_{11}(s) = M_{pc}s^2 + B^{*}_{pc}s + k^{*}_{pc}$ (11.3)

$$A_{12} = k_{ff}A_{pc}\left(x_{pc0}\right) - A_{pcs} \tag{11.4}$$

Equation (8.21) is rewritten as (Note: "Δ" is dropped)

$$K_{qpc}x_{pc} + A_{pcs}\dot{x}_{pc} + \left(K_{cv} + K_{cpc}\right)P_m = K_{qv}x_v + K_{cv}P_s + K_{cpc}P_L \tag{11.5}$$

Taking the Laplace transform of Equation (11.5) gives

$$A_{21}(s)X_{pc}(s)+A_{22}P_m(s)=K_{qv}X_v(s)+K_{cv}P_s(s)+K_{cpc}P_L(s) \tag{11.6}$$

where $A_{21}(s)=K_{qpc}+A_{pcs}s$ (11.7)

$$A_{22}=K_{cv}+K_{cpc} \tag{11.8}$$

Taking the Laplace transform of Equation (8.10) gives the load flow rate through the hydrostat orifice as

$$Q_{Lpc}(s)=K_{qpc}X_{pc}(s)+K_{cpc}\left(P_m(s)-P_L(s)\right) \tag{11.9}$$

Solving Equation sets (11.2) and (11.6) for state variables $X_{pc}(s)$ and $P_m(s)$, and then substituting them into Equation (11.9) yields the flow rate, $Q_{Lpc}(s)$, as a function of three input variables, $X_{pc}(s)$, $P_s(s)$ and $P_L(s)$. Appendix K presents the derivation of this function and is shown to be

$$Q_{Lpc}(s)=G_{xv}(s)X_v(s)+G_{psL}(s)\left(P_s(s)-P_L(s)\right) \tag{11.10}$$

where

$$G_{xv}(s)=K_{xv}\frac{s^2+b_{xv1}s+b_{xv0}}{s^2+a_1s+a_0} \tag{11.11}$$

$$G_{psL}(s)=K_{psL}\frac{s^2+b_{psL1}s+b_{psL0}}{s^2+a_1s+a_0} \tag{11.12}$$

The dynamic model of the PC system (Equation (11.10)) and the linarized equation for a simple orifices (Equation (5.45)) have a similar form. That is,

$Q(s)=K_qX(s)+K_c\left(P_s(s)-P_L(s)\right)$ for an orifice and

$Q_{Lpc}(s)=G_{xv}(s)X_v(s)+G_{psL}(s)\left(P_s(s)-P_L(s)\right)$ for the dynamic model. Therefore, $G_{xv}(s)$ can be considered as the “flow gain transfer function” (TF) which is equivalent to its counterpart, K_q, and $G_{psL}(s)$ as the “flow-pressure coefficient transfer function” (TF) equivalent to its counterpart, K_c. In order to accomplish flow control through an

appropriate change in the area of the adjustable orifice, $X_v(s)$, $G_{psL}(s)$ should be as small as possible (zero at best). Thus it is most important to investigate the relationship between $G_{psL}(s)$ and parameters of the PC system with an aim to minimize the effect on Q_{Lpc} through optimal design of the PC system.

The gains and coefficients of Equations (11.11) and (11.12) are derived in Appendix K and are listed as

$$K_{xv} = \frac{K_{qv} K_{cpc}}{K_{cv} + K_{cpv}} \tag{11.13}$$

$$K_{psL} = \frac{K_{cv} K_{cpc}}{K_{cv} + K_{cpv}} \tag{11.14}$$

$$a_1 = \frac{B_{pc}^*}{M_{pc}} + \frac{A_{pcs}\left(A_{pcs} - k_{ff} A_{pc}\left(x_{pc0}\right)\right)}{M_{pc}\left(K_{cv} + K_{cpc}\right)} \tag{11.15}$$

$$a_0 = \frac{k_{pc}^*}{M_{pc}} + \frac{K_{qpc}\left(A_{pcs} - k_{ff} A_{pc}\left(x_{pc0}\right)\right)}{M_{pc}\left(K_{cv} + K_{cpc}\right)} \tag{11.16}$$

$$b_{xv1} = \frac{B_{pc}^*}{M_{pc}} \tag{11.17}$$

$$b_{xv0} = \frac{k_{pc}^*}{M_{pc}} + \frac{K_{qpc}\left(A_{pcs} - k_{ff} A_{pc}\left(x_{pc0}\right)\right)}{M_{pc} K_{cpc}} \tag{11.18}$$

$$b_{psL1} = \frac{B_{pc}^*}{M_{pc}} + \frac{A_{pcs}^2}{M_{pc} K_{cv}} \tag{11.19}$$

$$b_{psL0} = \frac{k_{pc}^*}{M_{pc}} - \frac{K_{qpc} k_{ff} A_{pc}\left(x_{pc0}\right)}{M_{pc} K_{cpc}} \tag{11.20}$$

Equations (11.13) through (11.20) include six coefficients given in Chapter 8. They are repeated here for completeness.

$$B_{pc}^* = B_{pc} + \rho L K_{qpc} + A_{pcs}^2 R_{sh} \tag{11.21}$$

$$k_{pc}^{*} = k_{pc} + k_{ff} w_{pc} \left(P_{m0} - P_L \right) \tag{11.22}$$

$$K_{qv} = C_{dv} w_v \sqrt{\frac{2}{\rho} \left(P_s - P_{m0} \right)} \tag{11.23}$$

$$K_{cv} = \frac{C_{dv} w_v x}{\sqrt{2\rho \left(P_s - P_{m0} \right)}} \tag{11.24}$$

$$K_{qpc} = C_{dc} w_{pc} \sqrt{\frac{2}{\rho} \left(P_{m0} - P_L \right)} \tag{11.25}$$

$$K_{cpc} = \frac{C_{dc} A_{pc} \left(x_{pc} \right)}{\sqrt{2\rho \left(P_{m0} - P_L \right)}} \tag{11.26}$$

where w_{pc} represents the equivalent width of the hydrostat orifice, $\frac{dA_{pc}\left(x_{pc0}\right)}{dx_{pc}}$.

Equations (11.15) through (11.20) can be expressed into simpler form by substituting Equations (11.21) through (11.26) into Equations (11.13) through (11.20). In the following process, it is assumed that $A_{pcs} >> A_{pc}\left(x_{pc0}\right)$ (i.e. the spool cross sectional area, A_{pcs}, is much larger than the hydrostat orifice area, $A_{pc}(x_{pc0})$) and $k_{ff} < 1$ (reference to Equation (10.6)). With these conditions, Equations (11.15) through (11.20) become

$$a_1 = \frac{1}{M_{pc}} \left(B_{pc} + \rho L K_{qpc} + A_{pcs}^2 \left(R_{sh} + \frac{1}{K_{cv} + K_{cpc}} \right) \right) \tag{11.27}$$

$$\begin{aligned} a_0 &= \frac{1}{M_{pc}} \left(k_{pc} + \frac{K_{qpc} A_{pcs}}{K_{cv} + K_{cpc}} \right) \\ &= \frac{1}{M_{pc}} \left(k_{pc} + \frac{2 w_{pc} A_{pcs} \left(P_{m0} - P_L \right)}{A_{pc}\left(x_{pc0}\right) + A_v \sqrt{\frac{P_{m0} - P_L}{P_s - P_{m0}}}} \right) \end{aligned} \tag{11.28}$$

$$b_{xv1} = \frac{B_{pc} + \rho L K_{qpc} + A_{pcs}^2 R_{sh}}{M_{pc}} \tag{11.29}$$

$$b_{xv0} = \frac{1}{M_{pc}}\left(k_{pc} + \frac{2w_{pc}A_{pcs}\left(P_{m0} - P_L\right)}{A_{pc}\left(x_{pc0}\right)}\right) \tag{11.30}$$

$$b_{psL1} = \frac{1}{M_{pc}}\left(B_{pc} + \rho L K_{qpc} + A_{pcs}^2\left(R_{sh} + \frac{1}{K_{cv}}\right)\right) \tag{11.31}$$

$$b_{psL0} = \frac{1}{M_{pc}}\left(k_{pc} - k_{ff}\, w_{pc}\left(P_{m0} - P_L\right)\right) \tag{11.32}$$

In order to use Equation (11.10) in subsequenct analysis and design of the PC system, it is necessary to determine R_{sh} in Equation (11.27). R_{sh} represents the hydraulic resistance in the damping hole (3) in Figure 8.2. The damping hole can be considered a short tube orifice. Because the flow rate through the damping hole is small, the flow must be laminar. Merritt [1967] gave a discharge coefficient for a short tube orifice at laminar flow conditions to be

$$C_d = \frac{1}{8}\sqrt{\frac{D_{damp}\,Re}{L_{damp}}} \tag{11.33}$$

where D_{damp} is the diameter of the small hole, L_{damp} is the length of the small hole, and Re is the Reynolds numbers and is defined

$$Re = \frac{4\rho Q}{\pi\mu D_{damp}} \tag{11.34}$$

Substituting Equation (11.34) into Equation (11.33), and then substituting C_d into the general orifice flow equation yields

$$Q = \frac{D_{damp}^4\pi}{128\mu L_{damp}}\Delta P \tag{11.35}$$

Therefore, the hydraulic resistance, R_{sh}, is derived as a reciprocal of the coefficient in Equation (11.35), that is,

$$R_{sh} = \frac{128\mu L_{damp}}{D_{damp}^4 \pi} \tag{11.36}$$

11.1.2 Condition B (Hydrostat orifice fully opened)

Under Condition B, the hydrostat orifice of the PC system is fully opened. The PC system becomes essentially two cascade fixed orifices in series. In order to obtain the equivalent flow gain and flow pressure coefficient of the cascaded orifices, Equations (8.9) and (8.10) must be considered (Noted: the "Δ" due to linearization is dropped). For Condition B, $x_{pc} = x_{pcmax}$ and $Q_{Lv} = Q_{Lpc} = Q_L$. Therefore,

$$Q_L = K_{qv} x_v + K_{cv}\left(P_s - P_m\right) \tag{11.37}$$

$$Q_L = K_{cpc}\left(P_m - P_L\right) \tag{11.38}$$

Eliminating P_m from Equations (11.37) and (11.38) gives

$$Q_L = \frac{K_{qv}K_{cpc}}{K_{cv} + K_{cpc}} x_v + \frac{K_{cv}K_{cpc}}{K_{cv} + K_{cpc}}\left(P_s - P_L\right) \tag{11.39}$$

Based on Equation (11.39), the equivalent flow gain and flow pressure coefficient for the cascaded orifices are defined as

$$K_q^* = \frac{K_{qv}K_{cpc}}{K_{cv} + K_{cpc}} \tag{11.40}$$

$$K_c^* = \frac{K_{cv}K_{cpc}}{K_{cv} + K_{cpc}} \tag{11.41}$$

11.2 Theoretical Prediction of the Frequency Response of the Brand PC Valve

This section uses the model form of Equation (11.10) to predict the frequency response of the Brand PC flow control valve. The essential parameters of the PC system

must be measured or indirectly calculated. For various conditions, the Bode diagram of $G_{xv}(s)$ and $G_{psL}(s)$ are presented.

11.2.1 Parameters

Table 11.1 gives all essential parameters for plotting the Bode diagrams based on Equations (11.11) and (11.12). Parameters with a "*" have been evaluated directly or developed in earlier sections.

Table 11.1 Parameters of a Typical PC System

	Parameters	Expression	Value	Unit
Fluid characteristics and parameters	Fluid density	ρ	898	Kgm^{-3}
	Fluid temperature	T *	35	°C
	Discharge coefficient of fixed orifice	C_{dv} *	0.63	
	Discharge coefficient of hydrostat orifice	C_{dc} *	0.65	
Geometry parameters	Spool diameter	D_{pcs}	23.55×10^{-3}	m
	Width of fixed orifice (rectangular type (1))	w_v	49.83×10^{-3}	m
	Equivalent width of hydrostat orifice (crescent type (4))	w_{pc} *	20.8×10^{-3}	m
	Maximum displacement of the spool	x_{pcmax}	2.62×10^{-3}	m
	Diameter of the damping hole	D_{damp}	1×10^{-3}	m
	Length of the damping hole	L_{damp}	1×10^{-3}	m
	The axial length between hydrostat orifice and the center of conduit	L	1×10^{-2}	m
Dynamic parameters	Spool mass	M_{pc}	0.14	kg
	Spool damping coefficient	B_{pc}	10	Nsm^{-1}
	Pre-compressed spring coefficient	k_{pc}	9.1×10^{3}	Nm^{-1}
	Spring pre-compression	F_{pc}	142.3	N

Fluid temperature, T, is used to determine the dynamic viscosity, μ, required by Equation (11.36). For the fluid in this study, the fluid's viscosity (model: NUTO 68) can be expressed as

$$\mu = 0.182 \rho T^{-2.16} \tag{11.42}$$

Two discharge coefficients, C_{dv} and C_{dc}, given in Table 11.1 actually represent $C_{dv\infty}$ and $C_{dc\infty}$ obtained by the experiment in Chapter 10. The discharge coefficients can usually be considered as constant because the flow rate is relatively large and hence the flow is turbulent. Only when the adjustable orifice has a very small opening, the modified discharge coefficient model in Chapter 10 has to be applied.

w_{pc} represents the equivalent width of the hydrostat orifice at small openings. Although the hydrostat orifice is crescent type (See equation (8.3)), the orifice could be approximated as an equivalent rectangular shape about an operating point, x_{pc0}. The experimental result indicated that when x_{pc0} is larger than the certain value (e.g. 0.2 mm for this study) the width of the equivalent rectangular orifice is almost constant. The value of w_{pc} of 20.8 mm in Table 11.1 is an experimental result.

11.2.2 Procedure and Result of Calculations

It is necessary to explain the procedure for the evaluation of the frequency response at an operating point because the PC system is, in fact, a nonlinear system. All of Equations (11.13) through (11.26) depend on the operating point. Equation (11.21) does not explicitly show a dependency on temperature, but it is indirectly affected via Equations (11.36) and (11.42).

The operating point is determined by the input variables; x_v, P_s and P_L, and the fluid temperature, T, for the studied PC system. Assume that x_v is 0.2 mm, P_s is 4 MPa and P_L is 2 MPa. The operating point is calculated using the flow chart given in Figure 9.2 of Chapter 9. The results indicate that the PC system operates under Condition A (the normal condition): δP_{pcc} = 0.34 MPa which is less than ($P_s - P_L$) (2 MPa). Thus,

Operating point: x_{pc0} = 0.23 mm and P_{m0} = 3.63 MPa

$$G_{xv}(s) = \frac{0.17\left(s^2 + 4205s + 4.33\times10^7\right)}{(s+7479)(s+1122))} \tag{11.43}$$

$$G_{psL}(s) = \frac{4.63\times10^{-11}(s+9668)(s-4.57)}{(s+7479)(s+1122))} \tag{11.44}$$

Note that as $s \rightarrow 0$, $G_{psL}(0)$ becomes negative, i.e. the phase shift is 180^o at steady state.

Equations (11.43) and (11.44) are plotted in Figures 11.1 and 11.2. It can be observed from Figure 11.1 that the frequency band of flow control is very wide (1122 rad/s). In

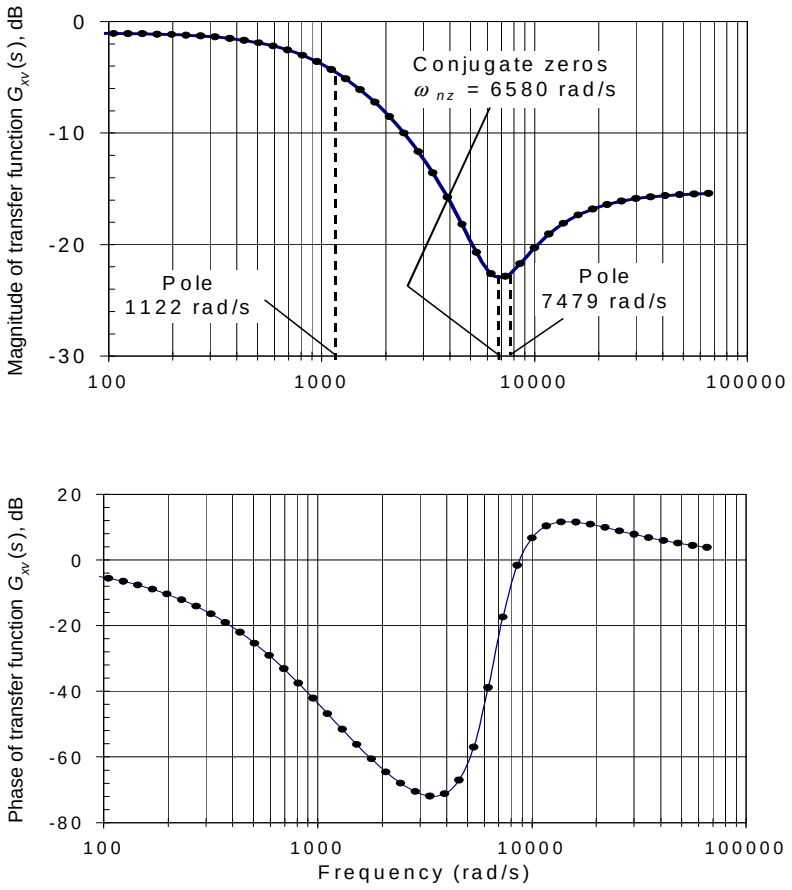

Figure 11.1 Frequency response of flow gain of the PC system, $G_{xv}(s)$

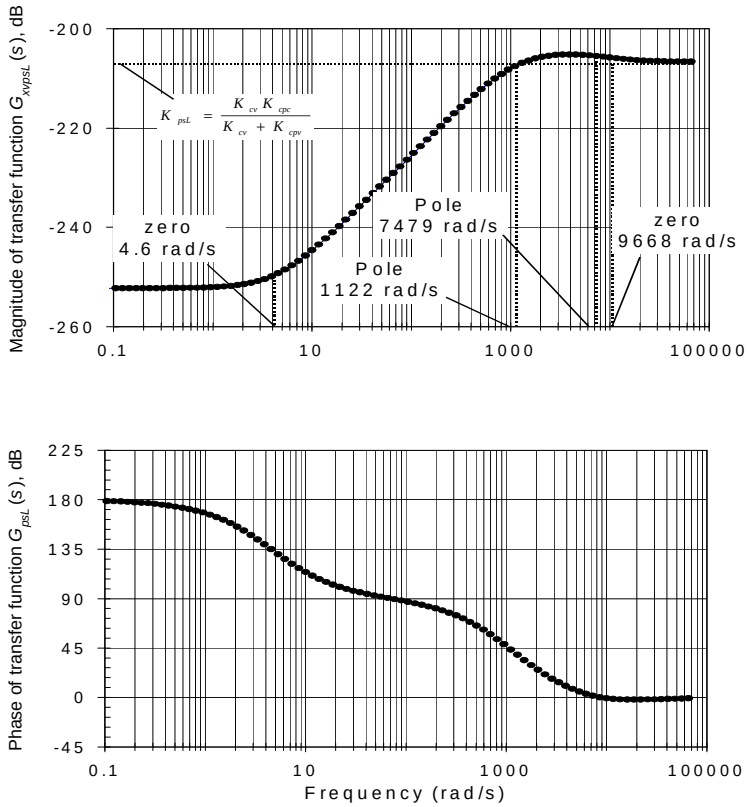

Figure 11.2 Frequency response of flow-pressure coefficient of the PC system, $G_{psL}(s)$

addition, it can be deduced that a conjugate zero and another pole with very high break frequencies, exist.

For $G_{psL}(s)$, Figure 11.2 and Equation (11.44) indicate that a small real zero exists in the right half of the s plane. In the low frequency region, the flow-pressure coefficient is very small (about -250 dB). It is known that the smaller $G_{psL}(s)$ is, the better that flow control over all frequencies can occur. The ideal situation is that a zero should be located at the origin. This is further discussed in the follow section. As mentioned above, at the very low frequency region (near the steady state condition) the phase of the flow-pressure coefficient TF is 180°. This is defined as an “over-compensated” situation and will now be considered.

11.3 Model Analysis and Design of the Pressure Compensated System

The objective of this section is to analyze the basic characteristics of the flow gain TF, G_{xv}(s), and the flow-pressure coefficient TF, G_{psL}(s), to use these to define three different dynamic operating conditions and to derive formulas which can be used to optimize the design of a PC system.

11.3.1 The Basic Feature of the Flow Gain Transfer Functions, $G_{xv}(s)$

The flow gain TF, $G_{xv}(s)$, is a low pass filter because a_0 in Equation (11.28) is smaller than b_{xv0} in Equation (11.30). The bandwidth of the low pass filter can be considered as the smallest one of two poles which is determined using Equations (11.27) and (11.28). The hydraulic resistance, R_{sh}, in Equations (11.27) affects the damping in the system. In order to obtain a proper damping ratio of the PC system, the size of the damping hole (3) in Figure 8.2 must be carefully calculated. When the hole is large (resulting in a small value of R_{sh}), the two poles of Equations (11.11) and (11.12) are complex conjugates; as a result, the damping ratio is very small. This can cause oscillatory behavior of the PC system. If the hole is very small (so that R_{sh} is large), the two poles become real, with one of the poles becoming very small. This reduces the flow control bandwidth of the PC system. In an ideal situation R_{sh} is selected such that the PC system has a pair of conjugate poles with a damping ratio of 0.7, thus, $\frac{a_1}{\sqrt{a_0}} = 2\zeta = 1.4$. Substituting Equations (11.27) and (11.28) into this equation and rearranging it gives

$$R_{sh} = \frac{1}{A_{pcs}^2}\left(\sqrt{2M_{pc}\left(k_{pc} + \frac{K_{qpc}A_{pcs}}{K_{cv}+K_{cpc}}\right)} - B_{pc} - \rho L K_{qpc}\right) - \frac{1}{K_{cv}+K_{cpc}} \qquad (11.45)$$

In this case, the bandwidth of the flow control is $\sqrt{a_0}$ (refer to Equation (11.12)). Figure 11.3 gives the magnitude plots of the flow gain TF's and the flow pressure coefficient TF's for two examples: Examples I and II. The flow gain TF's and flow pressure coefficient TF's are $G_{xv1}(s)$ and $G_{psL1}(s)$ for Example I and $G_{xv2}(s)$ and $G_{psL2}(s)$ for Example II respectively. The comparison between G_{xv1} and G_{xv2} indicates that further increase in the bandwidth can be obtained by increasing the spring coefficient, k_{pc}, the spool cross sectional area, A_{pcs}, or decreasing the mass, M_{pc}, (Equation 11.28).

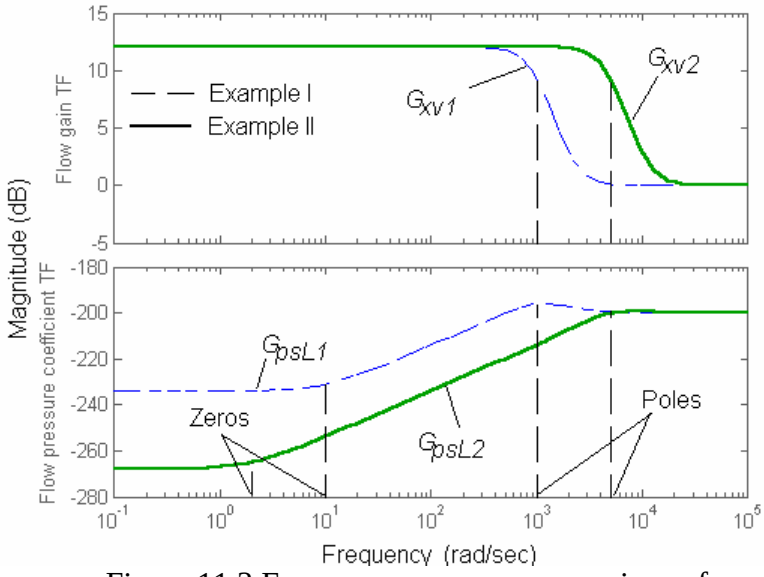

Figure 11.3 Frequency response comparison of $|G_{psL}(s)|$ of two PC systems

11.3.2 The Basic Feature of the Flow-Pressure Coefficient Transfer Functions, $G_{psL}(s)$

The flow-pressure coefficient TF, $G_{psL}(s)$, is a high pass filter. The function of the PC systems in hydraulic circuits is to control the flow rate through the valve by minimizing the effect of the pressure drop across the valve on the flow rate. To realize this, the

magnitude of flow-pressure coefficient TF, $G_{psL}(s)$, should be as small as possible in all frequency regions, especially in the low frequency region.

Factors affecting the magnitude of the flow-pressure coefficient TF, $G_{psL}(s)$, will now be explored. It can be observed from Equation (11.12) and Figure 11.2 that K_{psL} represents the flow-pressure coefficient in the high frequency region. K_{psL} is determined by the flow pressure coefficients of the adjustable orifice and the hydrostat orifice at a specific operating point and is independent of dynamic parameters such as M_{pc}, B_{pc}, k_{pc}, R_{sh}, etc. These dynamic parameters only affect the shape of the magnitude of $G_{psL}(s)$ at the low frequency region. Therefore, it is possible to reduce $|G_{psL}(s)|$ in the low frequency region by designing a set of proper dynamic parameters.

Figure 11.3 also shows the magnitude plots of flow pressure coefficient TF's, $G_{psL1}(s)$ and $G_{psL2}(s)$. When the pole of $G_{psL}(s)$ increases, $|G_{psL}(s)|$ decreases (compare $G_{psL1}(s)$ and $G_{psL2}(s)$). Section 11.3.1 has introduced the method of increasing the pole (i.e. expanding the bandwidth of flow control of the PC system). Therefore, increasing the pole results in two advantages: expanding the bandwidth of flow control and decreasing $|G_{psL}(s)|$.

The other approach of decreasing $|G_{psL}(s)|$ at low frequencies is to decrease the zero of $G_{psL}(s)$ (compare $G_{psL1}(s)$ and $G_{psL2}(s)$ again). The zero of $G_{psL}(s)$ in Figure 11.3 can be determined by (reference to Equation (11.12))

$$s_{z1} = 0.5\left|\sqrt{b_{psL1}^2 - 4b_{psL0}} - b_{psL1}\right| \tag{11.46}$$

It can be seen that, s_{z1} is reduced by decreasing the absolute value of b_{psl0} (ideally $b_{psl0} = 0$). In the ideal situation, s_{z1} is equal to zero and the flow rate is completely independent of the pressure drop across the PC system at steady state condition. It must

be emphasized that b_{psl0} can only be zero at some operating point, $P_{m0} = P_L + \dfrac{k_{pc}}{k_{ff} w_{pc}}$ (reference to Equation (11.32)). Indeed, P_{m0} can be larger, equal or less than $P_L + \dfrac{k_{pc}}{k_{ff} w_{pc}}$, which corresponds to, b_{psl0} being positive, zero or negative. This gives rise to different dynamic operating conditions.

11.3.3 Three "Pressure Compensated" Conditions

b_{psl0} can be positive, zero, or negative depending on which of the spring coefficients, k_{pc}, and the equivalent spring coefficient caused by the steady state flow force is largest. These cases reflect three different pressure compensation conditions. With the inspiration from the three damping conditions (under-damped, critically damped and over-damped conditions) of the 2nd order system, three different pressure compensation conditions are defined into under-compensated, critically compensated and over-compensated conditions.

Under-compensated Condition:

$$k_{pc} > k_{ff} w_{pc} \left(P_{m0} - P_L \right) \tag{11.47}$$

In the "under-compensated" condition, the flow pressure coefficient of the PC system is non-zero but positive at the steady state. When the pressure differential, $P_s - P_L$, increases, the flow rate, Q_{Lpc}, increases. This is similar to the case of a simple orifice, but the increase in Q_{Lpc} is much less than the increase in Q_L of a simple orifice for the same pressure drop across the PC system. As an example, $K_c = 1.8$ lpm per MPa for an orifice and K_c = 0.018 lpm per MPa for the PC system.

Critically Compensated Condition:

$$k_{pc} = k_{ff} w_{pc} \left(P_{m0} - P_L \right) \tag{11.48}$$

Under the critically compensated condition, the flow pressure coefficient of the PC system is zero at the steady state. Therefore, the steady state flow rate, Q_{psL0}, is independent of the pressure drop across the PC system, ($P_{s0} - P_{L0}$).

Over-compensated Condition:

$$k_{pc} < k_{ff} w_{pc} \left(P_{m0} - P_L \right) \tag{11.49}$$

In the "over-compensated" condition, the flow pressure coefficient of the PC system is negative at the steady state. When the pressure differential, $P_s - P_L$, increases, the flow rate, Q_{Lpc}, decreases. The example in Section 11.2.2 is such a case. The theoretical prediction of the phase angle under steady state conditions is 180 degrees (Figure 11.2). This result has been verified experimentally in which the flow rate has been measured as a function of the pressure drop across the PC system at several openings. It is clear that the slope (here K_{psL}) is negative reflecting the over-compensated condition (Figure 11.4).

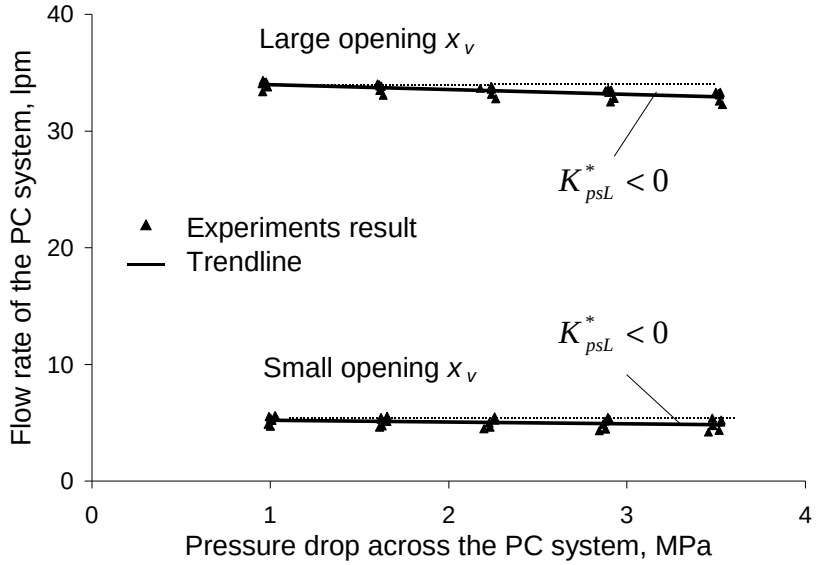

Figure 11.4 The relationship of flow rate and pressure drop across the PC system at steady state.

11.3.4 Simplification of the Dynamic Model of the Pressure Compensated System

Equations (11.11) and (11.12) can be simplified, because, except for a small zero in G_{psL}(s), the poles and zeros of $G_{xv}(s)$ and $G_{psL}(s)$ are very large and hence, only influencing the dynamics of the valve at very high frequency operating condition. This justification is true as long as R_{sh} is not extremely large. Figures 11.1 and 11.2 indicate that most of the corner (or break) frequencies are larger than 1000 rad/s. These frequencies can be neglected when the frequency response less than 1000 rad/s of the PC system is of concern.

Equation (11.10) can be simplified and expressed as

$$Q_{Lpc}(s) = K_{xv}^{*} X_v(s) + G_{psL}(s)\left(P_s(s) - P_L(s)\right) \tag{11.50}$$

where $$K_{xv}^{*} = \frac{K_{xv} b_{xv0}}{a_0} = \frac{K_{qv} K_{cpc}}{K_{cv} + K_{cpv}} \cdot \frac{k_{pc} + \dfrac{K_{qpc} A_{pcs}}{K_{cpc}}}{k_{pc} + \dfrac{K_{qpc} A_{pcs}}{K_{cv} + K_{cpc}}} \tag{11.51}$$

$$G_{psL}(s) = K_{psL}^{*}\left(\frac{s}{\omega_{pc0}} + 1\right) \tag{11.52}$$

where

$$K_{psL}^{*} = \frac{K_{cv} K_{cpc}}{K_{cv} + K_{cpv}} \cdot \frac{k_{pc} - k_{ff} w_{pc}\left(P_{m0} - P_L\right)}{k_{pc} + \dfrac{K_{qpc} A_{pcs}}{K_{cv} + K_{cpc}}} \tag{11.53}$$

$$\omega_{pc0} = \frac{k_{pc} - k_{ff} w_{pc}\left(P_{m0} - P_L\right)}{B_{pc} + \rho L K_{qpc} + A_{pcs}^2\left(R_{sh} + \dfrac{1}{K_{cv}}\right)} \tag{11.54}$$

The simplified dynamic model of the PC system is such that the flow gain TF, $G_{xv}(s)$, is a pure proportional gain, K_{xv}^{*}, and the flow pressure coefficient TF, $G_{psL}(s)$, is approximately as a first order TF with the corner frequency, ω_{pc0} (time constant, $\frac{1}{\omega_{pc0}}$).

For the critically compensated condition, substituting Equations (11.53) and (11.54) into Equation (11.52) gives

$$G_{psL}(s) = K_{psL}^{**} s \tag{11.55}$$

where

$$K_{psL}^{**} = \frac{K_{cv}K_{cpc}}{K_{cv}+K_{cpv}} \cdot \frac{B_{pc} + \rho L K_{qpc} + A_{pcs}^{2}\left(R_{sh} + \frac{1}{K_{cv}}\right)}{k_{pc} + \frac{K_{qpc}A_{pcs}}{K_{cv}+K_{cpc}}} \tag{11.56}$$

This indicates that the flow pressure coefficient, $G_{psL}(s)$, is a pure differential. At steady state condition ($s = 0$), the flow pressure coefficient is zero. Flow through the valve is completely independent of pressure drop.

For the over-compensated condition, it can be observed from Equations (11.53) and (11.54) that both K_{psL}^{*} and ω_0 are negative. Equation (11.52) can be expressed as

$$G_{psL}(s) = \left|K_{psL}^{*}\right|\left(\frac{s}{|\omega_0|} - 1\right) \tag{11.57}$$

Equation (11.57) indicates that the flow pressure coefficient at steady state is equal to $-\left|K_{psL}^{*}\right|$ (reference to Figure 11.4).

11.3.5 Discussion Relating to Experiments on the Pressure Compensated System

It must be explained that although the sign of the steady state gain, $K_{psL}^{*} = \frac{K_{psL}b_{psL0}}{a_0}$,

of Equation (11.44) has been experimentally verified (see Figure 11.4), it is extremely difficult to completely verify Equation (11.44) at all frequencies experimentally, because

- The flow pressure coefficient of PC valves is very small; that is, the dynamic component in the flow rate, resulting from the small dynamic excitation signal in the pressure drop across the PC valve, is quite small. Any change in measured flow which could be attributed to $K_{psL}(s)$ would be masked by a low signal to noise ratio at their levels.
- In order to increase the flow sensitivity to $K_{psL}(s)$, one method is to increase the amplitude of the dynamic excitation signal of the pressure drop across the PC valve. However, this would make the linearization method invalid. This can be further explained by examing Equations (11.12) and (11.32). When ($P_s - P_L$) (and hence ($P_m - P_L$)) varies over a large range, the coefficient, b_{psL0}, in Equation (11.12) would experience a significant variation, and indeed could change its sign. Consequently, the TF defined at the operating point would no longer be valid.
- It is very difficult to excite and measure break frequencies larger than 1000 rad/s.

As a final note, it should be mentioned that the three compensated conditions discussed above are often not of concern for a simple circuit which uses a PC system only for control of the flow rate, because $\left|K^*_{psL}\right|$ is much smaller than K_c for a simple orifice (typically one hundredth). However, when the PC system plays the role of both flow control and "pressure sensing" in complex circuits such as a LSPC system, the three compensated conditions can have completely different consequences for the performance of the system.

11.4 Summary

Based on the analysis of the PC system model given by Equations (11.10), (11.11) and (11.12), the following comments can be forwarded.

- Because it is preferred that a PC system display a very small flow pressure coefficient, the best condition is that the spring coefficient, k_{pc}, matches the equivalent spring coefficient caused by the steady state flow force (reference to Equation (11.48)).
- The PC system can exist in one of three dynamic compensation conditions which are defined as pressure "under-compensated", "critically compensated" and "over-compensated" conditions depending on the sign of b_{psL0} (Equation (11.32)).
- In order to extend the bandwidth of the flow control valve, the poles of the PC system TF's ($G_{xv}(s)$ and ($G_{psL}(s)$) should be as large as possible. Increasing the spring coefficient, k_{pc}, the spool cross sectional area, A_{pcs}, or decreasing the mass, M_{pc}, can expand the bandwidth.
- In order to obtain a good compromise between the bandwidth and dynamic behavior of the PC system, the size of the damping hole in Figure 8.2 must be properly selected using Equations (11.45) and (11.36). A very small R_{sh} (i.e. a very large damping hole) would result in high frequency oscillation. But a very large R_{sh}, (a very small damping hole) would reduce the bandwidth.

Chapter 12 Steady State Analysis of the Load Sensing and Pressure Compensated System

12.1 Introduction

In Chapter 2 through Chapter 7, it was established that flow control using a LS system demonstrated high efficiency, but at the expense of performance. In chapters 8 through 11, a PC valve for flow control was considered which demonstrated good dynamic characteristics, but was very inefficient from an energy point of view. In this chapter, a combination of the LS system and the PC valve is examined and is defined as a load sensing, pressure compensated (LSPC) system. The LSPC system is illustrated schematically in Figure 12.1.

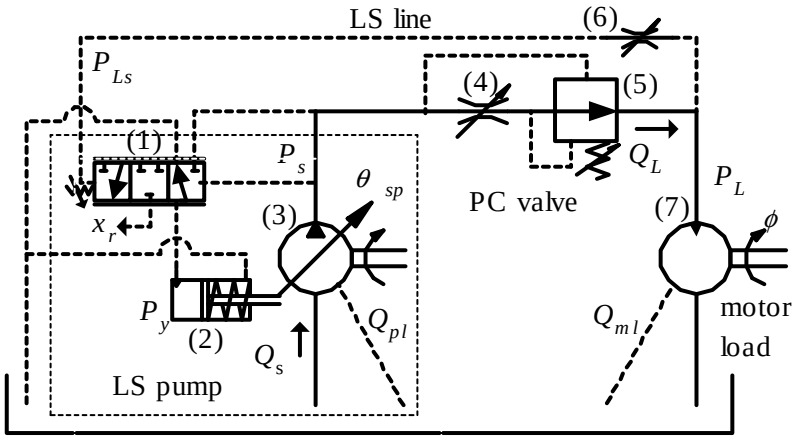

Figure 12.1 Schematic of the Load Sensing Pressure Compensating System

The LSPC system consists of a LS pump with the LS regulator (1), the control piston (2) and the pressure control pump (3), the PC valve with an adjustable orifice (4) and hydrostat (5), the LS line with a damping orifice (6), and the motor load (7). It can be observed that the PC system (defined by (4) and (5)) controls the load flow rate, Q_L,

through the load (7), while the LS pump ((1), (2) and (3)) delivers the necessary flow to the PC valve by measuring the pressure drop across the PC system via the LS line (6).

In order to investigate the performance of the LSPC system by the linearization approach, a procedure similar to that used to analyze the LS system and PC system must be followed. The basic steps include modeling, steady state analysis (operating condition analysis and solving for SSOP's), dynamic analysis, etc. However, because the LSPC system is an assembly of the LS system and the PC system, it is unnecessary to repeat modeling of each hydraulic component. This chapter analyzes the steady state operating condition of the LSPC system and presents the method of solving for SSOP's. The following chapter considers the modeling and analysis of the dynamic performance of the LSPC system.

12.2 Steady State Operating Conditions

The steady state operating conditions of the LSPS system are combinations of all operating conditions of the LS system and the PC system, that is, six different operating conditions (Condition I, II, and III for the LS system; Condition A and B for the PC system). It is now necessary to discuss these operating conditions.

According to Chapters 3 and 9, Conditions I and A are the normal operating conditions for both the LS system and the PC system. Therefore, the combination of Condition I for the LS and Condition A for the PC system is the normal operating condition of the LSPC system. For simplicity, this condition is defined as Condition N for the LSPC system. According to Equations (3.20) and (9.9), Condition N must satisfy the relationship

$$P_{s0} - P_{L0} = P_d \tag{12.1}$$

and

$$P_{s0} - P_{L0} > \delta P_{pcc}(x_v) \tag{12.2}$$

It is noted that P_s and P_L in the condition ($P_s - P_L > \delta P_{pcc}(x_v)$) of Condition A in Equation (9.9) is added with a subscript "$_0$" in Equation (12.2). This is because, when the PC system was independently studied, P_s and P_L were considered to be input variables, but P_s and P_L are now two state variables in the LSPC system. Combining Equations (12.1) and (12.2) gives

$$P_d > \delta P_{pcc}(x_v)$$

or

$$P_d > \left(P_{pc} - \frac{k_{pc}}{A_{pcs}} x_{pc\,max} \right) \lambda_2 \left(x_{pc\,max} \right) \tag{12.3}$$

where $\lambda_2 \left(x_{pc\,max} \right)$ is determined by Equation (9.6) with $x_{pc} = x_{pcmax}$. It gives

$$\lambda_2 \left(x_{pc\,max} \right) = \frac{A_{pcs} \left(A_{pc}^2 \left(x_{pc\,max} \right) + \eta^2 w_v^2 x_v^2 \right)}{k_{ff} \eta^2 A_{pc} \left(x_{pc\,max} \right) w_v^2 x_v^2 + A_{pc}^2 \left(x_{pc\,max} \right) A_{pcs}} \tag{12.4}$$

which can be approximated as (see Equation (9.7))

$$\lambda_2 \left(x_{pc\,max} \right) = 1 + \frac{\eta^2 w_v^2 x_v^2}{A_{pc}^2 \left(x_{pc\,max} \right)} \tag{12.5}$$

It is necessary to explain that Inequality (12.3) is an essential condition for Condition N. If Inequality (12.3) cannot be satisfied, the LSPC system cannot operate in Condition N. If Inequality (12.3) can be satisfied, it is possible for the LSPC system to operate in Condition N. This must be further determined by (P_s - P_L). As long as (P_s - P_L) lies in the region [δP_{pcc}, P_d], the LSPC system operates in Condition N (reference to Equations (12.1) and (12.2)).

It can be observed that $\lambda_2\left(x_{pc\max}\right)$ depends on the opening of the fixed orifice, x_v. For convenience, the six operating conditions are discussed in two cases:

Case 1: Inequality (12.3) is true and

Case 2: Inequality (12.3) is false.

It can be observed from Equation (12.5) that a critical opening value, x_{vc}, may exist and satisfies $P_d = \left(P_{pc} - \frac{k_{pc}}{A_{pcs}} x_{pc\,max}\right)\left(1+\frac{\eta^2 w_v^2 x_v^2}{A_{pc}^2\left(x_{pc\,max}\right)}\right)\Bigg|_{x_v = x_{vc}}$. When x_v is smaller than x_{vc}, the LSPC system is in Case 1. Beyond this opening value, Inequality (12.3) becomes false and hence the LSPC system is in Case 2. The critical value of the fixed orifice opening, x_{vc}, can be approximated by

$$x_{vc} = \frac{A_{pc}\left(x_{pc\max}\right)}{\eta w_v}\sqrt{\frac{P_d}{P_{pc} - \frac{k_{pc} x_{pc\max}}{A_{pcs}}} - 1} \qquad (12.6)$$

Case 1: (Inequality (12.3) is true)

In addition to Condition N, there are three possibilities: Condition O, P and Q, which are shown in Table 12.1. The operating condition must also be further determined by the load condition.

Table 12.1 Steady State Operating Conditions of the LSPC system (Case 1)

LS / PC / LSPC	Condition I	Condition II	Condition III
Condition A	Condition N	Condition O	Condition P
Condition B	×	××	Condition Q

× & ××: Impossible conditions

Condition N is the normal operating condition. Conditions O, P and Q would occur under "extreme" load conditions. Condition O is associated with the "runaway" load. Conditions P and Q are associated with the situation that the load flow demand is larger than the maximum flow delivery of the pump.

Consider the impossible operating conditions "×" in Table 12.1 (Condition I for the LS system and Condition B for the PC system). According to Equations (3.20) and (9.9), the combination of Condition I for the LS system and Condition B for the PC system implies $P_{s0} - P_{L0} = P_d$ and $P_{s0} - P_{L0} \le \delta P_{pcc}(x_v)$, and consequently $P_d \le \delta P_{pcc}(x_v)$ which contradicts the criterion (Inequality (12.3)). Therefore, the condition with a "×" could not occur.

Consider the second impossible operating condition with a "××" (Condition II for the LS system and Condition B for the PC system). Again, according to Equations (3.20) and (9.8), the combination of Condition II and Condition B implies $P_{s0} - P_{L0} > P_d$ and $P_{s0} - P_{L0} \le \delta P_{pcc}(x_v)$, and consequently $P_d < \delta P_{pcc}(x_v)$ which also contradicts the criterion (Inequality (12.3)). Therefore, this is also an impossible steady state operating condition.

The four different steady state operating conditions in Table 12.1 can be expressed by

$$\begin{cases} (P_{s0} - P_{L0}) = P_d > \delta P_{pcc} & \text{for } x_{r0} = 0 \text{ and } x_{pc0} < x_{pc\,max} \text{ (condition N)} \\ (P_{s0} - P_{L0}) > P_d > \delta P_{pcc} & \text{for } x_{r0} > 0,\ x_{pc0} < x_{pc\,max} \text{ and } P_y = P_s \text{ (condition O)} \\ P_d > (P_{s0} - P_{L0}) > \delta P_{pcc} & \text{for } x_{r0} < 0,\ x_{pc0} < x_{pc\,max} \text{ and } P_y = 0 \text{ (condition P)} \\ P_d > (P_{s0} - P_{L0}) \,\&\, \delta P_{pcc} \ge (P_{s0} - P_{L0}) & \text{for } x_{r0} < 0,\ x_{pc0} = x_{pc\,max} \text{ and } P_y = 0 \text{ (condition Q)} \end{cases} \tag{12.7}$$

Because $\lambda_2\left(x_{pc\,max}\right)$ increases as x_v increases, Inequality (12.3) is always true for all openings, x_v, as long as it is true for the maximum, x_{vmax}, of x_v, (refer to Equation (12.5). Therefore, a generic condition for Case 1 which is applicable for all x_v becomes

$$P_d > \left(P_{pc} - \frac{k_{pc}}{A_{pcs}} x_{pc\max} \right)\left(1 + \frac{\eta^2 w_v^2 x_{v\max}^2}{A_{pc}^2\left(x_{pc\max}\right)} \right) \tag{12.8}$$

Inequality (12.8) is an important criterion of the LSPC system, because it gives the LSPC system the "most chance" (for all x_v) to operate in the normal operating condition (Condition N). It is noted that, in addition to the LS pump parameter, P_d, Inequality (12.8) mainly deals with the parameters of the PC system. It does not relate to the load parameters such as J_m, B_m, D_m, T_{mf}, etc. Therefore, it can be used to select the PC system for the LSPC system.

Case 2: (Inequality (12.3) is false)

Under this Case, four operating conditions could possibly exist and are given in Table 12.2.

Table 12.2 Steady State Operating Conditions of the LSPC system (Case 2)

LS / PC / LSPC	Condition I	Condition II	Condition III
Condition A	×	Condition O	××
Condition B	Condition R	Condition S	Condition Q

× & ××: Impossible conditions

The steady state operating condition for Case 2 can be expressed by

$$\begin{cases} (P_{s0} - P_{L0}) = P_d \le \delta P_{pcc} & \text{for } x_{r0} = 0 \text{ and } x_{pc0} = x_{pc\,max} \text{ (Condition R)} \\ (P_{s0} - P_{L0}) > P_d \;\&\; (P_{s0} - P_{L0}) > \delta P_{pcc} & \text{for } x_{r0} > 0,\ x_{pc0} < x_{pc\,max} \text{ and } P_y = P_s \text{ (Condition O)} \\ P_d < (P_{s0} - P_{L0}) < \delta P_{pcc} & \text{for } x_{r0} > 0,\ x_{pc0} = x_{pc\,max} \text{ and } P_y = P_s \text{ (Condition S)} \\ P_d > (P_{s0} - P_{L0}) \;\&\; \delta P_{pcc} \ge (P_{s0} - P_{L0}) & \text{for } x_{r0} < 0,\ x_{pc0} = x_{pc\,max} \text{ and } P_y = 0 \text{ (Condition Q)} \end{cases} \quad (12.9)$$

Similar to Case 1, it can be verified that Condition P does not exist in Case 2.

An approximate criterion can also be found for Case 2. According to Equation (12.4), when the opening of the fixed orifice is zero, λ_2 (x_{pcmax}) is equal to 1. δP_{pcc} (Equation (9.8)) is very close to P_{pc}, because x_{pc} is very small at $x_v = 0$ (reference to Figures 10.6 through Figure 10.9). Therefore, Inequality (12.3) is false at $x_v = 0$ implies that

$$P_d < P_{pc} \quad (12.10)$$

If Inequality (12.10) is true, Inequality (12.3) would always be false for all values of x_v. Therefore, P_d and P_{pc} must be such selected such that Inequality (12.10) is always false.

In summary, Case 1 is preferred because it is possible for the LSPC system to operate in Condition N. Case 2 is an unexpected case for the LSPC system and the design parameters should be selected such that Case 2 would not occur.

It is now necessary to consider the non-linear equations used to solve for the operating point under the six operating conditions.

12.3 Solving for the Steady State Operating Point

In this section, the solutions of the steady state equations set with six conditions are discussed separately. For each condition, the general solution of the operating point is developed which is associated with x_{r0}, x_{pc0}, θ_{sp0}, P_{s0}, P_{L0}, P_{y0}.

12.3.1 Steady State Operating Point at Condition N

Because the pressure drop across the PC system, ($P_{s0} - P_{L0}$), is constant (P_d) (though P_{s0} or P_{L0} can be variable under Condition N), the SSOP of the LSPC system at Condition N can be independently calculated by the equations sets presented in Chapters 3 and 9 (with some minor modifications). First, x_{pc0} is calculated by (refer to Equation (9.5))

$$P_d = \left(P_{pc} - \frac{k_{pc}}{A_{pcs}} x_{pc} \right) \lambda_2 \left(x_{pc} \right) \tag{12.11}$$

where $\lambda_2 \left(x_{pc} \right) = \dfrac{A_{pcs} \left(A_{pc}^2 \left(x_{pc} \right) + \eta^2 w_v^2 x_v^2 \right)}{k_{ff} \eta^2 A_{pc} \left(x_{pc} \right) w_v^2 x_v^2 + A_{pc}^2 \left(x_{pc} \right) A_{pcs}}$ (12.12)

Equation (12.11) is a non-linear algebraic equation which must be solved by the iterative method presented in Figure 9.2.

In order to determine the load pressure, P_{L0}, with x_{pc0} generated from Equation (12.11), it is necessary to modify Equation (3.24). It can be observed from Equation (3.24) that the term, $C_d w x \sqrt{\dfrac{2P_d}{\rho}}$, represents the flow rate through a simple orifice. In the LSPC system, this term must be replaced by the flow rate through the PC valve which was presented in Equation (9.2). Consequently,

$$P_{L0} = \frac{1}{\left(c_{ml} + \dfrac{D_m^2}{B_m} \right)} \left[\frac{C_{dv} w_v x_v A_{pc} \left(x_{pc0} \right)}{\sqrt{A_{pc}^2 \left(x_{pc0} \right) + \eta^2 w_v^2 x_v^2}} \sqrt{\frac{2}{\rho} P_d} + \frac{D_m T_{mf}}{B_m} \right] \tag{12.13}$$

The pump pressure, P_{s0}, can be directly obtained by

$$P_{s0} = P_d + P_{L0} \tag{12.14}$$

To find the swash plate angle θ_{sp0}, the term, $C_d w x \sqrt{\frac{2P_d}{\rho}}$, in Equation (3.26) is replaced by Equation (9.2) to yield

$$\theta_{sp0} = tan^{-1}\left[\frac{\pi}{NA_p R_p \omega}\left(\frac{C_{dv} w_v x_v A_{pc}\left(x_{pc0}\right)}{\sqrt{A_{pc}^2\left(x_{pc0}\right)+\eta^2 w_v^2 x_v^2}}\sqrt{\frac{2}{\rho}P_d} + c_{pl}P_{s0}\right)\right] \tag{12.15}$$

Thus, the control pressure P_{y0}, is determined by Equation (3.27). For completeness, it is repeated here

$$P_{y0} = T_{sp}^{'} + K_{pr2}^{'}P_{s0} - \left(K_{sp}^{'} + K_{pr3}^{'}P_{s0}\right)\theta_{sp0} \tag{12.16}$$

12.3.2 Solution of the Steady State Equations Set with Condition O

Because the pressure drop across the PC system, ($P_{s0} - P_{L0}$), is not constant under Condition O, the SSOP of the LSPC system cannot be independently calculated by the equation sets presented in Chapter 3 and Chapter 9. The SSOP; x_{r0}, x_{pc0}, θ_{sp0}, P_{s0}, P_{L0}, P_{y0} has to be computed by solving a large non-linear equations set. In order to simplify the calculation, it is essential to manipulate some equations in Chapters 3 and 9 to reduce the number of the non-linear equations set.

Substituting Equation (9.5) into Equation (9.2) gives

$$Q_L\left(x_{pc}\right) = \frac{C_{dv}A_v\sqrt{A_{pcs}A_{pc}\left(x_{pc}\right)}}{\sqrt{k_{ff}\eta^2 A_v^2 + A_{pcs}A_{pc}\left(x_{pc}\right)}}\sqrt{\frac{2}{\rho}\left(P_{pc} - \frac{k_{pc}}{A_{pcs}}x_{pc}\right)} \tag{12.17}$$

Substituting Equation (12.17) into Equation (3.23) and then re-organizing the equation results in

$$P_L\left(x_{pc}\right) = \frac{1}{\left(c_{ml} + \frac{D_m^2}{B_m}\right)}\left[\frac{C_{dv}A_v\sqrt{A_{pcs}A_{pc}\left(x_{pc}\right)}}{\sqrt{k_{ff}\eta^2 A_v^2 + A_{pcs}A_{pc}\left(x_{pc}\right)}}\sqrt{\frac{2}{\rho}\left(P_{pc} - \frac{k_{pc}}{A_{pcs}}x_{pc}\right)} + \frac{D_m T_{mf}}{B_m}\right] \tag{12.18}$$

It is noted that the load pressure, P_L, and the displacement, x_{pc}, in Equation (12.18) are not labeled with the subscript 'o' because at this point x_{pc} is not known. Indeed, all subsequent equations will not bear the 'o' subscript until the x_{pc} can be solved.

Substituting Equation (12.18) into Equation (9.5) gives

$$P_s\left(x_{pc}\right)=\frac{1}{\left(c_{ml}+\frac{D_m^2}{B_m}\right)}\left[\frac{C_{dv}A_v\sqrt{A_{pcs}A_{pc}\left(x_{pc}\right)}}{\sqrt{k_{ff}\eta^2A_v^2+A_{pcs}A_{pc}\left(x_{pc}\right)}}\sqrt{\frac{2}{\rho}\left(P_{pc}-\frac{k_{pc}}{A_{pcs}}x_{pc}\right)}+\frac{D_mT_{mf}}{B_m}\right] \tag{12.19}$$
$$+\left(P_{pc}-\frac{k_{pc}}{A_{pcs}}x_{pc}\right)\frac{A_{pcs}\left(A_{pc}^2\left(x_{pc}\right)+\eta^2A_v^2\right)}{k_{ff}\eta^2A_{pc}\left(x_{pc}\right)A_v^2+A_{pc}^2\left(x_{pc}\right)A_{pcs}}$$

Equation (3.32) is repeated but P_s is now a variable dependent on x_{pc}.

$$\theta_{sp}\left(x_{pc}\right)=\frac{T_{sp}^{'}+\left(K_{pr2}^{'}-1\right)P_s\left(x_{pc}\right)}{K_{sp}^{'}+K_{pr3}^{'}P_s\left(x_{pc}\right)} \qquad 0\le\theta_{sp}\le\theta_{sp\max} \text{ and } P_y=P_s \tag{12.20}$$

Replacing the flow term, $C_d w x\sqrt{\frac{2}{\rho}\left(P_s-P_L\right)}$, in Equation (3.31) with Equation (12.17) and substituting Equations (12.20) into Equation (3.31) result in a non-linear algebraic equation of the displacement, x_{pc}, as

$$\frac{NA_pR_p\omega\tan\left(\frac{T_{sp}^{'}+\left(K_{pr2}^{'}-1\right)P_s\left(x_{pc}\right)}{K_{sp}^{'}+K_{pr3}^{'}P_s\left(x_{pc}\right)}\right)}{\pi}= \tag{12.21}$$
$$\frac{C_{dv}A_v\sqrt{A_{pcs}A_{pc}\left(x_{pc}\right)}}{\sqrt{k_{ff}\eta^2A_v^2+A_{pc}\left(x_{pc}\right)A_{pcs}}}\sqrt{\frac{2}{\rho}\left(P_{pc}-\frac{k_{pc}}{A_{pcs}}x_{pc}\right)}+c_{pl}P_s\left(x_{pc}\right)$$

where the function $P_s\left(x_{pc}\right)$ is given in Equation (12.19). For a given P_{pc}, the numeric solution of Equation (12.21), x_{pc0}, can be used to determine other variables, P_{L0}, P_{s0} (which is also equals to P_{y0}), and θ_{sp0} by Equations (12.18), (12.19) and (12.20).

It can be noted that the above derivation of the non-linear Equation (12.21) does not contain the variable x_r. In general, the actual value of the variable x_{r0} is usually not of concern since it is the pressure equality, $P_{s0} = P_{y0}$, that is important for condition O. However, x_{r0} can be determined by Equation (3.1) if required. Since x_{pc0} is now known, substituting Equation (9.5) into (3.1) gives the displacement of the LS regulator spool under steady state condition as

$$x_{r0} = \frac{A_r}{k_r}\left(\left(P_{pc} - \frac{k_{pc}}{A_{pcs}}x_{pc0}\right)\frac{A_{pcs}\left(A_{pc}^2\left(x_{pc0}\right)+\eta^2 A_v^2\right)}{k_{ff}\eta^2 A_{pc}\left(x_{pc0}\right)A_v^2 + A_{pc}^2\left(x_{pc0}\right)A_{pcs}} - P_d\right) \qquad (12.22)$$

12.3.3 Solution of the Steady State Equations Set with Condition P

Under Condition P of the LSPC system, the pump is in the fully "stroke" position but the PC system is in the normal operating condition. In order to solve for the SSOP in this condition, consider Equation (9.3).

The first term of Equation (9.3) includes the pressure drop across the adjustable or fixed orifice, ($P_s - P_m$). It can be alternately expressed as $\frac{\rho}{2}\left(\frac{Q_L}{C_{dv}A_v}\right)^2$. The third term of Equation (9.3) represents the steady state flow force. For convenience, the equation can be expressed in a form consistent with the model of the steady state flow force, F_{ff}, derived by Merrit [1967]. k_{ff} can be eliminated by rewriting the flow force as:

$F_{ff} = \frac{\cos 69^o \rho Q^2}{C_c A_{pc}\left(x_{pc}\right)}$. The contraction coefficient, C_c, equals to 0.611 [Merritt, 1967, p42]. Consequently, Equation (9.3) with the pump fully stroked becomes

$$A_{pcs}\left(P_{pc} - \frac{\rho}{2}\left(\frac{Q_{p\max}}{C_{dv}A_v}\right)^2\right) - k_{pc}x_{pc} - \frac{\rho\cos 69^0 Q_{p\max}^2}{C_c A_{pc}\left(x_{pc}\right)} = 0 \qquad (12.23)$$

If the hydrostat orifice can be approximated by an equivalent rectangular orifice with the width, w_{pc}, Equation (12.23) can be directly solved to give x_{pc0} as,

$$x_{pc0} = \frac{c_1 + \sqrt{c_1^2 - 4k_{pc}c_2}}{2k_{pc}} \tag{12.24}$$

where $c_1 = A_{pcs}\left(P_{pc} - \frac{\rho}{2}\left(\frac{Q_{p\max}}{C_{dv}A_v}\right)^2\right)$ and $c_2 = \frac{\rho\cos 69^0 Q_{p\max}^2}{C_c w_{pc}}$.

It is noted that the solution, x_{pc0}, of Equation (12.24) must be smaller than x_{pcmax}, otherwise, the LSPC system would operate in Condition Q.

12.3.4 Solution of the Steady State Equations Set with Condition Q

If the hydrostat orifice is fully opened and the pump fully stroked, the LSPC system operates under Condition Q. In this case, the cascade of two fixed orifices plays the part of a fixed orifice in the LS system with the pump fully stroked.

It can be observed from Equation (9.2) that the PC system can be regarded as an equivalent orifice whose area equals to the product of a factor, $\frac{A_{pc}(x_{pc})}{\sqrt{A_{pc}^2(x_{pc}) + \eta^2 A_v^2}}$, and the area, A_v, of the adjustable orifice. Therefore, the SSOP can be calculated by replacing A_v in Equation (3.35) with the equivalent orifice area, that is,

$$P_{s0} = P_{L0} + \frac{\rho}{2}\left(\frac{NA_pR_p\omega\tan\theta_{sp\,max}\sqrt{A_{pc}^2(x_{pc\,max}) + \eta^2 w_v^2 x_v^2}}{\pi C_{dv} w_v x_v A_{pc}(x_{pc\,max})}\right)^2 \tag{12.25}$$

where P_{L0} is determined by Equation (3.34) which is repeated here for convenience.

$$P_{L0} = \frac{1}{\left(c_{ml} + \frac{D_m^2}{B_m}\right)}\left[\frac{NA_pR_p\omega\tan\theta_{sp\max}}{\pi} + \frac{D_mT_{mf}}{B_m}\right] \tag{12.26}$$

It should be noted that x_{pc0} is known to be x_{pcmax} under Condition Q.

12.3.5 Solution of the Steady State Equations Set with Condition R

Condition R is an operating condition which the LS system operates in normal condition but the PC system is in the condition under which the hydrostat orifice is fully open (i.e. the spool reaches the end). The LSPC system now operates in the LS mode with an equivalent orifice of two fixed cascade orifices. The method of solving for the operating point is the same as that for Condition N, but it is unnecessary to calculate x_{pc0} using Equation (12.11) due to $x_{pc0} = x_{pcmax}$.

12.3.6 Solution of the Steady State Equations Set with Condition S

Similar to Conditions Q and R, Condition S also represents the LS mode. The model of the operating point can be obtained by modifying the orifice area, *wx*, in Equations (3.31) and (3.33) with the equivalent area of two cascade orifices (Equation (9.2)). The modified model equations are:

$$\frac{NA_p R_p \omega \tan(\theta_{sp})}{\pi} = \frac{C_{dv} w_v x_v A_{pc}(x_{pc\max})}{\sqrt{A_{pc}^2(x_{pc\max}) + \eta^2 w_v^2 x_v^2}} \sqrt{\frac{2}{\rho}(P_s - P_L)} - c_{pl} P_s \qquad (12.27)$$

$$\theta_{sp}(P_s) = \frac{T_{sp}^{'} + (K_{pr2}^{'} - 1)P_s}{K_{sp}^{'} + K_{pr3}^{'} P_s} \qquad 0 \le \theta_{sp} \le \theta_{sp\max} \text{ and } P_y = P_s \qquad (12.28)$$

$$P_L = \frac{-b_2 + \sqrt{b_2^2 - 4b_1 b_3}}{2b_1} \qquad (12.29)$$

where $b_1 = a_1^2$, $b_2 = a_3 - 2a_1 a_2$, and $b_3 = a_2^2 - a_3 P_s$. The coefficients, a_1, a_2, and a_3, can be further expressed as $a_1 = c_{ml} + \frac{D_m^2}{B_m}$, $a_2 = \frac{D_m T_{mf}}{B_m}$, and $a_3 = \frac{2}{\rho} \frac{C_{dv}^2 w_v^2 x_v^2 A_{pc}^2(x_{pc\max})}{A_{pc}^2(x_{pc\max}) + \eta^2 w_v^2 x_v^2}$.

12.4 Procedure of Solving for the Steady State Operating Point

Figure 12.2 shows the flow chart of solving for the SSOP of the LSPC system. First of all, the critical opening of the fixed orifice, x_{vc}, is calculated using Equation (12.6). If the opening setting, x_v, of the fixed orifice is less than x_{vc}, the LSPC system is in Case 1. Therefore, the LSPC system may operate in Condition N, O, P or Q. In order to justify which of the Conditions N, O, P and Q exist, it is necessary to initially assume that the LSPC system operates in its normal condition. Therefore, Equation (12.11) is used to iteratively calculate x_{pc0} and then values of other variables, P_{L0}, P_{s0}, P_{y0} and θ_{sp0}, are computed using Equations (12.13), (12.14), (12.15) and (12.16). At this point, Condition N must be validated. If the swash plate angle is less than the maximum ($\theta_{sp0} < \theta_{sp\,max}$) and the control pressure is less than the pump pressure ($P_{y0} < P_{s0}$), the LSPC system does operate in Condition N. Otherwise, the LSPC system must operate in one of the other three conditions. If $\theta_{sp0} < \theta_{sp\,max}$ and $P_{y0} > P_{s0}$, then an impossible condition exists. In this situation, the LSPC system might in fact be operating in Condition O. If $\theta_{sp0} > \theta_{sp\,max}$ is calculated, then this situation is also impossible. This condition indicates that the pump is fully stroked, that is, Condition P or Q (which depends on whether the PC valve is fully opened (Condition Q), or not (Condition P)). Similarly, the operating condition must be validated based on Equation (12.7).

It is noted that the dashed line box in Figure 12.2 indicates that some iterative computation is required. For Case 2, the procedure for justifying the validation of operating condition and calculating the SSOP is similar to Case 1 and hence it is not explained here.

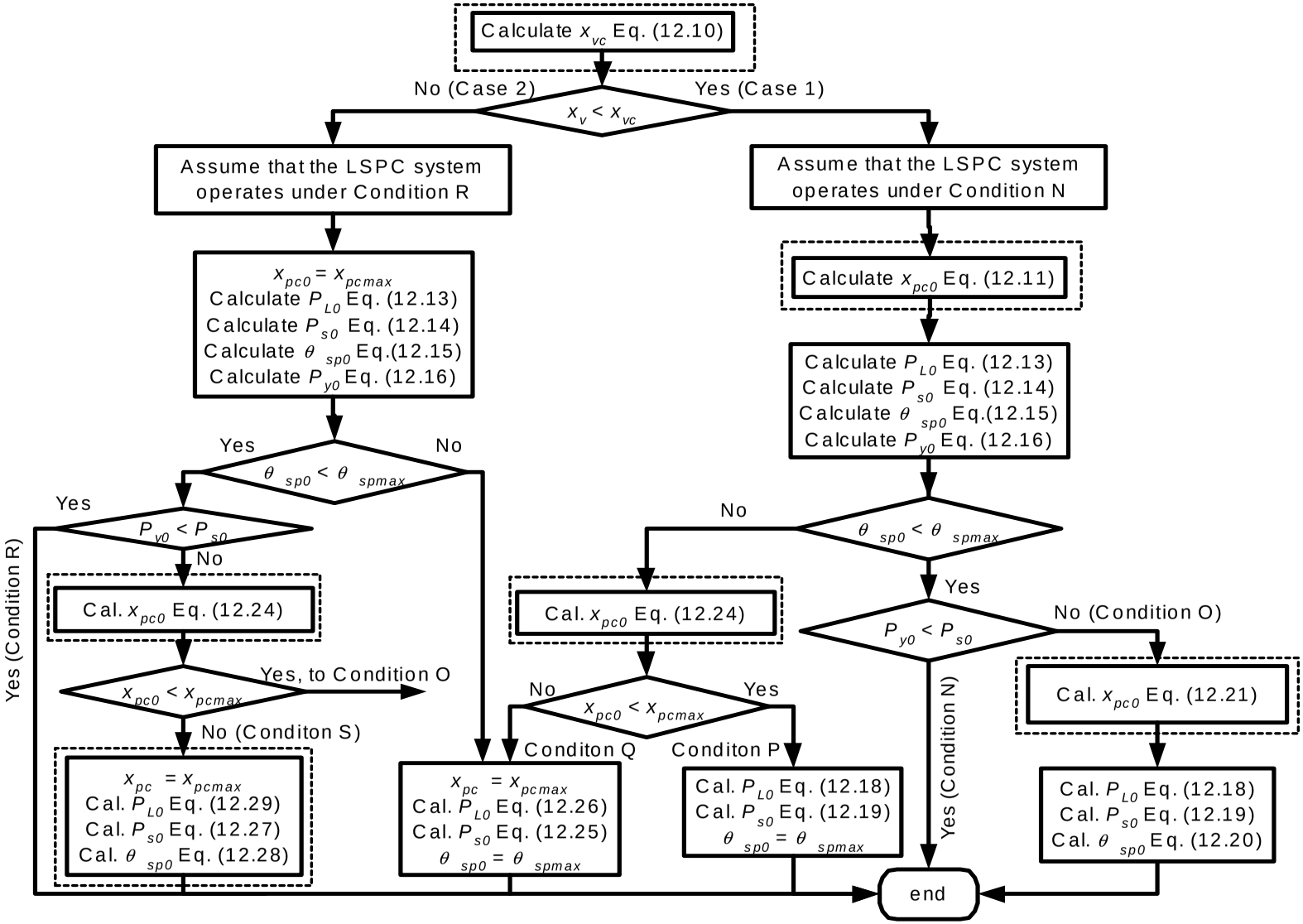

Figure 12.2 Flow Chart of Solving for the SSOP of the LSPC System

12.5 Summary

This Chapter has investigated all possible steady state operating conditions of the LSPC system. Theoretically, there are six different operating conditions which are all combination of the conditions of the LS system and the PC system. They are defined as Conditions N, O, …S. Condition N is the normal operating condition under which the LS system and the PC system normally operate.

The operating conditions can be classified into two groups: Case1 and Case 2. Case 1 reflects all combinations (N, O, P and Q) of the LS system and PC system operating conditions in which Inequality (12.3) is true. Case 2 represents all combinations (O, R, S and Q) of the LS system and PC system operating conditions in which Inequality (12.3) is false. When the adjustable orifice opening, x_v, is smaller than x_{vc} determined by Inequality (12.6), the LSPC system operates in Case 1. The load condition can be further used to determine which of Conditions N, O, P and Q the LSPC system is operating in.

For any adjustable orifice opening, the LSPC system is expected to operate in Case 1, because the normal operating Condition N is in Case 1. In other word, Inequality (12.8) is required to be true.

It is very important that the system be designed to avoid Inequality (12.10), a condition in which the PC system could not normally operate.

Based on the results of Chapters 3 and 9, this chapter has developed the models of the SSOP's of the LSPC system for all six operating conditions and presented a flow chart which can be used to validate the operating condition and to solve for the SSOP. These results are essential for the dynamic analysis of the LSPC system presented in the following chapter.

Chapter 13 Dynamic Model of the Load Sensing and Pressure Compensated System

13.1 Introduction

The objective of this chapter is to develop the TF of the LSPC system for each operating condition (N, O, P, Q, R and S) and to present the procedure of calculating the stability of the LSPC system. The TF of the LSPC system can be given by assembling the TF of the LS system (Chapter 5) and the TF of the PC system (Chapter 9). The block diagram of the LSPC system shown in Figure 13.1 is similar to that of the LS system presented by Figure 5.10 but the blocks, K_q and K_c, in Figure 5.10 are replaced with the transfer functions, $G_{xv}(s)$ and $G_{psL}(s)$, of the PC system respectively. The comprehensive TF can be developed and programmed based on the block diagram shown in Figure 13.1 via Mason flow formula [Ogata, 1970]. The actual development of the transfer functions using Mason's flow formula is not presented here. This Chapter considers only the simplified TF's of the LSPC system which can be used to calculate the frequency response in order to compare the results to the LS system without the PC valve.

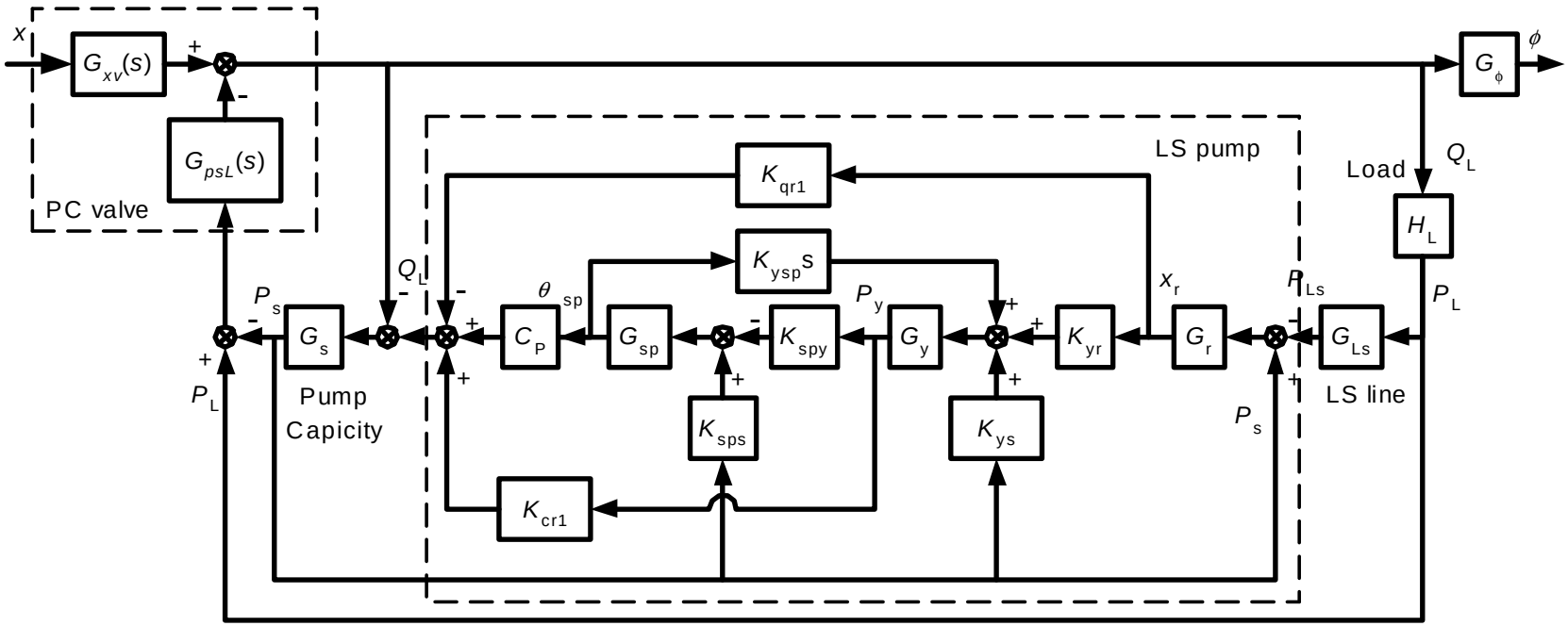

Figure 13.1 Complete Block Diagram of the LSPC System

13.2 Transfer Function of the Load Sensing and Pressure Compensated System

The objective of this section is to develop the simplified TF for Conditions N, O, P, and Q. The simplified TF's of the PC system, Equations (11.51) and (11.52), are used to replace K_q and K_c in Equations (5.81), (5.85) and (5.87) respectively.

- **Condition N (normal operating condition)**

Based on Equation (5.81), the simplified TF of the LSPC system at Condition N is

$$F(s)=\frac{K_q\left(1+G_pG_sH_p\right)G_\phi}{1+K_cH_L+K_cG_s+G_pG_sH_p+K_cH_LG_pG_s\left(H_p-G_{Ls}\right)}$$

$$=\frac{K_{xv}^*\left(1+\dfrac{K_pK_sH_p\left(\dfrac{s}{\omega_{p0}}+1\right)}{\left(\dfrac{s}{\omega_{ysp}}+1\right)\left(\dfrac{s}{\omega_s}+1\right)}\right)\dfrac{K_\phi}{\left(\dfrac{s^2}{\omega_L^2}+\dfrac{2\zeta_Ls}{\omega_L}+1\right)}}{1+\dfrac{K_{psL}^*K_L\left(\dfrac{s}{\omega_{L0}}+1\right)\left(\dfrac{s}{\omega_{pd0}}+1\right)}{\left(\dfrac{s^2}{\omega_L^2}+\dfrac{2\zeta_Ls}{\omega_L}+1\right)}+\dfrac{K_sK_{psL}^*\left(\dfrac{s}{\omega_{pd0}}+1\right)}{\left(\dfrac{s}{\omega_s}+1\right)}+\dfrac{K_pK_sH_p\left(\dfrac{s}{\omega_{p0}}+1\right)}{\left(\dfrac{s}{\omega_{ysp}}+1\right)\left(\dfrac{s}{\omega_s}+1\right)}+\dfrac{K_pK_sK_{psL}^*K_L\left(H_p-1\right)\left(\dfrac{s}{\omega_{Lp0}}+1\right)\left(\dfrac{s}{\omega_{L0}}+1\right)\left(\dfrac{s}{\omega_{p0}}+1\right)\left(\dfrac{s}{\omega_{pd0}}+1\right)}{\left(\dfrac{s}{\omega_{ysp}}+1\right)\left(\dfrac{s^2}{\omega_L^2}+\dfrac{2\zeta_Ls}{\omega_L}+1\right)\left(\dfrac{s}{\omega_s}+1\right)\left(\dfrac{s}{\omega_{Ls}}+1\right)}}$$

(13.1)

Equation (13.1) can be expressed as a 5th order TF of the form

$$F(s)=K\frac{b_3s^3+b_2s^2+b_1s+b_0}{a_5s^5+a_4s^4+a_3s^3+a_2s^2+a_1s+a_0} \tag{13.2}$$

The coefficients can be determined as presented in Appendix L.

- **Condition O**

Based on Equation (5.85), the simplified TF of the LSPC system at Condition O is

$$F(s)=\frac{K_q(1+G_sH_p)G_\phi}{1+K_cH_L+K_cG_s+G_sH_p+K_cH_LG_sH_p} \tag{13.3}$$
$$=\frac{K_{xv}^*\left(1+\frac{K_p^*K_s}{\left(\frac{s^2}{\omega_{sp}^2}+\frac{2\zeta_{sp}s}{\omega_{sp}}+1\right)\left(\frac{s}{\omega_s}+1\right)}\right)\frac{K_\phi}{\left(\frac{s^2}{\omega_L^2}+\frac{2\zeta_Ls}{\omega_L}+1\right)}}{1+\frac{K_{psL}^*K_L\left(\frac{s}{\omega_{L0}}+1\right)\left(\frac{s}{\omega_{pc0}}+1\right)}{\left(\frac{s^2}{\omega_L^2}+\frac{2\zeta_Ls}{\omega_L}+1\right)}+\frac{K_sK_{psL}^*\left(\frac{s}{\omega_{pc0}}+1\right)}{\left(\frac{s}{\omega_s}+1\right)}+\frac{K_p^*K_s}{\left(\frac{s^2}{\omega_{sp}^2}+\frac{2\zeta_{sp}s}{\omega_{sp}}+1\right)\left(\frac{s}{\omega_s}+1\right)}+\frac{K_p^*K_sK_{psL}^*K_L\left(\frac{s}{\omega_{L0}}+1\right)\left(\frac{s}{\omega_{pc0}}+1\right)}{\left(\frac{s^2}{\omega_{sp}^2}+\frac{2\zeta_{sp}s}{\omega_{sp}}+1\right)\left(\frac{s^2}{\omega_L^2}+\frac{2\zeta_Ls}{\omega_L}+1\right)\left(\frac{s}{\omega_s}+1\right)}}$$

Equation (13.3) can also be expressed as a 5th order TF as

$$F(s)=K\frac{b_3s^3+b_2s^2+b_1s+b_0}{a_5s^5+a_4s^4+a_3s^3+a_2s^2+a_1s+a_0} \tag{13.4}$$

The coefficients are presented in Appendix M.

- **Condition P**

Based on Equation (5.87), the simplified TF of the LSPC system at Condition P is

$$F(s)=\frac{K_{xv}^*\left(\frac{K_\phi}{\frac{s^2}{\omega_L^2}+\frac{2\zeta_Ls}{\omega_L}+1}\right)}{1+\frac{K_{psL}^*K_L\left(\frac{s}{\omega_{L0}}+1\right)\left(\frac{s}{\omega_{pc0}}+1\right)}{\frac{s^2}{\omega_L^2}+\frac{2\zeta_Ls}{\omega_L}+1}+\frac{K_sK_{psL}^*\left(\frac{s}{\omega_{pc0}}+1\right)}{\frac{s}{\omega_s}+1}} \tag{13.5}$$

Equation (13.5) can be expressed as a 3rd order TF as

$$F(s)=K\frac{b_1s+b_0}{a_3s^3+a_2s^2+a_1s+a_0} \tag{13.6}$$

The coefficients are presented in Appendix N.

- **Condition Q, R and S**

Under Conditions Q, R or S, the hydrostat orifice of the PC system is fully opened. The PC system, in effect, becomes two fixed orifices that are cascaded in series. The LSPC system actually operates in the LS mode. The TF of the system has the same expressions as Equations (5.81), (5.85) and (5.87) but the coefficients, K_q and K_c, in these equations have different meanings. K_q and K_c become the "equivalent flow-gain" and "equivalent flow-pressure coefficient" of two cascaded orifices which are independent of the frequency. They were defined as K_q^* and K_c^* in Chapter 11 and were determined by Equations (11.40) and (11.41).

13.3 Procedure to Calculate the Stability for the Load Sensing and Pressure Compensated System

The procedure for determining the LSPC system stability is similar to that presented in Table 5.2 of Chapter 5, but the parameters associated with the PC system at each step have to be evaluated. For purpose of comparison, Table 13.1 gives the counterpart of Table 5.2 for the LSPC system. The parameters printed in **bold** font are different from those in Table 5.2. It must be acknowledged that $\boldsymbol{A_v}$ in the LSPC system represents either the fixed or adjustable orifice flow area.

Table 13.1 is valid for only operating Conditions N, O and P. When the LSPC system operates in Condition Q, R or S, the procedure to evaluate the stability is the same as shown in Table 5.2 but K_q and K_c are replaced with K_q^* and K_c^* which are determined from Equations (11.40) and (11.41).

Table 13.1 Procedure for Conducting a Stability Analysis for the LSPC System

Calculation steps	Parameters
Input parameters	P_d V_p $\boldsymbol{A_v}$ V_m J_m B_m T_{mf} ω_{Ls}
⇩	
Operating point	P_{s0} P_{y0} P_{L0} x_{r0} $\boldsymbol{x_{pc0}}$ $\boldsymbol{P_{m0}}$ (Figure 12.2)
⇩	
linearization parameters	K_{qr1} K_{qr2} K_{c1} K_{c2} $\boldsymbol{\tilde{K}_{xv}}$ $\boldsymbol{\tilde{K}_{psL}}$ (Eqs.5.25 through 5.28, Eqs.12.52 and 12.53**)
⇩	
Coefficients of subsystem TFs	K_p K_p^* K_s K_L ω_s ω_L ω_{sp} ω_r ω_y ω_{ysp} ω_{L0} ω_{p0} ζ_L ζ_r ζ_{sp} $\boldsymbol{\omega_{pc0}}$
⇩	
Coefficients of closed loop TF	a_i b_i (Appendix K, L, and M)
⇩	
Poles and zeros of loop TF	$\sigma_{pi} + j\omega_{pi}$ (i = 1, 2, …9) and $\sigma_{zi} + j\omega_{zi}$ (i = 1, 2, …7) (Matlab programming)

** —— The flow rate, Q_L, through the adjustable orifice usually is turbulent. Therefore, it is unnecessary to use the more accurate flow rate model shown in Appendix D

13.4 Summary

This chapter has presented the block diagram of the LSPC system. In order to obtain the transfer function for the LSPC system, $G_{xv}(s)$ replaces K_q in the TF's for the LS system and $G_{psL}(s)$ replaces K_c. The coefficients, b_i, in the numerators of Equations (13.1), (13.3) and (13.5) are the same as those in Equations (5.81), (5.85) and (5.87). However, the coefficients, a_i and K, of the TF's for the LSPC system are different from those for the LS system. The different coefficients, a_i, in the denominator of their TF's would result in different dynamic performance compared to the LS system (which will be investigated in Chapter 14). This chapter also provides the procedure used to do the dynamic analysis of the LSPC system at an operating point.

Chapter 14 Stability Analysis of the Load Sensing and Pressure Compensated System

14.1 Introduction

The purpose of this chapter is to illustrate the stability of the LSPC system by tracing the root locus as the steady state operating points (SSOP) move along the special trajectories. The requirements of the designed PC valve are established which will result in the overall stabilization of the LSPC system. The approach to do this is based on carrying out a comparison of the root locus of the LSPC system with different parameters for the PC valve.

The dynamic performance of the LSPC system is also compared to that of the LS system by itself. It must be noted that the comparison is valid only if the same SSOP trajectory exists for both systems. Therefore, it is necessary to first explain the SSOP trajectory of the LSPC system and the LS system.

14.2 Trajectory of Steady State Operating Points

Assume that all parameters associated with the SSOP of the LS system in Figure 5.1 are the same as those of the LSPC system in Figure 12.1. The SSOP trajectories of the LS system (Figure 7.1 P_y vs P_s) as the result of varying x of the adjustable orifice (1) in Figure 5.1 should be same for the LSPC system as the result of varying x_v of the adjustable orifice (4) in Figure 12.1. However, for same opening, $x = x_v$, the actual SSOP "location" is a different point on the trajectory due to the different orifice width and the different pressure drop across adjustable orifice. The actual values of the openings, x and x_v, are unimportant, but it is important that the operating points on the SSOP (P_{y0} vs P_{s0}) trajectory must be the same. This is because the load flow rates, Q_{L0} or Q_{Lpc0}, and the load

pressure, P_{L0}, would be the same at same operating point for the LS system and LSPC system. Thus, the system's dynamics can be compared. It should be noted that the trajectory of the LSPC system, which is defined by the parameters, P_{s0}, P_{y0} and θ_{sp0}, of the LS pump, is the same as that of the LS system and hence, is not illustrated here.

It is necessary to illustrate the "trajectory" of the SSOP, x_{pc0} and P_{m0}, of the PC valve on Trajectory I (as presented in Figure 7.2). Figure 14.1 shows the plots of x_{pc0}, (P_{m0} - P_{L0}) and (P_{s0} - P_{L0}) as a function of the opening of the adjustable orifice, x_v. As the adjustable orifice opening, x_v, increases, the LSPC system operates in Condition N (See Figure 14.1). In this region, the pressure drop, $P_{s0} - P_{L0}$, is numerically equal to P_d (1.5 MPa); the pressure drop, $P_{m0} - P_{L0}$, increases slightly and the hydrostat orifice opening, x_{pc0}, is approximately proportional to adjustable orifice opening, x_v (Figure 14.1). At point x_{12}, in Figure 7.2, the pump is fully stroked; the LSPC system enters the region of Condition P where the pump is fully stroked but the PC valve has not fully opened. Because the pressure drop across the PC valve can no longer be controlled to 1.5 MPa as point x_{12} increases, $P_{s0} - P_{L0}$ rapidly decreases and hence, the hydrostat orifice increases to its maximum value, x_{pcmax}. At this point the pressure drop across the PC valve converges to a critical value, δP_{pcc}, (reference to Equation (12.2) and Figure 14.1). In this example, δP_{pcc} = 0.3 MPa at x_v = 1.75. Beyond this point, the LS pump is fully stroked and the PC valve is fully opened. Therefore, the region associated with Condition P in the LSPC system is very limited.

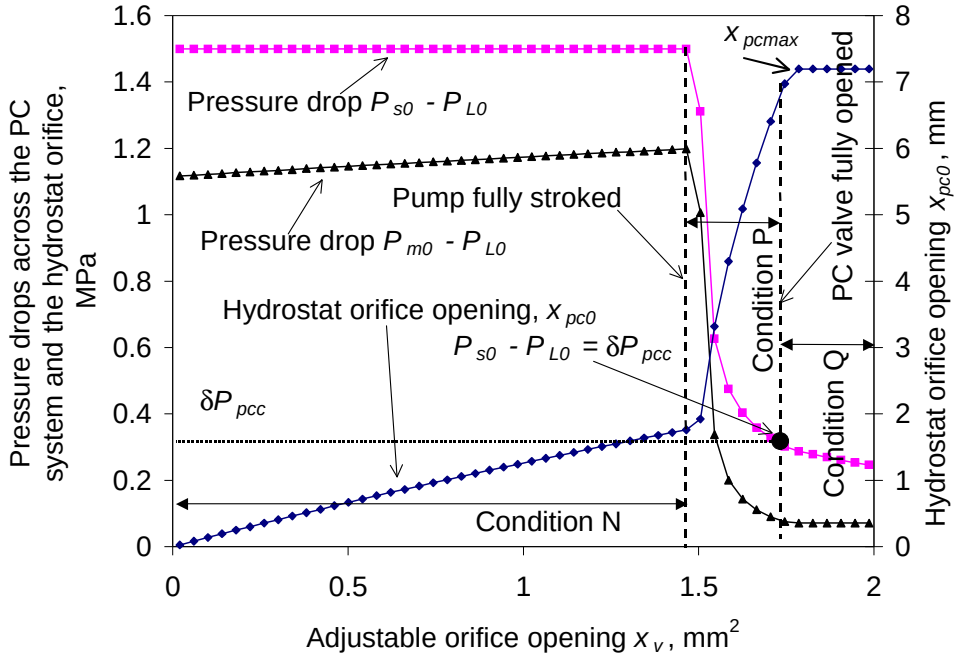

Figure 14.1 Hydrostat Orifice Opening and Pressure Drops Across the PC Valve and the Hydrostat Orifice on Trajectory I as a Function of the Control Orifice Opening

Figure 14.2 shows the hydrostat orifice opening, x_{pc0}, the pressure drop across the hydrostat orifice, $P_{m0} - P_{L0}$, and the pressure drop across the PC valve, $P_{s0} - P_{L0}$, (defined as Trajectory II in Figure 7.5) as a function of x_v. From Figure 7.5, it is noted that a "runaway" load with a negative torque of 6.94 Nm is applied to the rotary shaft. As the adjustable orifice opening is small, the LS pump operates in Condition II where $P_{s0} - P_{L0} > P_d$. Because $P_d > \delta P_{pcc}$ (P_d = 1.5 MPa and δP_{pcc} = 0.38 ~ 0.3 MPa at x_v = 0 ~ 0.3 mm), the PC valve operates in Condition A. Consequently, the LSPC system is in Condition O. At point x_{23} in Figures 7.5 and 14.2, the LSPC system enters the region of Condition N. Similar to Trajectory I, as the adjustable orifice opening, x_v, increases, the LSPC system passes from Condition N to Q via a short region of x_v in which Condition P exists (see Figure 14.2).

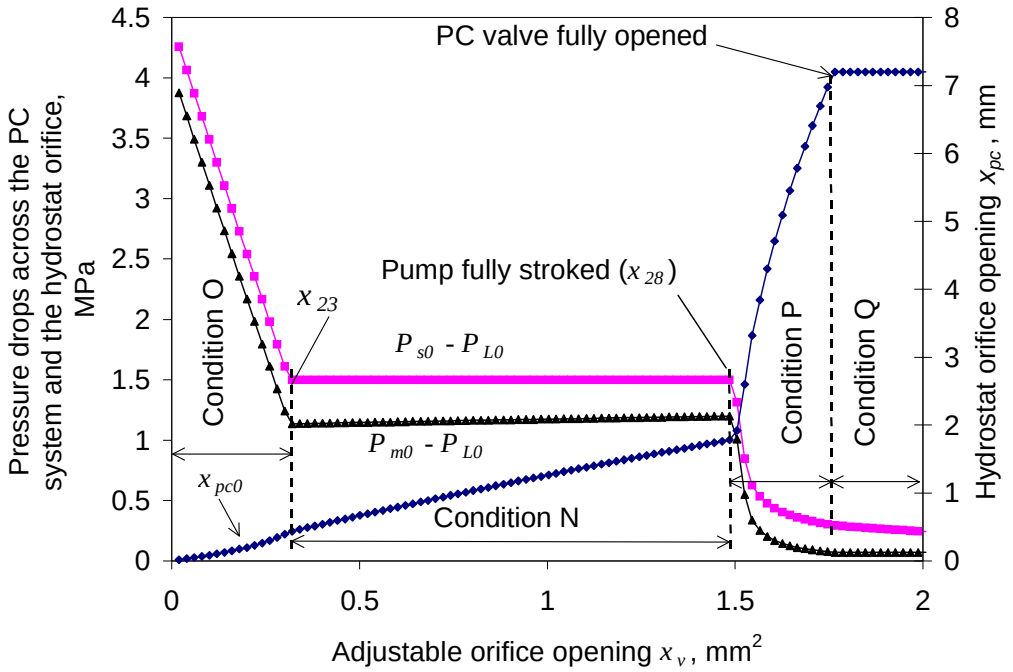

Figure 14.2 Hydrostat Orifice Opening and Pressure Drops Across the PC Valve and the Hydrostat Orifice on Trajectory II as a Function of the Control Orifice Opening

It is noted that Trajectory I defined in Chapter 7 consists of the SSOP at Condition I or Conditions I and III (see Figure 7.1). Therefore, for the LSPC system, Trajectory I can be one of four combinations: Condition N, Conditions N and P, Conditions N, P and Q, and Conditions R and Q (refer to Tables 12.1 and 12.2). In this study, only Conditions N for Trajectory I is considered, because, for Condition Q, R and S, the LSPC system actually operates in the LS mode and Condition P only exists in the limited transition region.

In a similar fashion, Trajectory II defined in Chapter 7, consists of the SSOP at Conditions II, I, and III, or II and III (see Figure 7.1). Trajectory II for the LSPC system can be Conditions O, N, P and Q, or Conditions O, P and Q. In this study, only Conditions O and N for Trajectory II are considered, because Condition P only exists in the limited transition region and Condition Q reflects the LS mode.

It is noted that Case 1 defined in Chapter 12 is only considered in this chapter, that is;

the PC valve must satisfy Inequality (12.3), because the other case, Case 2, reflects the saturation condition in which the hydrostat orifice of the PC valve is fully opened.

14.3 Stability Analysis of the LSPC System

The objective of this section is to compare the loci of the poles (especially the dominant poles) of the LSPC system and the LS system when the SSOP moves along the same trajectory (Trajectories I or II). The effect of the dynamics of the PC valve on the dynamic performance of the LSPC system is discussed.

14.3.1 Trajectory I (Conditions N (LSPC) and I (LS))

In order to illustrate the root locus of the LSPC system and compare them to that of the LS system, the parameters of the LS pump and the load are selected to be the same as those used in Section 7.2.1 of Chapter 7 and the PC valve parameters are also selected to be the same as those listed in Table 11.1 of Chapter 11. Using the procedure discussed in Table 13.1, the locus of the poles and zeros for the LSPC system can be plotted. The results of the zero-pole analysis for the LSPC system are worth repeating here: **in the region of Condition N, the dominant conjugate poles, whose frequency components were less than ω_L (the undamped natural frequency of the motor load), and a second pair of "non dominant" poles, with frequency components close to ω_s (the undamped natural frequency of the LS spool), mainly influence the stability of the LS system.**

For the non-dominant poles, the results of the calculation are similar to that illustrated in Figure 7.3; that is, the non-dominant poles are in the right half side of the s plane. It is noted that if the LS circuit is connected together with soft hoses (instead of pipe), the non-dominant poles shifts to the left half side of the s plane. When the orifice opening is

small, the poles and zeros of the LS system transfer function at these frequency points cancel or approximately cancel. Because these non-dominant poles mainly relate to the dynamics of the LS spool, any instability associated with these non-dominant poles is caused by the positive feedback loops in the LS pump (see Figure 13.1). There are three positive feedback loops: 1) $G_r \rightarrow K_{yr} \rightarrow G_y \rightarrow K_{cr1} \rightarrow G_s$, 2) $K_{ys} \rightarrow G_y \rightarrow K_{cr1} \rightarrow G_s$ and 3) $K_{sps} \rightarrow G_{sp} \rightarrow C_p \rightarrow G_s$. Therefore, replacing the simple orifice with the PC valve does not solve the instability problem associated with the non-dominant poles.

For the dominant poles shown in Figure 14.3, it can be observed that the difference in the dominant poles' loci indeed exists between the LS and LSPC systems. For the LS system, as the operating point moves along the trajectory shown in Figure 7.2, the dominant poles shown by Curve (1) in Figure 14.3 move directly towards the origin. In other words, the undamped natural frequency, ω_n, of the system decreases and the damping ratio, ζ, is approximately constant [1]. However, the LSPC system can become unstable due to the dominant poles shifting into the right half side of s plane (refer to Curve (2)).

In order to investigate why using the PC valve in the LS system makes the LS system performance worse, it is necessary to review the dynamic performance of the PC valve used in the LSPC system. Equation (11.44) and Figure 11.1 indicate that the PC valve is an over-compensated PC valve. At the steady state, there is a phase shift of 180°. This phase shift might be a problem, because, at the steady state and the low frequency region, the LS loop and the flow feedback loop (i.e. the load feedback loop: $G_{psL}(s) \rightarrow H_L(s)$ and the flow feedback ($G_{psL}(s) \rightarrow G_s(s)$)) in Figure 13.1 become a positive feedback loop but

[1] The undamped natural frequency, ω_n, of the LSPC system is equal to the distance between the poles and the origin in s plane. The damping ratio, ζ, is equal to the sine of the angle with respect to imaginary axis.

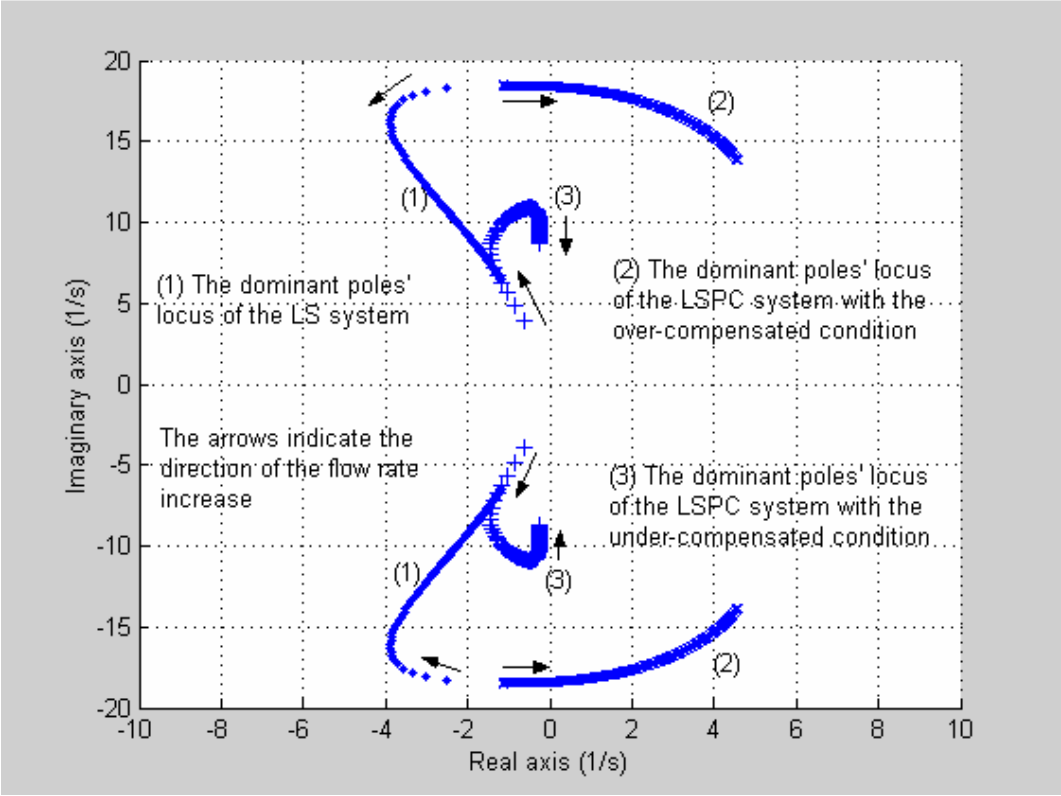

Figure 14.3 Comparison of the Dominant Poles' Loci between the LS and the LSPC Systems on Trajectory I

the pump pressure feedback loop ($G_{psL}(s) \rightarrow H_L(s) \rightarrow G_{Ls}(s) \rightarrow G_r(s) \rightarrow K_{yr} \rightarrow G_y(s) \rightarrow K_{spy} \rightarrow G_{sp}(s) \rightarrow C_p \rightarrow G_s(s)$) becomes negative due to the phase shift (180°) of $G_{psL}(s)$ itself. This scenario is opposite to the LS system.

According to Section 11.3.3 of Chapter 11, the PC valve can be one of three compensation conditions; critically compensated, under compensated and over compensated. Consider the under-compensated PC valve for the LSPC system. For a PC valve, there are four methods which can be used to change compensation conditions from over- to under-compensated (reference to Equations (11.47) and (11.49)): a) increasing the hydrostat spring coefficient, k_{pc}, b) decreasing the steady state flow force coefficient (i.e. decreasing k_{ff}), c) decreasing the equivalent width of the hydrostat orifice, w_{pc}, and d) decreasing the pressure drop across the hydrostat orifice, $P_{m0} - P_{L0}$. The first method is

physically feasible for the PC valve studied. It is noted that in order to make the comparison valid, P_d cannot be changed. When the hydrostat spring coefficient, k_{pc}, increases, the pressure drop across the hydrostat orifice, $P_{m0} - P_{L0}$, correspondingly decreases because increasing k_{pc} results in an increase in the pressure drop across the fixed orifice, $P_{s0} - P_{m0}$, (note: the pressure differential set, P_d, is constant and equal to $P_{s0} - P_{L0}$).

When k_{pc} increases from 9100 N/m to 37000 N/m, Inequality (11.47) is satisfied and the PC valve becomes under-compensated. Curve (3) in Figure 14.3 shows the locus of the dominant poles of the LSPC system with the under-compensated PC valve. It indicates that, although the dominant poles move outwards at small openings of the adjustable orifice, then change their direction and shift towards to the region of instability (Curve (3)), the dominant poles' locus of the LSPC system is always located in the left half side of s plane; that is, the LSPC system is stable. Therefore, the LSPC system can be stabilized by modifying the over-compensated condition into the under compensated condition for the PC valve.

It should be noted that even though the aforementioned improvement is accomplished, the dominant poles' locus (Curve 3) of the LSPC system for the large openings of the adjustable orifice is still to the right of the dominant poles' locus (Curve 1) of the LS system and is very close to imaginary axis. This implies that the dynamic performance of the LSPC system cannot be superior to that of the LS system.

14.3.2 Trajectory II (Conditions O & II and Conditions N & I)

The objective of this section is to compare the dominant poles' locus of the LSPC system when the LSPC system operates along trajectory II. Based on Figure 14.2, the

LSPC system operates at Conditions O, N, P and Q as the opening of the PC valve's adjustable orifice varies. Again, it is mentioned that Condition P only exists in the limited transition region P and Condition Q reflects the LS mode because the hydrostat orifice is fully open. Thus, Conditions P and Q are not discussed in this chapter. This section compares the dominant poles' loci of the LSPC systems at Conditions O ($P_{s0} = P_{y0}$) and N. Usually, Condition O would occur when the load becomes "runaway". In fact, if P_d is set to be less than P_{s2} (see Figure 7.1), the LSPC system when the opening, x_v, is small, can operate in Condition O even if the load is not a runaway load (reference to Equation (7.2)).

Figure 14.4 illustrates the dominant poles' loci for the LS system and the LSPC systems with the over- and under-compensated PC valve on Trajectory II (Figure 7.5 and Figure 14.2). The symbols, 'O' (Condition II) and '*' (Condition I) represent the root locus of the LS system. The symbols, '+', '×' (with under-compensated condition) and '•', '◊' (with over-compensated condition), identify the loci of the LSPC system. The loci with '+' and '•', are in Condition O and '×' and '◊' in Condition N. It can be observed that the loci of the LS system and the LSPC system with the under-compensated condition are always located in the left half side of the s plane. The loci of the LSPC system with the over-compensated condition are located in the right side of the s plane except the part of the locus with very small opening of the adjustable orifice.

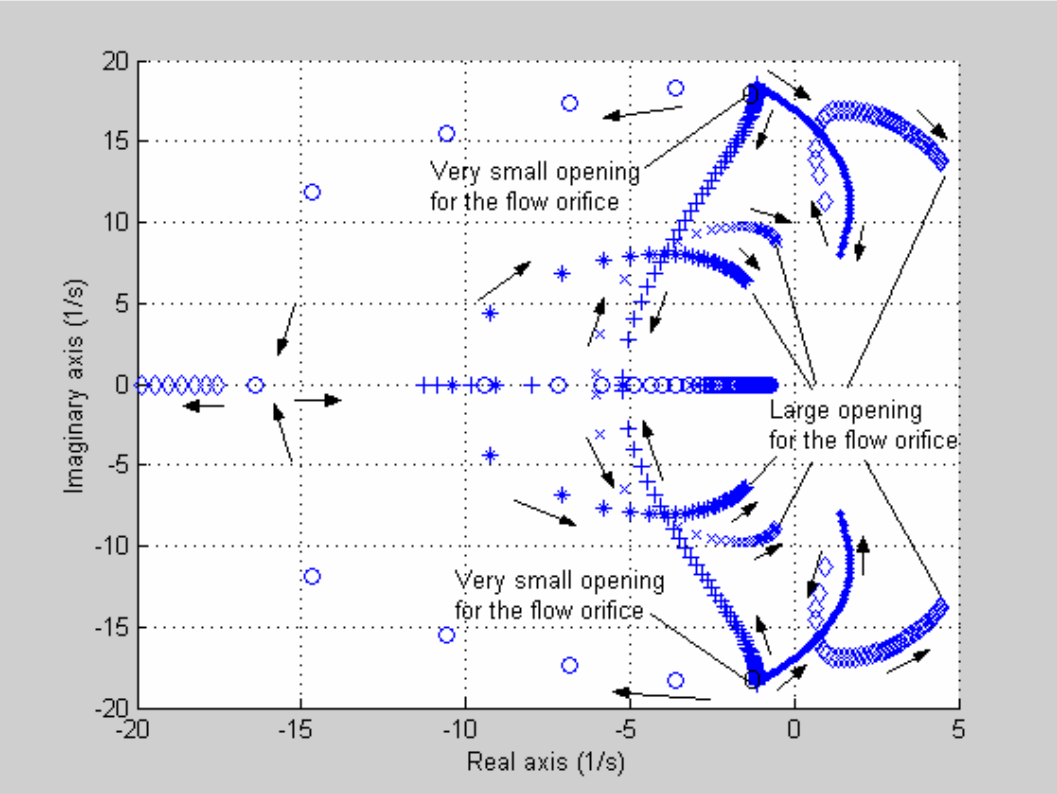

Note: 'O' and '*' — LS, '+' and '×' — LSPC (with under-compensated condition), '•' and '◊' — LSPC (with over-compensated condition), 'O' — Condition II, '*'— Condition I, '+' and '•' —Condition B, and '×' and '◊' — Condition A, Arrows indicate directions of increasing flow.

Figure 14.4 Comparison of the Dominant Poles' Loci between the LS and the LSPC Systems on Trajectory II

It is noted that the above comparisons for Conditions N and O in Sections 14.3.1 and 14.3.2 are accomplished under the certain condition such as the pressure drop, P_d, of 1.5 MPa, a specific load (J_m = 0.16 Nm/s^2, B_m = 0.056 Nm/s) and the temperature, T, of 30°C. For different conditions, particularly the different load, the locus of the dominant pole would be different. Figure 14.5 shows the root locus of the LS and LSPC system under the condition in which only the load inertia, J_m, is the tenth of that for Figure 14.4 and all other parameters are the same as those for Figure 14.4. Compared to Figure 14.4, it can be observed that the initial dominant poles change from 1.3±18j to 2.5±58j and the trend of the locus is also different.

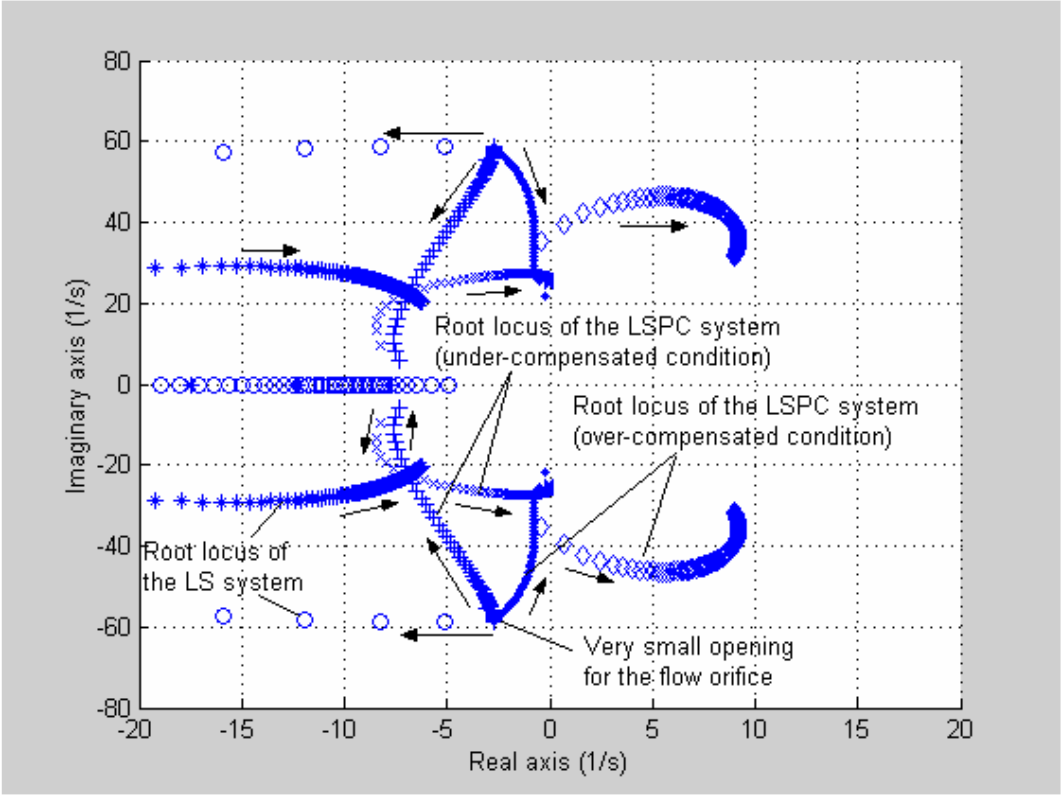

Note: 'O' — Condition II, '*'— Condition I, '+' and '•' —Condition B, and '×' and '◊' — Condition A, Arrows indicate directions of increasing flow.

Figure 14.5 Comparison of the Dominant Poles' Loci between the LS and the LSPC Systems on Trajectory II

Although the root locus of the LS and LSPC systems changes as the parameter varies, the root locus plots under different conditions can give rise to consistent conclusions such as:

- The over-compensated PC condition always makes the LSPC system unstable.
- The use of a PC valve does not improve the dynamic performance of the LS system. Therefore, the use of a PC valve in a LS system (LSPC system) has limited application, unless it is applied to the case of a multiple-load LS system where the PC valves have to be used to isolate the interaction between loads (refer to Chapter 1).

In addition to the above conclusions, the following observations can also be forwarded based on the result of the parameter sensitivity analysis about the particular trajectory.

- A decrease in the load resistance, T_{mf}, can make both the dominant poles and the non-dominant poles move towards the left half side of the s plane, thus the LSPC system tends to be more stable.
- A decrease in the pressure differential set, P_d, stabilizes the system but reduces the speed of response of the system.
- Increasing the damping in the LS line, i.e. decreasing ω_{ls}, reduces the speed of response of the LSPC system and tends to destabilize its operation.
- An increase in the capacity of the pump and motor (via increasing the volumes, V_p and V_m, or reducing the equivalent bulk module, β, using soft hoses, for example) reduces the speed of response of the LSPC system. However, the non-dominant poles (around 2000 rad/s) move into the left half side of the s plane (stabilizes), and the high frequency oscillation which would occur in the system pressures, P_s, P_y and P_L, and the displacement of the LS spool, x_r, no longer exist.
- In addition to the spring coefficient, k_{pc}, other parameters of the PC valve, such as the size of the damping orifice, significantly affect the dominant poles' loci.

14.4 Summary

When the PC valve is applied to the LS system (creating the LSPC system), the system becomes very complex in its steady state and dynamic performance. The steady state operating condition can be one of six different operating conditions as a result of the combination of Conditions I, II and III for the LS system and Conditions A and B for the

PC valve. They are defined as Conditions N, O, … S. Condition N is the normal operating condition. As the opening of the adjustable orifice of the PC valve increases, the SSOP of the LSPC system moves along Trajectory I (starting from Condition N through Q via P) or Trajectory II (starting from Condition O through Q via N and P).

The stability analysis of the LSPC system in this chapter results in two main conclusions: 1) the LSPC system can be stabilized using the under-compensated PC valve and 2) the dynamic performance of the LSPC system is not superior to that of the LS system for the case of the single load.

Chapter 15 Experimental Verification for the Results of Stability Analysis of the Load Sensing and Pressure Compensated system

15.1 Introduction

The purpose of this Chapter is to experimentally verify the main conclusions and observations which were forwarded in Chapter 14. The most important conclusions for the LSPC system is restated as: **1) the LSPC system can be stabilized using the under-compensated PC valve and 2) the dynamic performance of the LSPC system is not superior to that of the LS system for the case of the single load.** In order to experimentally verify the above statements, it is necessary to establish three dynamic experiments and compare the results to that predicted theoretically. The first experiment is associated with the LS system, the second the LSPC system (with over-compensated PC valve), and the third the LSPC system (with the under-compensated PC valve). The comparison of the behaviors of these three systems is done using step responses. Experimental verification is limited to the stability associated with the dominant poles of the LS system and the LSPC system and is undertaken only in the normal operating conditions (Conditions I and N). The experimental studies of the dynamic performance under "non-normal" operating conditions (Conditions II and III for the LS system and Conditions O, P, Q, R for the LSPC system) and the stability associated with the non-dominant poles of the LS and LSPC systems are deferred for future work.

It is noted that for the purpose of comparison the experimental operating conditions for the three experiments must be the same. In other words, the system parameters (e.g. the LS pump parameters, the load conditions -- J_m, B_m, T_{mf}, c_{ml}, the pressure drops across the PC valve and the needle valve, P_d) and the SSOP (e.g. the load flow rate at the steady

state, Q_{L0}) are required to be the same.

In order to conduct two of the experiments on the LSPC system, it was necessary to determine some method for modifying one or more parameters of the PC valve in order to create the under- and over-compensated conditions on the same PC valve.

15.2 Modification and Verification of the "Compensation Condition" for the Pressure Compensated Flow Control valve

The "Compensation Condition" denotes the three conditions: "under", "critical" or "over" compensation introduced in the earlier chapters. This section first introduces the approach for modifying the compensation condition for the existing PC valve. The particular experiments are then conducted to verify the modification.

In order for the PC valve shown in Figure 8.2 to operate under the desired compensation condition, the PC valve must be modified so as to satisfy Inequality (11.47) for the under-compensated condition, Equality (11.48) for the critically compensated condition, or Inequality (11.49) for the over-compensated condition. In order to further understand these criteria, Equality (11.48) is modified slightly as follows. Because the pressure drop across the fixed orifice, $P_s - P_{m0}$, is approximately equal to P_{pc} (refer to Section 10.1.1 in Chapter 10), the pressure drop, $P_{m0} - P_L$, can be approximated by ($P_s - P_L$) - P_{pc} = ($P_s - P_L$) - $\frac{k_{pc} x_{spring\_def}}{A_{pcs}}$ (refer to Equation (10.4)). Consequently, Equation (11.48) can be approximated by

$$k_{pc} = \frac{k_{ff} w_{pc} (P_s - P_L)}{1 + \frac{k_{ff} w_{pc} x_{spring\_def}}{A_{pcs}}} \qquad (15.1)$$

Equation (15.1) indicates that the compensation condition can be related to the value of spring coefficient, k_{pc}, the equivalent width of the hydrostat orifice, w_{pc}, the coefficient k_{ff} (where $k_{ff} = 0.7C_{dc}$. See Equation (10.6)), the cross-sectional area of the hydrostat spool at the ends, A_{pcs}, the spring deformation, x_{spring_def}, at $x_{pc} = 0$, and the pressure drop across the PC valve, $P_s - P_L$. For the existing PC valve, it is difficult to modify w_{pc}, k_{ff} and A_{pcs}. The pressure drop, $P_s - P_L$, is equal to the system parameter, P_d, in the LSPC system and is required to be constant for comparison purposes. Therefore, a feasible approach for modifying the compensated condition is to change the spring size, that is, selecting different k_{pc} and x_{spring_def}. Practically, it is more restrictive physically to choose different values of the spring deformation, x_{spring_def}, than it would be for changing the spring coefficient, k_{pc}. Thus the spring coefficient, k_{pc}, was changed to reflect a value which would be larger or smaller than the value of the term on the right hand side of Equation (15.1) for the corresponding compensation conditions (under or over-compensated conditions).

For the critically compensated condition, k_{pc} is calculated to be 10140 N/m for P_d = 1.5MPa. Thus two springs were selected to which had spring coefficients of 37000 N/m for the under-compensated condition (Century Spring Co., #3057) and 5000 N/m for the over-compensated PC valve(Century Spring Co., #11511).

In order to verify the under-compensated condition and the over-compensated condition, the measured value of the steady state flow-pressure coefficient, K^*_{psL} (refer to Equation (11.52)), must be a positive number for the rigid spring and a negative number for the soft spring (refer to Equation (11.53)).

Figure 15.1 shows a comparison of the measured steady state flow-pressure coefficients of the PC valve using a rigid hydrostat spring and a soft spring. When the pressure drop across the PC valve, $P_s - P_L$, is constant (P_d = 1.5MPa), the slope of the experimental curve is a positive number ($K^*_{psL} > 0$) for the rigid spring and a negative number ($K^*_{psL} < 0$) for the soft spring as predicted by theory. Therefore, the use of these hydrostat springs does indeed create the desired compensation conditions for the same PC valve.

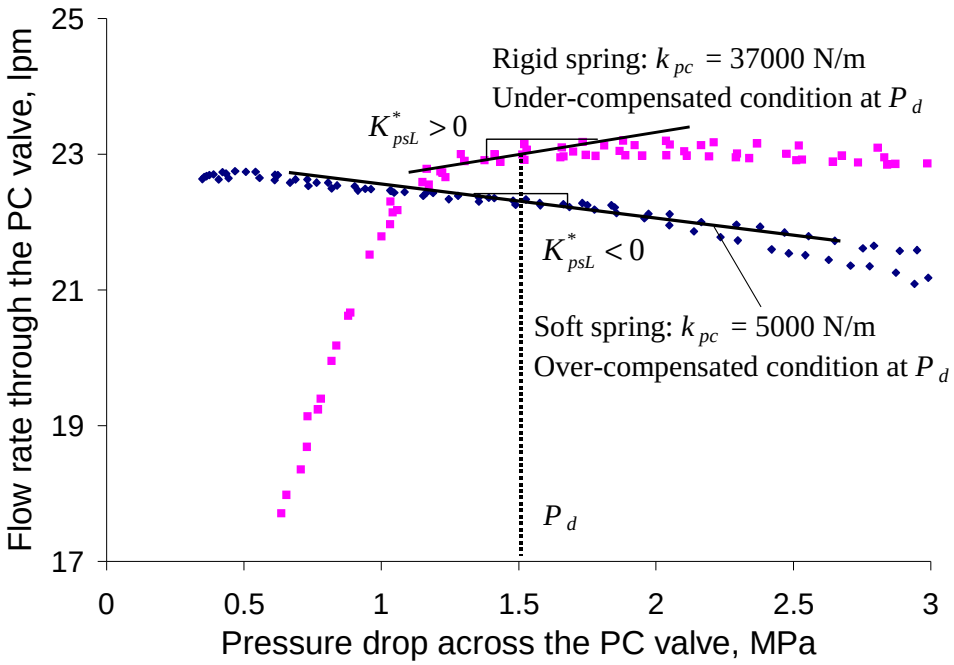

Figure 15.1 Comparison of the Experimental Flow-Pressure Coefficients of the PC Valve between a Rigid Hydrostat Spring and a Soft Hydrostat Spring

15.3 Procedure of the Experiment and Signal Processing

The purpose of this section is to explain the procedure used to create the step response experiments for the LS and LSPC system with under-compensated and over-compensated PC valves. The input signal is the opening, $x(t)$, of the needle valve or the opening, $x_v(t)$, of the adjustable orifice of the PC valve. The output is the motor rotary speed, $\phi(t)$. The

parameters of the LS pump and the load (developed in Appendix H) are P_d = 1.5 MPa, ω_{ls} = 450 rad/s (the LS damping orifice is fully opened), and T_{mf} = 0.2 Nm. The fluid temperature was in the region of 25 ~ 35 °C. With these defined parameters, Trajectory I can be created experimentally. The procedure was to select several SSOP's on this trajectory and to carry out step responses with a small step input signal, ($x_{final}(t)$ - $x_{initial}(t)$). The procedure can be summarized as

Step 1: Construct the LS circuit with a needle valve as the control orifice. Initialize the data acquisition system.

Step 2: Power on the LS system; continuously adjust the opening of the adjustable orifice until the load flow rate is equal to 5 l/min.

Step 3: When steady state conditions are reached, the adjustable orifice is opened as a small step about SSOP. The magnitude of the step is such that the output flow rate variation is 3 l/min. This is accomplished using trial-and-error process.

Step 4: Measure and collect the output signal, $\phi(t)$, using the data acquisition system.

Step 5: Repeat Steps 2, 3 and 4 with the several SSOP's (load flow rates of 10, 15, 20 l/min).

Step 6: Replace the needle valve with the PC valve (containing the soft hydrostat spring) and repeat Steps 2, 3 and 4.

Step 7: Replace the soft hydrostat spring in the PC valve with the rigid hydrostat spring and repeat Steps 2, 3 and 4.

It is noted that the load flow rate of 20 l/min can result in a motor speed of 1337 rpm for the piston motor used. For safety reasons, experiments for flow rates greater than 20 l/min were not conducted. However, the flow range used was considered sufficient to

verify the stated conclusions of Chapter 14.

The data collected during the experiments must be properly processed in order to facilitate comparison. As stated in Section 15.1, the stability associated with the dominant poles is only considered; therefore, it is necessary to filter out any high frequency signal from the collected data. Because the undamped natural frequency, ω_n, of the LS system and the LSPC system associated with the dominant poles is usually less than the undamped natural frequency, ω_L (3 Hz in this study), a 5th order Chebyshev II filter with the cutoff frequency of 4.5 Hz was applied.

15.4 Experimental Results and Analysis

In order to understand the relationship between the experimental result and the location of the dominant poles, Figure 14.3 is re-plotted as Figure 15.2 in which only the experimental operating points (Q_L = 5, 10, 15 and 20 l/min.) are illustrated. This is the stability prediction based on the experiment condition.

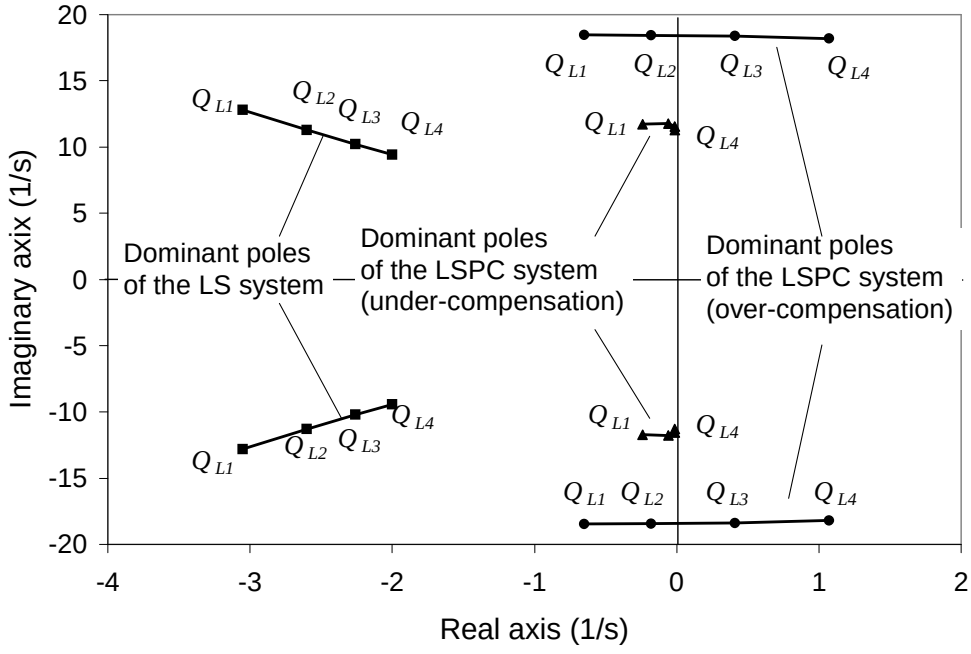

Figure 15.2 Dominant poles' Loci of the LS System and the LSPC System for the Experimental Condition

Figures 15.3 through 15.6 illustrate the step responses about the operating points, Q_{L1}, Q_{L2}, Q_{L3} and Q_{L4}. It can be observed in Figure 15.3 that the step response of the LSPC system demonstrates more oscillation than the LS system. This reflects the fact that the dominant poles of the LSPC system are very close to the imaginary axis (see Figure 15.2). For two situations of the LSPC system, the case of the under-compensated condition demonstrates a significant oscillation which is identical to that predicted by the dominant poles of the LS system as they move close to the imaginary axis (see Figure 15.2).

Figure 15.4 indicates that the step response of the LSPC system tends to be more oscillatory. The LS system and the LSPC system are stable for the flow rate of 5 and 10 l/min which was shown in Figures 15.3 and 15.4.

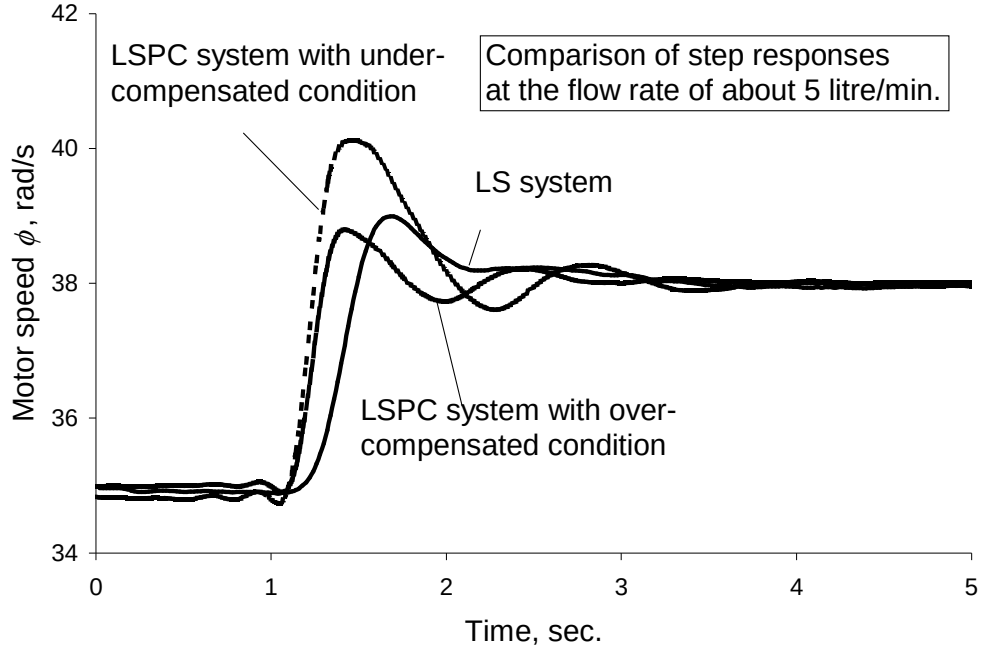

Figure 15.3 Comparison of the Measured Motor Rotary Speed, ϕ, at the Load Flow Rate of 5 l/min

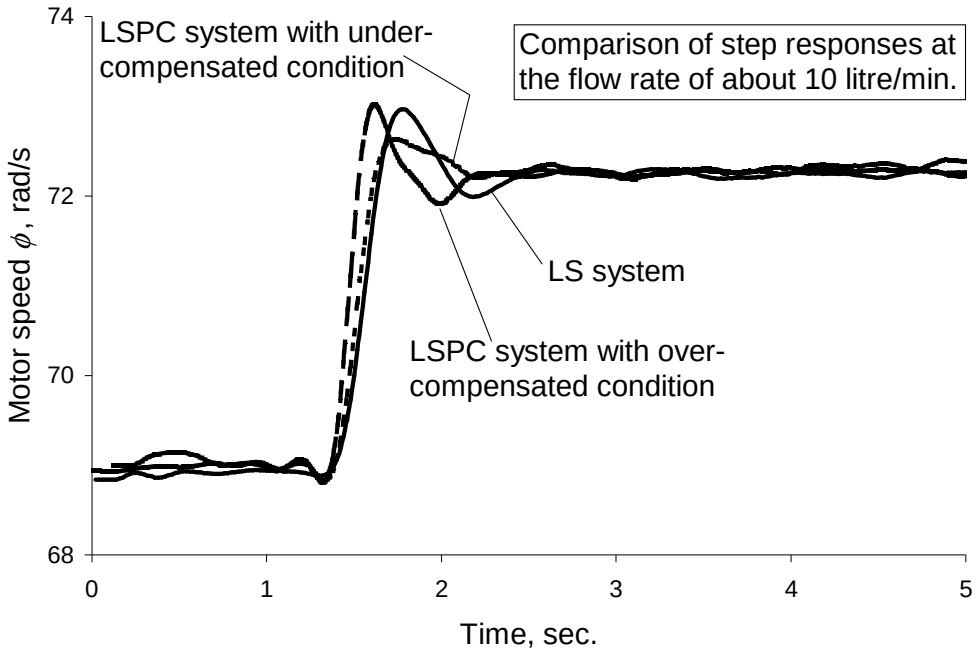

Figure 15.4 Comparison of the Measured Motor Rotary Speed, ϕ, at the Load Flow Rate of 10 l/min

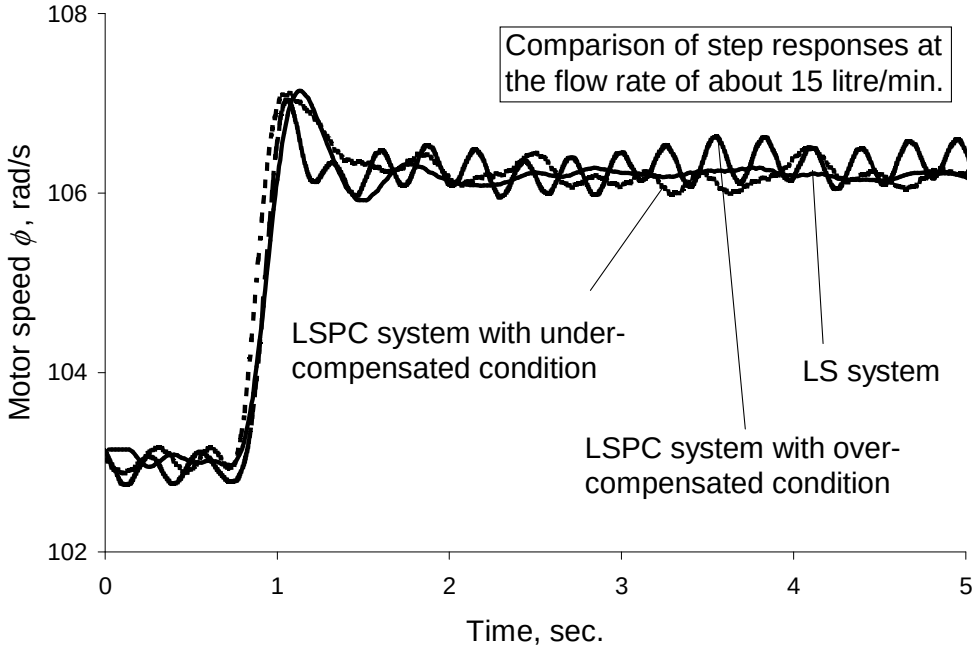

Figure 15.5 Comparison of the Measured Motor Rotary Speed, ϕ, at the Load Flow Rate of 15 l/min

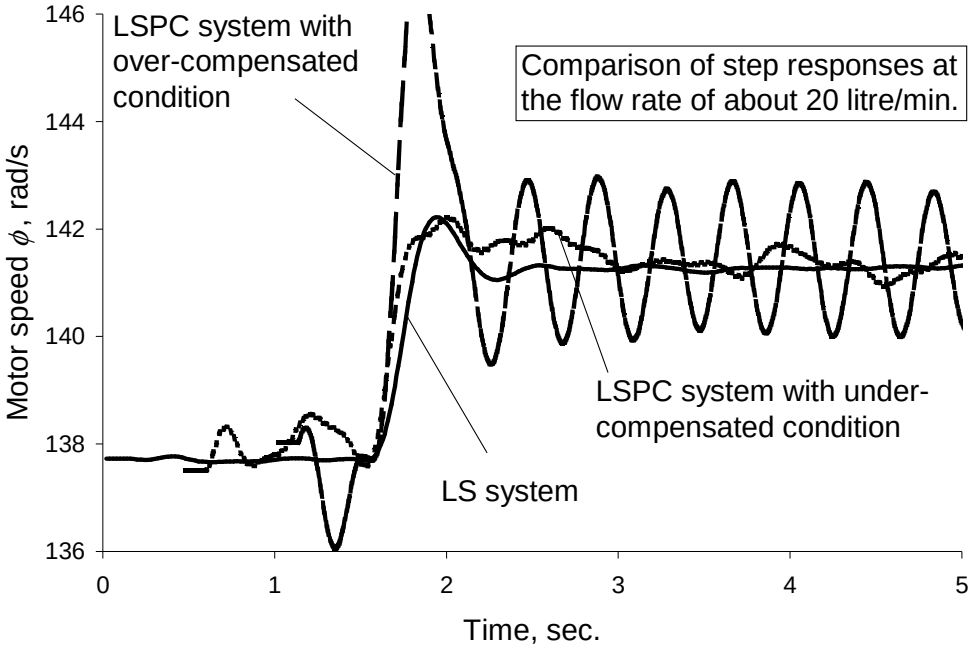

Figure 15.6 Comparison of the Measured Motor Rotary Speed, ϕ, at the Load Flow Rate of 20 l/min.

The step response with the over-compensated condition in Figure 15.5 indicates that the LSPC system is in a limit cycle oscillation. This kind of the oscillation represents the "marginally stable status" on the basis of the linear theory. This experimental result is inconsistent with the "unstable state" predicted theoretically as the dominant poles have moved into the right half side of the s plane (see Figure 15.2). The inconsistence was caused by the application of the linear theory to the non-linear system. The "instability" predicted by the linearization approach for a practical nonlinear system always demonstrates a limit cycle oscillation. If the pole located in the right half side of the s plane is very close to the imaginary axis, the magnitude of the limit cycle oscillation is small. If the poles are far away the imaginary axis, the magnitude of the limit cycle oscillation becomes large. The step response with the over-compensated condition in Figure 15.5 demonstrates a low frequency fluctuation with small magnitude. This is consistent with the prediction that the dominant pole of the LSPC system is very close to

the imaginary axis.

Figure 15.6 shows the existence of the significant oscillations in the LSPC system with the over-compensated condition compared to its partner in Figure 15.5. This is consistent with the prediction that Q_{L3} is closer to imaginary axis than Q_{L4}. But the difference of the step responses of the LSPC system with the under-compensated condition in Figures 15.5 and 15.6 is not evident. This is also consistent with the prediction that the location of dominant poles is almost invariable.

It can also be observed through a comparison of the step responses of the LS system in Figures 15.3 through 15.6 that the percent overshoot is almost the same. This is also consistent with the fact that the damping ratio associated with dominant pole location of the LS system is the same.

15.5 Summary

This Chapter experimentally verifies the main conclusion obtained in Chapter 14. The result of the dynamic response in time domain and the theoretical prediction in frequency domain are basically consistent. Both methods indicate that the LSPC system can be stabilized using the under-compensated PC valve but the dynamic performance of the LSPC system seems to be inferior to that of the LS system for the operation of a single load.

Chapter 16 Conclusions and Recommendations

This thesis presents a comprehensive study of a LS and LSPC system -- a highly nonlinear system. To compromise between efficiency and fast dynamic response, a LS system is sometimes equipped with a LS regulator with a critically lapped spool. This brings about a situation where the system model not only is non-linear but also varies depending on which operating region it is in. Therefore, the system analysis initially started by identifying the operating regions to establish the order of the system model, and then secondly, solving for the operating points to define appropriate linearized coefficients of the models. Finally, a standard stability analysis procedure was carried out.

16.1 Main Achievements

The following sections summarize the main achievements of this thesis.

16.1.1 Load Sensing System

In order to summarize the achievement of the research for the LS system, it is necessary to recall the objectives for this thesis. The objectives associated with the LS system were (1) to investigate the steady state operating condition and the SSOP's of a LS system with a critically lapped LS regulator spool in the LS pump; (2) to develop the stability models of the LS system under different steady state operating conditions using the linearization method based on the knowledge about the SSOP of the LS system; and (3) to determine the dependence of the system stability on the SSOP of the LS system.

The following section itemizes the achievements accomplished in meeting the objectives.

- Steady state operating conditions and steady state models of the LS system

  In this research, the LS system equipped with a LS regulator with a critically lapped spool has been defined as operating in three different operating regions Conditions I, II, & III. Operating Condition I is the normal operating condition of the LS system. The boundary conditions of the three conditions can be given as

  Condition I: $x_{r0} = 0;\ P_{s1} < P_{y0} < P_{s0};\ \theta_{sp0} < \theta_{sp\max}$ and $P_{s0} - P_{L0} = P_d$ (16.1)

  Condition II: $x_{r0} > 0;\ P_{s1} < (P_{y0} = P_{s0}) < P_{s2};\ \theta_{sp0} < \theta_{sp\max}$ and $P_{s0} - P_{L0} > P_d$ (16.2)

  Condition III: $x_{r0} < 0;\ P_{y0} = 0;\ \theta_{sp0} = \theta_{sp\max}$ and $P_{s0} - P_{L0} < P_d$ (16.3)

  Under each operating condition, the model for solving for the SSOP was presented and experimentally verified.

- Empirical orifice flow model at small openings

  In order to develop the transfer function of the LS system for stability analysis, it was necessary to obtain the flow gain and flow-pressure coefficient of the orifice flow rate for the LS regulator. The traditional form of the flow gain ($K_q = C_d w\sqrt{\frac{2}{\rho}\Delta P}$), and the flow-pressure coefficient ($K_c = \frac{C_d w x}{\sqrt{2\rho\Delta P}}$), for an orifice are not sufficiently accurate to use in the modeling of a LS system because of the following three factors:

  1. C_d may not be a constant but a function of the orifice Reynolds number (i.e. a function of the flow rate through orifice, orifice geometry and fluid temperature) because of laminar flow, or the transient region from laminar to turbulent flow status. Except for the generation of graphical representations [Merritt, 1967; Borghi et al, 1998; Vescovo et al, 2002; Ellman et al, 1996;

Gromala et al, 2002], an analytical expression of such a function has not been found.

2. Traditionally used flow gain and flow-pressure coefficient models are discontinuous at the null position ($x = 0$) where the LS regulator operates at most time.
3. The flow cross sectional area (wx) is usually inaccurate about the null position because of chamfers, clearances and other factors caused by machining limitations.

These problems also exists when modeling other hydraulic valves which have the spool operating at the "null" point, such as, pilot valves of two stage valves or compensators of pumps and motors.

This research provides a closed form empirical model for C_d as a function of the Reynolds number which can be applied to different types of orifices (see Equation (4)[1] in Appendix C). Based on this model, a technique to evaluate flow without having to use iteration (given an orifice area and pressure drop) is introduced. A novel modification to the flow cross-sectional area is introduced (see Equation (10) in Appendix D) and the resulting empirical closed form of the flow equation is presented (see Equation (14) in Appendix D). This closed form equation greatly facilitates the transient and steady state analysis of low flow regions at small or null point operating regions of the spool valve. The derived flow gain (Equation (15) in Appendix D) and the flow-pressure coefficient (Equation (16) in Appendix D) are reasonably accurate and no longer influenced by the aforementioned three factors.

[1] The use of "(4)" rather than "(C.4)" for the equations in necessitated because the appendix is a reprint of the journal article.

Journal papers based on this particular research have now been published [Wu, et al, 2002 and Wu, et al, 2003].

- Frequency response models of the LS system

The transfer function of the flow control with the LS system is defined as (see Figure 6.2)

$$F(s) = \frac{\phi(s)}{X(s)} \tag{16.4}$$

where the input signal, X, is the opening of the adjustable orifice. The output signal, ϕ, is the motor's rotary speed. The transfer functions for operating Conditions I, II and III are given by Equations (5.76), (5.80) and (5.82) respectively. These frequency response models in the low frequency regions have been experimentally verified. These transfer functions can be summarized as following:

Condition I: The transfer function Equation (5.76) is 5^{th} order and neglects the effects of system characteristic frequencies higher than 1000 rad/s of the LS pump. It can be used to investigate the stability of the LS system in the frequency range less than 1000 rad/s. A complete 9^{th} order transfer function can be used to determine the high frequency dynamic behavior of the LS pump caused by the LS spool with a high undamped natural frequency, ω_r, (1954 rad/s). High frequency dynamic behavior cannot be identified with respect to the motor rotary speed due to the filter effects of the load inertia.

Condition II: The 5^{th} order transfer function Equation (5.80) reflects the dynamic behavior of the LS system in which the "charge orifice" is fully opened (see Figure 5.15). The LS pump dynamics are dominated by the pump pressure and are not affected by the LS path via $G_{Ls}(s)$ and $G_r(s)$ (compare Figures 5.16 and 5.10). This situation is

similar to the operation of a compensated pump/valve system in which the cut-off pressure of the compensated pump is P_{s1} and the deadhead pressure is P_{s2} (see Figure 3.2). Therefore, this model can be applicable to a compensated pump/valve system.

Condition III: The 3rd order transfer function Equation (5.82) reflects the operating behavior of the LS system in which the pump is fully stroked. The LS system is shown to be stable (see Appendix G). This condition is similar to that of a fixed displacement pump/valve system in which swash plate angle, θ, is fixed. Therefore, this model is applicable to a simple pump/valve system.

16.1.2 The Pressure Compensated System

In order to summarize the research achievements for the PC system, the objective associated with the PC system is restated. The objective was to analyze the steady state and dynamic performance of a typical PC system. The following section itemizes the achievements accomplished in meeting the objective.

- Steady state operating conditions and steady state analysis of the PC system

The PC system has been defined as operating in two different operating regions defined as operating Conditions A & B. Operating Condition A is a normal operating condition of the PC system while Condition B represents the situation in which the hydrostat orifice is fully opened. The boundary conditions of the two conditions can be determined by Equation (9.8). Equation (9.9) can also be used to solve for the SSOP of the PC system, x_{pc0}. The intermediate pressure, P_{m0}, can be calculated using Equation (9.1).

The operating point, x_{pc0} and P_{m0}, has been measured on a typical PC valve and the measured x_{pc0} was compared to the theoretical prediction. The experimental result was consistence with the theoretical prediction.

- Frequency response model of the PC system

The PC system can be considered as an "equivalent orifice" in which the flow gain, $G_{xv}(s)$, and the flow-pressure coefficient, $G_{psL}(s)$, are a function of the operating point and the input frequency of the adjustable orifice opening and the pressure drop across the PC system. $G_{xv}(s)$ and $G_{psL}(s)$ have been defined as the flow gain TF and flow-pressure coefficient TF respectively. $G_{xv}(s)$ is a "low pass" filter and $G_{psL}(s)$ is a "high pass" filter.

- Criterions for optimized design of the PC system

Based on the study of the steady state and dynamic behavior of the PC system, a PC system can be optimized. The objective of the optimization is to expand the bandwidth of the flow control, $G_{xv}(s)$, and to decrease the gain of the flow-pressure coefficient TF, $G_{psL}(s)$, at the low frequency region as much as possible. Equations (11.45) and (11.48) are used to in optimizing performance as a function of the damping orifice's size and spring coefficient, etc.

16.1.3 Load Sensing and Pressure Compensated System

In order to summarize the research achievements for the LSPC system, the objective associated with the LSPC system is restated. The objective was to investigate the stability of the LSPC system which consists of both the LS and the PC system. The following section itemizes the accomplishments in meeting the objective.

- Steady state operating conditions and steady state analysis of the LSPC system

The LSPC system has six different operating conditions which are all combinations of the LS system and PC system operating conditions. These operating conditions can be classified into two groups: Case 1 and Case 2. Case 1 given in Table 12.1 reflects the combinations at a typical design condition that Inequality (12.3) is true. Case 2 represents combinations (B, E, F and D) of the LS system and PC system operating conditions in which Inequality (12.3) is false. Case 1 is an expected design condition, because the normal operating Condition A belongs to Case 1. When the adjustable orifice opening, x_v, is smaller than x_{vc} determined by Inequality (12.6), the LSPC system operates in Case 1. The load condition can be further used to determine which of Conditions A, B, C and D the LSPC system is operating in.

- Frequency response model of the LSPC system

The TF's of the LSPC system are the same in form as the TF's of the LS system, but with a replacement of the K_q and K_c by $G_{xv}(s)$ and $G_{psL}(s)$ of the PC system. When the simplified models of $G_{xv}(s)$ and $G_{psL}(s)$ (Equations (11.51) and (11.52)) are applied to the simplified TF's of the LS system (Equations (5.76), (5.80) and (5.82)), the order and zero point locations of the frequency response models of the LSPC system and the LS system are the same, that is, 5^{th}, 5^{th} and 3^{rd} order respectively. Only their poles are different.

A dynamic analysis for the LSPC system using the above models was undertaken. A set of experiments were conducted in order to verify the main conclusions drawn from the dynamic analysis for the LSPC system.

16.2 Contributions (Summary)

This Ph. D. research makes seven original contributions in the field of fluid power. They are:

- An empirical model of an orifice discharge coefficient as a function of Reynolds number has been developed which is suitable for different types of orifices (sharp-edged type, needle valve and long tube orifice) and for different flow conditions (laminar flow, turbulent flow and the transition region between them).
- An analytical expression of the orifice flow model has also been developed which can facilitate the modeling and simulation of a complete hydraulic system with pilot stage valves or pump/motor compensators.
- Three pressure compensated conditions (under-compensated, critically compensated and over-compensated conditions) of a PC flow control valve have been defined which provide a design criterion for valve designers.
- Three steady state operating conditions (Condition I, Condition II and Condition III) for a typical LS system have been identified which can aid in the design of LS pumps.
- A practical method of analyzing LS & LSPC systems has been provided which includes identifying all possible steady state operating conditions, solving for steady state operating point for each operating condition, justifying linearized models and illustrating the relative stability. This method can be used to design stable LS & LSPC system and to minimize the energy losses.

16.3 Main Conclusions

Based on the extensive modeling and experimental verification of the describing equations for the LS and PC systems, the following conclusions are drawn:

16.3.1 Load Sensing System

For the load sensing system, it is concluded that:

- The LS system usually operates in Condition I.
- When the orifice opening is large, the LS system tends to operate in the region of Condition III.
- When a runaway load occurs, the LS system tends to operate in the region of Condition II.
- In the region of Condition I, as the adjustable orifice opening increases, the LS system tends to be unstable because a pair of poles near the undamped natural frequency of the LS spool (1954 rad/s) is in the right half side of s plane. The limit cycle oscillation caused by this instability cannot be observed in the motor rotary speed due to the “low pass” filtering function of the motor and load.
- The LS system tends to be the low frequency oscillation as the adjustable orifice opening increases.
- The damping orifice in the LS line can be used to stabilize the system but the bandwidth of the LS system is compromised.
- The LS system is always unstable in the region of Condition II.
- The LS system is always stable in the region of Condition III.

16.3.2 Pressure Compensated System

For the pressure compensated system, it is concluded that:

- When the PC system operates in the steady state operating Condition A, the hydrostat orifice is automatically adjusted.
- Depending on the parameters of the PC system and the SSOP, the dynamic behavior of the PC system can be one of three dynamic operating conditions which are defined as the under-compensated, critically compensated and over-compensated conditions. The criterion developed was expressed by Equation (11.48)
- For the critically compensated condition ($k_{pc} = k_{ff} w_{pc} (P_{m0} - P_L)$), the flow rate through the PC system is completely independent of the pressure drop across the PC system.
- For the under-compensated condition ($k_{pc} > k_{ff} w_{pc} (P_{m0} - P_L)$), the flow rate through the PC system increases as the pressure drop across the PC system increases.
- For the over-compensated condition ($k_{pc} < k_{ff} w_{pc} (P_{m0} - P_L)$), the flow rate through the PC system decreases as the pressure drop across the PC system increases.
- Usually, these three dynamic operating conditions are not of concern. However, when the PC system plays the role of both “flow control” and a “pressure sensing” in complex circuits such as the LSPC system, the three compensated conditions produce distinctly different consequences (for example, positive feedback or negative feedback).

16.3.3 Load Sensing and Pressure Compensated System

For load sensing and pressure compensated system, it is concluded that:

- ♦ The over-compensated PC condition always makes the LSPC system unstable. The LSPC system can be stable in the low frequency region provided a PC valve with the under-compensated condition is used.
- ♦ There was no evident that the dynamic performance of the LS system was improved using a PC valve. Therefore, it is questionable that a PC valve can be applied to a LS system (creating the LSPC system) in order to improve the dynamic performance of the LS system. The exception is the case of a multiple-load LS system where the PC valves are used to isolate the interaction between loads (refer to Chapter 1).

16.4 Future Work and Recommendations

In general, a LS system seems to be good compromise between energy saving, controllability, reliability, price and maintenance. It is necessary to further investigate and optimize the system performance of the LS system. There is a substantial amount of future work that could be conducted regarding this research.

- It has been mentioned above that the actual LS system always uses a pressure regulator assembly which consists of a LS regulator and a pressure limiter. There is a region in which the pressure limiter and the regulator could operate together. This operating condition could be defined as the “fourth” operating condition of a practical LS system. Therefore, it is necessary to model and analyze this condition.
- The contributions in this thesis has provided a practical and reliable method to determine the stability of a LS system and a LSPC system at any operating point. It

is possible to optimize the design of the LS system using these models in the future.

- The models developed in this thesis could be extended to the case with an underlapped spool LS regulator.
- Chapters 12 through 15 investigate the LSPC system from the point view of the flow control because only the transfer function, $\frac{\phi(s)}{X(s)}$, was developed and analyzed. In fact, the main purpose for using the PC system in the LSPC system is to decrease the interaction between loads in a multi-load LSPC system. Therefore, more theoretical study is required.

References

Andresson, B. R. and Ayres, J. L., 1997. Load sensing directional valve, current technology and future development. *Proceeding of the fifth scandinavian international conference on fluid power.* Linköping, Sweden). pp99-119.

Backe, W. 1993. Research projects in hydraulics. *Fluid power.* pp1-27.

Bitner, D. and Burton, R. T. 1984. Experimental Measurement of Load Sensing Pump Parameters. *Proceeding of the 40th National Conference on Fluid Powe*r, Chicago, p153.

Bitner, D. and Burton, R. T. 1984. Small Signal Model of a Load Sensing Pump. *Proceeding of the 40th National Conference on Fluid Power,* Chicago, p107.

Bitner, D. 1986. *Analytical and Experimental Analysis of a Load Sensing Pump.* M. Sc. thesis, University of Saskatchewan, Canada.

Bitner, D. 1996. Parameters of the LS pump (Vickers PVE19Q). Fluid Power Laboratory in University of Saskatchewan, Canada.

Book, R. and Goering, C. E. 1997. Load Sensing Hydraulic System Simulation. *Applied Engineering in Agriculture.* ASAE Vol.13(1), p17-25

Borghi, M., Cantore, G., Milani, M. and Paoluzzi, R. 1998. Analysis of Hydraulic Components using Computational Fluid Dynamics Models. *Proceedings of the Institute of Mechanical Engineers*. V212 Part C. pp619.

Chaimowitsch, M. 1967**.** Ölhydraulik: Grundlagen und Anwendung. Veb Verlag Technik Berlin**.**

Coleman, H. W. and Steele, W. G. 1999. *Experimentation and uncertainty analysis for engineers*. Wiley, New York.

Ding, K. 1989. The Simplification of Transfer Function with Literal Coefficients in Hydraulic System. *Proceeding. of the 2nd International Conference on Fluid Power Transmission and Control*. Hangzhou, China, p409.

Dobchuk, J. W., Burton, R.T., Nikiforuk, P. N., and Ukrainetz, P. R. 1999**.** Mathematical Modeling of a Variable Displacement Axial Piston Pump. *Fluid Power Systems and Technology.* ASME. Vol. 6, p1-8.

Dobchuk, J. W., Nikiforuk, P. N., Ukrainetz, P. R. and Burton, R.T., 2000. Effect of Internal Pump Dynamics on Control Piston Pressure Ripple. Presented on the sixth triennial International Symposium on Fluid Power, Measurement and Visualization. Sherbrooke, QC, Canada.

Elfving, M. and Palmberg, J-O. and Jansson, A. 1997. Distributed Control of Fluid Power Actuators - a Load Sensing Application of a Cylinder with Decoupled Chamber Pressure Control. *Proceeding of the Fifth Scandinavian International Conference on Fluid Power, SICFP'97*, Linkoping, Sweden, p159.

Ellman, A. and Piche, R. 1996. A Modified Orifice Flow Formula for Numerical Simulation of Fluid Power Systems. *Fluid Power Systems and Technology, ASME*, Vol. 3, pp59-63.

Erkkila, M. 1999. Practical Modelling of Load-Sensing Systems. *Proceeding of the Sixth Scandinavian International Conference on Fluid Power, SICFP'99*, Tampere, Finland, p445

Friedrichsen, W. 1989. Investigation of the Dynamic Behavior of Hydrostatic Steering in Load-Sensing Hydraulic Systems. *Fluid power treansmission and control--Proc. Of the 2nd international conference*. P361.

Gromala, P., Domagal, M. and Lisowski, E. 2002. Research on Pressure Drop in Hydraulic Components by Means of CFD Method on Example of Control Valve. *Proceedings of the 2nd International FPNI PhD Symposium on Fluid Power*. Modena, Italy.

Huh, J. Y., Burton, R., and Schoenau, G. 2000. Estimation of Friction and Spring Characteristics of a Variable Displacement Pump using the Extended Kalman Filter Approach. *Internal research report* from Fluid power Laboratory of University of Saskatchewan.

Jarboe, H. R. 1983. Agricultural Load-Sensing Hydraulic Systems. ASAE *distinguished lecture series: tractor design*. 16p

Johnson, O. 1991. Load-Sensing Systems Control Speed Accurately. *Hydraulics & pneumatics*. Vol 4 No 3 pp3

Kappl, T.J. 2001. Semiempirical Model for Variable Displacement Pump with Load Sensing Regulator and Power Restrictor. *Proceedings of 2001 ASME International Mechanical Engineering Congress and Exposition*. New York, NY, USA. Nov. 11.

Kauranne, H., Kajaste, J. and Heiskanen, K. 1999. Problems in Using Pressure Controlled Pumps with Long Pipelines? *Proceedings of the 6th Scandinavian International Conference on Fluid Power*. SICFP'99. Tampere, Finland.

Kavanagh, G. P. 1987. The Dynamic Modeling of an Axial Piston Hydraulic Pump. *M.Sc. thesis*, University of Saskatchewan.

Kim, S. D., Cho, H. S. and Lee, C. O., 1987. On the Order Reduction of the Dynamic Model of a Pressure-Compensated Variable Displacement Hydraulic Pump. *Presented at the ASME Winter Annual Meeting.* Boston, Massachusetts, USA, Dec. 13-18.

Kim, S. D., Cho, H. S. and Lee, C. O., 1987. A Parameter Sensitivity Analysis for the Dynamic Model of a Variable Displacement Axial Piston Pump. *Proceedings of Institute of Mechanical Engineers.* Vol 201, No C4, pp235-243.

Kim, S. D. and Cho, H. S. 1988. Stability Analysis of a Load-Sensing Hydraulic System. *Proceedings of Institute of Mechanical Engineering.* Part A. Vol 202 pp79-88.

Kim, S. D. and Cho, H. S. 1991. A Suboptimal Controller Design Method for the Energy Efficiency of a Load-sensing Hydraulic Servo System. *Journal of Dynamics Systems, Measurement, and Control.* Vol. 113, p487-493.

Krus, P. 1988. On Load Sensing Fluid Power Systems. *Dissertation No.198*. Linkoping University, Sweden.

Lantto, B., Palmberg, J.O. and Krus, P. 1990. Static and Dynamic Performance of Mobile Load-sensing Systems with Two Different Types of Pressure-Compensated Valves. *SAE Technical Paper Series*. *SAE*. Sept 10-13, p251.

Lantto, B., Krus, P. and Palmberg, J.O. 1991. Interaction between Loads in Load-sensing Systems. *Proceeding of the 2nd Tampere International Conference on Fluid Power*. Linkoping, Sweden, p53.

Li, J. 1999. Study of Pressure-Compensated Plants of Load Sensing System with one Pump and Multi-load. *Proceedings of the 3rd Scandinavian International conference on fluid power.* P297-301.

Lin, S. J. and Akers, A. 1988. The Control of an Axial Piston Pump: Use of a Two-stage Electrohydraulic Servovalve. *Proceeding of the 43rd National Conference on Fluid Power,* Chicago, p443.

Luomaranta, M. 1999. A Stable Electrohydraulic Load Sensing System Based on a Microcontroller. *Proceedings of The sixth Scandinavian International conference on fluid power.* SICFP'99, Tampere, Finland. P419-432.

Mai, V.K.L. 1982. Dynamic Performance of Hydraulic Control Systems Employing Load-Sensitive Variable Delivery Pump with Single and Multiple Loads. *Ph.D. thesis*, Monash University, Australia.

Mai, V.K.L., and Dransfield, P. 1989. Load-sensitive Pump Control Performance. *Mechanical Engineering Transactions –Institution of Engineers*. ME14(3) p149-157.

Maiti, R, Pan, S. and Bera, D. 1996. Analysis of a Load Sensing Hydraulic Flow Control Valve. *Fluid power--Third JHPS international symposium*. p213.

Mattila, J. 1997. Computed Force Control of Hydraulic Servo drive with a Novel LS-System. *Fluid power transmission and control—Proceedings Of the 4th international conference*. p97.

Merritt, H.E. 1967. *Hydraulic control systems.* John Wiley & Sons, Inc.

Miller, R.W. 1996. *Flow Measurement Engineering Handbook,* 3rd. McGraw-Hill, New York.

Ogata, K. 1970. Modern Control Engineering, Prentice-Hall, Inc., Englewood Cliffs, N.J.

Palmberg, J. O., Krus, P. and Ding, K. 1985. Dynamic Response Characteristics of Pressure-Control Pumps. *The First International Conference on Fluid Power Transmission and Control*. Zhejiang University, Hangzhou, China, p110.

Pettersson, H., Krus, P., Jansson, A. and Palmberg, J.O. 1996. The Design of Pressure Compensators for Load Sensing Hydraulic Systems. UKACC International Conference on Control'96. IEE 427. University of Exeter, UK, p1456.

Pizon, A. and Sikora, K. 1993. Conputer Simulation Research of Load Sensing Systems. *Fluid power treansmission and control--Proceedings. of the 3nd international conference*. p404

Ramachandran,S. and Ukrainetz,P.R. 1985. Performance of a Load Sensing Pump under Multi-Load Conditions. *Proceedings of the First International Conference on Fluid Power Transmission and Control,* Zhejiang University Hangzhou, China, p770-789.

Ruan, J., Burton, R. and Ukrainetz, P., 2002. An Investigation Into the Characteristics of a Two Dimensional "2D" Flow Control Valve. *Journal of Dynamic Systems, Measurement and Control*. Vol. 124. March. pp214-220.

Sakurai, Y. and Takahashi, K. 1997. Modelling and Simulation of a Load Sensing System by Bond-Graph Method. *Proceedings of the fifth scandinavian international conference on fluid power*. Linkoping university. Vol 3, p187-198

Sakurai, Y. and Takahashi, K. 2000. Calculation of Dynamic Overall Efficiency of a Load Sensing Hydraulic System by Bondgraphs. *Proceeding of IECON (Industrial Electronics conference) and the 26th Annual Conference of the IEEE Electronics Society IECON 2000*. p1568-1573

Scholz, D. and Engelhardt, J. 1997. Direct Steady State Calculations of Hydraulic Power Systems. *Proceedings of the fifth scandinavian international conference on flow power SICFP'97*. Linkoping university. Vol 2, p 249

Stallbaumer, R. 1986. Application of Load Sensing Systems on Articulated Manlift Vehicles. *Fluid Power Technology & Systems*. ASE, warrendale, PA. p33-38

Tahler, G. J., 1989. *Automatic Control Systems*. St. Paul West Publish Company.

Ukrainetz, P. R., Bitner, D. and Nikiforuk, P. 1986. Load Interaction in a Multi-Load Load Sensing Pump Driven Hydraulic System. *Proceeding of the 41st national conference on fluid power.* Detroit, April, 29, 1986, pp83-93.

Vescovo, G. D. and Lippolis, A. 2002. Flow Forces Analysis on a Four-way Valve. *Proceedings of the 2nd International FPNI PhD Symposium on Fluid Power* . Modena, Italy.

Viall, E. and Zhang, Q. 2000. Spool Valve Discharge Coefficient Determination. *Proceedings of the 48th National Conference on Fluid Power*. Milwaukee, Wisconsin, USA. pp491.

Wu, D. 2002. Steady State Analysis of the Load Sensing Systems, *Proceeding of the Second International Ph.D. Conference, FPNI*, Modena, Italy, July.

Wu, D., Burton, R., and Schoenau, G., 2002. An Empirical Discharge Coefficient Model for Orifice Flow. *Journal International of Fluid Power*. Vol 3 No 3.

Wu, D., Burton, R., Schoenau, G., and Bitner, D., 2003. Modeling of orifice flow rate at very small openings. *Journal International of Fluid Power*. Vol 4 No1

Zhang, Z. and Hou, S. 1989. Experiment and Research of Model XBPOC-F75FF Pressure-flow Compensated Load-sensing Axial Piston Pump. *Proceeding of the 2nd International Conference on Fluid Power Transmission and Control*. Zhejiang University, Hangzhou, China, p317.

Zarotti, L. G. and Nervegna, N. 1988. Saturation Problems in Load Sensing Architectures. *Proceeding of the 43rd National Conference on Fluid Power, NCFP,* Chicago, p393.

Zarotti, Luca G. and Paoluzzi, R. 1993. Automatic Displacement Controls in Competition. *Fluid Power Transmission and Control--Proceedings of the 3rd international conference*. p235.

Zhang, Z. and Hou, S. 1989. Experiment and Research of Model XBPOC-F75FF Pressure-Flow Compensated Load-Sensing Axial Piston Pump. *Fluid Power Transmission and Control- Proceedings of the 2nd international Conference.* P317-319.

Zhang, Z., Lei, X., Hou, S. and Li, J. 1999**.** The Study of Power-Matching Energy-Saving Hydraulic System. *Fluid power transmission and control—Proceedings of the 3rd international symposium*. p227.

Zheng, X. and Guan, Z., 1993. A Study on Digital Control Constant Pressure Axial Plunger Pump. *Fluid power transmission and control--Proceedings of the 3rd international conference.* p329

Appendix A Linearization of Non-Linear Hydraulic Systems

In this appendix, the linearization process for a non-linear function and non-linear dynamic system are considered. The approach is to present the general form and then illustrate the procedure with common examples found in hydraulic applications.

A.1 Linearization of a Non-Linear Function

Consider the relationship where y is a non-linear function of *x*, $y = f(x)$. This non-linear function can be expressed by the Taylor series for *f(x)* as

$$y = f(x) = f(x_0) + \left.\frac{df}{dx}\right|_{x_0} \Delta x + \left.\frac{d^2 f}{dx^2}\right|_{x_0} \Delta x^2 + \cdots \tag{A.1}$$

Usually, the high order terms are negligible about the steady state operating points as long as the higher order derivatives are not infinite. Thus Equation (A.1) simplifies to

$$y = f(x_0) + \left.\frac{df}{dx}\right|_{x_0} \Delta x$$

or

$$\Delta y = K(x_0)\Delta x \tag{A.2}$$

where $\Delta y = y - f(x_0)$ and $K(x_0) = \left.\frac{df}{dx}\right|_{x_0}$. The linearization can be generally represented as illustrated in Figure A.1. Equation (A.2) is the straight line in Figure A.1 and is tangent to curve *f(x)* at (x_0,y_0). Within a small range about (x_0,y_0), there is little error between the straight line and the curve. It may also be that the output, y, of a component is a non-linear function of two inputs or two independent variables. Similarly, for the case where y is a non-linear function of two variables, this can be expressed as

$$y = f(x,z) = f(x_0,z_0) + \left.\frac{\partial f}{\partial x}\right|_{x_0,z_0}\Delta x + \left.\frac{\partial f}{\partial z}\right|_{x_0,z_0}\Delta z + \left.\frac{\partial^2 f}{\partial x^2}\right|_{x_0,z0}\Delta x^2 + \left.\frac{\partial^2 f}{\partial x \partial z}\right|_{x_0,z0}\Delta x\Delta z + \left.\frac{\partial^2 f}{\partial z^2}\right|_{x_0,z0}\Delta z^2 + \cdots \quad \text{(A.3)}$$

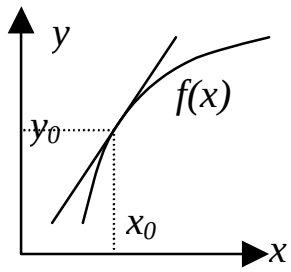

Figure A.1 Linearization of a Non-Linear Function

For small excursions about a steady state operating point [(x_0, z_0), y_0], the items with higher order derivatives are negligible and Equation (A.3) can be simplified to

$$\Delta y = K_1(x_0,z_0)\Delta x + K_2(x_0,z_0)\Delta z \quad \text{(A.4)}$$

where $\Delta y = y - f(x_0,z_0), K_1(x_0,z_0) = \left.\frac{\partial f}{\partial x}\right|_{(x_0,z_0)}$, $K_2(x_0,z_0) = \left.\frac{\partial f}{\partial z}\right|_{(x_0,z_0)}$

Consider an example involving a hydraulic system in which valve flow, Q, is a function of valve opening, x, and the pressure drop, P, across the valve orifice. Mathematically, this is given by

$$Q = f(x,P) = C_d w x\sqrt{\frac{2}{\rho}P} \quad \text{(A.5)}$$

where w is the width of rectangular-shaped orifice, C_d the discharge coefficient of the valve orifice and ρ the density of fluid oil. The linearization model for small variations Δx and ΔP about a steady state operating point (x_0, P_0) is

$$\Delta Q = K_q(x_0,P_0)\Delta x + K_c(x_0,P_0)\Delta P \quad \text{(A.6)}$$

where $K_q(x_0, P_0) = K_q(P_0) = C_d w\sqrt{\frac{2}{\rho}P_0}$ is the flow gain and $K_c(x_0, P_0) = \frac{C_d w x_0}{\sqrt{2\rho P_0}}$ is the flow-pressure coefficient of the valve orifice.

A.2 Linearization of a Simple Non-Linear Dynamic System

A non-linear dynamic system may consist of one or more non-linear components with dynamic parameters. The generic form of the model of a simple non-linear system can be expressed as

$$f(\dot{x}, x, u) = 0 \tag{A.7}$$

where x is the state variable, $\dot{x}$ the time derivative of state variable and u is the input variable. Linearization of Equation (A.7) (retaining only first order terms) gives

$$\left.\frac{\partial f}{\partial \dot{x}}\right|_{\dot{x}_0, x_0, u_0} \Delta\dot{x} + \left.\frac{\partial f}{\partial x}\right|_{\dot{x}_0, x_0, u_0} \Delta x + \left.\frac{\partial f}{\partial u}\right|_{\dot{x}_0, x_0, u_0} \Delta u = 0 \tag{A.8}$$

or

$$\Delta\dot{x} = K_x \Delta x + K_u \Delta u \tag{A.9}$$

where the linearization coefficients are $K_x = -\frac{\left.\frac{\partial f}{\partial x}\right|_{\dot{x}_0, x_0, u_0}}{\left.\frac{\partial f}{\partial \dot{x}}\right|_{\dot{x}_0, x_0, u_0}}$ and $K_u = -\frac{\left.\frac{\partial f}{\partial u}\right|_{\dot{x}_0, x_0, u_0}}{\left.\frac{\partial f}{\partial \dot{x}}\right|_{\dot{x}_0, x_0, u_0}}$, if $\left.\frac{\partial f}{\partial \dot{x}}\right|_{\dot{x}_0, x_0, u_0} \neq 0$. When $\left.\frac{\partial f}{\partial \dot{x}}\right|_{\dot{x}_0, x_0, u_0} = 0$, the system is no longer a dynamic system and this linearization has no physical meaning.

Consider the simple hydraulic system shown in Figure A.2. Assume that the upstream pressure, P_s, of the flow control orifice is constant. The damping coefficient,

B_m, of the load is also assumed constant. The inertia of the motor and load and the leakage are considered to be negligible. The dynamic equations of the system can thus be expressed by

$$Q = C_d w x \sqrt{\frac{2}{\rho}(P_s - P_L)} \tag{A.10}$$

$$\dot{P}_L = \frac{\beta}{V}(Q - D_m \dot{\theta}) \tag{A.11}$$

$$B_m \dot{\theta} = D_m P_L \tag{A.12}$$

where w, C_d and ρ are explained previously in Equation (A.5). β is the bulk modulus of hydraulic oil, D_m the volumetric displacement of the motor and V the volume of the inlet chamber of the motor.

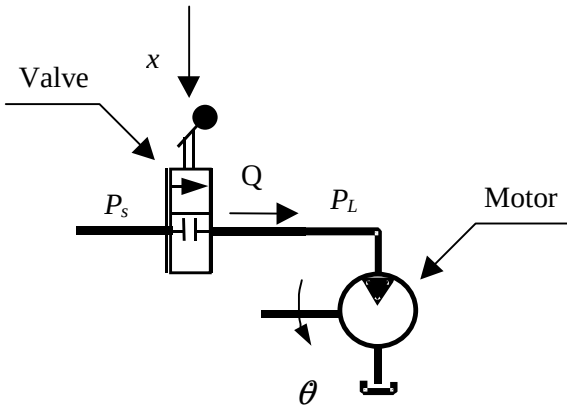

Figure A.2 A Valve- Motor Control System

Substituting Equations (A.10) and (A.12) into Equation (A.11), a non-linear dynamic equation is obtained given by

$$f(\dot{P}_L, P_L, x) = \dot{P}_L - \frac{\beta}{V}\left(C_d w x \sqrt{\frac{2}{\rho}(P_s - P_L)} - \frac{D_m^2}{B_m} P_L \right) = 0 \tag{A.13}$$

where load pressure, P_L, is the state variable, $\dot{P}_L$ is the time derivative of the state variable and x is the control input to the system. The linearization model of the non-linear dynamic system can be described as

$$\Delta\dot{P}_L = K_p \Delta P_L + K_x \Delta x \tag{A.14}$$

where

$$K_p = -\frac{\beta}{V}\left(\frac{C_d w x_0}{\sqrt{2\rho(P_s - P_{L0})}} + \frac{D_m^2}{B_m} \right) \tag{A.15}$$

$$K_x = \frac{\beta C_d w}{V}\sqrt{\frac{2}{\rho}(P_s - P_{L0})} \tag{A.16}$$

A.3 Generic Formulation of the Linearization of a Non-Linear Dynamic System

Most control systems in industry are non-linear and complex, such as LSPC hydraulic systems, robot control systems, etc. The system variables and inputs are sometimes coupled. The motion of a system may be described by more than one non-linear equation. For example, it could be described as

$$\begin{cases} f_1(\dot{x}_1, \dot{x}_2, \cdots \dot{x}_n; x_1, x_2, \cdots x_n; u_1, u_2, \cdots u_m) = 0 \\ f_2(\dot{x}_1, \dot{x}_2, \cdots \dot{x}_n; x_1, x_2, \cdots x_n; u_1, u_2, \cdots u_m) = 0 \\ \\ f_n(\dot{x}_1, \dot{x}_2, \cdots \dot{x}_n; x_1, x_2, \cdots x_n; u_1, u_2, \cdots u_m) = 0 \end{cases} \tag{A.17}$$

$$\begin{cases} y_1 = g_1(\dot{x}_1, \dot{x}_2, \cdots \dot{x}_n; x_1, x_2, \cdots x_n; u_1, u_2, \cdots u_m) \\ y_2 = g_2(\dot{x}_1, \dot{x}_2, \cdots \dot{x}_n; x_1, x_2, \cdots x_n; u_1, u_2, \cdots u_m) \\ \vdots \\ y_p = g_p(\dot{x}_1, \dot{x}_2, \cdots \dot{x}_n; x_1, x_2, \cdots x_n; u_1, u_2, \cdots u_m) \end{cases} \tag{A.18}$$

In Equations (A.17) and (A.18), n is the number of system dynamic equations or state variables, x_i (i=1 ..n), m is the number of input variables, u_i (i=1 ..m), and p is the number of the output variable y_i (i=1 ..p). The system represented by Equations (A.17) and (A.18) is defined as multi-input, multi-output (MIMO) system. The system control Equations (A.17) and (A.18) can be re-written in a matrix format as

$$F\left(\dot{X}, X, U\right) = 0 \tag{A.19}$$

$$Y = g\left(\dot{X}, X, U\right) \tag{A.20}$$

Equation (A.19) and (A.20) can be linearized as

$$\left.\frac{\partial F}{\partial \dot{X}}\right|_{op} \Delta\dot{X} + \left.\frac{\partial F}{\partial X}\right|_{op} \Delta X + \left.\frac{\partial F}{\partial U}\right|_{op} \Delta U = 0 \tag{A.21}$$

$$\Delta Y = \left.\frac{\partial g}{\partial \dot{X}}\right|_{op} \Delta\dot{X} + \left.\frac{\partial g}{\partial X}\right|_{op} \Delta X + \left.\frac{\partial g}{\partial U}\right|_{op} \Delta U \tag{A.22}$$

where $\left.\frac{\partial F}{\partial \dot{X}}\right|_{op}$ and $\left.\frac{\partial F}{\partial X}\right|_{op}$ are n×n matrices, $\left.\frac{\partial F}{\partial U}\right|_{op}$ is a n×m matrix. $\left.\frac{\partial g}{\partial \dot{X}}\right|_{op}$ and $\left.\frac{\partial g}{\partial X}\right|_{op}$ are 1×n matrices, $\left.\frac{\partial g}{\partial U}\right|_{op}$ is a 1×m matrix as shown in detail below.

$$\left.\frac{\partial F}{\partial \dot{X}}\right|_{op} = \left[\begin{array}{cccc} \frac{\partial f_1}{\partial \dot{x}_1} & \frac{\partial f_1}{\partial \dot{x}_2} & \cdots & \frac{\partial f_1}{\partial \dot{x}_n} \\ \frac{\partial f_2}{\partial \dot{x}_1} & \frac{\partial f_2}{\partial \dot{x}_2} & \cdots & \frac{\partial f_2}{\partial \dot{x}_n} \\ \vdots & \vdots & \ddots & \\ \frac{\partial f_n}{\partial \dot{x}_1} & \frac{\partial f_n}{\partial \dot{x}_2} & \cdots & \frac{\partial f_n}{\partial \dot{x}_n} \end{array}\right]_{op}, \quad \left.\frac{\partial F}{\partial X}\right|_{op} = \left[\begin{array}{cccc} \frac{\partial f_1}{\partial x_1} & \frac{\partial f_1}{\partial x_2} & \cdots & \frac{\partial f_1}{\partial x_n} \\ \frac{\partial f_2}{\partial x_1} & \frac{\partial f_2}{\partial x_2} & \cdots & \frac{\partial f_2}{\partial x_n} \\ \vdots & \vdots & \ddots & \\ \frac{\partial f_n}{\partial x_1} & \frac{\partial f_n}{\partial x_2} & \cdots & \frac{\partial f_n}{\partial x_n} \end{array}\right]_{op}$$

$$\left.\frac{\partial F}{\partial U}\right|_{op} = \left[\begin{array}{cccc} \frac{\partial f_1}{\partial u_1} & \frac{\partial f_1}{\partial u_2} & \cdots & \frac{\partial f_1}{\partial u_m} \\ \frac{\partial f_2}{\partial u_1} & \frac{\partial f_2}{\partial u_2} & \cdots & \frac{\partial f_2}{\partial u_m} \\ \vdots & \vdots & \ddots & \\ \frac{\partial f_n}{\partial u_1} & \frac{\partial f_n}{\partial u_2} & \cdots & \frac{\partial f_n}{\partial u_m} \end{array}\right]_{op}, \quad \left.\frac{\partial g}{\partial \dot{X}}\right|_{op} = \left[\begin{array}{cccc} \frac{\partial g}{\partial \dot{x}_1} & \frac{\partial g}{\partial \dot{x}_2} & \cdots & \frac{\partial g}{\partial \dot{x}_n} \end{array}\right]$$

$$\left.\frac{\partial g}{\partial X}\right|_{op} = \left[\begin{array}{cccc} \frac{\partial g}{\partial x_1} & \frac{\partial g}{\partial x_2} & \cdots & \frac{\partial g}{\partial x_n} \end{array}\right], \quad \left.\frac{\partial g}{\partial U}\right|_{op} = \left[\begin{array}{cccc} \frac{\partial g}{\partial u_1} & \frac{\partial g}{\partial u_2} & \cdots & \frac{\partial g}{\partial u_m} \end{array}\right]$$

As long as the inverse matrix of $\left.\frac{\partial F}{\partial \dot{X}}\right|_{op}$ exists, the linearized Equations (A.21) and (A.22) can be expressed in a generic form as

$$\Delta \dot{X} = A\Delta X + B\Delta U \tag{A.23}$$

$$\Delta Y = C\Delta X + D\Delta U \tag{A.24}$$

where

$$A = \left(\left.\frac{\partial F}{\partial \dot{X}}\right|_{op}\right)^{-1} \left.\frac{\partial F}{\partial X}\right|_{op} \qquad (n \times n) \tag{A.25}$$

$$B = \left(\left.\frac{\partial F}{\partial \dot{X}}\right|_{op}\right)^{-1} \left.\frac{\partial F}{\partial U}\right|_{op} \qquad (n \times m) \tag{A.26}$$

$$C = \left(\left.\frac{\partial g}{\partial X}\right|_{op} + \left.\frac{\partial g}{\partial \dot{X}}\right|_{op} \cdot A\right) \qquad (1 \times n) \tag{A.27}$$

$$D = \left(\left.\frac{\partial g}{\partial U}\right|_{op} + \left.\frac{\partial g}{\partial \dot{X}}\right|_{op} \cdot B\right) \qquad (1 \times m) \tag{A.28}$$

For convenience, the "Δ" is often dropped from Equations (A.22) and (A.23) yielding

$$\dot{X} = AX + BU \tag{A.29}$$

$$Y = CX + DU \tag{A.30}$$

Equations (A.29) and (A.30) are a common generalized form of the state space model of dynamic systems. In this case, the matrixes A, B, C, and D are dependent on the steady state operating point. Within small variations about a particular steady state operating point, these parameter matrixes can be regarded as being invariant. Thus, a complex non-linear system can be subjected to linear system theory, including frequency domain analysis.

Equations (A.29) and (A.30) can usually be used to analyze the dynamic behavior in the frequency domain. Matlab® software has provided many functions which can be directly used for Equations (A.29) and (A.30) to illustrate the result of the frequency response in the way of a Bode diagram or a root locus. This is a direct method. Another method is the traditional frequency analysis method — transfer function (TF) analysis. The second method requires (1) to do the Laplace transform to Equations (A.29) and (A.30); (2) to present all Laplace transform equations in block diagrams; (3) to simplify these block diagrams, if necessary; (4) to develop the TF of the system; and (5) to illustrate the TF in a Bode diagram or the root locus. It seems that, comparing to the first method, the second method has some extra steps ((1), (2), (3) and (4)). In fact, the second method can help to provide a thorough understanding and subsequent simplification for the physical system, especially for systems with high non-linearities. Therefore, this thesis will use the second method.

Appendix B Calibration of Measurement System of the Load Sensing System

B.1 Pressure sensing calibration—measurement of pump, control and load pressures

Three pressures (P_s, P_y, and P_L) are measured using three sets of variable inductance type of pressure transducers (Model: DP15 differential pressure transducer) and specialized signal conditioning amplifiers by Validyne Engineering Corporation (Model: CD15 sine wave carrier demodulator). The signal conditioner applies a 5kHz sinusoidal wave excitation to two inductance ratio arms of the pressure transducer. The resulting output of the transducer is demodulated and amplified using the integrated circuit. The DC output is obtained from an active filter circuit and gives a uniform response from steady state to 1000 Hz. The DC output is read by the DAQ system directly connected to computer.

The system is calibrated using a deadweight tester [model 5525]. Selected weights (representing pressure) are applied to the tester and the output voltage recorded. The results of this procedure are shown for one transducer in Figure B.1. The calibration curve shown is, in fact, four calibration curves in which two are obtained before the experiment was started and the other two after the tests was completed. The calibration curve shown in Figure B.1 indicates that the measurement gain is 1V per 300 psi. The scatter associated with the four measurements is shown on an expended scale on Figure B.1. The scatter lies within a range of ±0.01V which corresponds to an error band of

±0.02MPa. The calibration also indicates that no difference exists in the calibration before and after the experiments were conducted.

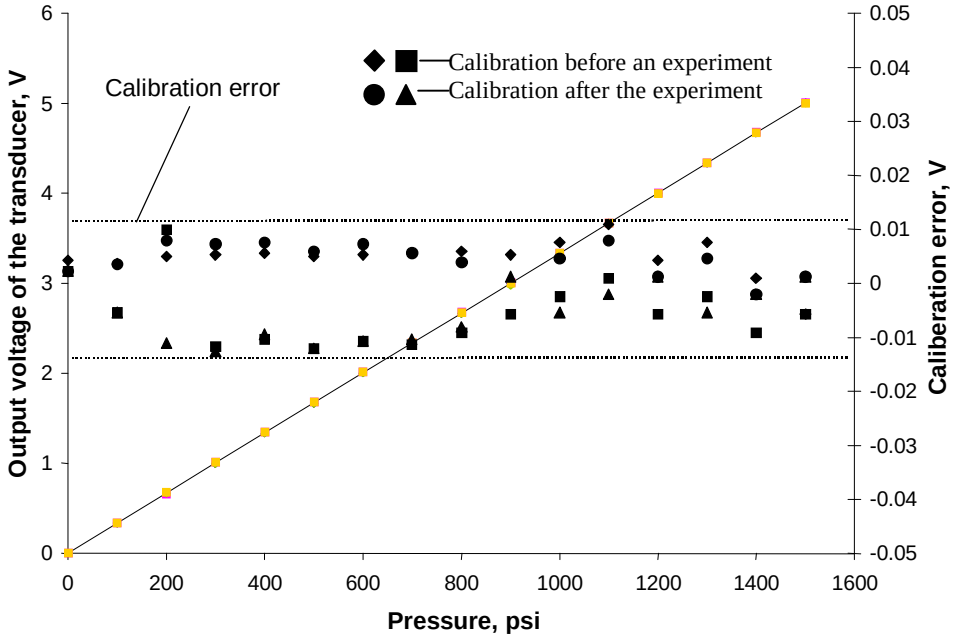

Figure B.1 Calibration of one of the pressure transducers

B.2 Angular position transducer calibration—measurements of the pump swash plate angle

The swash plate angle is measured by a RVDT (Rotary Variable Differential Transformer, R30D). The output of the transducer produces a voltage whose magnitude varies linearly with the angular position of the shaft. The DC-operated RVDT accepts a DC input voltage that is internally converted to an AC carrier signal to excite the primary coil. An integral demodulator and filter converts the signal which is subsequently amplified.

The calibration of the transducer is based on data provided by the manufacturer. Calibration in the laboratory was not possible due to the precision of the calibration

equipment which would be required to do this. Such equipment was not available in our laboratory. The RVDT operates within a range of ± 40° with a linearity (the maximum deviation from a straight line fit over the full range) less than ±0.5 percent. However, over smaller angular displacements, linearity improves substantially. For this application, the maximum of the swash plate angle is 18° (0.314 radian) when the pump is fully stroked. The calibration of this transducer over the full range is shown in Figure B.2. The calibration error which is expressed as a function of deviation of the experimental points from a least square best fit of these points is also shown in this figure. The maximum deviation at any point is within ±0.04V and the maximum deviation in the range of operation is less than ±0.01V.

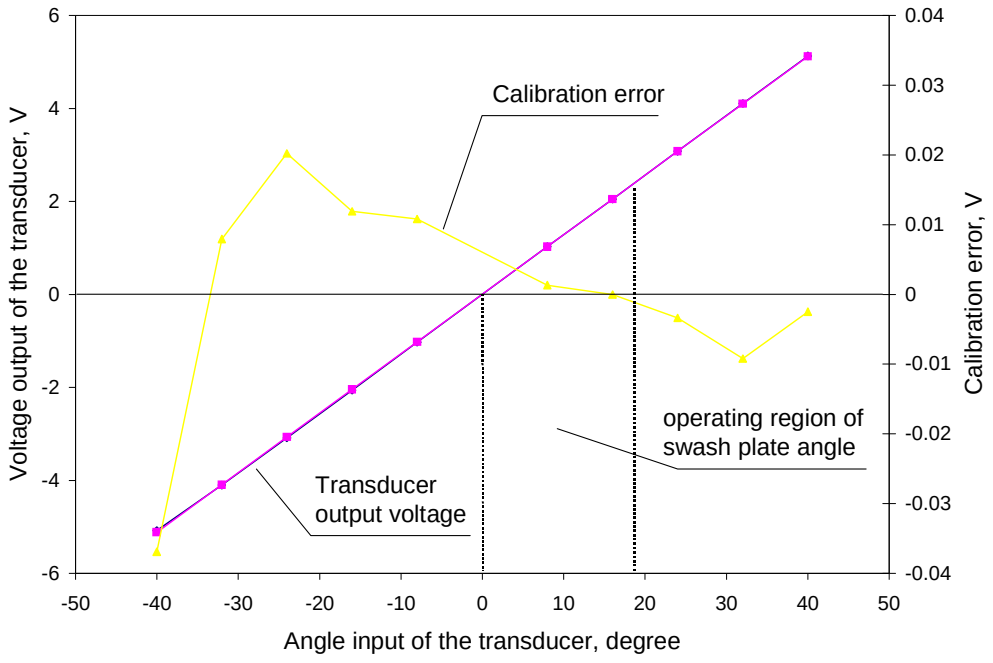

Figure B.2 Calibration curve of the RVDT (R30D)--angular position transducer

B.3 Proximitor sensor calibration — measurement of the LS spool displacement

The spool displacement of the LS pressure regulator is measured by a proximitor which consists of a signal conditioning circuit (model: Bently Proximitor 3106) and an eddy current probe (model: Bently Probe 306J). The Bently Probe is mounted at the end of the LS spool sleeve and is driven by the signal from the Proximitor (see Figure B.3). The displacement measurement is derived directly from the end of the transducer to the nearest conductive body (spool) facing the probe. The output voltage is highest at high gap distances, decreasing toward a zero level as the gap decreases. The output voltage readings are not affected by the gap medium, in this case — hydraulic oil. Installation of the probe and the amount of the gap spacing for the null position of the spool is based on a trade-off between the resolution of the transducer and probe safety. If the gap between the probe and spool end is too large (to protect the probe from contacting the spool under any circumstances), the probe would operate in a non-linear (saturation) region where the signal produced by the spool motion is almost independent of the spool displacement. To obtain the best probe sensitivity, the gap should be small. But the spool would contact the probe during expected oscillations. Based on an assumed maximum displacement of the spool and the actual null position of the spool, the gap was set to be 1.6 mm.

Before calibrating the probe (Figure B.3), the probe must be seated into the casing by pressurizing the probe at port P_s. When the system was pressurized for the first time, some plastic and elastic deformation in the seat between the probe and the casing may be expected. Since plastic deformation occurs only once, any subsequent deformation upon pressurization would be elastic in behavior. The comparison of experiments before

seating and after (fist time pressurization) indicated that the plastic deformation was in the order of 0.29 mm.

Two possible factors might affect the elastic deformation of the probe; the pressure, P_s, and temperature, T, of the hydraulic oil. Increasing P_s could result in a small longitudinal elastic deformation of the probe head and spool metal. To determine this, another experiment using a fixed spool was conducted to check the effect of P_s. The results of this experiment indicated that a small elastic deformation did exist with a pressure sensitivity of 0.002 mm/MPa. Thus, the maximum elastic deformation at 10MPa was 0.02mm which is only a 1% error over the expected measurement range of ±1mm.

Temperature can affect the measurement of the spool displacement via the thermal expansion of the spool metal. A calculation indicated that the maximum expansion of the spool (for the length of 50mm) with 25 ~ 45°C is 0.01 mm which is only about 0.5% of the measurement range of ±1mm. Therefore, the effects of the pressure and temperature on the measurement of the spool position were considered negligible.

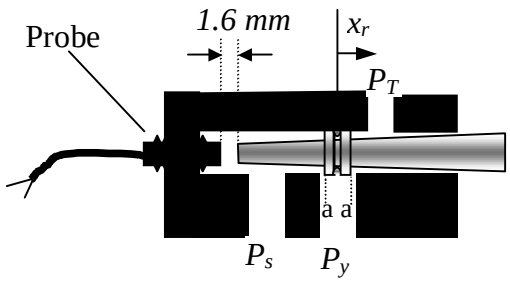

Figure B.3 Measurement of the LS spool displacement

Figure B.4 shows the calibration of the measurement system for LS spool displacement. The null position was considered as the origin point of coordinate x_r. It was identified visually. The calibration curve of Figure B.4 presents a significant

nonlinearity. Normally, the spool operates at the null position where the output voltage of the proximitor is about –3.64 V and the sensitivity is 0.577 V/mm. The fitting error of the polynomial function of the spool displacement is also shown in the secondary axis. The deviation is within ±0.5mV.

Because the null point was done visually, it is quite possible that a “bias” could exist in the actual calculation curve.

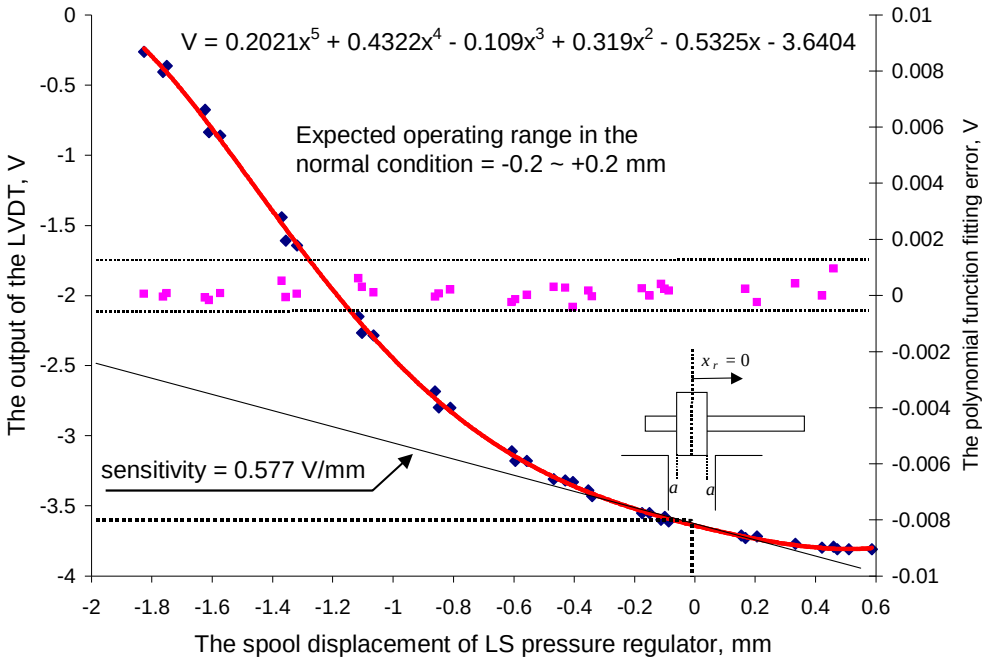

Figure B.4 Calibration of the LS spool position measurement

Appendix C An Empirical Discharge Coefficient Model for Orifice Flow

(Reprinted from *International Journal of Fluid Power*, Vol. 3, No. 3)

An Empirical Discharge Coefficient Model for Orifice Flow

D. Wu, R. Burton, and G. Schoenau

Department of Mechanical Engineering, University of Saskatchewan
57 Campus Drive, Saskatoon, Saskatchewan, Canada, S7N 5A9
duw612@mail.usask.ca

Abstract

In fluid power systems, flow control is mainly achieved by throttling the flow across valve orifices. Lumped parameter models are generally used to model the flow in these systems. The basic orifice flow equation, derived from Bernoulli's equation of flow, is proportional to the orifice sectional area and the square root of the pressure drop and is used to model the orifice coefficient of proportionality. The discharge coefficient, C_d, is often modeled as being constant in value, independent of Reynolds number.

However, for very small orifice openings, C_d varies significantly and can result in substantial error if assumed constant. In this situation, modelers usually revert to graphs or look–up tables to determine C_d. This paper provides a closed form model for C_d as a function of the Reynolds number which can be applied to different types of orifices. Based on this model, a technique to evaluate flow given an orifice area and pressure drop without having to use iteration is introduced.

Keywords: fluid power, hydraulic, flow control, orifice equation, discharge coefficient, Reynolds number

1 Introduction

The well known equation of the volumetric flow rate through an orifice (Fig. 1) is derived from Bernoulli's equation by assuming (1) an incompressible fluid and (2) turbulent flow as

$$Q = C_d A \sqrt{\frac{2}{\rho}(P_u - P_{vc})} \tag{1}$$

where

$$C_d = \frac{C_v C_c}{\sqrt{1 - C_c^2 (A/A_u)^2}} \tag{2}$$

C_v: flow velocity coefficient (approximately 0.98).

C_c: area contraction coefficient (equal to A_{vc}/A). For sharp-edged orifices, it is 0.611.

A_{vc}, the cross-sectional area at *vena contracta*.

A_u, the cross-sectional area at upstream.

P_u, the pressure at upstream.

P_{vc}, the pressure at vena contracta.

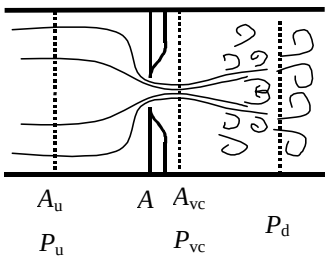

Fig. 1: *Flow through a sharp-edged orifice*

Because A_u is much larger than A, the discharge coefficient, C_d, is almost equal to $C_v C_c$.

Because in many situations, the flow through an orifice is turbulent, the discharge coefficient, C_d, is commonly considered as a constant. Application of Eq. 1 can also be extended to the case of laminar flow. In this case, the discharge coefficient is a function of the Reynolds number as well as the orifice geometry and is

usually determined by experimental methods and presented graphically [Merritt, 1967]. Viall et al [2000] experimentally determined the discharge coefficient of a typical spool valve. Borghi et al [1998] and Vescovo et al [2002] employed computational fluid dynamics (CFD) models to numerically compute the discharge coefficient and compared the computational and experimental results. None of these studies or other CFD studies [Ellman et al, 1996; Gromala et al, 2002], etc. developed a functional relationship between the discharge coefficient and Reynolds number. A main reason is that the Reynolds number also depends on the flow rate requiring an iterative numerical solution [Miller, 1996].

This paper provides an empirical model of the discharge coefficient with respect to square root of Reynolds number. This empirical model can be directly applied to traditional graphically-expressed functions, $C_d = f(\sqrt{\mathrm{Re}})$, for sharp-edged orifices (such as that provided by Merritt [1967]), or to experimentally derived discharge coefficients (such as that provided in this paper). The paper will also consider the determination of parameters in the generalized empirical model for an orifice. Finally, a new calculation method for the flow rate, which does not need iteration, with the empirical model is developed.

2 Empirical modelling of discharge coefficient for orifices

From the literature, it is well known that there is a transition in a plot of discharge coefficient vs. $\sqrt{\mathrm{Re}}$ from being proportional to the square root of the Reynolds number, *Re*, at low Reynolds number, to being constant at high *Re*. Although the curve shapes vary as the orifice geometry varies, they can be approximated by an empirical model as an exponential function, i.e:

$$C_d = C_{d\infty}\left(1 - e^{-\frac{\delta}{C_{d\infty}}\sqrt{\mathrm{Re}}}\right) \tag{3}$$

where $C_{d\infty}$ is the turbulent discharge coefficient for a specific orifice. δ is a laminar discharge coefficient, and is similar to the coefficient introduced graphically by Merritt [1967].

Eq. 3 is simple and the two parameters have a clear physical interpretation. $C_{d\infty}$ is the turbulent discharge coefficient because C_d converges to $C_{d\infty}$ for high Reynolds numbers. δ is called as "laminar discharge coefficient" because Eq. 3 can be approximated by $C_d = \delta\sqrt{\mathrm{Re}}$ at very small Reynolds numbers ($\left.\frac{\partial C_d}{\partial\sqrt{\mathrm{Re}}}\right|_{\sqrt{\mathrm{Re}}=0} = \delta$). However, Eq. 3 cannot always be satisfied for a variety of orifices with different geometries, especially when fitting the transition from the laminar flow to turbulent flow.
Therefore, another form of the discharge coefficient is proposed as

$$C_d = C_{d\infty}\left(1 + ae^{-\frac{\delta_1}{C_{d\infty}}\sqrt{\mathrm{Re}}} + be^{-\frac{\delta_2}{C_{d\infty}}\sqrt{\mathrm{Re}}}\right) \tag{4}$$

where the parameters, a, b, δ_1 and δ_2 are specific flow dependent coefficients to be determined. Eq. 4 can be applied to most types of orifice.

Three types of orifices with the different geometries shown in Fig. 2 are modeled using the generalized empirical model (Eq. 4). The sharp-edged orifice (Fig. 2(a)) has zero length and near 180° trumpet mouth downstream. The spool orifice (Fig. 2(b)) has a 90° downstream mouth. The needle orifice (Fig. 2(c)) has a downstream mouth less than 90°. The shape of discharge coefficient curves for each would be different and it is now necessary to consider the application of the empirical model (Eq. 4) to these typical orifices.

(a) Sharp-edged Orifice (b) Sharp-edged spool orifice (c) Needle valve orifice

Fig. 2: *Three types of orifice*

2.1 Application of the empirical model to typical curve of discharge coefficient

Merritt [1967] has presented a "smooth" discharge coefficient curve with respect to square root of Reynolds number for a typical sharp-edged orifice (Fig. 2(a)). This smooth curve has been generated from experimental data. For this curve, the parameters, a, b, δ_1 and δ_2 in Eq. 4 can be determined using the following mathematical manipulation. The laminar discharge coefficient, δ, the turbulent discharge coefficient, $C_{d\infty}$, and the maximum discharge coefficient, C_{dm}, at a specific Reynolds number, Re_m, can be found by applying an appropriate measurement on a given curve. The four parameters, a, b, δ_1, and δ_2 can be solved by applying the following four conditions common to most types of orifices;

1. Initial condition.

$$C_d\big|_{\sqrt{\mathrm{Re}}=0} = 1 + a + b = 0 \tag{5}$$

2. Laminar discharge coefficient condition:

$$\left.\frac{\partial C_d}{\partial\sqrt{\mathrm{Re}}}\right|_{\sqrt{\mathrm{Re}}=0} = -a\delta_1 - b\delta_2 = \delta \tag{6}$$

For a sharp edged orifice, $\delta \approx 0.2$.

3. Maximum value conditions

$$C_{\mathrm{dm}} = C_{\mathrm{d}\infty}\left(1 + ae^{-\frac{\delta_1}{C_{\mathrm{d}\infty}}\sqrt{\mathrm{Re_m}}} + be^{-\frac{\delta_2}{C_{\mathrm{d}\infty}}\sqrt{\mathrm{Re_m}}}\right) \tag{7}$$

and

$$\left.\frac{\partial C_{\mathrm{d}}}{\partial\sqrt{\mathrm{Re}}}\right|_{\sqrt{\mathrm{Re_m}}} = -a\delta_1 e^{-\frac{\delta_1}{C_{\mathrm{d}\infty}}\sqrt{\mathrm{Re_m}}} - b\delta_2 e^{-\frac{\delta_2}{C_{\mathrm{d}\infty}}\sqrt{\mathrm{Re_m}}} = 0 \tag{8}$$

Eqs. 5 through 8 can be solved to determine *a*, *b*, δ_1, and δ_2. These equations can be simplified into a non-linear algebraic equation of δ_1 as

$$\delta_1 = \frac{\delta e^{-\frac{\delta_2}{C_{\mathrm{d}\infty}}\sqrt{\mathrm{Re_m}}}}{\frac{C_{\mathrm{dm}}}{C_{\mathrm{d}\infty}} - 1 + e^{-\frac{\delta_2}{C_{\mathrm{d}\infty}}\sqrt{\mathrm{Re_m}}}} \tag{9}$$

where

$$\delta_2 = \frac{\delta e^{-\frac{\delta_1}{C_{\mathrm{d}\infty}}\sqrt{\mathrm{Re_m}}}}{\frac{C_{\mathrm{dm}}}{C_{\mathrm{d}\infty}} - 1 + e^{-\frac{\delta_1}{C_{\mathrm{d}\infty}}\sqrt{\mathrm{Re_m}}}} \tag{10}$$

Eqs.9 and 10 can be solved numerically. Parameters, *a* and *b*, can be determined by

$$a = \frac{\delta - \delta_2}{\delta_2 - \delta_1} \tag{11}$$

$$b = \frac{\delta - \delta_1}{\delta_1 - \delta_2} \tag{12}$$

Note that a maximum value of discharge coefficient does not always exist in the transition region from the laminar to the turbulent flow. In this case, Re_{m} can be considered to be an intersecting point of two asymptote lines for the laminar and turbulent flow regions. Thus, the right hand side of Eq. 8 would not be zero, but some finite value, $\dot{C}_{\mathrm{dm}}$. Eqs. 9 and 10 then become

$$\delta_1 = \frac{\delta e^{-\frac{\delta_2}{C_{\mathrm{d}\infty}}\sqrt{\mathrm{Re}_m}} - \dot{C}_{\mathrm{dm}}}{\frac{C_{\mathrm{dm}}}{C_{\mathrm{d}\infty}} - 1 + e^{-\frac{\delta_2}{C_{\mathrm{d}\infty}}\sqrt{\mathrm{Re_m}}}} \tag{13}$$

and

$$\delta_2 = \frac{\delta e^{-\frac{\delta_1}{C_{\mathrm{d}\infty}}\sqrt{\mathrm{Re_m}}} - \dot{C}_{\mathrm{dm}}}{\frac{C_{\mathrm{dm}}}{C_{\mathrm{d}\infty}} - 1 + e^{-\frac{\delta_1}{C_{\mathrm{d}\infty}}\sqrt{\mathrm{Re_m}}}} \tag{14}$$

The method is applied to the typical discharge coefficient curve given by Merritt [1967] (pp44). The input and output parameters for the model calculations are listed in Table 1.

Table 1 Empirical model parameters for a typical coefficient curve

Input Parameters	$C_{\mathrm{d}\infty}$	δ	C_{dm}	$\sqrt{\mathrm{Re_m}}$
	0.61	0.23	0.69	11
Output Parameters	A	b	δ_1	δ_2
	1.07	-2.07	0.077	0.15

Using these parameters, the empirical model of the discharge coefficient for Merritt's curve becomes

$$C_{\mathrm{d}} = 0.61\left(1 + 1.07e^{-0.126\sqrt{\mathrm{Re}}} - 2.07e^{-0.246\sqrt{\mathrm{Re}}}\right) \tag{15}$$

and is shown in Fig. 3. Excellent agreement between the original curve and the empirical model predictions is obtained.

2.2 Application of the empirical model to experimental data plot of discharge coefficient

Although Fig. 3 is a commonly used plot of discharge coefficient for a sharp-edged orifice, in practice, the clearance, chamfer, and other factors of valves (due to machining accuracy limitation) generate a different shaped curve. Thus, it is necessary to measure the discharge coefficient for the orifice of specific valves. The method of the experimental determination of the discharge coefficient, C_{d}, and the corresponding Reynolds number, *Re*, for an orifice are also based on the general flow equations:

$$C_{\mathrm{d}} = \frac{Q}{A\sqrt{\frac{2}{\rho}\Delta P}} \tag{16}$$

$$\mathrm{Re} = \frac{\rho\left(Q/A\right)D_{\mathrm{h}}}{\mu} \tag{17}$$

where Q is the flow rate through the orifice, A is the cross-sectional area of the orifice, ΔP is the pressure drop cross the orifice, D_{h} is the hydraulic diameter, ρ is the fluid density and μ is the fluid absolute viscosity.

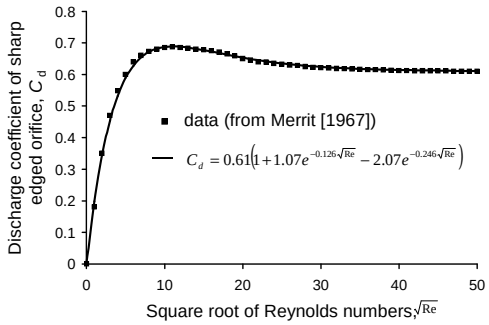

Fig. 3: *Comparison between typical discharge coefficient and the empirical model predictions*

The experimental hydraulic circuit was so designed such that the pressure differential, ΔP, of the tested

orifice could be adjusted. In order to create a variety of flow conditions, each of the orifice opening, x, the fluid temperature, T, and the pressure differential, ΔP, was set at different levels to carry out the experiment. The purpose of varying the fluid temperature, T, was to change in a controlled form, the fluid absolute viscosity, μ. The three variables were selected so that the orifice flow condition could span the laminar, the transient and turbulent regions. For these different flow conditions through the orifice, Q, ΔP, x, and T, are measurable. A and D_h can be calculated from x, based on the orifice geometry. Consequently, the discharge coefficient, C_d, and the Reynolds number, Re, can be determined from Eqs. 16 and 17.

Experimental results for the discharge coefficient for a specific sharp-edged spool orifice used in the study are given in Fig. 4. The data was obtained for the fixed orifice of a PC valve manufactured by Brand Hydraulics Inc (model: EFC12-10-12).

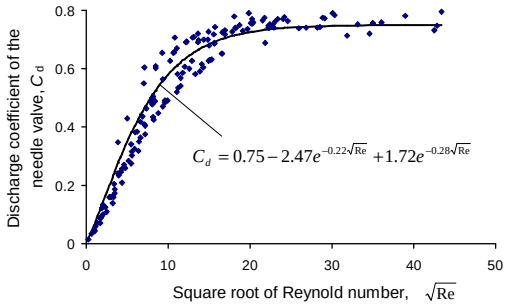

Fig. 5: *Comparison between the measured results and empirical model of the discharge coefficient for a typical needle valve orifice*

The discharge coefficient of a typical needle valve orifice was also experimentally determined (Fig.5) for a ¾" needle valve manufactured by Deltrol Fluid Prod (Model: EN-35).

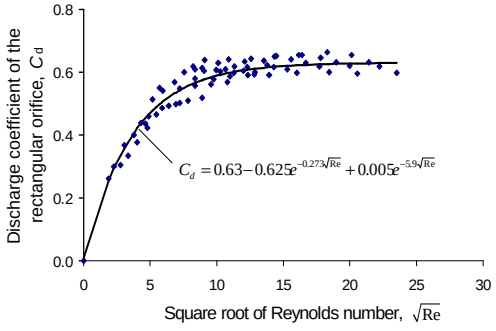

Fig. 4: *Comparison between the measured results and empirical model of the discharge coefficient for a typical sharp-edged spool orifice*

Consider the application of the empirical model to these two experimental results. It is noted that the mathematical method introduced in Section 2.1 cannot be applied to these experimental data because the input parameters, $C_{d\infty}$, δ, $\mathrm{Re_m}$, C_{dm}, and $\dot{C}_{dm}$, cannot be accurately measured from the plot of the experimental data. Therefore, an alternate technical method is introduced to evaluate the various coefficients from experimental data with normal scatter.

This alternative method of obtaining model coefficients, $C_{d\infty}$, a, b, δ_1, and δ_2, is nothing more than the direct application of curve fitting. In this case, the typical parameters, $C_{d\infty}$, C_{dm}, δ, Re_m, and $\dot{C}_{dm}$ do not need to be known. The solution of $C_{d\infty}$, a, b, δ_1, and δ_2 should make the following objective function a minimum.

$$J = \sum_{i=1}^{N} \left[w_i \left(C_{di} - C_{d\infty} \left(1 + ae^{-\frac{\delta_1}{C_{d\infty}}\sqrt{\mathrm{Re_i}}} + be^{-\frac{\delta_2}{C_{d\infty}}\sqrt{\mathrm{Re_i}}} \right) \right) \right]^2 \quad (18)$$

where w_i is the weight coefficient at Re_i. C_{di} is the experimental discharge coefficient at the point Re_i. The optimal method of searching multi-parameters is suitable for solving $C_{d\infty}$, a, b, δ_1, and δ_2 from the direct experimental results. It must be recognized, however, that a significant amount of computation is necessary because the curve fit using Eq.18 includes five unknown parameters. Models generated using the curve fitting method (as well as the predicted values) were also illustrated in Figs. 4 and 5.

3 Application in fluid power simulations

In section 2 of this paper, a method has been presented for developing equations for directly calculating C_d as a function of Re from experimental data which has been smoothed or with experimental scatter. However, to make use of the curve for modelling purposes, iterative procedures must be used because the Reynolds number is a function of flow rate. This can be observed from the equation relating flow to pressure drop across an orifice obtained by substituting Eq. 4 into the general flow Eq. 1 which gives

$$Q = C_{d\infty} \left(1 + ae^{-\frac{\delta_1}{C_{d\infty}}\sqrt{\mathrm{Re}}} + be^{-\frac{\delta_2}{C_{d\infty}}\sqrt{\mathrm{Re}}} \right) A \sqrt{\frac{2}{\rho}\Delta P} \quad (19)$$

and the equation for Reynolds number expressed as a function of flow rate by

$$\mathrm{Re} = \frac{\rho\left(Q/A\right)D_h}{\mu} \quad (20)$$

Consider a rectangular orifice of width, w, and opening of a small distance, x, where $w >> x$. Re can be expressed as

$$\mathrm{Re} = \frac{2Q\rho}{w\mu} \tag{21}$$

Substituting Eq. 21 into Eq.19 gives

$$Q = C_{d\infty}\left(1 + ae^{-\frac{\delta_1}{C_{d\infty}}\sqrt{\frac{2Q\rho}{w\mu}}} + be^{-\frac{\delta_2}{C_{d\infty}}\sqrt{\frac{2Q\rho}{w\mu}}}\right)wX \tag{22}$$

where $X = x\sqrt{\frac{2}{\rho}\Delta P}$ (23)

An iterative solution to this equation is required for all combinations of the variable, X. This means that, for each time step in a simulation, a series of interactions must be implemented as follows. Given a specific value for X, the initial flow rate, Q_0, is calculated using the discharge coefficient for large Reynolds numbers, $C_{d\infty}$. This would be used to calculate an initial Reynolds number, Re_0 which would be used to calculate a new C_d, and subsequently, a new Q. The process is repeated until the difference in calculated flow rate between iterations reaches some accepted value.

Alternatively, for a specific value of X, it is possible to solve for C_d "off line" before the simulation is in fact started. This requires that the converged value of C_d be plotted as a function of some convenient variable. In this work, the initial Reynolds number Re_0 is used. This essentially eliminates the need for time consuming iterative solutions during dynamic simulation. The process requires calculating Re_0 off line (from X), using iterations to find the converged value for C_d and then plotting C_d vs. $\sqrt{Re_0}$. To use this new plot, either a look-up table or a functional empirical relationship can be used.

To demonstrate this, the off line process was applied to the sharp-edged orifice of Merritt [1967]. This is shown in Fig. 6. It is noted worthy that the shape of the curve is similar to the original C_d vs. $\sqrt{\mathrm{Re}}$ curve. Thus Eq. 4 could be used to approximate the curve with reasonable accuracy.

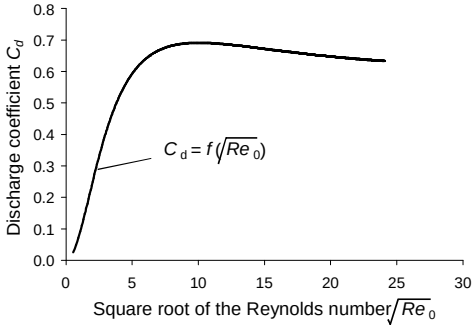

Fig. 6: *The modified discharge coefficient of the sharp-edged orifice*

4 Conclusions

This paper provides an empirical discharge coefficient model of flow rate through orifices. It can be applied to a variety of orifices with different geometries. Two approaches for solving the parameters in the empirical model are also developed. They can be applied to the "smooth" representations of the discharge coefficient and to experimentally determined C_d (with scatter) as a function of the Reynolds number. A simple method of using an off line value of C_d vs. the initial Reynolds numbers is introduced for use in modelling applications. This reduces the need for on line iterations. As a final note, the closed form of discharge coefficient as a function of Reynolds number makes it possible to mathematically manipulate the orifice flow rate equation, such as differentiating the flow rate to obtain the analytical expression of the flow gain, K_q, and flow-pressure coefficient, K_c. This is extremely important in determining stability criterion using small signal analysis of hydraulic systems at small orifice openings.

Nomenclature

A	orifice cross-sectional area	[m^2]
a, b	coefficients in the empirical model	
A_u	flow cross-sectional area at upstream	[m^2]
A_{vc}	flow cross-sectional area at *vena contracta*	[m^2]
C_c	area contraction coefficient	
C_d	discharge coefficient	
$C_{d\infty}$	turbulent discharge coefficient	
C_{dm}	maximum of discharge coefficient	
$\dot{C}_{dm}$	tangent of discharge coefficient at $\sqrt{\mathrm{Re}_m}$	
C_v	velocity coefficient	
D_h	hydraulic diameter	[m]
ΔP	pressure drop cross orifice	[Pa]
P_d	downstream pressure	[Pa]
P_u	upstream pressure	[Pa]
P_{vc}	pressure at *vena contracta*	[Pa]
Q	volumetric flow rate	[m^3/s]
Q_0	initial volumetric flow rate calculated from the turbulent discharge coefficient, $C_{d\infty}$.	[m^3/s]
Re	Reynolds number	
Re_m	Reynolds number at maximum value or a specific point	
Re	initial Reynolds number calculated from Q_0 associated with the turbulent discharge coefficient, $C_{d\infty}$.	
S	orifice perimeter	[m]
w	rectangular orifice width	[m]
w_i	weight	
X	variable associated with x, ΔP and ρ.	
x	orifice opening	[m]

δ	laminar discharge coefficient	
δ_1, δ_2	attenuation coefficients of the empirical model	
μ	absolute viscosity	[Pas]
ρ	fluid density	[kg/m³]

Acknowledgements

The authors are grateful to visiting professor Jian Ruan from Zhejiang University of Technology of China and engineer Doug Bitner for their beneficial suggestions and help. This research was possible through the financial support of NSERC grants RGPIN 17061-99 and RGPIN 3689-00.

References

Borghi, M., Cantore, G., Milani, M. and Paoluzzi, R. 1998. Analysis of Hydraulic Components using Computational Fluid Dynamics Models. *Proceedings of the Institute of Mechanical Engineers*. V212 Part C. pp619.

Ellman, A. and Piche, R. 1996. A Modified Orifice Flow Formula for Numerical Simulation of Fluid Power Systems. *Fluid Power Systems and Technology, ASME*, Vol. 3, pp59-63.

Gromala, P., Domagal, M. and Lisowski, E. 2002. Research on Pressure Drop in Hydraulic Components by Means of CFD Method on Example of Control Valve. *Proceedings of the 2nd International FPNI PhD Symposium on Fluid Power*. Modena, Italy.

Merritt, H. E. 1967. *Hydraulic Control Systems.* John Wiley & Sons, Inc.

Miller, R.W. 1996. *Flow Measurement Engineering Handbook*, 3rd. McGraw-Hill, New York.

Vescovo, G. D. and Lippolis, A. 2002. Flow Forces Analysis on a Four-way Valve. *Proceedings of the 2nd International FPNI PhD Symposium on Fluid Power* . Modena, Italy.

Viall, E. and Zhang, Q. 2000. Spool Valve Discharge Coefficient Determination. *Proceedings of the 48th National Conference on Fluid Power*. Milwaukee, Wisconsin, USA. pp491.

Duqiang Wu
Graduate student for Ph.D. at present, Mechanical Engineering Department, University of Saskatchewan in Canada. Master (1984) at Nanjing University of science and Technology in China. Engineer (1986) at Shaanxi Mechanical and Electrical Institute in China. Visiting Scholar (1997) at University of Illinois at Urbana-Champaign.

Richard Burton
P.Eng, Ph.D, Assistant Dean of the college of Engineering, Professor, Mechanical Engineering, University of Saskatchewan. Burton is involved in research pertaining to the application of intelligent theories to control and monitoring of hydraulics systems, component design, and system analysis. He is a member of the executive of ASME, FPST Division, a member of the hydraulics' advisory board of SAE and NCFP and a convenor for FPNI.

Greg Schoenau
Professor of Mechanical Engineering at the University of Saskatchewan. He was head of that Department from 1993 to 1999. He obtained B.Sc. and M. Sc. Degrees from the University of Saskatchewan in mechanical engineering in 1967 and 1969, respectively. In 1974 he obtained his Ph.D. from the University of New Hampshire in fluid power control systems. He continues to be active in research in this area and in the thermal systems area as well. He has also held positions in numerous outside engineering and technical organizations.

Appendix D Modelling of Orifice Flow Rate at Very Small Openings

(Reprinted from *International Journal of Fluid Power*, Vol. 4, No. 1)

Modelling of Orifice Flow Rate at Very Small Openings

Duqiang Wu, Richard Burton, Greg Schoenau and Doug Bitner

Department of Mechanical Engineering, University of Saskatchewan
57 Campus Drive, Saskatoon, Saskatchewan, Canada, S7N 5A9
duw612@mail.usask.ca

Abstract

Modelling hydraulic control systems that contain flow modulation valves is highly influenced by the accuracy of the equation describing flow through an orifice. Classically, the basic orifice flow equation is expressed as the product of cross-sectional area, the square root of the pressure drop across the orifice and a "flow discharge coefficient", which is often assumed constant. However, at small Reynolds numbers (such the case of valve pilot stage orifices), the discharge coefficient of the flow equation is not constant. Further, the relationship between the flow cross-sectional area and the orifice opening are extremely complex due to clearances, chamfers, and other factors as a result of machining limitations. In this work, a novel modification to the flow cross-sectional area is introduced and the resulting closed form of the flow equation is presented. As a secondary benefit, an analytical form of the orifice flow gain and flow-pressure coefficient can be obtained. This closed form equation greatly facilitates the transient and steady state analysis of low flow regions at small or null point operating regions of spool valve.

Keywords: pilot valve, flow control, orifice, flow rate equation, discharge coefficient, Reynolds number

1 Introduction

In many fluid power applications, spool valves are used to modulate flow to a load. This flow can be quite large and demonstrate turbulent behavior. Under these conditions, the discharge coefficient is known to be constant and independent of the Reynolds number. However in other applications, the flow through the valve can be very small and show a strong dependency on the Reynolds number. Such applications of low flow rate are often found in pilot valves of two stage valves or in compensators of pumps and motors. For these kinds of applications, it is very difficult to model the flow rate because the flow cross-sectional area around the null position often cannot be exactly defined or because the flow may not be turbulent. Due to these difficulties, other means such as experimental techniques are often used to model the flow (Bitner (1986)). Chaimowitsch (1967) developed a flow model for a rectangular orifice as a function of pressure drop and geometry parameters (clearance, chamfer angle, openings, the maximum lap, etc.). The model is difficult to use due to its extremely complex form. Therefore, an accurate and relatively simple analytical expression of flow as a function of orifice geometry and pressure drop is absolutely essential in order to develop a complete dynamic model of any hydraulic control system.

Consider the classical square-type orifice flow equation. As derived from Bernoulli's equation, flow is proportional to the product of the orifice width, the orifice opening, the square root of the pressure drop and a flow coefficient which is defined as the discharge coefficient. The equation is derived by assuming the fluid is inviscid, incompressible, one dimensional and turbulent. Thus,

$$Q = C_d w x \sqrt{\frac{2}{\rho}\Delta P} \tag{1}$$

In most applications, for large Reynolds numbers, C_d, is modeled as being constant. Merritt (1967) suggests that the application of the general turbulent flow equation (Eq.1) can also be extended to the case of laminar flow. However, the discharge coefficient, C_d, is now a function of the Reynolds number, as well as the orifice geometry. C_d is usually determined experimentally and presented graphically. However, in Wu (2002), a closed form model of the discharge

coefficient was developed for different types of orifice geometries. This closed form expression for a square-type orifice is

$$Q = C_{d\infty}\left(1 + ae^{-\frac{\delta_1}{C_{d\infty}}\sqrt{\mathrm{Re}}} + be^{-\frac{\delta_2}{C_{d\infty}}\sqrt{\mathrm{Re}}}\right) wx\sqrt{\frac{2}{\rho}\Delta P} \qquad (2)$$

The advantage of Eq.2 is that it is possible to differentiate the flow rate to obtain flow gain, $K_q = \frac{\partial Q}{\partial x}$, and flow-pressure coefficient, $K_c = \frac{\partial Q}{\partial P}$, for use in transient and stability studies. Palmberg (1985) and Wu (2002) showed that stability in a load sensing system is influenced by the parameters K_q and K_c, which are important factors in determining the overall pump gain and dynamic behavior of the pump. Others (Krus (1988), Lantto (1990, 1991) and Peterson (1996)) have also shown that stability is influenced by overall pump gain.

At small orifice openings around the null point, Eqs.1 and 2 are often invalid. This is because the actual flow cross-sectional area, *A*, is not defined due to clearances, chamfers and other factors which result from machining limitations. Fig.1 shows a comparative plot of an ideal flow rate based on Eqs.1 or 2 and a measured flow rate about the null point. It is evident that a significant error between the measured and ideal flow does occur at the null position. Further, for the curve illustrated in this figure, the flow gain, which from Eqs.1 or 2 should be constant for $x > 0$, is not constant in actual practice. For $x < 0$, the theoretical flow gain is zero, but in actual practice is still a positive, finite value. Thus, it is necessary to develop an empirical expression that will approximate the typical flow rate for $-\alpha < x < \alpha$. To do this, it is necessary to accurately model the orifice area in some empirical function.

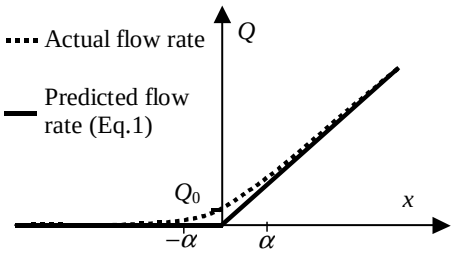

Fig.1: *Comparison of measured and ideal flow rates for a typical pilot valve*

The objective of this paper is to present an empirically modified closed form of the flow cross-sectional area, *A*, which would replace *wx* in Eq.2 and which could be used to accurately model the flow equation in the null region. This empirical form will allow the flow orifice equation to be valid at small openings (positive and negative), as well as large spool displacements, *x*.

2 Modelling of the cross-sectional area of an orifice

The model of flow cross-sectional area of an orifice, $A(x)$, is highly dependent on the geometry of the orifice (often defined as "square", "crescent", "short slot tube" etc). This study assumes that the orifice is rectangular, which is the most common types. Other types can be modeled in a similar fashion. Fig.2 illustrates a typical rectangular orifice in a spool valve. At the null position, the existence of clearances result in null position flow; thus at $x = 0$, an equivalent flow cross-sectional area must be defined. In the absence of any chamfers on the land, the cross-sectional area is

$$A = \frac{\left(D_2^2 - D_1^2\right)\pi}{4} \qquad (3)$$

where D_1 and D_2 are the diameters of the spool and sleeve respectively. For convenience, the cross-sectional area, *A*, can be alternatively expressed in terms of the clearance between the spool and sleeve, *c*, and the average diameter, *D*. In order to do this, consider the relationships as follows (see Fig.2)

$$D_1 = D - c \qquad (4)$$

$$D_2 = D + c \qquad (5)$$

Substituting Eqs.4 and 5 into Eq.3 gives

$$A = \pi Dc = wc \qquad (6)$$

where *w* is defined as the width of the square orifice at the null position and is equal to the average of the perimeters of the spool and sleeve. *c* is defined as the height of the square orifice. It is noted that Eq.6 has the same form as the cross-sectional area term, *wx*, in Eq.2. However, at the null position, *A* would be zero but in practical applications, the existence of spool clearances means this is not valid.

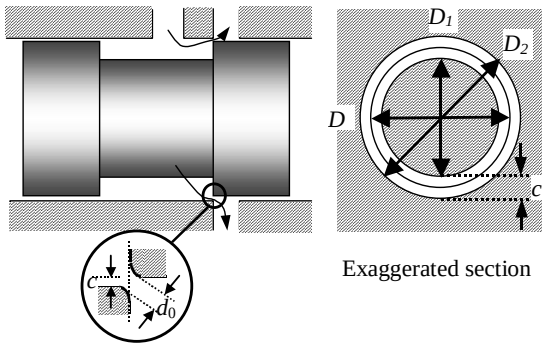

Fig. 2: *Flow cross sectional areas of a rectangular orifice*

The flow cross-sectional area due to clearances is even larger than *wc* at the null position due to chamfers. The height of the rectangular orifice is, in fact, d_0, instead of *c* (see Fig.3(b)). Assuming that the

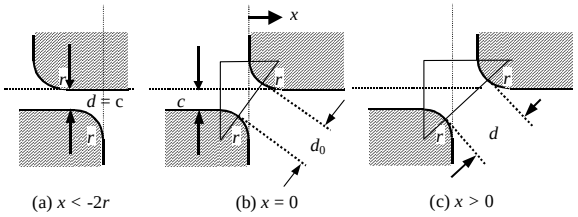

Fig. 3: *The enlarged scenario of the spool and sleeve chamfers*

chamfer angle radius is *r*. The height of the orifice, d_0, can now be expressed as

$$d_0 = \sqrt{(2r+c)^2 + 4r^2} - 2r \tag{7}$$

When the spool is not at null position (see Figs.3(a) and 3(c)), the height, d_0, becomes

$$d(x) = \begin{cases} \sqrt{(2r+c)^2 + (2r+x)^2} - 2r & x > -2r \\ c & x < -2r \end{cases} \tag{8}$$

Therefore, the cross-sectional area becomes

$$A(x) = wd(x) = \begin{cases} w\left(\sqrt{(2r+c)^2 + (2r+x)^2} - 2r\right) & x > -2r \\ wd_0 & x = 0 \\ wc & x < -2r \end{cases} \tag{9}$$

However, it is not convenient to use Eq.9 in Eq.2, because:

- Eq.9 is valid only for a known quarter circular chamfer. Whereas the actual land chamfer geometry would not be known,
- Eq.9 includes two parameters, *r* and *c* which would be very difficult to measure and
- Eq.9 is complex and piecewise.

When the spool displacement, *x*, is less than –2*r*, the orifice cross-sectional area in Eq.9 becomes constant and subsequently for a constant pressure drop, the flow rate would become a constant (Eq.2). However in reality, the flow rate is not constant but decreases as the lap increases (Fig.3(a)). This is because the orifice now becomes a short slot tube and hence the coefficients (i.e. $C_{d\infty}$, *a*, *b*, δ_1, and δ_2) in the discharge coefficient model for a typical square orifice become invalid. For the above reasons, it is necessary to consider developing an empirical flow area model that reflects the behaviors of Eq.9 for $x > -2r$ and approximates the flow of short slot tube orifice for $x < -2r$ in the same flow rate model.

Any empirical model requires experimentally generated data. Consider Fig.2. If the spool is fixed at a certain position, the pressure drop across the orifice, ΔP, and the flow rate through the orifice, *Q*, are readily measured. The flow cross-sectional area, *A*, can be estimated by Eq.1 (accounting for the changing C_d as in Wu (2002)). As in any experimental procedure, measurement error will have an effect on the estimated value of *A*. This results in the vertical scatter in the data in Fig.4. Any error in estimating C_d will also contribute to the scatter.

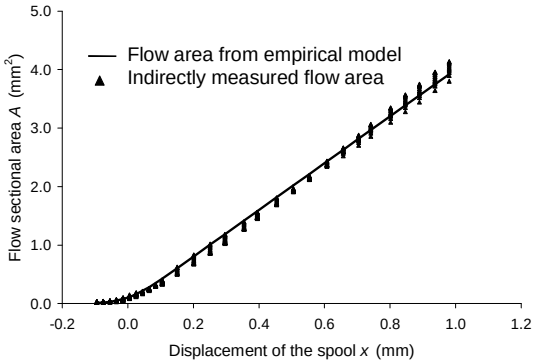

Fig. 4: *The measurement and modelling of the orifice flow cross sectional area*

The objective is to find an empirical relationship between the flow cross-sectional area, *A*, and the spool displacement, *x*, which will best fit the experimental results. There are many functions that can be used to fit the data, including an n[th] order polynomial. However, the function that would be most desirable is one that would satisfy the following constraints:

- The functional form should be as simple as possible.
- The function should not include more than two parameters (one would be ideal) in addition to the orifice width, *w* ($w = D\pi$). These parameters should have some physical significance.
- The fit should be acceptable at large spool displacements as well as in the region about the null position.

In this study, an empirical model which satisfies the above criteria is proposed as

$$A(x) = \frac{wx}{1 - e^{-\frac{x}{d_0}}} \tag{10}$$

where *w* is the width of the square type orifice and d_0 is a parameter which can be related to the equivalent orifice height at the null position (refer to Fig.3(b)). The clearances and chamfers influence the model though the term, $\frac{1}{1 - e^{-\frac{x}{d_0}}}$. Because it is difficult to obtain d_0 analytically from Eq.7, d_0 is experimentally determined from

$$d_0 = \frac{A|_{x=0}}{w} \tag{11}$$

where

$$A|_{x=0} = \frac{1}{N}\sum_{i=1}^{N} \frac{Q_i}{C_d\sqrt{\frac{2}{\rho}\Delta P_i}} \tag{12}$$

In Eq.12, N is the number of measurements at different pressure drops, ΔP_i. C_d is determined by Wu (2002)'s model. For non-rectangular orifice, w varies with position. In this case, Eq.10 is used with a small non-zero valve displacement to generate another equation in w and d_0 from which an effective valve width can be calculated. In Fig.4, Eq.10 is plotted as the solid line for the valve used in this study. Fig.5 shows more closely the information in Fig.4 about the null position.

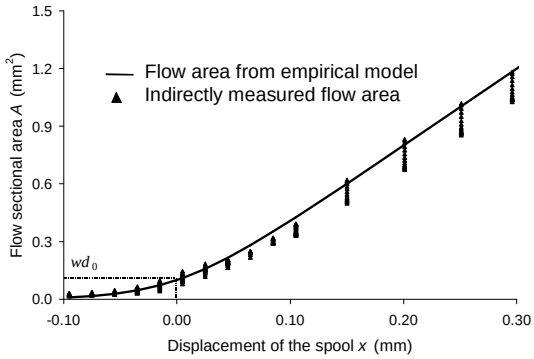

Fig. 5: *The measurement and modeling of the orifice flow cross sectional area about the null position*

The model must satisfy the following boundary conditions:

- When x is a large negative number (large lapped amounts), $A \rightarrow 0$ and $\frac{\partial A}{\partial x} = 0$.
- When $x = 0$, $A = wd_0$.
- When x is a large positive number (large openings), $A \rightarrow wx$.

From Figs.4 and 5, it is apparent that the first and third boundary conditions are satisfied. When $x = 0$, Eq.2 tends to $\frac{0}{0}$. Applying L'Hopital rule to Eq.10 gives

$$A\big|_{x=0} = \lim_{x\to 0} A(x) = \frac{\left.\frac{d(wx)}{dx}\right|_{x=0}}{\left.\frac{d}{dx}\left(1-e^{-\frac{x}{d_0}}\right)\right|_{x=0}} = wd_0 \qquad (13)$$

Thus, the second condition is satisfied.

Eq.13 and Fig.5 indicate that, although the null position is a singular point, Eq.10 is continuous. As a consequence, the flow rate equation (Eq.2) is also continuous.

3 Analytical model of the flow gain and flow-pressure coefficient

Using the modified form of Eq.10 for the flow cross-sectional area, the flow through the orifice becomes

$$Q = C_{d\infty}\left(1 + ae^{-\frac{\delta_1}{C_{d\infty}}\sqrt{\mathrm{Re}}} + be^{-\frac{\delta_2}{C_{d\infty}}\sqrt{\mathrm{Re}}}\right)\frac{wx}{1-e^{-X}}\sqrt{\frac{2}{\rho}\Delta P} \qquad (14)$$

where $X = \frac{x}{d_0}$. X is a dimensionless variable.

The flow gain and the flow-pressure coefficient can be obtained by differentiating Eq.14 with respect to the opening, x, and pressure drop, ΔP. As developed in Appendix A, the closed forms for K_q and K_c become

$$K_q = \frac{\partial Q}{\partial x} = \frac{C_d w}{1-\varepsilon}\frac{\left(1-(1+X)e^{-X}\right)}{\left(1-e^{-X}\right)^2}\sqrt{\frac{2}{\rho}\Delta P} \qquad (15)$$

and

$$K_c = \frac{\partial Q}{\partial \Delta P} = \frac{C_d wx}{(1-\varepsilon)\left(1-e^{-X}\right)\sqrt{2\rho\Delta P}} \qquad (16)$$

where

$$\varepsilon = \frac{\left(-a\delta_1 e^{-\frac{\delta_1}{C_{d\infty}}\sqrt{\mathrm{Re}}} - b\delta_2 e^{-\frac{\delta_2}{C_{d\infty}}\sqrt{\mathrm{Re}}}\right)\sqrt{\mathrm{Re}}}{2C_d} \qquad (17)$$

It is apparent that the "modification" quantity, ε, is also a function of the Reynolds number (Eq.17). It can be shown that at $Re = 0$, $\varepsilon = 0.5$ (Note: as $Re \rightarrow 0$, $C_d \rightarrow 0$ as well). For a typical sharp-edged orifice, ε is plotted in Fig.6 and varies from 0.5 at very low Reynolds numbers to zero at large Reynolds numbers. It should be noted here that at $x = 0$, Eqs.A12, A13 and A14 should be used rather than Eqs.15, 16 and 17. A simple "IF" statement can be used to facilitate this in a dynamic simulation.

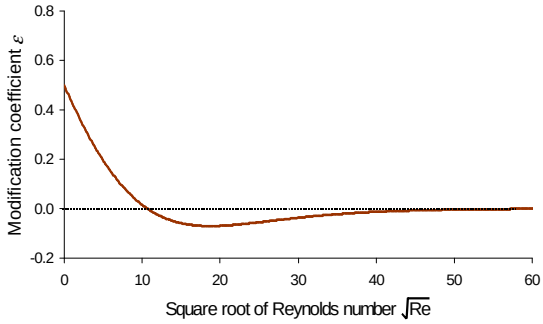

Fig. 6: *The modification of the discharge coefficient for orifice flow gain and flow-pressure coefficient*

Eqs.14, 15 and 16 are the general forms of the flow rate through a square orifice, the flow gain and flow-pressure coefficient respectively, which can be applied to cases of laminar flow, turbulent flow, as well as the transition from laminar to turbulent flow. For both laminar flow and turbulent flow, Eqs.15 and 16 can be simplified as follows.

As the orifice opening, x, and/or the pressure drop, ΔP, increase, the Reynolds number increases. C_d and ε converges to $C_{d\infty}$ and 0 respectively. If $x >> d_0$ (i.e.

$X >> 1$), the term, $\frac{\left(1-(1+X)e^{-X}\right)}{\left(1-e^{-X}\right)^2}$, also converges to 1. As a result, the flow gain becomes the well-known form of

$$K_q\big|_{turbulent} = C_{d\infty} w \sqrt{\frac{2}{\rho}\Delta P} \tag{18}$$

and the flow-pressure coefficient becomes the familiar expression

$$K_c\big|_{turbulent} = \frac{C_{d\infty} w x}{\sqrt{2\rho\Delta P}} \tag{19}$$

It would appear from Eq.19 that K_c could become infinite when $\Delta P = 0$. This is not true as K_c is always a finite value. When ΔP approaches zero, the flow rate is very small and the flow becomes laminar. Therefore, Eq.19 is really not applicable. In this situation, the Reynolds number is very small and thus Eq.16 should be used under the limit, C_d approaches zero. Thus, as shown in Appendix B, the closed forms of the flow gain and the flow-pressure coefficient under laminar flow conditions are

$$K_a\big|_{\text{laminar}} = \frac{8\delta^2 w x \Delta P}{\mu} \cdot \frac{1-(1+X)e^{-X}}{\left(1-e^{-X}\right)^3} \tag{20}$$

$$K_c\big|_{laminar} = \frac{4wx^2\delta^2}{\mu\left(1-e^{-\frac{x}{d_0}}\right)^2} \tag{21}$$

where δ is the laminar discharge coefficient, as defined in Wu (2002). Under these conditions, it can be observed that the flow-pressure coefficient, K_c, is independent of the pressure drop, ΔP, across the orifice under the laminar flow conditions.

When $x = 0$, the flow rate (leakage) is through the clearances and hence is small. The flow is usually laminar. Therefore, Eqs.20 and 21 are applicable. The flow gain and the flow-pressure coefficient at $x = 0$ thus become

$$K_{q0} = \left.\frac{\partial Q}{\partial x}\right|_{x=0} = \frac{4\delta^2 w d_0 \Delta P}{\mu} \tag{22}$$

$$K_{c0} = \left.\frac{\partial Q}{\partial \Delta P}\right|_{x=0} = \frac{4\delta^2 w d_0^2}{\mu} \tag{23}$$

Eqs.14, 15 and 16 can also be extended to the case of non-rectangular orifices. The general forms of the flow rate, the flow gain and the flow-pressure coefficient for any type orifice can be expressed by

$$Q = C_d \frac{A(x)}{1-e^{-X}} \sqrt{\frac{2}{\rho}\Delta P} \tag{24}$$

$$K_q = \frac{C_d w}{1-\varepsilon} \frac{\left(1-(1+X)e^{-X}\right)}{\left(1-e^{-X}\right)^2} \sqrt{\frac{2}{\rho}\Delta P} \tag{25}$$

$$K_c = \frac{C_d A(x)}{(1-\varepsilon)\left(1-e^{-X}\right)\sqrt{2\rho\Delta P}} \tag{26}$$

where $A(x)$ represents the ideal area as a function of the orifice opening (without considering clearances and chamfers). C_d employs Wu (2002)'s model. X and w represent the area ratio of the ideal area function, $A(x)$, and the practical leakage area, A_0, at the null position, and the equivalent orifice width respectively, i.e.

$$C_d = C_{d\infty}\left(1 + ae^{-\frac{\delta_1}{C_{d\infty}}\sqrt{\text{Re}}} + be^{-\frac{\delta_2}{C_{d\infty}}\sqrt{\text{Re}}}\right) \tag{27}$$

$$X = \frac{A(x)}{A_0} \tag{28}$$

$$w = \frac{dA(x)}{dx} \tag{29}$$

4 A comparison of the analytical and experimental results

The orifice flow rate models expressed by Eqs. 14, 15, and 16 can be verified experimentally. A pilot valve was used in the experimental verification (Fig. 7). With the orifice opening, x, fixed, the flow rate, Q, and the pressure drop, $\Delta P = P_u - P_d$, were measured. Experimental results of flow through a pilot valve with a crescent orifice were obtained and illustrated using the function, $Q(x)$ at a specific pressure drop, ΔP, and the function, $Q(\Delta P)$ at a specific opening, x.

In order to calculate the flow rate using the empirical model provided in this study, parameters for the cross-sectional area model, w and d_0, and parameters for the discharge coefficients model, $C_{d\infty}$, a, b, δ_1, and δ_2, must be known. Although the cross-sectional area is a crescent type (see Fig.7), experimental results indicate that, within small orifice openings, such as less than 1 mm (in this study), the orifice could be approximated as a rectangular type. For the pilot valve used in this study, the identified model parameters, w and d_0, are listed in Table 1. Wu (2002)'s research indicated that model parameters of the discharge coefficient, $C_{d\infty}$, a, b, δ_1, and δ_2, were highly dependent on the orifice geometry, such as "sharp-edged", "short slot tube", or "needle valve" types. In this study, the pilot valve used was a sharp-edged type and the model parameters are also given in Table 1.

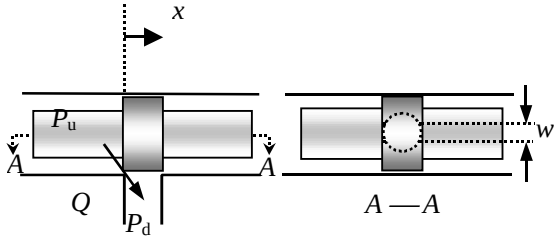

Fig. 7: *A simple spool orifice*

Table 1 Model parameters

d_0(mm)	w(mm)	$C_{d\infty}$	a	δ_1	b	δ_2
0.025	4	0.63	-0.99	0.20	-0.01	3.7

Fig.8 shows a comparison of the flow rate using Eq.14 and the experimental results for orifice flow rates at small openings ($x > 0$) and small lapped amounts ($x < 0$) for a pressure drop of 5 MPa. All the experimental data is contained in the region between the two dashed lines. Although the empirically calculated flow is not a perfect fit to the experimental results, it is far superior to that obtained using the more common model, as illustrated in Fig.8. Fig. 9 shows a comparison at large orifice openings. It is clear that the representation of the empirical model at large orifice openings is excellent.

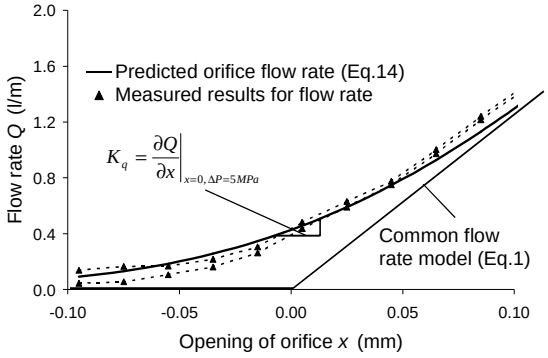

Fig. 8: *Comparison of model-based and experimental results of orifice flow rate at ΔP = 5MPa (for small openings (x > 0) and small lapped amounts (x < 0))*

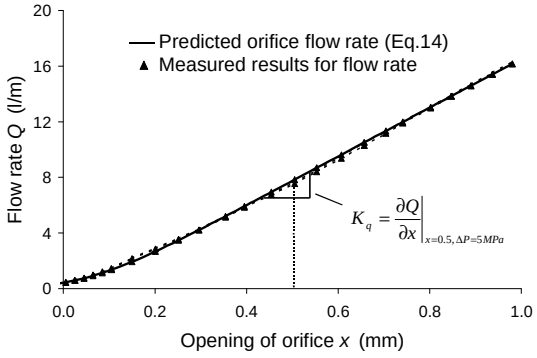

Fig. 9: *Comparison of model-based and experimental results of orifice flow rate at ΔP = 5MPa (for large openings)*

Fig.10 shows a comparison of the empirically predicted and measured flow rates as a function of pressure drop across the orifice at the null position ($x = 0$). The tangent on the curve represents the flow-pressure coefficient at operating points, $x = 0$ and $\Delta P = 6$ MPa. Fig.11 also shows a comparison of the flow rate as a function of pressure drop across the orifice at an opening of 0.5 mm.

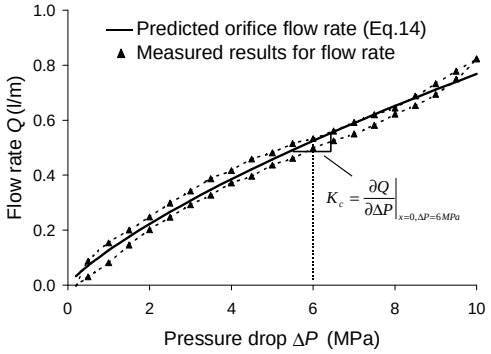

Fig 10 *Comparison of model-based and experimental results of orifice flow rate at x*

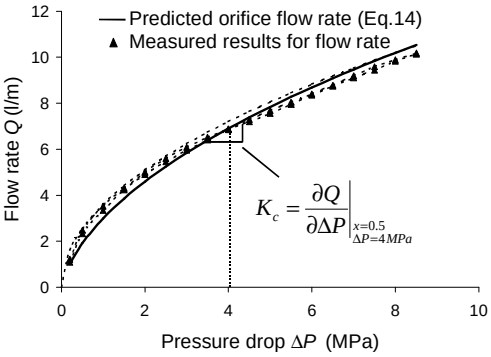

Fig 11 *Comparison of model-based and experimental results of orifice flow rate at x = 0.5 mm*

Fig.12 shows a comparison of the orifice flow gains, K_q, based on the empirical model and experimental results. The two curves plotted with "triangles" represent experimental flow gains, i.e. the slopes of the upper and lower dashed lines shown in Figs.8 & 9. The experimental results show a flat region at about $x = 0.2$ mm. This is attributed to the fact that K_q (experimental) is obtained graphically and in this region, small variations can lead to large errors in the slope.

Fig.13 compares the orifice flow-pressure coefficients, K_c, based on the empirical model and slope values obtained from the experimental results. The solid line represents the predicted results from the empirical model. The scatter evident in the experimental results of Fig.13 is attributed to the process of differentiation of the experimental data, which also has a significant amount of scatter.

There is a relatively good agreement between the empirical model predictions and the experimental results. The determination of K_q and K_c using Eqs.15 and 16 is a valid approach.

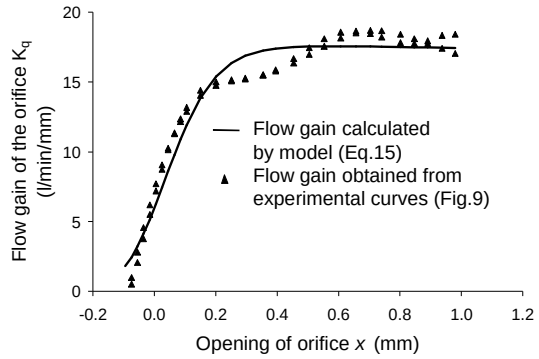

Fig. 12 *Comparison of modeled and experimental flow gain with the pressure drop of 5 MPa*

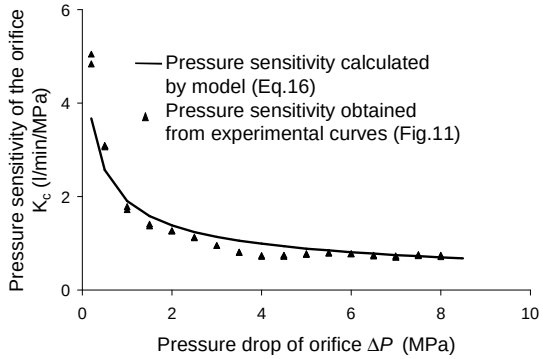

Fig. 13 *Comparison of modeled and experimental pressure sensitivity with the orifice opening of 0.5 mm*

5 Conclusions

The flow rate through a pilot valve usually is small due to small orifice openings. A problem occurs in using the classical orifice flow equation in this case. The discharge coefficient is not a constant due to laminar flow conditions. In addition, it is difficult to determine the actual orifice cross-sectional area about the null position due to clearances, chamfers, and machining limitations. This paper provides an empirical flow cross-sectional area model that includes only one parameter, d_0, or only two parameters, d_0 and w, for non-rectangular orifice. In practice, C_d must also be measured (for example, Wu (2002), which requires measurement of other parameters). It is thus possible to differentiate the flow equations with respect to the orifice opening and pressure drop in order to obtain the flow gain and flow-pressure coefficient of the pilot valve. Thus, the discontinuity problem of applying the traditional flow rate model at $x = 0$ no longer exists. A comparison between experimental and empirical models show that this approach is valid.

Nomenclature

A	orifice cross-sectional area
A_0	orifice cross-sectional area at the zeroed orifice opening
a, b	coefficients in the empirical model C_d, or polynomials
C_d	discharge coefficient
$C_{d\infty}$	turbulent discharge coefficient
d	height of square type orifice
d_0	height of square type orifice at the null position
K_q	flow gain
K_{q0}	flow gain at the zeroed orifice opening
K_c	flow-pressure coefficient
K_{c0}	flow-pressure coefficient at the zeroed orifice opening
N	the number of experiments
P_d	downstream pressure
P_u	upstream pressure
ΔP	pressure drop across orifice
Q	volumetric flow rate
Re	Reynolds number
w	rectangular orifice width
x	orifice opening
X	dimensionless orifice opening
α	a small orifice opening
δ	laminar flow discharge coefficient
δ_1 δ_2	attenuation coefficients of the empirical model
ε	modification associated with discharge coefficient
ρ	fluid density

Acknowledgements

The authors are grateful to visiting professor Jian Ruan from Zhejiang University of Technology of China for his helpful suggestions. This research was made possible through the financial support of NSERC grants RGPIN 17061-99 and RGPIN 3689-00.

References:

Bitner, D. 1986. *Analytical and Experimental Analysis of a Load Sensing Pump.* M. Sc. thesis, University of Saskatchewan, Canada.

Chaimowitsch, M. 1967. *Ölhydraulik: Grundlagen und Anwendung*. Veb Verlag Technik Berlin.

Krus, P. 1988. *On Load Sensing Fluid Power Systems.* Dissertation No. 198, Linkoping University, Sweden.

Lantto, B., Palmberg, J.O. and Krus, P. 1990. Static and Dynamic Performance of Mobile Load-sensing Systems with Two Different Types of Pressure-

Compensated Valves. *SAE Technical Paper Series*. *SAE*. Sept 10-13, p251.

Lantto, B., Krus, P. and Palmberg, J.O. 1991. Interaction between Loads in Load-sensing Systems. *Proceeding of the 2nd Tampere International Conference on Fluid Power*. Linkoping, Sweden, p53.

Merritt, H.E. 1967. *Hydraulic Control Systems.* John Wiley & Sons, Inc.

Palmberg, J.O., Krus, P. and **Ding, K.** 1985. Dynamic Response Characteristics of Pressure-Control Pumps. *The 1st International Conference on Fluid Power Transmission and Control*, Zhejiang University, Hangzhou, China, p.110.

Pettersson, H., **Krus, P., Jansson, A.** and **Palmberg, J.O.** 1996. The Design of Pressure Compensators for Load Sensing Hydraulic systems. *UKACC International Conference on Control'96*, IEE 427. University of Exeter, UK, p.1456.

Wu, D. 2002**.** *Analysis and Simulation of LSPC Hydraulic Systems*. Ph.D. thesis. University of Saskatchewan, work in progress.

Appendix A: Derivation of the general form of flow gain and flow-pressure coefficient through orifices

For simplicity, the orifice flow equation (Eq.2) can be re-expressed as

$$Q = C_d A\sqrt{\frac{2}{\rho}\Delta P} \tag{A1}$$

where

$$C_d = C_{d\infty}\left(1 + ae^{-\frac{\delta_1}{C_{d\infty}}\sqrt{\mathrm{Re}}} + be^{-\frac{\delta_2}{C_{d\infty}}\sqrt{\mathrm{Re}}}\right) \tag{A2}$$

$$A = \frac{wx}{1 - e^{-\frac{x}{d_0}}} \tag{A3}$$

For a rectangular orifice with width w, when the orifice opening, x, is much less than width w (i.e. $x << w$), the Reynolds number can be expressed as (Wu (2002))

$$\mathrm{Re} = \frac{2Q\rho}{w\mu} \tag{A4}$$

Differentiating Eq.A1 with respect to orifice opening, x, gives

$$K_q = \frac{\partial Q}{\partial x} = A\sqrt{\frac{2}{\rho}\Delta P}\frac{\partial C_d}{\partial x} + C_d\sqrt{\frac{2}{\rho}\Delta P}\frac{\partial A}{\partial x} \tag{A5}$$

where

$$\frac{\partial C_d}{\partial x} = \frac{dC_d}{d\sqrt{\mathrm{Re}}}\frac{d\sqrt{\mathrm{Re}}}{dQ}\frac{\partial Q}{\partial x} \tag{A6}$$
$$= \left(-a\delta_1 e^{-\frac{\delta_1}{C_{d\infty}}\sqrt{\mathrm{Re}}} - b\delta_2 e^{-\frac{\delta_2}{C_{d\infty}}\sqrt{\mathrm{Re}}}\right)\cdot\sqrt{\frac{\rho}{2w\mu Q}}\cdot\frac{\partial Q}{\partial x}$$

$$\frac{\partial A}{\partial x} = w\frac{\left(1-(1+X)e^{-X}\right)}{\left(1-e^{-X}\right)^2} \tag{A7}$$

X is a dimensionless number ($X = \frac{x}{d_0}$). Substituting Eqs.A6 &A7 into Eq.A5 gives

$$\frac{\partial Q}{\partial x} = \left(-a\delta_1 e^{-\frac{\delta_1}{C_{d\infty}}\sqrt{\mathrm{Re}}} - b\delta_2 e^{-\frac{\delta_2}{C_{d\infty}}\sqrt{\mathrm{Re}}}\right)\cdot\sqrt{\frac{\rho}{2w\mu Q}}\cdot A\sqrt{\frac{2}{\rho}\Delta P}\frac{\partial Q}{\partial x} + C_d w\frac{\left(1-(1+X)e^{-X}\right)}{\left(1-e^{-X}\right)^2}\sqrt{\frac{2}{\rho}\Delta P} \tag{A8}$$
$$= \frac{\left(-a\delta_1 e^{-\frac{\delta_1}{C_{d\infty}}\sqrt{\mathrm{Re}}} - b\delta_2 e^{-\frac{\delta_2}{C_{d\infty}}\sqrt{\mathrm{Re}}}\right)\sqrt{\mathrm{Re}}}{2C_d}\frac{\partial Q}{\partial x} + C_d w\frac{\left(1-(1+X)e^{-X}\right)}{\left(1-e^{-X}\right)^2}\sqrt{\frac{2}{\rho}\Delta P}$$

The first term in the right hand side can be considered as the product of a coefficient, ε, and $\frac{\partial Q}{\partial x}$. K_q (i.e. $\frac{\partial Q}{\partial x}$) is then solved to be

$$K_q = \frac{\partial Q}{\partial x} = \frac{C_d w}{1-\varepsilon}\frac{\left(1-(1+X)e^{-X}\right)}{\left(1-e^{-X}\right)^2}\sqrt{\frac{2}{\rho}\Delta P} \tag{A9}$$

where

$$\varepsilon = \frac{\left(-a\delta_1 e^{-\frac{\delta_1}{C_{d\infty}}\sqrt{\mathrm{Re}}} - b\delta_2 e^{-\frac{\delta_2}{C_{d\infty}}\sqrt{\mathrm{Re}}}\right)\sqrt{\mathrm{Re}}}{2C_d} \tag{A10}$$

Similarly, Differentiating Eq.A1 with respect to pressure drop, ΔP, gives

$$K_c = \frac{\partial Q}{\partial \Delta P} = A\sqrt{\frac{2}{\rho}\Delta P}\frac{\partial C_d}{\partial \Delta P} + \frac{C_d A}{\sqrt{2\rho\Delta P}}$$
$$= \varepsilon K_c + \frac{C_d A}{\sqrt{2\rho\Delta P}}$$

or

$$K_c = \frac{\partial Q}{\partial \Delta P} = \frac{C_d wx}{(1-\varepsilon)\left(1-e^{-X}\right)\sqrt{2\rho\Delta P}} \tag{A11}$$

It is notable that when $x = 0$ (hence $X = 0$), Q, K_q and K_c show the form of $\frac{0}{0}$. Similar to Eq.13, the value of Q, K_q and K_c at the null position can be calculated by

$$Q_0 = C_d wd_0\sqrt{\frac{2}{\rho}\Delta P} \tag{A12}$$

$$K_{q0} = \frac{\partial Q}{\partial x} = \frac{C_d w}{2(1-\varepsilon)}\sqrt{\frac{2}{\rho}\Delta P} \tag{A13}$$

$$K_{c0} = \frac{\partial Q}{\partial \Delta P} = \frac{C_d wd_0}{(1-\varepsilon)\sqrt{2\rho\Delta P}} \tag{A14}$$

Appendix B: Derivation of the flow gain and the flow-pressure coefficient for the laminar flow through orifices

Eq. 2 is an empirical orifice flow equation that can be applied to both laminar and turbulent flow. Eqs.15 and 16 are the flow gain, K_q, and the flow-pressure coefficient, K_c, developed from Eq.2. When the flow through orifices becomes laminar, the Reynolds number of the orifice flow is very small and the discharge coefficient can be approximated by its linearization model, i.e.

$$C_d = \delta\sqrt{\mathrm{Re}} \tag{B1}$$

where $\delta = -a\delta_1 - b\delta_2$. Substituting Eq.A4 into Eq.B1 gives

$$C_d = \delta\sqrt{\frac{2Q\rho}{w\mu}} \tag{B2}$$

Replacing Eq.A2 by Eq.B2, Eq.A1 becomes

$$Q = \frac{2\delta x}{1-e^{-\frac{x}{d_0}}}\sqrt{\frac{wQ\Delta P}{\mu}}$$

or

$$\sqrt{Q} = \frac{2\delta x}{1-e^{-\frac{x}{d_0}}}\sqrt{\frac{w\Delta P}{\mu}} \tag{B3}$$

Squaring both sides of Eq.B3 results in the laminar flow equation of an orifice as

$$Q = \frac{4\delta^2 x^2 w\Delta P}{\mu\left(1-e^{-\frac{x}{d_0}}\right)^2} \tag{B4}$$

Eq.B4 shows a linear relationship between the orifice flow and pressure drop. Eq.B4 can be compared to Eq.(3-39) of Merritt (1967) (note: the term of $4x^2w$ is same as $2D_hA$ in Merritt). The only difference is that the term of the exponential function, $\left(1-e^{-\frac{x}{d_0}}\right)^2$, exists in the denominator of Eq.B4.

Differentiating Eq.B4 with respect to x and ΔP gives the flow gain and the flow-pressure coefficient at the laminar flow condition as

$$K_a = \frac{\partial Q}{\partial x} = \frac{8\delta^2 wx\Delta P}{\mu}\cdot\frac{1-(1+X)e^{-X}}{\left(1-e^{-X}\right)^3} \tag{B5}$$

$$K_c = \frac{\partial Q}{\partial \Delta P} = \frac{4wx^2\delta^2}{\mu\left(1-e^{-\frac{x}{d_0}}\right)^2} \tag{B6}$$

Duqiang Wu
Graduate student for Ph.D. at present, Mechanical Engineering Department, University of Saskatchewan in Canada. Master (1984) at Nanjing University of science and Technology in China. Engineer (1986) at Shaanxi Mechanical and Electrical Institute in China. Visiting Scholar (1997) at University of Illinois at Urbana-Champaign.

Richard Burton
P.Eng, Ph.D, Assistant Dean of the college of Engineering, Professor, Mechanical Engineering, University of Saskatchewan. Burton is involved in research pertaining to the application of intelligent theories to control and monitoring of hydraulics systems, component design, and system analysis. He is a member of the executive of ASME, FPST Division, a member of the hydraulics' advisory board of SAE and NCFP and a convenor for FPNI.

Greg Schoenau
Professor of Mechanical Engineering at the University of Saskatchewan. He was head of that Department from 1993 to 1999. He obtained B.Sc. and M. Sc. Degrees from the University of Saskatchewan in mechanical engineering in 1967 and 1969, respectively. In 1974 he obtained his Ph.D. from the University of New Hampshire in fluid power control systems. He continues to be active in research in this area and in the thermal systems area as well. He has also held positions in numerous outside engineering and technical organizations.

Doug Bitner
MSc. Departmental Assistant Mechanical Engineering, University of Saskatchewan. Manager Fluid Power Laboratory and Control Systems Laboratory University of Saskatchewan.

Appendix E Transfer Function of the Load Sensing System (Condition I)

The appendix is to express the TF (see Equation (5.81)) of the LS system under the operating Condition I in a more general form as Equation (5.82) so that it is possible to use Matlab® programming to plot the Bode diagram and/or the zeros & poles in phase plane. Equations (5.81) and (5.82) are rewritten as

$$F(s)=\frac{K_q\left(1+G_pG_sH_p\right)G_\phi}{1+K_cH_L+K_cG_s+G_pG_sH_p+K_cH_LG_pG_s\left(H_p-G_{Ls}\right)}$$

$$=\frac{K_q\left(1+\dfrac{K_pK_sH_p\left(\dfrac{s}{\omega_{p0}}+1\right)}{\left(\dfrac{s}{\omega_{ysp}}+1\right)\left(\dfrac{s}{\omega_s}+1\right)}\right)\dfrac{K_\phi}{\left(\dfrac{s^2}{\omega_L^2}+\dfrac{2\zeta_Ls}{\omega_L}+1\right)}}{1+\dfrac{K_cK_L\left(\dfrac{s}{\omega_{L0}}+1\right)}{\left(\dfrac{s^2}{\omega_L^2}+\dfrac{2\zeta_Ls}{\omega_L}+1\right)}+\dfrac{K_sK_c}{\left(\dfrac{s}{\omega_s}+1\right)}+\dfrac{K_pK_sH_p\left(\dfrac{s}{\omega_{p0}}+1\right)}{\left(\dfrac{s}{\omega_{ysp}}+1\right)\left(\dfrac{s}{\omega_s}+1\right)}+\dfrac{K_pK_sK_cK_L\left(H_p-1\right)\left(\dfrac{s}{\omega_{Lp0}}+1\right)\left(\dfrac{s}{\omega_{L0}}+1\right)\left(\dfrac{s}{\omega_{p0}}+1\right)}{\left(\dfrac{s}{\omega_{ysp}}+1\right)\left(\dfrac{s^2}{\omega_L^2}+\dfrac{2\zeta_Ls}{\omega_L}+1\right)\left(\dfrac{s}{\omega_s}+1\right)\left(\dfrac{s}{\omega_{Ls}}+1\right)}} \tag{E1}$$

$$F(s)=K\frac{b_3s^3+b_2s^2+b_1s+b_0}{a_5s^5+a_4s^4+a_3s^3+a_2s^2+a_1s+a_0} \tag{E2}$$

For the convenience, it is necessary to define some variables as

$$t_{L2}=\frac{1}{\omega_L^2} \tag{E3}$$

$$t_L=\frac{2\zeta_L}{\omega_L} \tag{E4}$$

$$t_{Ls}=\frac{1}{\omega_{Ls}} \tag{E5}$$

$$t_s=\frac{1}{\omega_s} \tag{E6}$$

$$t_{L0}=\frac{1}{\omega_{L0}} \tag{E7}$$

$$t_{p0} = \frac{1}{\omega_{p0}} \tag{E8}$$

$$t_{ysp} = \frac{1}{\omega_{ysp}} \tag{E9}$$

$$t_{Lp0} = \frac{1}{\omega_{Lp0}} = \frac{H_p}{\left(H_p - 1\right)\omega_{Ls}} \tag{E10}$$

$$K_{cl} = K_c K_L = \frac{K_c B_m}{c_{ml} B_m + D_m^2} \tag{E11}$$

$$K_{sc} = K_s K_c = \frac{K_c}{c_{pl} + K_{cr1}} \tag{E12}$$

$$\begin{aligned} K_{ps} &= K_p K_s H_p \\ &= \frac{A_r H_p}{k_r \left(c_{pc} + K_{cr1}\right)} \left(\frac{C_p R_{py} A_y \left(K_{qr1} + \left|K_{qr2}\right|\right)\left(1 - \dfrac{K_{cr1}\left(K_{sp} + K_{pr3} P_{s0}\right)}{C_p R_{py} A_y}\right)}{\left(K_{cr1} + K_{cr2}\right)\left(K_{sp} + K_{pr3} P_{s0}\right)} + K_{qr1} \right) \end{aligned} \tag{E13}$$

$$\begin{aligned} K_{pscl} &= K_p K_s K_c K_L \left(H_p - 1\right) \\ &= \frac{A_r K_c B_m \left(H_p - 1\right)}{k_r \left(c_{pc} + K_{cr1}\right)\left(c_{ml} B_m + D_m^2\right)} \left(\frac{C_p R_{py} A_y \left(K_{qr1} + \left|K_{qr2}\right|\right)\left(1 - \dfrac{K_{cr1}\left(K_{sp} + K_{pr3} P_{s0}\right)}{C_p R_{py} A_y}\right)}{\left(K_{cr1} + K_{cr2}\right)\left(K_{sp} + K_{pr3} P_{s0}\right)} + K_{qr1} \right) \end{aligned} \tag{E14}$$

$$K = K_q K_\phi = \frac{K_q}{D_m + \dfrac{c_{ml} B_m}{D_m}} \tag{E15}$$

The coefficients in Equation (E2) can be calculated by Tables E.1 and E.2

Table E.1 Determination of the coefficients, b_i, of s polynomial in the numerator of LS system's TF in Condition I

	s^3	s^2	s^1	s^0
1	$t_s t_{ysp} t_{Ls}$	$t_s t_{ysp} + t_s t_{Ls} + t_{Ls} t_{ysp}$	$t_s + t_{ysp} + t_{Ls}$	1
2		$K_{ps}(t_{p0} t_{Ls})$	$K_{ps}(t_{p0} + t_{Ls})$	K_{ps}
Σ	b_3	b_2	b_1	b_0

Table E2 Determination of the coefficients, a_i, of s polynomial in the denominator of LS system's TF in Condition I

	s^5	s^4	s^3	s^2	s^1	S^0
1	$t_{L2} t_s t_{ysp} t_{Ls}$	$t_{L2} t_s t_{ysp} + t_{L2} t_s t_{Ls} + t_{L2} t_{ysp} t_{Ls} + t_L t_s t_{ysp} t_{Ls}$	$t_{L2} t_s + t_{L2} t_{Ls} + t_{L2} t_{ysp} + t_L t_s t_{ysp} + t_L t_s t_{Ls} + t_L t_{Ls} t_{ysp} + t_s t_{Ls} t_{ysp}$	$t_{L2} + t_L t_s + t_L t_{ysp} + t_L t_{Ls} + t_{ysp} t_s + t_{Ls} t_s + t_{Ls} t_{ysp}$	$t_L + t_s + t_{ysp} + t_{Ls}$	1
2		$K_{cL} t_{L0} t_s t_{ysp} t_{Ls}$	$K_{cL}(t_{L0} t_s t_{ysp} + t_{L0} t_{Ls} t_s + t_{L0} t_{Ls} t_{ysp})$	$K_{cL}(t_{L0} t_s + t_{L0} t_{ysp} + t_{L0} t_{Ls} + t_s t_{ysp} + t_s t_{Ls} + t_{ysp} t_{Ls})$	$K_{cL}(t_{L0} + t_s + t_{ysp} + t_{Ls})$	K_{cL}
3		$K_{sc} t_{L2} t_{ysp} t_{Ls}$	$K_{sc}(t_{L2} t_{ysp} + t_{L2} t_{Ls} + t_L t_{Ls} t_{ysp})$	$K_{sc}(t_{L2} + t_L t_{ysp} + t_L t_{Ls} + t_{ysp} t_{Ls})$	$K_{sc}(t_L + t_{ysp} + t_{Ls})$	K_{sc}
4		$K_{ps} t_{L2} t_{p0} t_{Ls}$	$K_{ps}(t_{L2} t_{p0} + t_{L2} t_{Ls} + t_L t_{Ls} t_{p0})$	$K_{ps}(t_{L2} + t_L t_{p0} + t_L t_{Ls} + t_{p0} t_{Ls})$	$K_{ps}(t_L + t_{p0} + t_{Ls})$	K_{ps}
5			$K_{pscl} t_{L0} t_{p0}\ t_{Lp0}$	$K_{pscl}(t_L\ t_{Lp0} + t_{p0}\ t_{Lp0} + t_L\ t_{p0})$	$K_{pscl}(t_L + t_{p0} + t_{Lp0})$	K_{pscl}
Σ	a_5	a_4	a_3	a_2	a_1	A_0

Appendix F The Transfer Function of the Load Sensing System (Condition II)

The appendix is to express the TF (see Equation (5.85)) of the LS system under the operating Condition II in a more general form as Equation (5.86) so that it is possible to use Matlab® programming to plot the Bode diagram and/or the zeros and poles in the phase plane. Equations (5.85) and (5.86) are rewritten as

$$F(s)=\frac{K_q(1+G_sH_p)G_\phi}{1+K_cH_L+K_cG_s+G_sH_p+K_cH_LG_sH_p}$$
$$=\frac{K_q\left(1+\frac{K_p^*K_s}{\left(\frac{s^2}{\omega_{sp}^2}+\frac{2\zeta_{sp}s}{\omega_{sp}}+1\right)\left(\frac{s}{\omega_s}+1\right)}\right)\frac{K_\phi}{\left(\frac{s^2}{\omega_L^2}+\frac{2\zeta_Ls}{\omega_L}+1\right)}}{1+\frac{K_cK_L\left(\frac{s}{\omega_{L0}}+1\right)}{\left(\frac{s^2}{\omega_L^2}+\frac{2\zeta_Ls}{\omega_L}+1\right)}+\frac{K_sK_c}{\left(\frac{s}{\omega_s}+1\right)}+\frac{K_p^*K_s}{\left(\frac{s^2}{\omega_{sp}^2}+\frac{2\zeta_{sp}s}{\omega_{sp}}+1\right)\left(\frac{s}{\omega_s}+1\right)}+\frac{K_p^*K_sK_cK_L\left(\frac{s}{\omega_{L0}}+1\right)}{\left(\frac{s^2}{\omega_{sp}^2}+\frac{2\zeta_{sp}s}{\omega_{sp}}+1\right)\left(\frac{s^2}{\omega_L^2}+\frac{2\zeta_Ls}{\omega_L}+1\right)\left(\frac{s}{\omega_s}+1\right)}} \quad \text{(F1)}$$

$$F(s)=K\frac{b_3s^3+b_2s^2+b_1s+b_0}{a_5s^5+a_4s^4+a_3s^3+a_2s^2+a_1s+a_0} \quad \text{(F2)}$$

For the convenience, it is necessary to define some variables as

$$t_{L2}=\frac{1}{\omega_L^2} \quad \text{(F3)}$$

$$t_{sp2}=\frac{1}{\omega_{sp}^2} \quad \text{(F4)}$$

$$t_L=\frac{2\zeta_L}{\omega_L} \quad \text{(F5)}$$

$$t_{sp}=\frac{2\zeta_{sp}}{\omega_{sp}} \quad \text{(F6)}$$

$$t_s=\frac{1}{\omega_s} \quad \text{(F7)}$$

$$t_{L0}=\frac{1}{\omega_{L0}} \quad \text{(F8)}$$

$$K_{cl} = K_c K_L = \frac{K_c B_m}{c_{ml} B_m + D_m^2} \tag{F9}$$

$$K_{sc} = K_s K_c = \frac{K_c}{c_{pl}} \tag{F10}$$

$$K_{ps}^* = K_p^* K_s = \frac{C_p \left(R_{py} A_y - K_{pr2} + K_{pr3} \theta_{sp0} \right)}{\left(K_{sp} + K_{pr3} P_{s0} \right) c_{pl}} \tag{F11}$$

$$K_{pscl}^* = K_p^* K_s K_c K_L = \frac{C_p \left(R_{py} A_y - K_{pr2} + K_{pr3} \theta_{sp0} \right)}{\left(K_{sp} + K_{pr3} P_{s0} \right) c_{pl}} \cdot \frac{K_c B_m}{c_{ml} B_m + D_m^2} \tag{F12}$$

Consequently, the coefficients in Equation (F2) can be calculated by Equation (F13), Tables F1 and F2.

$$K = K_q K_\phi = \frac{K_q}{D_m + \frac{c_{ml} B_m}{D_m}} \tag{F13}$$

Table F.1 Determination of the coefficients, b_i, of s polynomial in the numerator of LS system's TF in Condition II

	s^3	s^2	s^1	s^0
1	$t_{sp2}t_s$	$t_{sp2}+t_{sp}t_s$	$t_s + t_{sp}$	1
2				K_{sp}^*
Σ	b_3	b_2	b_1	b_0

Table F.2 Determination of the coefficients, a_i, of s polynomial in the denominator of LS system's TF in Condition II

	s^5	s^4	s^3	s^2	s^1	s^0
1	$t_{L2}t_st_{sp2}$	$t_{L2}t_st_{sp}+t_{L2}t_{sp2}$ $+t_Lt_st_{sp2}$	$t_{L2}t_s+ t_{L2}t_{sp}+ t_Lt_st_{sp}+$ $t_Lt_{sp2}+ t_st_{sp2}$	$t_{L2}+ t_Lt_s+ t_Lt_{sp}+$ $t_{sp2}+ t_st_{sp}$	$t_L+ t_s+ t_{sp}$	1
2		$K_{cL}t_{L0}t_st_{sp2}$	$K_{cL}(t_{L0}t_{sp2}+ t_{sp2}t_s+$ $t_{L0}t_st_{sp})$	$K_{cL}(t_{L0}t_s+ t_{L0}t_{sp}+$ $t_st_{sp}+ t_{sp2})$	$K_{cL}(t_{L0}+ t_s+$ $t_{sp})$	K_{cL}
3		$K_{sc}t_{L2}t_{sp2}$	$K_{sc}(t_Lt_{sp2}+ t_{L2}t_{sp})$	$K_{sc}(t_{L2}+ t_{sp2}+t_{sp}t_L)$	$K_{sc}(t_L+ t_{sp})$	K_{sc}
4				$K_{ps}^*\ t_{L2}$	$K_{ps}^*\ t_L$	K_{ps}^*
5					$K_{pscl}^*\ t_{L0}$	K_{pscl}^*
Σ	a_5	a_4	a_3	a_2	a_1	a_0

Appendix G The Transfer Function of the Load Sensing System (Condition III)

The appendix is to express the TF (see Equation (5.87)) of the LS system under the operating Condition I in a more general form as Equation (5.88) so that it is possible to use Matlab® programming to plot the Bode diagram and/or the zeros and poles in the phase plane. Equations (5.87) and (5.88) are rewritten as

$$F(s)=\frac{K_q\left(\dfrac{K_\phi}{\dfrac{s^2}{\omega_L^2}+\dfrac{2\zeta_L s}{\omega_L}+1}\right)}{1+\dfrac{K_c K_L\left(\dfrac{s}{\omega_{L0}}+1\right)}{\dfrac{s^2}{\omega_L^2}+\dfrac{2\zeta_L s}{\omega_L}+1}+\dfrac{K_s K_c}{\dfrac{s}{\omega_s}+1}} \tag{G1}$$

$$F(s)=\frac{K(b_1 s+b_0)}{a_3 s^3+a_2 s^2+a_1 s+a_0} \tag{G2}$$

For convenience, it is necessary to define variables as

$$t_{L2}=\frac{1}{\omega_L^2} \tag{G3}$$

$$t_L=\frac{2\zeta_L}{\omega_L} \tag{G4}$$

$$t_s=\frac{1}{\omega_s} \tag{G5}$$

$$t_{L0}=\frac{1}{\omega_{L0}} \tag{G6}$$

$$K_{cl}=K_c K_L=\frac{K_c B_m}{c_{ml} B_m+D_m^2} \tag{G7}$$

$$K_{sc} = K_s K_c = \frac{K_c}{c_{pl} + K_{cr1}} \tag{G8}$$

Consequently, the coefficients can be obtained as follows.

$$K = K_q K_\phi = \frac{K_q}{D_m + \frac{c_{ml} B_m}{D_m}} \tag{G9}$$

$$a_3 = t_{L2} t_s \tag{G10}$$

$$a_2 = t_{L2}(1 + K_{sc}) + t_L t_s + K_{cL} t_s t_{L0} \tag{G11}$$

$$a_1 = t_L(1 + K_{sc}) + t_s + K_{cL}(t_{L0} + t_s) \tag{G12}$$

$$b_1 = t_s \tag{G13}$$

$$a_0 = 1 + K_{cL} + K_{sc} \tag{G14}$$

$$b_0 = 1 \tag{G15}$$

In order to prove the LS system is always stable at Condition III, apply the Routh-stability criterion.

a_3	a_1
a_2	a_0
$\frac{a_2 a_1 - a_3 a_0}{a_2}$	

$$\begin{aligned}
a_2 a_1 &= [t_{L2}(1 + K_{sc}) + t_L t_s + K_{cL} t_s t_{L0}] \cdot [t_L(1 + K_{sc}) + t_s + K_{cL}(t_{L0} + t_s)] \\
&> [t_{L2}(1 + K_{sc})] \cdot [t_L(1 + K_{sc}) + t_s + K_{cL}(t_{L0} + t_s)] \\
&> [t_{L2}(1 + K_{sc})] \cdot [t_s + K_{cL}(t_{L0} + t_s)] \\
&> [t_{L2}(1 + K_{sc})] \cdot [t_s(1 + K_{cL})] = t_{L2} t_s (1 + K_{sc})(1 + K_{cL}) \\
&> t_{L2} t_s (1 + K_{cL} + K_{sc}) \\
&= a_3 a_0
\end{aligned}$$

It can be observed that the term, $\frac{a_2 a_1 - a_3 a_0}{a_2}$, is larger than zero. Therefore, the LS system is stable at Condition III.

Appendix H Parameters for the Stability Analysis of the LS System

Components	Parameter definition	Symbol	Value	Unit
Fluid properties	Bulk modulus	β	1.38×10^{9}	Nm^{-2}
	Fluid density	ρ	898	kgm^{-3}
	Fluid absolute viscosity at 25°C	μ	1.74×10^{-4}	m^2s^{-1}
LS regulator	Pressure differential of the adjustable orifice	P_d *	0.3 ~ 2.5	MPa
	LS spool cross-sectional area	A_r	3.2×10^{-5}	m^2
	LS spool balance spring constant	k_r	6.1×10^{4}	Nm^{-1}
	LS spool mass	m_r	1.6×10^{-2}	kg
	LS spool damp	B_r	2.21	Nsm^{-1}
	Equivalent opening of two orifices at null point	d_r	2.5×10^{-5}	m
	Equivalent width of two orifices at null point	W_r	4×10^{-3}	m
Control piston	Moment arm of the control piston about the shaft	R_{py}	5.5×10^{-2}	m
	Cross-sectional area of the control piston	A_y	3.36×10^{-4}	m^2
	Minimum volume of the control piston chamber	V_{ymin}	1.38×10^{-6}	m^3
Pressure pump	Moment arm of the pump pistons about the shaft	R_p	3.48×10^{-2}	m
	Cross-sectional area of pump pistons	A_p	2.07×10^{-4}	m^2
	Pump outlet volume including the hose volume	V_p	2.0×10^{-4}	m^3
	Pump leakage coefficient	c_{pl}	2.0×10^{-12}	$m^5s^{-1}N^{-1}$
	Pump shaft speed	ω	183.5	$rad\text{-}s^{-1}$
	Angle coefficient of swash plate spring	K_{sp}	1.42×10^{6}	$N\text{-}m^{-2}rad^{-1}$
	Angle precompression of swash plate spring	T_{sp}	1.11×10^{6}	$N\text{-}m^{-2}$
	Pressure torque constant	K_{pr2}	2.84×10^{-1}	
	Pressure torque constant	K_{pr3}	4.53×10^{-1}	rad^{-1}
	Damp coefficient of the swash plate	B_{sp}	5.5×10^{-1}	Nsm
	Inertial of the swash plate	J_{sp}	1.32×10^{-3}	kgm^2
	Maximum swash plate angle	θ_{spmax}	3.14×10^{-1}	rad
Adjustable orifice	Discharge coefficient	C_d	0.63	
	Cross area of the flow control orifice	A_v *	Variable	m^2
Motor and load	Damp coefficient of the motor and the load	B_m	0.056	Nms
	Motor inlet volume including the hose volume	V_m	1.4×10^{-4}	m^3
	Inertial of the motor and the load	J_m	1.62×10^{-1}	kgm^2
	Resistant torque of the load on the motor axis	T_{mf} *	0.2 ~	Nm
	Motor leakage coefficient	c_{ml}	2.0×10^{-13}	$m^5s^{-1}N^{-1}$
	Volumetric displacement of motor	D_m	2.57×10^{-6}	m^3rad^{-1}
LS line	Damp frequency of the LS line	ω_{ls} *	0 ~ 500	$rad\text{-}s^{-1}$

Appendix I Determination of Parameters of the Motor with an Inertial Load

Based on the dynamic model developed in Chapter 7, the stability of the LS system depends on the parameters of the LS pump, in addition to the parameters of the motor load (V_m, J_m, B_m, T_{mf}, D_m and c_{ml}). The volume of the motor inlet, V_m, can be estimated by the size of the hose between the adjustable orifice and the motor. The inertia of the motor and flywheel load, J_m, can be calculated by the dimension of the flywheel. The volumetric displacement, D_m, and the leakage coefficient of the motor, c_{ml}, can be found from the motor's specification. The damping coefficient, B_m, and the Coulomb resistant torque, T_{mf}, of the motor with the inertial load (flywheel) had to be experimentally determined.

Consider Equation (2.22) of the motor load. When the motor operates at the steady state, $\dot{\phi}$ becomes zero. Therefore,

$$-B_m\phi + D_m P_L - T_{mf} = 0 \tag{I.1}$$

or

$$T = B_m\phi + T_{mf} \tag{I.2}$$

where $T = D_m P_L$. ϕ and P_L are measurable. D_m is known. Equation (I.2) indicates that the unknown parameters, B_m and T_{mf}, could be identified by a linear regression of the steady state experimental results at different operating points.

Figure I.1 shows a simple experimental circuit of obtaining B_m and T_{mf}. The orifice opening was set to a series of values; the steady state values of the load pressure, P_L, and the rotary speed of the motor, ϕ, were subsequently measured. The experimental results are shown in figure I2. The slope of the fitted straight line is B_m and the zero-intercept

of the line is T_{mf}. In the study, B_m and T_{mf} are determined to be 0.056 Nms and 0.16 Nm respectively.

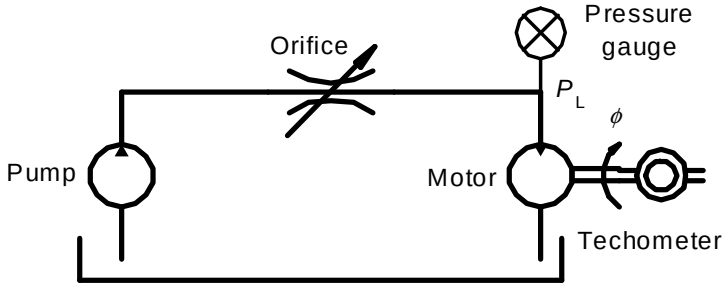

Figure I.1 Parameters measurement circuit of the motor load

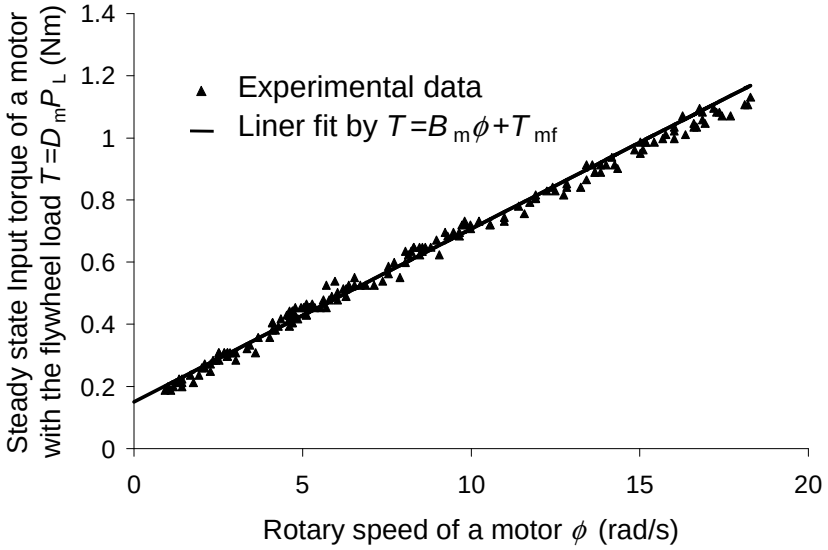

Figure I.2 Parameter estimation of the motor load

Appendix J Determination of the Damping Characteristics in the Load Sensing Line

The damping characteristics in the LS line has a significant effect on the stability of the LS system under certain conditions, because the LS line, $G_{Ls}(s)$, in Figure 7.2 lies in the loop path with positive feedback (i.e. $H_L \rightarrow G_{Ls} \rightarrow G_p \rightarrow G_s \rightarrow K_c$ path). A preliminary dynamic analysis in the frequency domain indicated that the more damping the LS line has, the more stable the LS system would be. However, the response would become slower. In order to quantitatively analyze the effect of the damping of the LS line on the stability, it was necessary to determine the damping time constant, t_{Ls} (or, damping frequency $\omega_{Ls} = 1/t_{Ls}$), for different LS lines (a long line without restriction orifice or a short line with a restriction).

Figure J.1 shows the experimental layout. The measured LS line was pressurized by a deadweight loader. Two pressure gauges were installed at the two terminals of the LS line. The instrumentation was comprised of a signal analyzer which could directly give the frequency response in the way of a Bode plot. The procedure for the experiment was (1) to select the proper deadweight load, (2) to pressurize (via a hand pump) the line in order to set the operating point pressure selected by the deadweight load, (3) to strike the

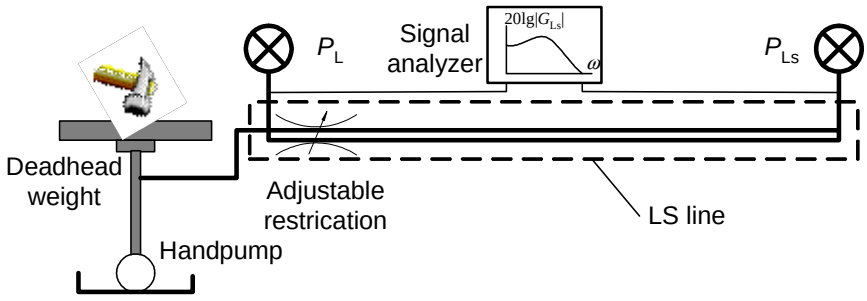

Figure J.1 Measurement of the damping performance of the LS line

deadweight loader to generate a pressure pulse signal and (4) to start the frequency response analyzer.

In this study, the LS line consisted of a soft hose of diameter 6.35 mm and length 700mm (model: H425 04), and a small needle valve (model: Parker N200S). Figures J.2 and J.3 show an experimental frequency response result at the operating point with pressure of 500psi and restriction orifice opening of 0.5 turn on the valve knob. The break frequency is measured to be about 8 rad/s.

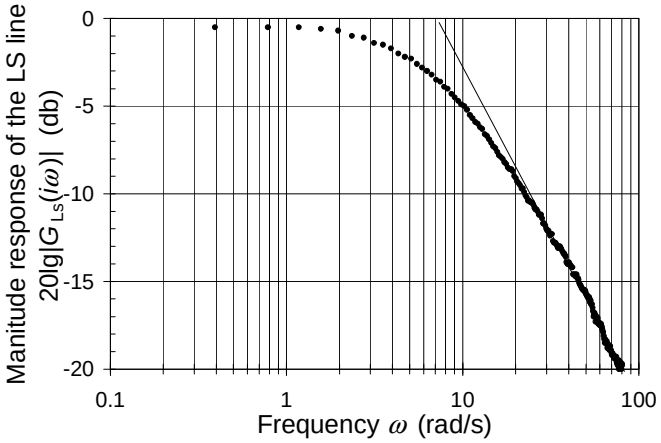

Figure J.2 Magnitude response of the LS line

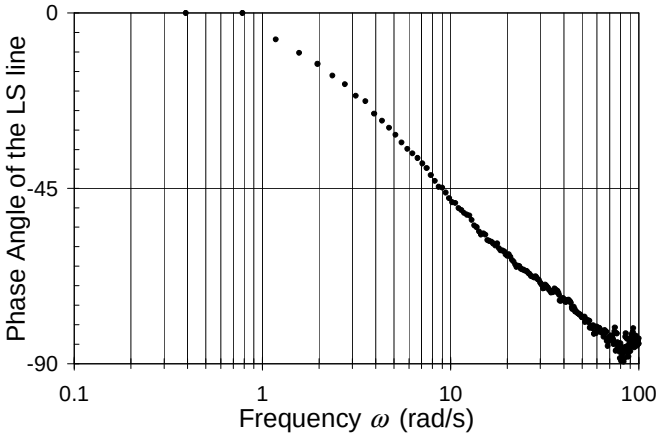

Figure J.3 Phase angle of the LS line

Figure J.4 shows the experimental results of the break frequency, ω_{Ls}, as a function of the number of valve knob turns.

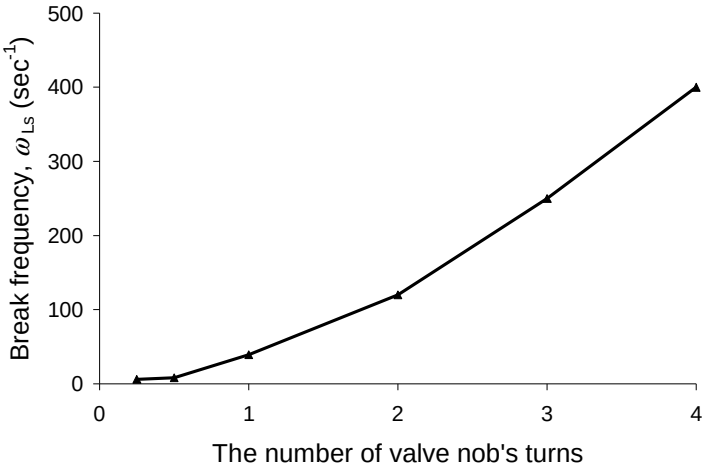

Figure J.4 Break frequency of the LS line as a function of the number of turns on knob of the restriction valve

Appendix K Derivation of the Transfer Function of the Pressure Compensated System

The objective of this appendix is to derive the TF of the PC system based on the Laplace transform of the linearized dynamic equations of the PC system. For convenience, these equations (Equations (11.2), (11.6), and (11.10)) are repeated as

$$A_{11}(s)X_{pc}(s)+A_{12}P_m(s)=-A_{pcs}P_s(s)+k_{ff}A_{pc}(x_{pc0})P_L(s) \quad \text{(K1)}$$

$$A_{21}(s)X_{pc}(s)+A_{22}P_m(s)=K_{qv}X_v(s)+K_{cv}P_s(s)+K_{cpc}P_L(s) \quad \text{(K2)}$$

$$Q_{Lpc}(s)=K_{qpc}X_{pc}(s)+K_{cpc}(P_m(s)-P_L(s)) \quad \text{(K3)}$$

Solving Equations (K1) and (K2) for $X_{pc}(s)$ and $P_m(s)$ gives

$$X_{pc}(s)=\frac{-A_{12}K_{qv}X_v(s)}{A_{11}(s)A_{22}-A_{21}(s)A_{12}}+\frac{-(A_{22}A_{pcs}+A_{12}K_{cv})P_s(s)}{A_{11}(s)A_{22}-A_{21}(s)A_{12}}+\frac{(A_{22}k_{ff}A_{pc}(x_{pc0})-A_{12}K_{cpc})P_L(s)}{A_{11}(s)A_{22}-A_{21}(s)A_{12}} \quad \text{(K4)}$$

$$P_m(s)=\frac{A_{11}(s)K_{qv}X_v(s)}{A_{11}(s)A_{22}-A_{21}(s)A_{12}}+\frac{(A_{11}(s)K_{cv}+A_{21}(s)A_{pcs})P_s(s)}{A_{11}(s)A_{22}-A_{21}(s)A_{12}}+\frac{(A_{11}(s)K_{cpc}-A_{21}(s)k_{ff}A_{pc}(x_{pc0}))P_L(s)}{A_{11}(s)A_{22}-A_{21}(s)A_{12}} \quad \text{(K5)}$$

Substituting A_{12} and A_{22} expressed by Equations (11.4) and (11.8) in Chapter 11 into Equations (K4) and (K5) and then substituting Equations (K4) and (K5) into Equation (K3) give

$$Q_{Lpc}(s)=\frac{K_{qv}K_{cpc}\left(A_{11}(s)+\frac{K_{qpc}(A_{pcs}-k_{ff}A_{pc}(x_{pc0}))}{K_{cpc}}\right)X_v(s)}{(K_{cv}+K_{cpc})\left(A_{11}(s)+\frac{A_{21}(s)(A_{pcs}-k_{ff}A_{pc}(x_{pc0}))}{(K_{cv}+K_{cpc})}\right)}$$

$$+\frac{K_{cpc}K_{cv}\left[\left(A_{11}(s)+\frac{A_{pcs}A_{21}(s)}{K_{cv}}\right)-\frac{K_{qpc}(K_{cpc}A_{pcs}+K_{cv}k_{ff}A_{pc}(x_{pc0}))}{K_{cpc}K_{cv}}\right](P_s(s)-P_L(s))}{(K_{cv}+K_{cpc})\left(A_{11}(s)+\frac{A_{21}(s)(A_{pcs}-k_{ff}A_{pc}(x_{pc0}))}{(K_{cv}+K_{cpc})}\right)} \quad \text{(K6)}$$

Equation (K6) can be expressed as

$$Q_{Lpc}(s) = G_{xv}(s)X_v(s) + G_{psL}(s)\left(P_s(s) - P_L(s)\right) \tag{K7}$$

It is noted that Equation (K6) links with the frequency operator, "*s*", through two terms, $A_{11}(s)$ and $A_{21}(s)$. Substituting $A_{11}(s)$ and $A_{21}(s)$ expressed by Equations (11.3) and (11.7) in Chapter 11 into Equation (K6) can present $G_{xv}(s)$ and $G_{psL}(s)$ by the normalized TF form as

$$G_{xv}(s) = K_{xv}\frac{s^2 + b_{xv1}s + b_{xv0}}{s^2 + a_1 s + a_0} \tag{K8}$$

$$G_{psL}(s) = K_{psL}\frac{s^2 + b_{psL1}s + b_{psL0}}{s^2 + a_1 s + a_0} \tag{K9}$$

$$K_{xv} = \frac{K_{qv}K_{cpc}}{K_{cv} + K_{cpv}} \tag{K10}$$

$$K_{psL} = \frac{K_{cv}K_{cpc}}{K_{cv} + K_{cpv}} \tag{K11}$$

$$a_1 = \frac{B_{pc}^*}{M_{pc}} + \frac{A_{pcs}\left(A_{pcs} - k_{ff}A_{pc}\left(x_{pc0}\right)\right)}{M_{pc}\left(K_{cv} + K_{cpc}\right)} \tag{K12}$$

$$a_0 = \frac{k_{pc}^*}{M_{pc}} + \frac{K_{qpc}\left(A_{pcs} - k_{ff}A_{pc}\left(x_{pc0}\right)\right)}{M_{pc}\left(K_{cv} + K_{cpc}\right)} \tag{K13}$$

$$b_{xv1} = \frac{B_{pc}^*}{M_{pc}} \tag{K14}$$

$$b_{xv0} = \frac{k_{pc}^*}{M_{pc}} + \frac{K_{qpc}\left(A_{pcs} - k_{ff}A_{pc}\left(x_{pc0}\right)\right)}{M_{pc}K_{cpc}} \tag{K15}$$

$$b_{psL1} = \frac{B_{pc}^*}{M_{pc}} + \frac{A_{pcs}^2}{M_{pc}K_{cv}} \tag{K16}$$

$$b_{psL0} = \frac{k_{pc}^*}{M_{pc}} - \frac{K_{qpc}k_{ff}A_{pc}\left(x_{pc0}\right)}{M_{pc}K_{cpc}} \tag{K17}$$

Appendix L Transfer Function of the Load Sensing and Pressure Compensated System (Condition N)

The appendix is to express the TF (see Equation (13.1)) of the LSPC system under the operating Condition N in a more general form as Equation (13.2) so that it is possible to use Matlab® programming to plot the Bode diagram and/or the zeros & poles in phase plane. Equations (13.1) and (13.2) are rewritten as

$$F(s)=\frac{K_q\left(1+G_pG_sH_p\right)G_\phi}{1+K_cH_L+K_cG_s+G_pG_sH_p+K_cH_LG_pG_s\left(H_p-G_{Ls}\right)}$$

$$=\frac{K_{xv}^*\left(1+\dfrac{K_pK_sH_p\left(\dfrac{s}{\omega_{p0}}+1\right)}{\left(\dfrac{s}{\omega_{ysp}}+1\right)\left(\dfrac{s}{\omega_s}+1\right)}\right)\dfrac{K_\phi}{\left(\dfrac{s^2}{\omega_L^2}+\dfrac{2\zeta_Ls}{\omega_L}+1\right)}}{1+\dfrac{K_{psL}^*K_L\left(\dfrac{s}{\omega_{L0}}+1\right)\left(\dfrac{s}{\omega_{p0}}+1\right)}{\left(\dfrac{s^2}{\omega_L^2}+\dfrac{2\zeta_Ls}{\omega_L}+1\right)}+\dfrac{K_sK_{psL}^*\left(\dfrac{s}{\omega_{p0}}+1\right)}{\left(\dfrac{s}{\omega_s}+1\right)}+\dfrac{K_pK_sH_p\left(\dfrac{s}{\omega_{p0}}+1\right)}{\left(\dfrac{s}{\omega_{ysp}}+1\right)\left(\dfrac{s}{\omega_s}+1\right)}+\dfrac{K_pK_sK_{psL}^*K_L\left(H_p-1\right)\left(\dfrac{s}{\omega_{Lp0}}+1\right)\left(\dfrac{s}{\omega_{L0}}+1\right)\left(\dfrac{s}{\omega_{p0}}+1\right)\left(\dfrac{s}{\omega_{p0}}+1\right)}{\left(\dfrac{s}{\omega_{ysp}}+1\right)\left(\dfrac{s^2}{\omega_L^2}+\dfrac{2\zeta_Ls}{\omega_L}+1\right)\left(\dfrac{s}{\omega_s}+1\right)\left(\dfrac{s}{\omega_{Ls}}+1\right)}}$$

(L1)

$$F(s)=K\frac{b_3s^3+b_2s^2+b_1s+b_0}{a_5s^5+a_4s^4+a_3s^3+a_2s^2+a_1s+a_0} \tag{L2}$$

In addition to Equations (E3) through (E10) and (E13) in Appendix E, other coefficients associated to K_c and K_q must be redefined. They are

$$t_{pc0}=\frac{1}{\omega_{pc0}} \tag{L3}$$

$$K_{cl}=K_{psL}^*K_L=\frac{K_{psL}^*B_m}{c_{ml}B_m+D_m^2} \tag{L4}$$

$$K_{sc}=K_sK_{psL}^*=\frac{K_{psL}^*}{c_{pl}+K_{cr1}} \tag{L5}$$

$$K_{pscl} = \frac{A_r K_{psL}^* B_m \left(H_p - 1\right)}{k_r \left(c_{pc} + K_{cr1}\right)\left(c_{ml} B_m + D_m^2\right)} \left(\frac{C_p R_{py} A_y \left(K_{qr1} + \left|K_{qr2}\right|\right)\left(1 - \frac{K_{cr1}\left(K_{sp} + K_{pr3} P_{s0}\right)}{C_p R_{py} A_y}\right)}{\left(K_{cr1} + K_{cr2}\right)\left(K_{sp} + K_{pr3} P_{s0}\right)} + K_{qr1} \right) \quad \text{(L6)}$$

$$K = K_{xv}^* K_\phi = \frac{K_{xv}^*}{D_m + \frac{c_{ml} B_m}{D_m}} \quad \text{(L7)}$$

The coefficients of s-polynomial in the numerator in Equation (L2), b_i, are same as those in Equation (E2) and hence can be calculated by Table E1. The coefficients of s-polynomial in the denominator in Equation (L2), a_i, must be calculated by Table L1.

Table L.1 Determination of the coefficients, a_i, of s-polynomial in the denominator of LSPC system's TF in Condition N

	s^5	s^4	s^3	s^2	s^1	s^0
1	$t_{L2}t_s t_{ysp} t_{Ls}$	$t_{L2}t_s t_{ysp} + t_{L2}t_s t_{Ls} + t_{L2}t_{ysp}t_{Ls} + t_L t_s t_{ysp} t_{Ls}$	$t_{L2}t_s + t_{L2}t_{Ls} + t_{L2}t_{ysp} + t_L t_s t_{ysp} + t_L t_s t_{Ls} + t_L t_{Ls} t_{ysp} + t_s t_{Ls} t_{ysp}$	$t_{L2} + t_L t_s + t_L t_{ysp} + t_L t_{Ls} + t_{ysp} t_s + t_{Ls} t_s + t_{Ls} t_{ysp}$	$t_L + t_s + t_{ysp} + t_{Ls}$	1
2	$K_{cL} t_{L0} t_s t_{ysp} t_{Ls} t_{pc0}$	$K_{cL}(t_{L0} t_s t_{ysp} t_{Ls} + t_{pc0}(t_{L0} t_s t_{ysp} + t_{L0} t_{Ls} t_s + t_{L0} t_{Ls} t_{ysp}))$	$K_{cL}(t_{L0} t_s t_{ysp} + t_{L0} t_{Ls} t_s + t_{L0} t_{Ls} t_{ysp} + t_{pc0}(t_{L0} t_s + t_{L0} t_{ysp} + t_{L0} t_{Ls} + t_s t_{ysp} + t_s t_{Ls} + t_{ysp} t_{Ls}))$	$K_{cL}(t_{L0} t_s + t_{L0} t_{ysp} + t_{L0} t_{Ls} + t_s t_{ysp} + t_s t_{Ls} + t_{ysp} t_{Ls} + t_{pc0}(t_{L0} + t_s + t_{ysp} + t_{Ls}))$	$K_{cL}(t_{L0} + t_s + t_{ysp} + t_{Ls} + t_{pc0})$	K_{cL}
3	$K_{sc} t_{L2} t_{ysp} t_{Ls} t_{pc0}$	$K_{sc}(t_{L2} t_{ysp} t_{Ls} + t_{pc0}(t_{L2} t_{ysp} + t_{L2} t_{Ls} + t_L t_{Ls} t_{ysp}))$	$K_{sc}(t_{L2} t_{ysp} + t_{L2} t_{Ls} + t_L t_{Ls} t_{ysp} + t_{pc0}(t_{L2} + t_L t_{ysp} + t_L t_{Ls} + t_{ysp} t_{Ls}))$	$K_{sc}(t_{L2} + t_L t_{ysp} + t_L t_{Ls} + t_{ysp} t_{Ls} + t_{pc0}(t_L + t_{ysp} + t_{Ls}))$	$K_{sc}(t_L + t_{ysp} + t_{Ls} + t_{pc0})$	K_{sc}
4		$K_{ps} t_{L2} t_{p0} t_{Ls}$	$K_{ps}(t_{L2} t_{p0} + t_{L2} t_{Ls} + t_L t_{Ls} t_{p0})$	$K_{ps}(t_{L2} + t_L t_{p0} + t_L t_{Ls} + t_{p0} t_{Ls})$	$K_{ps}(t_L + t_{p0} + t_{Ls})$	K_{ps}
5		$K_{pscl} t_{L0} t_{p0} t_{pc0} t_{Lp0}$	$K_{pscl}(t_{L0} t_{p0} t_{pc0} + t_{L0} t_{p0} t_{Lp0} + t_{L0} t_{pc0} t_{Lp0} + t_{p0} t_{pc0} t_{Lp0})$	$K_{pscl}(t_{L0} t_{p0} + t_{pc0}(t_{L0} + t_{p0}) + t_{Lp0}(t_{pc0} + t_{L0} + t_{p0}))$	$K_{pscl}(t_{L0} + t_{p0} + t_{pc0} + t_{Lp0})$	K_{pscl}
Σ	a_5	a_4	a_3	a_2	a_1	a_0

Appendix M Transfer Function of the Load Sensing and Pressure Compensated System (Condition O)

The appendix is to express the TF (see Equation (13.3)) of the LSPC system under the operating Condition O in a more general form as Equation (13.4) so that it is possible to use Matlab® programming to plot the Bode diagram and/or the zeros and poles in the phase plane. Equations (13.3) and (13.4) are rewritten as

$$F(s)=\frac{K_q\left(1+G_sH_p\right)G_\phi}{1+K_cH_L+K_cG_s+G_sH_p+K_cH_LG_sH_p}$$

$$=\frac{K_{xv}^*\left(1+\dfrac{K_p^*K_s}{\left(\dfrac{s^2}{\omega_{sp}^2}+\dfrac{2\zeta_{sp}s}{\omega_{sp}}+1\right)\left(\dfrac{s}{\omega_s}+1\right)}\right)\dfrac{K_\phi}{\left(\dfrac{s^2}{\omega_L^2}+\dfrac{2\zeta_Ls}{\omega_L}+1\right)}}{1+\dfrac{K_{psL}^*K_L\left(\dfrac{s}{\omega_{L0}}+1\right)\left(\dfrac{s}{\omega_{pc0}}+1\right)}{\left(\dfrac{s^2}{\omega_L^2}+\dfrac{2\zeta_Ls}{\omega_L}+1\right)}+\dfrac{K_sK_{psL}^*\left(\dfrac{s}{\omega_{pc0}}+1\right)}{\left(\dfrac{s}{\omega_s}+1\right)}+\dfrac{K_p^*K_s}{\left(\dfrac{s^2}{\omega_{sp}^2}+\dfrac{2\zeta_{sp}s}{\omega_{sp}}+1\right)\left(\dfrac{s}{\omega_s}+1\right)}+\dfrac{K_p^*K_sK_{psL}^*K_L\left(\dfrac{s}{\omega_{L0}}+1\right)\left(\dfrac{s}{\omega_{pc0}}+1\right)}{\left(\dfrac{s^2}{\omega_{sp}^2}+\dfrac{2\zeta_{sp}s}{\omega_{sp}}+1\right)\left(\dfrac{s^2}{\omega_L^2}+\dfrac{2\zeta_Ls}{\omega_L}+1\right)\left(\dfrac{s}{\omega_s}+1\right)}} \quad \text{(M1)}$$

$$F(s)=K\frac{b_3s^3+b_2s^2+b_1s+b_0}{a_5s^5+a_4s^4+a_3s^3+a_2s^2+a_1s+a_0} \quad \text{(M2)}$$

In addition to Equations (F3) through (F8) and (F11) in Appendix F, other coefficients associated to K_c and K_q must be redefined. They are

$$t_{pc0}=\frac{1}{\omega_{pc0}} \quad \text{(M3)}$$

$$K_{cl}=K_{psL}^*K_L=\frac{K_{psL}^*B_m}{c_{ml}B_m+D_m^2} \quad \text{(M4)}$$

$$K_{sc}=K_sK_{psL}^*=\frac{K_{psL}^*}{c_{pl}+K_{cr1}} \quad \text{(M5)}$$

$$K_{pscl}=\frac{A_rK_{psL}^*B_m}{k_r\omega_{Ls}\left(c_{pc}+K_{cr1}\right)\left(c_{ml}B_m+D_m^2\right)}\left(\frac{NR_pA_p\omega\left(K_{qr1}+\left|K_{qr2}\right|\right)R_{py}A_y}{\pi\cos^2\theta_{sp0}\left(K_{cr1}+K_{cr2}\right)\left(K_{sp}+K_{pr3}P_{s0}\right)}+K_{qr1}\right) \quad \text{(M6)}$$

$$K = K_{xv}^{*} K_{\phi} = \frac{K_{xv}^{*}}{D_m + \frac{c_{ml} B_m}{D_m}} \tag{M7}$$

The coefficients of s-polynomial in the numerator in Equation (M2), b_i, are same as those in Equation (F2) and hence can be calculated by Table F1. The coefficients of s-polynomial in the denominator in Equation (M2), a_i, must be calculated by Table M1.

Table M1 Determination of the coefficients, a_i, of s polynomial in the denominator of LSPC system's TF in Condition O

	s^5	s^4	s^3	s^2	s^1	s^0
1	$t_{L2}t_s t_{sp2}$	$t_{L2}t_s t_{sp}+t_{L2}t_{sp2}$ $+t_L t_s t_{sp2}$	$t_{L2}t_s+ t_{L2}t_{sp}+ t_L t_s t_{sp}+$ $t_L t_{sp2}+ t_s t_{sp2}$	$t_{L2}+ t_L t_s+ t_L t_{sp}+$ $t_{sp2}+ t_s t_{sp}$	$t_L+ t_s+ t_{sp}$	1
2	$K_{cL}t_{L0}t_s$ $t_{sp2}t_{pc0}$	$K_{cL}(t_{L0}t_s t_{sp2}+$ $t_{pc0}(t_{L0}t_{sp2}+$ $t_{sp2}t_s+$ $t_{L0}t_s t_{sp}))$	$K_{cL}(t_{L0}t_{sp2}+ t_{sp2}t_s+$ $t_{L0}t_s t_{sp} + t_{pc0}(t_{L0}t_s+$ $t_{L0}t_{sp} + t_s t_{sp} + t_{sp2}))$	$K_{cL}(t_{L0}t_s+ t_{L0}t_{sp} +$ $t_s t_{sp} + t_{sp2}+$ $t_{pc0}(t_{L0}+ t_s+ t_{sp}))$	$K_{cL}(t_{L0}+ t_s+$ $t_{sp}+ t_{pc0})$	K_{cL}
3	$K_{sc}t_{L2}$ t_{sp2} t_{pc0}	$K_{sc}(t_{L2}t_{sp2}+$ $t_{pc0}(t_L t_{sp2}+$ $t_{L2}t_{sp}))$	$K_{sc}(t_L t_{sp2}+ t_{L2}t_{sp}+$ $t_{pc0}(t_{L2}+ t_{sp2}+t_{sp}t_L))$	$K_{sc}(t_{L2}+$ $t_{sp2}+t_{sp}t_L+ t_{pc0}(t_L+$ $t_{sp}))$	$K_{sc}(t_L+ t_{sp}+$ $t_{pc0})$	K_{sc}
4				K_{ps}^{*} t_{L2}	K_{ps}^{*} t_L	K_{ps}^{*}
5				K_{pscl}^{*} t_{L0} t_{pc0}	$K_{pscl}^{*}(t_{L0}+$ $t_{pc0})$	K_{pscl}^{*}
Σ	a_5	a_4	a_3	a_2	a_1	a_0

Appendix N Transfer Function of the Load Sensing and Pressure Compensated System (Condition P)

The appendix is to express the TF (see Equation (13.5)) of the LSPC system under the operating Condition P in a more general form as Equation (13.6) so that it is possible to use Matlab® programming to plot the Bode diagram and/or the zeros and poles in the phase plane. Equations (13.5) and (13.6) are rewritten as

$$F(s)=\frac{K_{xv}^{*}\left(\dfrac{K_{\phi}}{\dfrac{s^2}{\omega_L^2}+\dfrac{2\zeta_L s}{\omega_L}+1}\right)}{1+\dfrac{K_{psL}^{*}K_L\left(\dfrac{s}{\omega_{L0}}+1\right)\left(\dfrac{s}{\omega_{pc0}}+1\right)}{\dfrac{s^2}{\omega_L^2}+\dfrac{2\zeta_L s}{\omega_L}+1}+\dfrac{K_s K_{psL}^{*}\left(\dfrac{s}{\omega_{pc0}}+1\right)}{\dfrac{s}{\omega_s}+1}} \tag{N1}$$

$$F(s)=\frac{K(b_1 s+b_0)}{a_3 s^3+a_2 s^2+a_1 s+a_0} \tag{N2}$$

In addition to Equations (G3) through (G6) in Appendix G, other coefficients associated to K_c and K_q must be redefined. They are

$$t_{pc0}=\frac{1}{\omega_{pc0}} \tag{N3}$$

$$K_{cl}=K_{psL}^{*}K_L=\frac{K_{psL}^{*}B_m}{c_{ml}B_m+D_m^2} \tag{N4}$$

$$K_{sc}=K_s K_{psL}^{*}=\frac{K_{psL}^{*}}{c_{pl}+K_{cr1}} \tag{N5}$$

$$K=K_{xv}^{*}K_{\phi}=\frac{K_{xv}^{*}}{D_m+\dfrac{c_{ml}B_m}{D_m}} \tag{N6}$$

The coefficients of s-polynomial in the numerator in Equation (N2), b_i, are same as those in Equation (G2) in Appendix G and hence b_1 and b_0 are t_s and 1 respectively (Equations (G13) and (G15)). The coefficients of s-polynomial in the denominator in Equation (N2), a_i, must be calculated by

$$a_3 = t_{L2}t_s + K_{cL}t_s t_{L0}t_{pc0} + K_{sc}t_{L2}t_{pc0} \tag{N7}$$

$$a_2 = t_{L2} + t_L t_s + K_{sc}\left(t_{L2} + t_L t_{pc0}\right) + K_{cL}\left(t_s t_{L0} + t_{pc0}\left(t_{L0} + t_s\right)\right) \tag{N8}$$

$$a_1 = t_L + t_s + K_{sc}\left(t_L + t_{pc0}\right) + K_{cL}\left(t_{L0} + t_s + t_{pc0}\right) \tag{N9}$$

$$a_0 = 1 + K_{cL} + K_{sc} \tag{N11}$$